VOL. 607 NO. 1 AUGUST 21, 1992

JOURNAL OF CHROMATOGRAPHY

INCLUDING ELECTROPHORESIS AND OTHER SEPARATION METHODS

ELSEVIER

JOURNAL OF CHROMATOGRAPHY

INCLUDING ELECTROPHORESIS AND OTHER SEPARATION METHODS

Scope. The *Journal of Chromatography* publishes papers on all aspects of chromatography, electrophoresis and related methods. Contributions consist mainly of research papers dealing with chromatographic theory, instrumental development and their applications. The section *Biomedical Applications*, which is under separate editorship, deals with the following aspects: developments in and applications of chromatographic and electrophoretic techniques related to clinical diagnosis or alterations during medical treatment; screening and profiling of body fluids or tissues with special reference to metabolic disorders; results from basic medical research with direct consequences in clinical practice; drug level monitoring and pharmacokinetic studies; clinical toxicology; analytical studies in occupational medicine.

Submission of Papers. Manuscripts (in English; *four* copies are required) should be submitted to: Editorial Office of *Journal of Chromatography*, P.O. Box 681, 1000 AR Amsterdam, Netherlands, Telefax (+31-20) 5862 304, or to: The Editor of *Journal of Chromatography, Biomedical Applications*, P.O. Box 681, 1000 AR Amsterdam, Netherlands. Review articles are invited or proposed by letter to the Editors. An outline of the proposed review should first be forwarded to the Editors for preliminary discussion prior to preparation. Submission of an article is understood to imply that the article is original and unpublished and is not being considered for publication elsewhere. For copyright regulations, see below.

Publication. The *Journal of Chromatography* (incl. *Biomedical Applications*) has 39 volumes in 1992. The subscription prices for 1992 are:

J. Chromatogr. (incl. *Cum. Indexes, Vols. 551–600*) + *Biomed. Appl.* (Vols. 573–611):
Dfl. 7722.00 plus Dfl. 1209.00 (p.p.h.) (total *ca.* US$ 4880.25)

J. Chromatogr. (incl. *Cum. Indexes, Vols. 551–600*) only (Vols. 585–611):
Dfl. 6210.00 plus Dfl. 837.00 (p.p.h.) (total *ca.* US$ 3850.75)

Biomed. Appl. only (Vols. 573–584):
Dfl. 2760.00 plus Dfl. 372.00 (p.p.h.) (total *ca.* US$ 1711.50).

Subscription Orders. The Dutch guilder price is definitive. The US$ price is subject to exchange-rate fluctuations and is given as a guide. Subscriptions are accepted on a prepaid basis only, unless different terms have been previously agreed upon. Subscriptions orders can be entered only by calender year (Jan.–Dec.) and should be sent to Elsevier Science Publishers, Journal Department, P.O. Box 211, 1000 AE Amsterdam, Netherlands, Tel. (+31-20) 5803 642, Telefax (+31-20) 5803 598, or to your usual subscription agent. Postage and handling charges include surface delivery except to the following countries where air delivery via SAL (Surface Air Lift) mail is ensured: Argentina, Australia, Brazil, Canada, China, Hong Kong, India, Israel, Japan*, Malaysia, Mexico, New Zealand, Pakistan, Singapore, South Africa, South Korea, Taiwan, Thailand, USA. *For Japan air delivery (SAL) requires 25% additional charge of the normal postage and handling charge. For all other countries airmail rates are available upon request. Claims for missing issues must be made within three months of our publication (mailing) date, otherwise such claims cannot be honoured free of charge. Back volumes of the *Journal of Chromatography* (Vols. 1–572) are available at Dfl. 217.00 (plus postage). Customers in the USA and Canada wishing information on this and other Elsevier journals, please contact Journal Information Center, Elsevier Science Publishing Co. Inc., 655 Avenue of the Americas, New York, NY 10010, USA, Tel. (+1-212) 633 3750, Telefax (+1-212) 633 3990.

Abstracts/Contents Lists published in Analytical Abstracts, Biochemical Abstracts, Biological Abstracts, Chemical Abstracts, Chemical Titles, Chromatography Abstracts, Clinical Chemistry Lookout, Current Contents/Life Sciences, Current Contents/Physical, Chemical & Earth Sciences, Deep-Sea Research/Part B: Oceanographic Literature Review, Excerpta Medica, Index Medicus, Mass Spectrometry Bulletin, PASCAL-CNRS, Pharmaceutical Abstracts, Referativnyi Zhurnal, Research Alert, Science Citation Index and Trends in Biotechnology.

US Mailing Notice. *Journal of Chromatography* (main section ISSN 0021-9673, *Biomedical Applications* section ISSN 0378-4347) is published (78 issues/year) by Elsevier Science Publishers (Sara Burgerhartstraat 25, P.O. Box 211, 1000 AE Amsterdam, Netherlands). Annual subscription price in the USA US$ 4880.25 (subject to change), including air speed delivery. Application to mail at second class postage rate is pending at Jamaica, NY 11431. **USA POSTMASTERS:** Send address changes to *Journal of Chromatography*, Publications Expediting, Inc., 200 Meacham Avenue, Elmont, NY 11003. Airfreight and mailing in the USA by Publication Expediting.

See inside back cover for Publication Schedule, Information for Authors and information on Advertisements.

0021-9673/92/$05.00

Printed in the Netherlands

CONTENTS

(Abstracts/Contents Lists published in Analytical Abstracts, Biochemical Abstracts, Biological Abstracts, Chemical Abstracts, Chemical Titles, Chromatography Abstracts, Current Awareness in Biological Sciences (CABS), Current Contents/Life Sciences, Current Contents/Physical, Chemical & Earth Sciences, Deep-Sea Research/Part B: Oceanographic Literature Review, Excerpta Medica, Index Medicus, Mass Spectrometry Bulletin, PASCAL-CNRS, Referativnyi Zhurnal, Research Alert and Science Citation Index)

REGULAR PAPERS

Column Liquid Chromatography

Gas Chromatography

Supercritical Fluid Chromatography

Planar Chromatography

(Continued overleaf)

JOURNAL OF CHROMATOGRAPHY

VOL. 607 (1992)

JOURNAL of CHROMATOGRAPHY

INCLUDING ELECTROPHORESIS AND OTHER SEPARATION METHODS

ELSEVIER

AMSTERDAM — LONDON — NEW YORK — TOKYO

0021-9673/92/$05.00

Printed in the Netherlands

Journal of Chromatography, 607 (1992) 1–6
Elsevier Science Publishers B.V., Amsterdam

CHROM. 24 345

Determination of glycerol in bacterial cell wall teichoic acid by high-performance liquid chromatography

Juha-Pekka Himanen

Department of Molecular Bacteriology, and Molecular Biology Programme, National Public Health Institute, Mannerheimintie 166, SF-00300 Helsinki (Finland)

(First received March 10th, 1992; revised manuscript received May 8th, 1992)

ABSTRACT

A high-performance liquid chromatography method for the determination of glycerol in teichoic acid was developed. The phosphodiester linkages between repeating glycerol units were hydrolysed by treatment with 5.8 *M* HCl at 100°C for 75 h. The degree of hydrolysis was verified by gas chromatography–mass spectrometry. The hydrolysed samples were applied to an ion-exclusion column and the amount of glycerol determined as the area of the peak at 12.6 min. Using glycerol standards an r^2 value of 0.999, a relative standard deviation of 2.2% and a detection limit of 0.1 μg were obtained.

INTRODUCTION

The cell surface of gram-positive bacteria contains lipoteichoic acid (LTA) and a peptidoglycan–teichoic acid complex (PG–TA) as the major and biologically important molecules. Interest in these molecules is based on their role in the structure and function of the bacterial cell wall [1] and on their potential participation in modifying the course of infection and response to vaccines [2,3].

The basic structure of LTA and TA consists of a long hydrophilic chain of 20–60 repeating phosphoglycerol units where the individual glycerol (Gro) molecules are joined by a phosphodiester linkage [1]. Thus the determination of Gro in these compounds is of crucial importance to structure–function studies. This is usually carried out after cleavage of the phosphodiester bond by treatment with acid or alkaline phosphatase, or both. The liberated Gro is then determined by gas chromatography (GC) [4,5], enzymatically by a glycerol kinase-based assay [6,7], by potentiometric [8] or luminometric [9] methods. A preliminary report has been published describing the determination of Gro in grape juice by high-performance liquid chromatography (HPLC) [10].

The purpose of this study was to develop and validate a simple HPLC-method for the determination of Gro in bacterial cell surface compounds. The goal was to avoid the use of tedious enzyme reactions or toxic HF for the liberation of Gro and the multi-step sample preparations for the liberated Gro. The data obtained demonstrate the feasibility of applying the Gro sample directly after hydrochloric acid treatment to an ion exclusion column coupled to a refractive index (RI) detector using commercial α-phosphoglycerol (P-Gro) and PG-TA of *Bacillus subtilis* to standardize the method.

EXPERIMENTAL

Reagents

All chemicals used were commercially available and of analytical purity. P-Gro and Gro were from

Correspondence to: Dr. J.-P. Himanen, Department of Molecular Bacteriology, and Molecular Biology Programme, National Public Health Institute, Mannerheimintie 166, SF-00300 Helsinki, Finland.

0021-9673/92/$05.00

Sigma (St.Louis, MO, USA) and iodomethane from Fluka (Buchs, Switzerland).

Chemical methods

The hydrolyses were carried out in sealed glass tubes. Inorganic and total phosphate were determined by the spectrophotometric method of Lowry *et al.* [11]. The amount of organic phosphate was calculated from the difference between inorganic and total phosphate. Permethylation was performed by CH_3I in a basic solution of dimethyl sulphoxide after diazomethane treatment according to the method of Ciucanu and Kerek [12].

Gas chromatography–mass spectrometry

Combined GC–mass spectrometry (MS) analyses were performed using a Hewlett-Packard 5890 Series II gas–liquid chromatograph (Avondale, PA, USA) and a Hewlett-Packard 5971A mass selective detector equipped with an HP-5 fused-silica capillary column (25 m × 0.2 mm I.D.). Helium was used as the carrier gas. The initial temperature of 100°C was held for 1 min and then increased at a rate of 7°C/min to the final temperature of 250°C. The injector temperature was 250°C and the ion-source temperature 185°C. Electron impact mass spectra were recorded at 70 eV.

High-performance liquid chromatography

The HPLC analyses were carried out using a Waters Model 510 pump (Milford, MA, USA) with a 20-μl injection loop equipped with a Pharmacia 2142 RI detector (Bromma, Sweden) and a Shimadzu C-R3A integrator (Tokyo, Japan). The ion-exclusion column (Aminex HPX-87H) and the guard column were from Bio-Rad (Richmond, CA, USA). Sulphuric acid (0.004 *M*) in distilled and deionized water was used as the eluent at a flow-rate of 0.6 ml/min.

RESULTS AND DISCUSSION

Optimum conditions for the hydrolysis of glycerol-phosphoester bonds

The liberation of phosphate from P-Gro was first tested in 0.1 *M* HCl. Table I shows that after 3 days of this treatment at 100°C only 50% of the P-Gro was hydrolysed to inorganic phosphate and Gro. Total hydrolysis was achieved only after a prolonged hydrolysis of up to 11 days.

TABLE I

ORGANIC PHOSPHATE DETECTED AFTER PROLONGED HYDROLYSIS OF P-Gro IN 0.1 *M* HCl

P-Gro (1 mg/ml) was hydrolysed in 0.1 *M* HCl at 100°C for various times and organic phosphate (P_{org}) determined as described under Experimental.

Time (h)	P_{org} (%)
0	100
1	100
2	97
6	94
24	78
65	50
260	0.1

Increasing the HCl concentration from 0.1 to 2.0 *M* did not influence the rate of hydrolysis (Table II), apparently because the mechanism of hydrolysis at low concentrations is based on an intramolecular rearrangement reaction [13]. An increase in the concentration of acid to above 2.0 *M* increased the rate of hydrolysis, consistent with the change of the reaction to second-order kinetics. Thus after 65 h at 100°C, 87% of P-Gro was hydrolysed in 4.0 *M* HCl and 98% in 5.8 *M* HCl (Table II).

Fig.1 shows the time course of the hydrolysis of P-Gro in 5.8 *M* HCl. About 70% of P-Gro was hydrolysed after 1 day and about 90% after 2 days. The hydrolysis was completed within 75 h.

TABLE II

ORGANIC PHOSPHATE DETECTED AFTER A 65 h HYDROLYSIS OF P-Gro IN HCl

P-Gro (1 mg/ml) was hydrolysed for 65 h at 100°C in HCl of various concentrations and organic phosphate (P_{org}) determined as described under Experimental.

Concentration of HCl (*M*)	P_{org} (%)
0	100
0.1	50
0.5	50
1.0	50
2.0	58
4.0	13
5.8	2.4

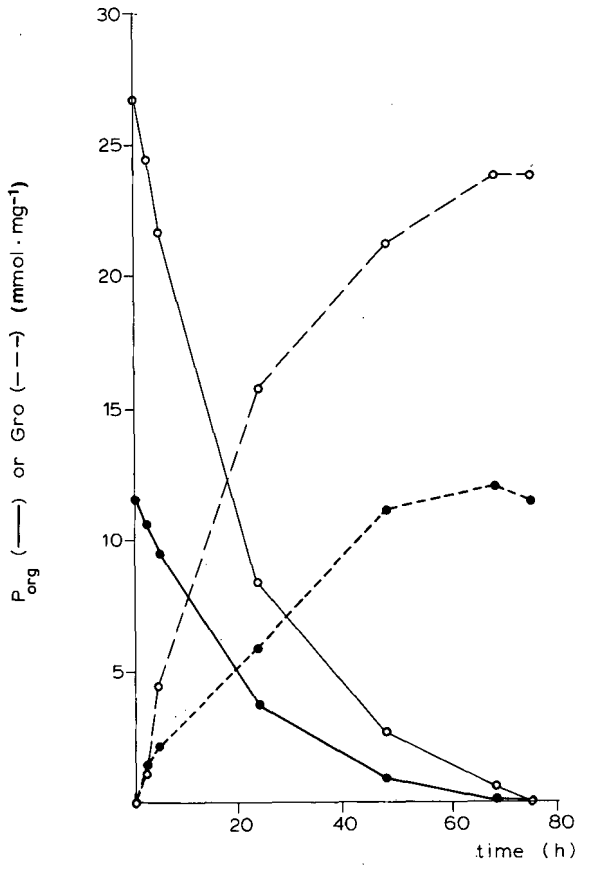

Fig. 1. Kinetics of hydrolysis of P-Gro (○) and PG-TA (●) in 5.8 *M* HCl at 100°C. Solutions (1 mg/ml) of the samples were hydrolysed in HCl and organic phosphate (solid lines) and Gro (dotted lines) were determined at different times as described under Experimental.

The production of Gro by the hydrolysis of P-Gro with HCl was verified by GC. Intact and hydrolysed (5.8 *M* HCl, 100°C, 75 h) samples of P-Gro were permethylated and investigated using GC–MS. Intact, permethylated P-Gro was detected by GC as one major peak (retention time 8.1 min). This peak yielded the electron impact mass spectrum shown in Fig. 2a, showing characteristic fragments of methylated phosphate at *m/z* 109 and 127. In the hydrolysed sample this peak was negligible and instead a prominent peak at 3.7 min appeared. The mass spectrum of this peak (Fig.2b) was indistinguishable from that obtained with authentic Gro, including the molecular ion of permethylated Gro (*m/z* 134).

The results show that the use of HCl is applicable in hydrolysing phosphoglycerol compounds. Both HCl and the commonly used HF [14] demand prolonged treatment, but HF is more expensive, potentially toxic and inconvenient to use.

Determination of glycerol

In the HPLC analysis authentic Gro yielded a single peak with a retention time of 12.6 min. The calibration graph for Gro was obtained by applying Gro standards to the ion exclusion column and comparing the areas of the peaks at 12.6 min. The results followed the linear regression equation $y = 1.087x + 0.580$ ($r^2 = 0.999$), where y is the relative area and x is the amount of glycerol (Fig.3).

The reproducibility was determined by five independent injections of 20 μg of glycerol. The areas varied from 21.382 to 22.833 and a relative standard deviation of 2.2% was obtained.

The detection limit for glycerol was 0.1 μg, corresponding to a signal-to-noise ratio of 2. As an injection volume of 20 μl was used this is equal to a concentration of 5 μg/ml. This is better than those reported for the potentiometric (10 μg/ml) [8], enzymatic (10 μg/ml) [15] and preliminary HPLC (25 μg/ml) [10] methods. On the other hand, it is clearly less good than the sensitivity of a bioluminescent method (0.3 μg/ml) [9]. When investigating cell surface compounds, however, such extreme sensitivities are rarely required. The correlation was linear up to 100 μg. Above this level tailing of the peaks reduced the accuracy.

Study of PG-TA of the cell wall of Bacillus subtilis

PG-TA was purified from *Bacillus subtilis* and shown in chemical analysis to be composed of essentially pure teichoic acid and peptidoglycan covalently linked to each other [16]. PG-TA (1 mg/ml) was hydrolysed for various times in 5.8 *M* HCl (100°C). The hydrolysis of phosphoester bonds was found to show essentially similar kinetics as the hydrolysis of P-Gro (Fig.1). A typical chromatogram of an HPLC analysis of hydrolysed PG-TA is shown in Fig.4. The glycerol peak at 12.6 min resolved well from other peaks which represent amino sugars and amino acids generated from PG-TA. Fig.1 shows a good correlation between the amount of organic phosphate before hydrolysis and the amount of glycerol after hydrolysis. Decomposition

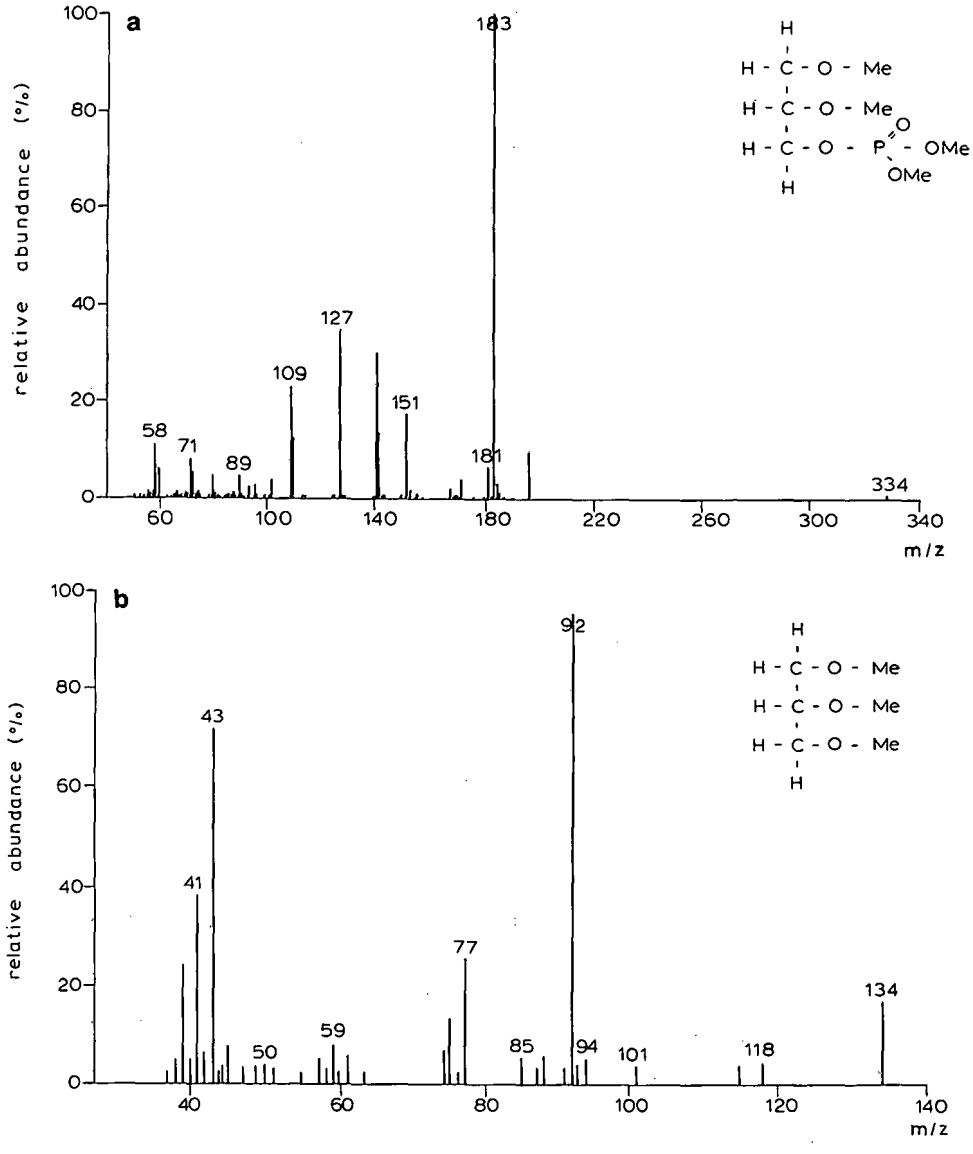

Fig. 2. Electron impact GC–MS spectra of P-Gro. P-Gro was hydrolysed in 5.8 *M* HCl for 75 h at 100°C and determined by GC–MS as described under Experimental before (a) and after (b) hydrolysis. Me = Methyl.

of Gro in HCl did not occur as the area of the peak at 12.6 min was the same before and after treating Gro for 75 h in 5.8 *M* HCl at 100°C.

The described method using ion-exclusion HPLC and a RI detector is fast and accurate for the determination of glycerol. The correlation coefficient (0.999) of the calibration graph indicates a high reproducibility of the method. Chromatography immediately after the hydrolysis, without extra sample preparation steps, eliminates the tedious and time-consuming steps of the enzymatic [15] and bioluminescent [9] assays and diminishes the errors. Especially with GC, sample preparation can be problematic because of the substantial volatility of glycerol [17]. According to experience in this laboratory, one evaporation to dryness decreases the amount of

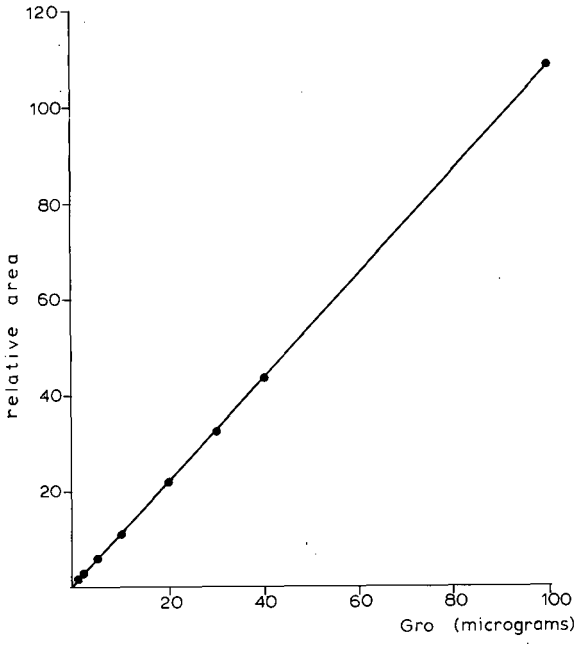

Fig. 3. Calibration graph for the determination of Gro by HPLC. Samples (20 μl; 1–100 μg) of Gro were applied to the HPX-87H ion-exclusion column and the effluent monitored by an RI detector. The area of the peak at 12.6 min was plotted against the amount of Gro in the sample.

peracetylated glycerol to 30% of the original amount.

ACKNOWLEDGEMENTS

The author is grateful to T. K. Korpela for fruitful discussions and for providing technical help, and to P. H. Mäkelä and I. M. Helander for critical reading of the manuscript. The work was financially supported by the Academy of Finland.

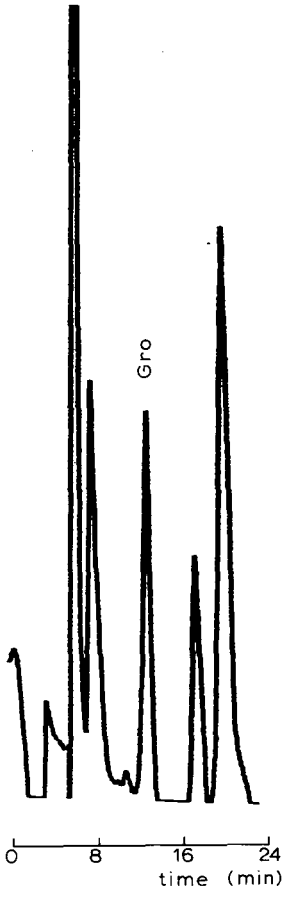

Fig. 4. Typical example of the determination of Gro in purified PG-TA. PG-TA (1 mg/ml) was hydrolysed in 5.8 *M* HCl for 75 h at 100°C and applied to the HPX-87H ion-exclusion column. The amount of Gro in the sample (2.5 μg in 20 μl) was determined by comparing the area of the peak at 12.6 min with the calibration graph.

REFERENCES

1 M. Duckworth, in I. Sutherland (Editor), *Surface Carbohydrates of the Prokaryotic Cell*, Academic Press, London, 1977, Ch. 5, p. 177.
2 D. E. S. Stewart-Dull, *Ann. Rev. Microbiol.*, 34 (1980) 311.
3 W. Fischer, *Adv. Microb. Physiol.*, 29 (1988) 233.
4 Y. Sasaki, Y. Araki and E. Ito, *Eur. J. Biochem.*, 132 (1983) 207.
5 N. Kojima, Y. Araki and E. Ito, *J. Biol. Chem.*, 258 (1983) 9043.
6 Y. Sasaki, Y. Araki and E. Ito, *Biochem. Biophys. Res. Commun.*, 96 (1980) 529.
7 C. Bublitz and O. Wieland, *Methods Enzymol.*, 5 (1962) 354.
8 A. K. Chen and J. A. Starzmann, *Biotechnol. Bioeng.*, 24 (1982) 971.
9 H. Kather, F. Schröder and B. Simon, in M. Serió and M. Pazzagli (Editors), *Luminescent Assays: Perspectives in Endocrinology and Clinical Chemistry*, Raven Press, New York, 1982, p. 53.
10 S. A. Kupina, *Am. J. Enol. Vitic.*, 35 (1984) 59.
11 O. H. Lowry, N. R. Roberts, K. Y. Leiner, M. L. Wu and A. L. Farr, *J. Biol. Chem.*, 207 (1954) 1.
12 I. Ciucanu and F. Kerek, *Carbohydr. Res.*, 131 (1984) 209.
13 R. G. Kallen, T. K. Korpela, A. E. Martell, Y. Matsushima, C. M. Metzler, D. E. Metzler, Y. V. Morozov, I. M. Ralston, F. A. Savin, Y. M. Torchinsky and H. Ueno, in P. Christen and D. E. Metzler (Editors), *Transaminases*, Wiley, New York, 1985, p. 37.

14 I. M. Helander, B. Lindner, H. Brade, K. Altmann, A. A. Lindberg, E. T. Rietschel and U. Zähringer, *Eur. J. Biochem.*, 177 (1988) 483.
15 C.-N. Ou and V. L. Frawley, *Clin. Biochem.*, 18 (1985) 37.
16 J.-P. Himanen. L. Pyhälä, R.-M. Ölander, O. Merimskaya, T. Kuzina, A. Pronin, A. Sanin, I. M. Helander and M. Sarvas, submitted for publication.
17 J. C. Dittmer and M. A. Wells, *Methods Enzymol.*, 14 (1969) 489.

Journal of Chromatography, 607 (1992) 7–18
Elsevier Science Publishers B.V., Amsterdam

CHROM. 24 359

Separation of glucose polymers by hydrophilic interaction chromatography on aqueous size-exclusion columns using gradient elution with pulsed amperometric detection

Andrew S. Feste and Iftikhar Khan

US Department of Agriculture/Agricultural Research Service Children's Nutrition Research Center, Baylor College of Medicine, 1100 Bates Street, Houston, TX 77030 (USA)

(First received February 18th, 1992; revised manuscript received May 12th, 1992)

ABSTRACT

Maltooligosaccharides were submitted to hydrophilic interaction chromatography on three aqueous size-exclusion columns. When mobile phase compositions were 0% to 40% (v/v) acetonitrile in water, the chromatographic mechanism was by size exclusion on all three columns; at concentrations $\geq 50\%$ (v/v) acetonitrile, the carbohydrates were fractionated by partition chromatography ($0.88 > k' > 143$; where k' is the solute capacity factor), and the order of elution was reversed. When maltooligosaccharides were eluted from the three columns using isocratic mobile phases in which the concentration of acetonitrile was varied from 50% to 75% (v/v), a negative linear relationship ($R^2 > -0.973$) existed between retention and solvent strength; retention increased as the polarity of the mobile phase was decreased. When the composition of the mobile phase was 65% acetonitrile in water, a correlation ($R^2 > 0.99$) was found in all three columns between the degree of polymerization and the retention of the oligosaccharide. With gradient elution, the Protein-Pak 60 column resolved N-acetylneuraminic acid, rhamnose, arabinose and a mixture of commercially available glucose polymers; the between-run precision of the retention times ($n = 16$) for the chromatography varied from 0.09 to 0.64% (relative standard deviation). The chromatography was applied to the analysis of enzyme-hydrolyzed starch digests.

INTRODUCTION

The analysis of monosaccharides, non-protein-bound oligosaccharides, and glycoprotein-derived oligosaccharides is necessary in certain disciplines in both biomedicine and industry. Sulfonated polystyrene-divinylbenzene cation-exchange supports with various counter ions [1-6], reversed-phase columns with C_{18} bound to silica [7] or polyvinyl alcohol [8] supports, and more recently, pellicular quaternary amine-bonded anion exchange supports [9–16] have been used to separate a variety of mono-, di- and oligosaccharides. Carbohydrates separated on the cation-exchange and reversed-phase supports were observed by refractive index detection [1–8], while those separated by anion exchange were observed by the more sensitive pulsed amperometric detection [9–16].

Carbohydrates have also been separated on columns that contain hydrophilic, polar-bonded phases. Mono-, di- and oligosaccharides have been separated on silica-bound amine [17–22], diol [20] and polyol [23] supports. A hydroxylated polymeric support was used to separate neutral oligosaccharides derived from glycoproteins [24]. A feature common to all these separations was the resolution of highly polar solutes on polar, hydrophilic bonded phases; the separations were performed with mobile phases of acetonitrile and water. Retention of the polar solutes increased with the volume percent of acetonitrile, and evidence suggested that carbohydrate separation occurred by partition [19,22]. At higher percentages of acetonitrile, proportionally

Correspondence to: Dr. Andrew S. Feste, Children's Nutrition Research Center, 1100 Bates Street, Houston, TX 77030, USA.

0021-9673/92/$05.00

more water was adsorbed to the hydrophilic group on the support than was present in the mobile phase, and the establishment of the static layer of water was required for partitioning and separation to occur (19,22).

Solutes other than carbohydrates have been separated on polar-bonded phases. Silica-bound polyol [23] was used to separate phenols and polyphenols with a mobile phase of hexane-methanol-tetrahydrofuran; when the mobile phase was phosphate buffer, however, proteins were separated by size exclusion. On chitosan (de-acetylated chitin) adsorbed to a silica support, amino acids, nucleotides, and dipeptides were separated by mobile phases of acetonitrile in water [25]. Binding of a hydrophilic group to a polystyrene–divinylbenzene support enabled separation of solutes by either reversed-phase or normal-phase chromatography [26]. Alpert has introduced the term "hydrophilic interaction chromatography" [27] to describe the previous polar-bonded phase separations [17–26], as well as the separation of amino acids, cyclodipeptides, phosphorylated amino acids, dipeptides, 3-hydroxyl-2-nitropyridyl-β-maltooligoglycosides, and oligonucleotides on polyhydroxyethyl-aspartamide-bound silica columns.

Our objectives in this study were to determine whether commercially available size-exclusion columns could function as hydrophilic interaction columns, and if so, to separate glucooligosaccharides using gradient elution and pulsed amperometric detection.

EXPERIMENTAL

Materials

Durapore hydrophilic filters (0.22 μm, 47 mm) and the Protein-Pak 60 column were from Waters (Milford, MA, USA). The TSK-G 2000 SW column was from Phenomenex (Torrance, CA, USA) and the G-Oligo-PW column was from TosoHaas (Philadelphia, PA, USA). All monosaccharides, disaccharides, maltooligosaccharides and starch were purchased from Sigma (St. Louis, MO, USA). Sodium acetate (HPLC grade), acetonitrile (HPLC grade) and sodium hydroxide solution (50%, w/w) were obtained from Fisher Scientific (Houston, TX, USA). Monitrol level II sera were purchased from American Dade (Miami, FL, USA).

Chromatography

Apparatus. Chromatography was performed on a Waters 860 system; the host computer was a MicroVAX 2000 which employed the VMS operating system. DECnet software enabled multisystem networking via Ethernet connections. Connections were made to the Ethernet via a DEC transceiver, which was connected in turn to the Laboratory Acquisition and Communications/Enviroment (LAC/E) Module. Communication with the chromatography instruments was accomplished by IEEE interface (direct or via System Interface Module).

Isocratic separations. Three high-performance size-exclusion chromatography (HPSEC) columns were used to separate standard monosaccharides, disaccharides, and maltooligosaccharides: the Waters Protein-Pak 60 column (300 mm × 7.9 mm I.D., 10 μm), the Phenomenex TSK-G 2000 SW (300 mm × 7.6 mm I.D., 10 μm), and the TosoHaas G-Oligo-PW column (300 mm × 7.8 mm I.D., 6 μm). Samples (50μl) were injected by a Waters Model 710 WISP autoinjector; two Waters Model 510 pumps produced isocratic mobile phases which eluted the solutes at a flow rate of 1.0 ml/min. Solvents were sparged with helium and maintained in a helium atmosphere during all separations. Post-column eluate was delivered into a 3-way PTFE mixing tee and mixed with 0.5 *M* sodium hydroxide, which was delivered at a flow rate of 0.4 ml/min; helium, at 50 p.s.i., was used to deliver the sodium hydroxide solution to the mixing tee. After the eluate was mixed with sodium hydroxide, the peaks were detected with a Dionex pulsed amperometric detection (PAD) system (Sunnyvale, CA, USA). The potentials and time periods were set as follows: E1 was 0.05 V, E2 was 0.6 V, E3 was −0.6 V, T1 was 480 ms, T2 was 120 ms, and T3 was 60 ms. The sensitivity of the pulsed amperometric detector was set at 30 μA unless otherwise specified.

Determination of capacity factors. Separate stock solutions of α-D-glucose (DP 1; DP = degree of polymerization), maltose (DP 2), maltotriose (DP 3), maltotetraose (DP 4), maltopentaose (DP 5), maltohexaose (DP 6) and maltoheptaose (DP 7) were prepared at a concentration of 1.0 mg/ml, then diluted 1:9 with Milli-Q water (Millipore, Bedford, MA, USA). To determine the capacity factors of DP 1 through DP 7 on all three columns, 50 μl containing 5.0 μg of each individual standard was in-

jected and eluted isocratically; the mobile phase compositions were 0, 10, 20, 30, 40, 50, 55, 60, 65, 70 and 75% (v/v) acetonitrile in water.

Solutions of N-acetylneuraminic acid, α-L-rhamnose, α-L-fucose, D(+)-xylose, D(−)-arabinose, β-D-fructose, D(+)-mannose, α-D-glucose, D(+)-galactosamine, D(+)-glucosamine, D(+)-galactose, sucrose, lactulose, maltose and lactose were prepared at a concentration of 1.0 mg/ml, then diluted 1:9 with Milli-Q water. A 50-μl volume of each individual standard was chromatographed separately on both the Protein-Pak 60 and G-Oligo-PW columns. An isocratic mobile phase consisting of 75% acetonitrile in water, at a flow-rate of 1.0 ml/min, was used to elute the mono- and disaccharides.

Chromatography of maltooligosaccharide mixtures. A mixture of maltooligosaccharides (DP 1 through DP 10) was run on the three columns, with gradient elution; DP 1, DP 2 and DP 3 were each mixed to a final concentration of 0.25 mg/ml, and a standard mixture of DP 4 to DP 10 (powder) was mixed to a final concentration of 2.5 mg/ml. A 50-μl injection containing 12.5 μg each of DP 1, DP 2, DP 3, and 125 μg (total) of DP 4 through DP 10 was made on to each column. The gradient program for the separation on the Protein-Pak 60 column was 70% (v/v) acetonitrile in water for 5.0 min, a linear gradient to 50% in 30 min, held at 50% for 20 min. For the TSK-G 2000 SW column, the gradient program was 70% (v/v) acetonitrile in water for 15 min, a linear gradient to 65% in 15 min, a linear gradient to 50% in 30 min, held at 50% for 20 min. The gradient program for the separation of the maltooligosaccharides on the G-Oligo-PW column was identical to that used for the Protein-Pak 60 column, except that the final condition was held at 50% for 50 min.

Separation of selected monosaccharides and glucose polymers. The Protein-Pak 60 column was used to separate a commercially available mixture of glucose polymers (Polycose) to which were added selected monosaccharides; 100 μg of N-acetylneuraminic acid, 25 μg of rhamnose, 25 μg of arabinose and 7.0 mg of Polycose were dissolved in Milli-Q water to final concentrations of 0.12, 0.03, 0.03 and 8.23 mg/ml, respectively. The column was injected with 50 μl containing 1.45 μg each of rhamnose and arabinose, 5.85 μg N-acetylneuraminic acid and 411 μg Polycose, and the solutes were separated by gradient elution. The gradient program was 70% (v/v) acetonitrile in water for 10.0 min, a linear gradient to 50% in 30 min, held at 50% for 20 min.

To determine whether the separation was reproducible, eight samples of the Polycose and monosaccharide mixture were run consecutively on the Protein-Pak 60 column on each of two separate days; the within-run and between-run precision of the retention times of the monosaccharides and oligosaccharides were determined. Eighty min after injection, the column was allowed to equilibrate for 20 min at starting conditions, *i.e.*, 70% acetonitrile.

To demonstrate the sensitivity of detection and to optimize the separation, 10 μl containing 0.8 μg each of rhamnose and arabinose, 3.33 μg of N-acetylneuraminic acid and 33.3 μg of Polycose were injected on to the Protein-Pak 60 column. The gradient program consisted of 70% (v/v) acetonitrile for 1.0 min, a linear gradient to 50% for 39 min, held at 50% for 20 min.

Separation of starch hydrolysates. In one set of experiments, 0.9 ml of a 2.0 g/100 ml solution of starch was mixed with 0.1 ml of Monitrol level 2 serum containing 500 U/ml of α-amylase. The mixtures were allowed to incubate at 37°C for 4.0 h; at 1.0, 2.0, 3.0, and 4.0 h, the tubes were heated at 100°C for 2.0 min, then 50 μl containing 450 μg of hydrolysate was injected on to the Protein-Pak 60 column. The enzyme control consisted of adding 0.1 ml of Monitrol serum to 0.9 ml of water, while the substrate control consisted of adding 0.1 ml water to 0.9 ml of starch solution. The enzyme and substrate controls were incubated in the same manner as were the enzyme–substrate mixtures. The controls and incubation mixtures were separated by gradient elution. The gradient program was 70% (v/v) acetonitrile for 1.0 min, a linear gradient to 50% for 49 min, held at 50% for 20 min. The column was then equilibrated for 20 min with 70% (v/v) acetonitrile before the next injection.

In a separate set of experiments, 0.1 ml of Monitrol serum was added to 0.1, 0.2, 0.3, 0.4, 0.5, 0.6, 0.7, 0.8 and 0.9 ml of a 1.0 g/ml solution of starch. Water was added to each solution to bring the volume to 1.0 ml. The solutions were incubated at ambient temperature for 16.0 h, then heated at 100°C for 2.0 min. A 50-μl volume was injected and separated by the gradient used for the starch hydrolysates.

RESULTS

The isocratic elution of maltooligosaccharides DP 1 through DP 7, with water as the mobile phase, are depicted for the Protein-Pak 60 (Fig. 1a), TSK-G 2000 SW (Fig. 1c), and the G-Oligo-PW (Fig. 1e) columns. Neither the Protein-Pak 60 nor the TSK-G 2000 SW columns resolved these oligomers by size exclusion. The G-Oligo-PW column, however, did give some resolution; the maltooligosaccharides DP 7, DP 6 and DP 5 eluted at 7.75 min, DP 4 at 7.96 min, DP 3 at 8.34 min, DP 2 at 8.82 min and DP 1 at 9.48 min. Although the Protein-Pak 60 and TSK-G 2000 SW columns did not resolve the components in the mixture under these conditions, chromatography of individual standards demonstrated that the maltooligosaccharides were separated by size exclusion, *i.e.*, they were eluted in descending size order from DP 7 through DP 1.

Chromatography of the maltooligosaccharides using a mobile phase composition of 65% (v/v) acetonitrile in water is shown for the Protein-Pak 60 (Fig. 1b), TSK-G 2000 SW (Fig. 1d) and G-Oligo-PW columns (Fig. 1f). All three columns exhibited retention behavior opposite to that observed for the

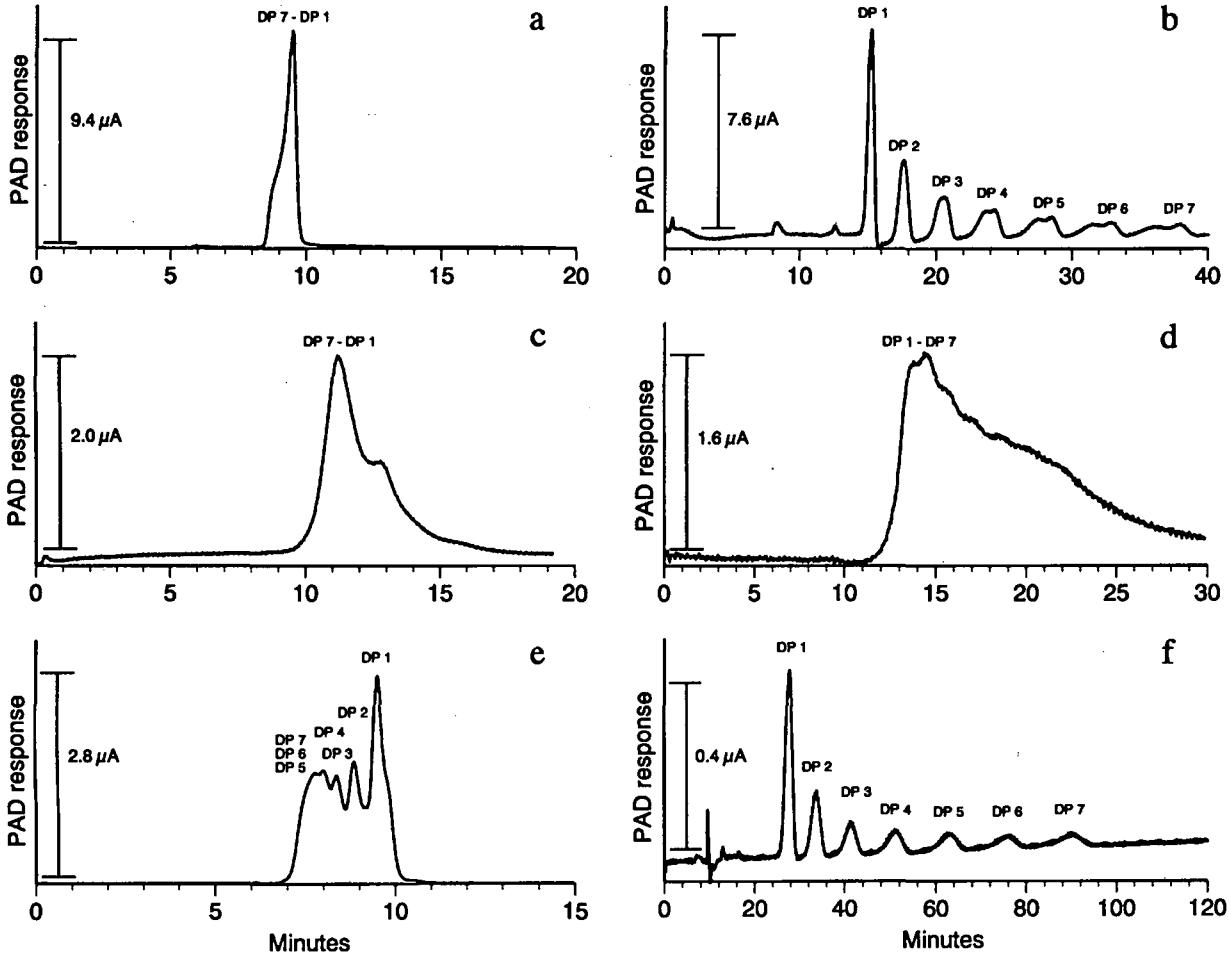

Fig. 1. Chromatography of glucose (DP 1) and maltooligosaccharides (DP 2 through DP 7) on HPSEC columns: using water as the mobile phase, the chromatography of DP 1 through DP 7 on the Protein-Pak 60 (a), TSK-G 2000 SW (c) and G-Oligo-PW (e) columns; using 65% (v/v) acetonitrile in water as the mobile phase, the partition chromatography of DP 1 through DP 7 on the Protein-Pak 60 (b), TSK-G 2000 SW (d), and G-Oligo-PW (f) columns.

size-exclusion separations; the order of elution was reversed. When the maltooligosaccharides were separated on the Protein-Pak 60 column under these conditions (Fig. 1b), their retention times were 15.1 (DP 1), 17.6 (DP 2), 20.6 (DP 3), 24.2 (DP 4), 28.4 (DP 5), 32.8 (DP 6) and 37.9 min (DP 7). In addition, DP 4 through DP 7 were separated into α and β anomers. The TSK-G 2000 SW column (Fig. 1d) was unable to resolve the mixture, even though the maltooligosaccharides were retained and eluted in the order observed for the Protein-Pak 60 column. The maltooligosaccharides were separated in the same order on the G-Oligo-PW column (Fig. 1f) as on the Protein-Pak 60 column; they were retained, however, to a greater degree. The retention times were 27.7 (DP 1), 33.8 (DP 2), 41.3 (DP 3), 51.0 (DP 4), 63.0 (DP 5), 75.6 (DP 6), and 90.0 min (DP 7).

Table I lists the capacity factor (k') values for the maltooligosaccharides DP 1 through DP 7 after elution from the three columns using mobile phase compositions where the percentage (v/v) of acetonitrile in water was 0, 10, 20, 30, 40, 50, 55, 60, 65, 70 and 75, respectively. For all three columns, chromatography with mobile phase compositions consisting of 0 to 40% (v/v) acetonitrile produced k' values for the retention of DP 1 to DP 7 that were inversely proportional to chain length at each composition, *i.e.* the k' values decreased as chain length increased (size exclusion). Conversely, at acetonitrile concentrations from 50 to 75% (v/v) the k' values at each concentration were proportional to

TABLE I

THE EFFECT OF MOBILE PHASE COMPOSITION ON THE RETENTION OF MALTOOLIGOSACCHARIDES DP 1 THROUGH DP 7 ON THE PROTEIN-PAK 60, TSK-G 2000 SW AND G-OLIGO-PW COLUMNS

	Capacity factor										
	Acetonitrile in Milli-Q water (%, v/v)										
	0	10	20	30	40	50	55	60	65	70	75
Protein-Pak 60											
DP 1	0.59	0.62	0.62	0.64	0.71	0.88	1.03	1.18	1.52	1.98	2.65
DP 2	0.56	0.60	0.60	0.61	0.70	0.92	1.13	1.37	1.93	2.76	4.15
DP 3	0.53	0.56	0.58	0.59	0.69	0.96	1.23	1.60	2.43	3.80	6.43
DP 4	0.51	0.53	0.55	0.58	0.68	0.99	1.37	1.80	3.03	5.20	9.82
DP 5	0.49	0.51	0.54	0.57	0.66	1.02	1.50	2.05	3.73	6.93	14.6
DP 6	0.48	0.50	0.52	0.56	0.65	1.06	1.62	2.20	4.46	8.93	21.3
DP 7	0.46	0.48	0.51	0.55	0.63	1.06	1.75	2.58	5.32	11.5	29.8
TSK-G 2000 SW											
DP 1	1.03	1.05	1.08	1.12	1.19	1.31	1.79	1.74	2.06	2.54	2.94
DP 2	1.03	1.05	1.07	1.12	1.17	1.32	1.87	1.70	2.15	2.86	3.77
DP 3	1.01	1.04	1.06	1.11	1.17	1.34	1.97	1.86	2.41	3.53	5.08
DP 4	0.99	1.01	1.05	1.10	1.17	1.36	2.03	2.04	2.76	4.34	6.96
DP 5	0.98	1.00	1.03	1.09	1.16	1.39	2.13	2.19	3.08	5.32	9.45
DP 6	0.97	1.00	1.03	1.08	1.16	1.41	2.19	2.42	3.54	6.33	12.2
DP 7	0.96	1.00	1.02	1.08	1.16	1.41	2.24	2.62	3.72	7.49	16.0
G-Oligo-PW											
DP 1	1.01	1.07	1.15	1.29	1.65	2.28	2.87	3.67	4.91	7.08	11.0
DP 2	0.87	0.93	0.99	1.11	1.50	2.30	3.06	4.26	6.30	10.2	18.8
DP 3	0.74	0.82	0.88	0.95	1.40	2.34	3.32	4.91	8.01	14.8	32.3
DP 4	0.68	0.74	0.80	0.87	1.31	2.41	3.59	5.78	10.3	21.1	54.8
DP 5	0.63	0.67	0.73	0.83	1.23	2.49	3.93	6.72	13.0	29.9	89.3
DP 6	0.60	0.63	0.66	0.79	1.16	2.55	4.24	7.65	15.9	40.5	117
DP 7	0.57	0.59	0.63	0.75	1.10	2.64	4.62	8.72	18.9	54.4	142

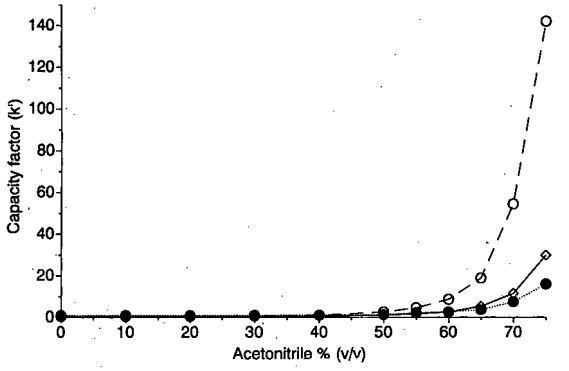

Fig. 2. The effect of mobile phase composition on the retention of maltooligosaccharide DP 7 on HPSEC columns. Maltoheptaose (DP 7) was applied to and eluted from the G-Oligo-PW (○), Protein-Pak 60 (◇) and the TSK-G 2000 SW (●) columns; isocratic mobile phase compositions consisting of 0, 10, 20, 30, 40, 50, 55, 60, 65, 70 and 75% (v/v) acetonitrile in water were used for elution on each column.

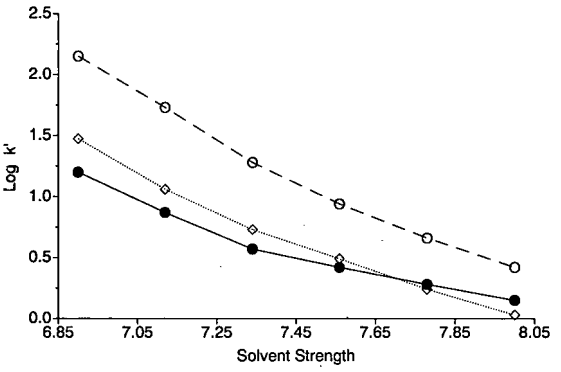

Fig. 4. The effect of solvent strength on the retention of oligosaccharide DP 7 when chromatographed by partition on HPSEC columns. DP 7 was eluted from the G-Oligo-PW (○), Protein-Pak 60 (◇), and TSK-G 2000 SW (●) columns using mobile phase compositions of 50, 55, 60, 65, 70 and 75% (v/v) acetonitrile in water.

chain length, *i.e.*, the k' values increased for the retention of DP 1 to DP 7.

Fig. 2 further illustrates the trend that occurred for all three columns; at 50% (v/v) acetonitrile, the k' values began to increase and continued to do so for concentrations of 60, 65, 70 and 75% (v/v). The only difference among the three columns was the degree of interaction at each concentration. The G-Oligo-PW column exhibited stronger interaction with the oligosaccharide at all solvent compositions than did the Protein-Pak 60 column; in turn, the Protein-Pak 60 column exhibited a greater interaction than did the TSK-G 2000 SW column.

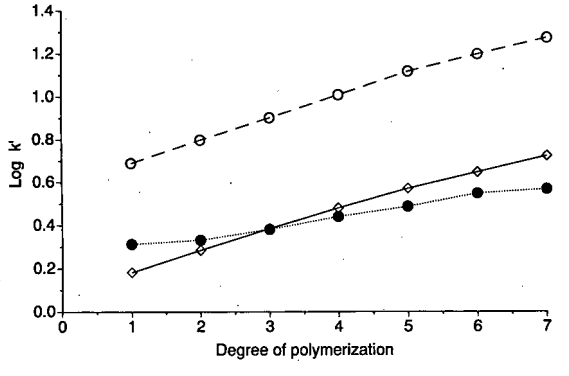

Fig. 3. The effect of the degree of polymerization of maltooligosaccharides on their retention when chromatographed by partition on HPSEC columns. Using a mobile phase composition of 65% (v/v) acetonitrile in water, DP 1 through DP 7 were applied to and eluted from the G-Oligo-PW (○), Protein-Pak 60 (◇), and TSK-G 2000 SW (●) columns..

For all three columns, when maltooligosaccharides DP 1 through DP 7 were eluted with a mobile phase composition of 65% (v/v) acetonitrile (Fig. 3), a linear relationship existed between the degree of polymerization of the maltooligosaccharide and log k'. The correlation coefficient (R^2) values were 0.998 for the G-Oligo-PW, 0.998 for the Protein-Pak 60, and 0.993 for the TSK-G 2000 SW columns. Chromatography of DP 1 through DP 7 on the G-Oligo-PW, Protein-Pak 60, and TSK-G 2000 SW columns at acetonitrile concentrations of 50, 55, 60, 65, 70 and 75% (v/v) produced a negative linear relationship ($R^2 > -0.973$, $p < 0.001$, for DP 1 to DP 7) between log k' and solvent strength (Fig. 4). The total solvent strength, S_T, for each mixture of acetonitrile and water was calculated using the following equation (28): $S_T = \Sigma_i S_i -_i$, where S_i is the solvent weighting factor and $-_i$ is the volume fraction of solvent in the mixture. The weighting factor was 10.2 for water and 5.8 for acetonitrile [28]. Increasing the polarity of the mobile phase resulted in decreased retention of all maltooligosaccharides on all three columns.

A maltooligosaccharide mixture comprised of DP 1 to DP 10 was separated by gradient elution on the Protein-Pak 60, TSK-G 2000 SW and G-Oligo-PW columns (Fig. 5). The separation of the mixture

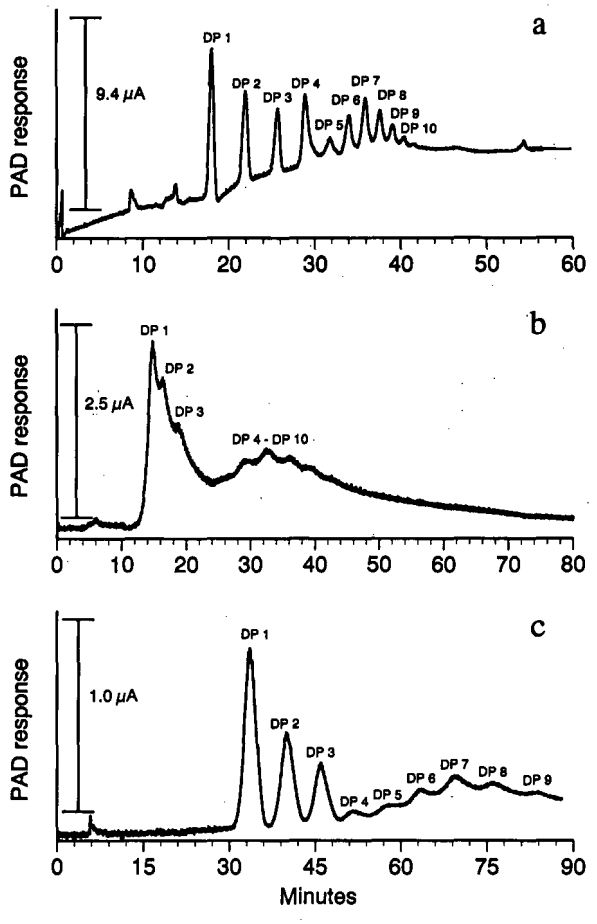

Fig. 5. Chromatography of standard maltooligosaccharides DP 1 through DP 10 on HPSEC columns by gradient elution: Protein-Pak 60 column (a), TSK-G 2000 SW column (b) and G-Oligo-PW column (c).

on the Protein-Pak 60 column was complete in 40 min; all peaks were resolved, and peak widths were narrow. The components were not resolved, however, on the TSK-G 2000 SW column, even when a shallow gradient was used for separation of the mixture. When the mixture was run on the G-Oligo-PW column, DP 1 through DP 9 were fractionated within 90 min; peak widths were wide, and DP 10 was not, therefore, observed.

Mono- and disaccharides exhibited similar retention behavior on the Protein-Pak 60 and G-Oligo-PW columns; however, differences did occur (Table II). Like the maltooligosaccharides, monosaccharides were retained longer on the G-Oligo-PW column than on the Protein-Pak 60 column. On the Protein-Pak 60 column, glucose and galactosamine were eluted at 18.1, glucosamine at 18.3 and galactose at 18.6 min; chromatography on the G-Oligo-PW column resulted in the early elution (after N-acetylneuraminic acid) of galactosamine (8.95 min) and glucosamine (9.49 min). On the Protein-Pak 60 column, glucose was eluted before galactose, and sucrose before lactulose; the converse occurred on the G-Oligo-PW column, *i.e.*, galactose was eluted before glucose, and lactulose before sucrose. Although there were differences in retention times, neither the Protein-Pak 60 nor the G-Oligo-PW column was suitable for the complete separation of all the mono- and disaccharides that were examined.

TABLE II

RETENTION TIMES (t_R) OF MONO- AND DISACCHARIDES SEPARATED ON THE PROTEIN-PAK 60 AND G-OLIGO-PW COLUMNS WITH A MOBILE PHASE COMPOSITION OF 75% (v/v) ACETONITRILE IN WATER

Solute	t_R (min)	
	Protein-Pak 60	G-Oligo-PW
N-acetylneuraminic acid	6.50	5.62
α-L-Rhamnose	14.4	23.1
α-L-Fucose	15.5	24.9
D(+)-Xylose	15.8	29.3
D(−)-Arabinose	16.3	29.2
β-D-Fructose	16.8	31.4
D(+)-Mannose	17.1	33.7
α-D-Glucose	18.1	38.2
D(+)-Galactosamine	18.1	8.95
D(+)-Glucosamine	18.3	9.49
D(+)-Galactose	18.6	37.7
Sucrose	21.2	45.7
Lactulose	22.1	43.6
Maltose	22.7	52.8
Lactose	23.5	52.8

A mixture of N-acetylneuraminic acid, rhamnose, arabinose and the glucose polymer mixture Polycose, was separated by gradient elution on the Protein-Pak 60 column (Fig. 6); Table III lists the retention times and identities of the peaks depicted in Fig. 6. The within-run precision (relative standard deviation, R.S.D., $n = 8$) of the retention times for the separation of the glucose polymer and monosaccharide mixture consisted of values from 0 to 0.26%; the between-run precision ($n = 16$) of the

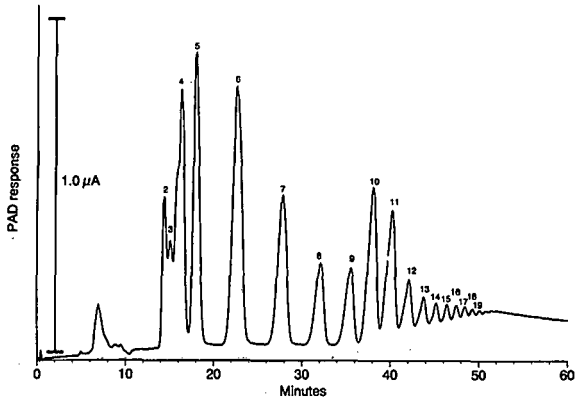

Fig. 6. The separation of selected monosaccharides and a commercial glucose polymer mixture by gradient elution on the Protein-Pak 60 column. The identity and retention times of the peaks are given in Table III.

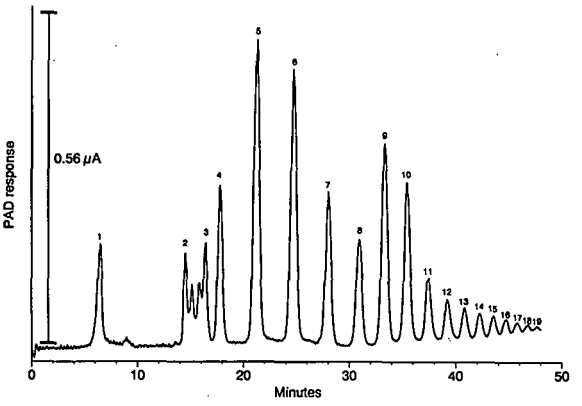

Fig. 7. Optimized gradient elution and detection of glucose polymers. The pulsed amperometric detector was in this case set at 1.0 μA full scale. The identity and retention times of the peaks are given in Table III.

retention times had values from 0.09 to 0.46% for 19 of the components and 0.64% for N-acetylneuraminic acid.

Fig. 7 depicts the optimized separation of the glucose polymer and monosaccharide mixture. The detector was set at 1.0 μA; the recorder at 0.56 μA.

TABLE III

WITHIN- AND BETWEEN-RUN PRECISION OF RETENTION TIMES FOR THE GRADIENT ELUTION SEPARATION OF SELECTED MONOSACCHARIDES AND GLUCOSE POLYMERS (Gp) ON THE PROTEIN-PAK 60 COLUMN

Peak No.	Solute	t_R			
		Within-run		Between-run	
		Mean ± S.D. (min)	R.S.D. (%)	Mean ± S.D. (min)	R.S.D. (%)
1	N-Acetylneuraminic acid	6.90 ± 0	0	6.92 ± 0.04	0.64
2	Rhamnose	14.4 ± 0.03	0.24	14.4 ± 0.03	0.24
3	Arabinose	16.3 ± 0.03	0.22	16.3 ± 0.05	0.31
4	DP 1	18.0 ± 0.05	0.26	18.0 ± 0.08	0.43
5	DP 2	22.5 ± 0.05	0.23	22.6 ± 0.10	0.46
6	DP 3	27.8 ± 0.07	0.25	27.8 ± 0.10	0.37
7	DP 4	32.0 ± 0.06	0.20	32.0 ± 0.10	0.30
8	DP 5	35.4 ± 0.05	0.15	35.5 ± 0.08	0.23
9	DP 6	38.0 ± 0.05	0.14	38.1 ± 0.08	0.20
10	DP 7	40.2 ± 0.04	0.09	40.2 ± 0.06	0.15
11	DP 8	42.0 ± 0.05	0.12	42.1 ± 0.08	0.18
12	DP 9	43.7 ± 0.04	0.08	43.7 ± 0.06	0.14
13	DP 10	45.1 ± 0.03	0.08	45.1 ± 0.06	0.14
14	Gp peak 11	46.3 ± 0.06	0.14	46.3 ± 0.06	0.14
15	Gp peak 12	47.4 ± 0.04	0.10	47.4 ± 0.04	0.13
16	Gp peak 13	48.3 ± 0.04	0.10	48.4 ± 0.07	0.15
17	Gp peak 14	49.2 ± 0.05	0.09	49.2 ± 0.05	0.09
18	Gp peak 15	50.0 ± 0.00	0.00	50.0 ± 0.06	0.12
19	Gp peak 16	50.7 ± 0.05	0.10	50.7 ± 0.07	0.14

The separation of rhamnose, arabinose, N-acetylneuraminic acid and Polycose was conducted by using a more shallow gradient than was used for the separations depicted in Figs. 5a and 6. Detector response increases in proportion to the% (v/v) of water in the mobile phase, and the decreased rate of

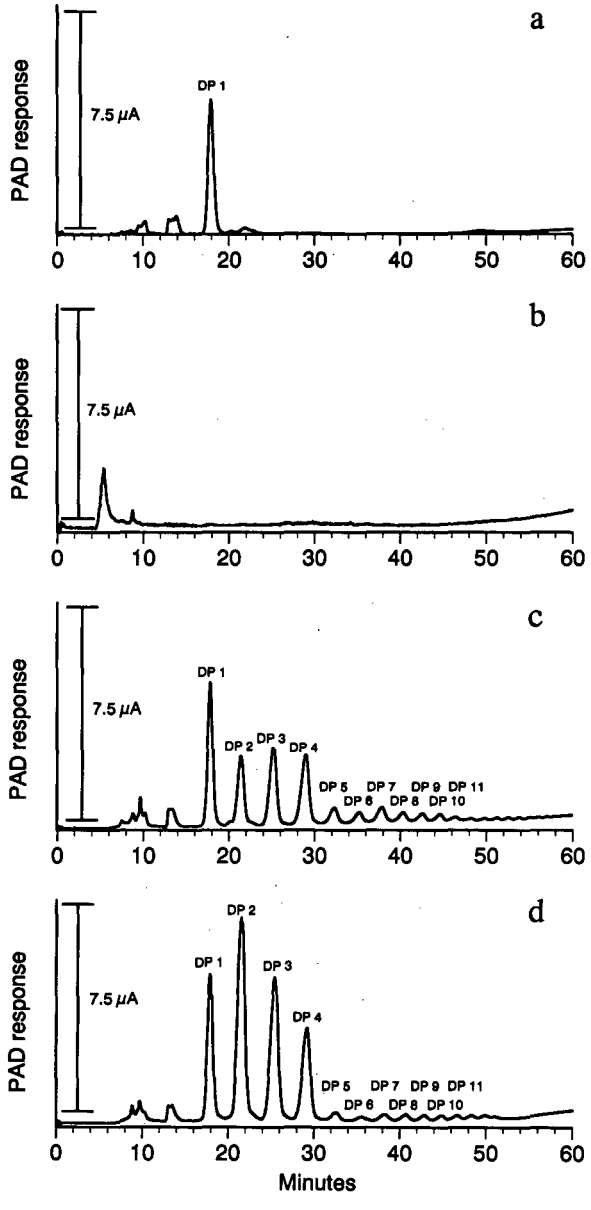

Fig. 8. The gradient elution chromatography of sera, starch and starch hydrolysates after incubation at 37°C. Monitrol serum (a), starch (b), starch hydrolysate (450 μg) after 1 h at 37°C (c) and starch hydrolysate (450 μg) after 4 h at 37°C (d) were injected after the treatment and eluted using the gradient conditions described in the Experimental section.

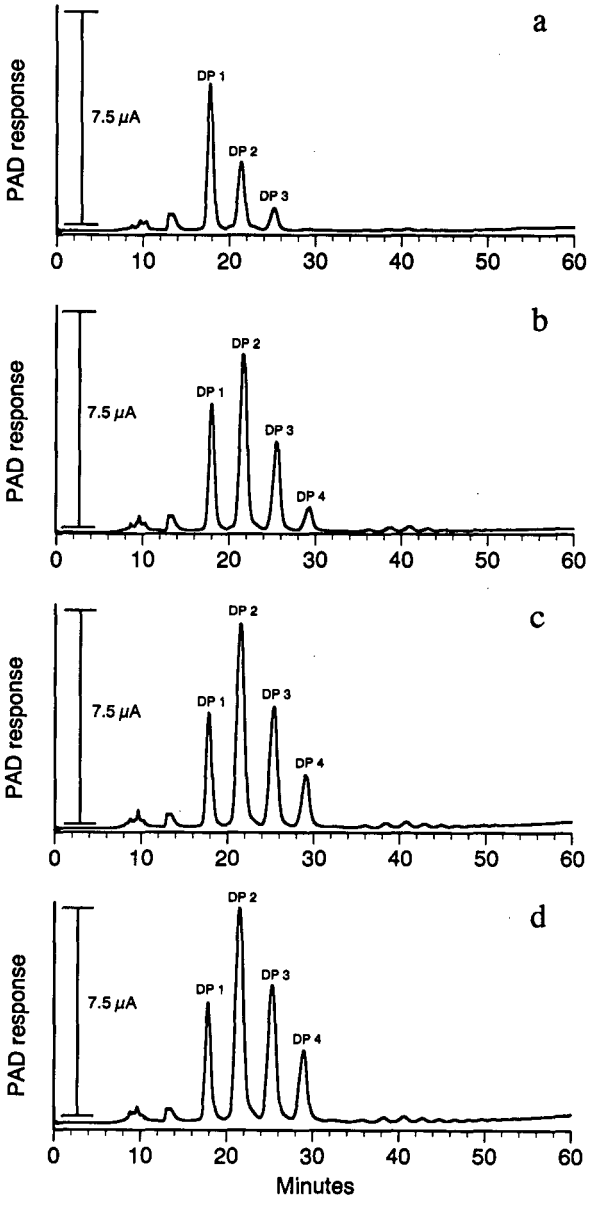

Fig. 9. The gradient elution chromatography of the products of starch digestion using different enzyme:substrate ratios. The chromatography of starch hydrolysates using enzyme:substrate ratios of (a) 1:1, (b) 1:4, (c) 1:7 and (d) 1:9 was performed after the treatment and by the gradient conditions described in the Experimental section. Starch hydrolysate was injected in amounts of 50 μg (a), 200 μg (b), 350 μg (c) and 450 μg (d).

water delivery resulted in a slower and more steady rise in the baseline than was observed in Figs. 5a and 6.

When starch was hydrolyzed with serum that contained α- and β-amylase, oligosaccharides were produced. The chromatographic separations are depicted in Fig. 8. Monitrol serum contains glucose, which was eluted at 18.1 min (Fig. 8a); all other solutes detected in the serum were eluted before the glucose peak. Fig. 8b represents the nonhydrolyzed starch that was eluted in the void volume. The chromatograms in Fig. 8c and 8d represent the products of starch hydrolysis after 1 and 4 h at 37°C, respectively; the degree of hydrolysis can be easily visualized and shows that, under these conditions, maltose was the major product of hydrolysis. Altering the enzyme:substrate ratio to values of 1:1. 1:4, 1:7, and 1:9 and incubating at ambient temperature for 16 h produced the maltooligosaccharide patterns depicted in Fig. 9. Increasing the amount of substrate resulted in the increased formation of DP 2, DP 3 and DP 4.

DISCUSSION

The Protein-Pak 60 column is a diol-bound silica support, the TSK-G 2000 SW column has hydrophilic groups bound to a silica support and the G-Oligo-PW column has hydrophilic groups bound to a polymeric support. With mobile phases containing from 0 to 40% (v/v) acetonitrile in water, maltooligosaccharides were fractionated by size exclusion on all three columns (Fig. 1a, c, e). Chromatography of the maltooligosaccharides with mobile phases containing from 50 to 75% (v/v) acetonitrile in water resulted in retention on the column and a reversal of the order of elution (Fig. 1b, d, e); at 50% (v/v) acetonitrile in water, all three size-exclusion columns became hydrophilic interaction columns.

Studies on the mechanism of retention of carbohydrates to amine-bonded silica supports, using mobile phases containing from 60 to 90% (v/v) acetonitrile in water, have demonstrated that as the percentage of acetonitrile in the mobile phase increases, the proportion of water bound to the support relative to that in the mobile phase increases [19,22]; as the amount of water bound to the column increases, the k' value of various mono- and disaccharides increases, and separation results from the partitioning of the solutes between the two water phases.

At 50% (v/v) acetonitrile, all three columns, irrespective of support or bonded phase, retained the oligosaccharides; the only difference at compositions above 50% (v/v) acetonitrile was the degree of interaction between the oligosaccharide and the support (Fig. 2, Table I). Because the hydrophilic group bonded to the polymeric support on the G-Oligo-PW column cannot be identified, it is difficult to determine whether the bonded group or the polymeric support is responsible for the higher k' values obtained for all of the oligosaccharides. However, neutral oligosaccharides separated on a hydroxylated polymeric support demonstrated the same trend as that observed for the G-Oligo-PW column, *i.e.*, very high k' values and broad peaks at higher acetonitrile concentrations [24]. It is possible, therefore, that the support on the G-Oligo-PW column contributes to the increase in k' values over those observed for either the TSK-G 2000 SW or Protein-Pak 60 columns.

Although data in the literature suggest that separation is due to partitioning of the carbohydrates between a static, adsorbed layer of water and the mobile phase [19,22], it is significant that all three columns retained the carbohydrates only when the concentration of acetonitrile was 50% (v/v) or greater. The amount of water bound to the three columns probably determined the value of k', *i.e.*, the degree of interaction, but the polarity of the carbohydrate and its relationship to the polarity of the mobile phase may have provided the driving force required for interaction with the adsorbed layer of water.

At concentrations $\geqslant 50\%$ (v/v) acetonitrile, a linear relationship existed between retention (k') and the degree of polymerization of the oligosaccharide; a representative example, using a mobile phase composition of 65% (v/v) acetonitrile, is given in Fig. 3. This linear relationship was observed with the separation of deoxymonosaccharides, monosaccharides, disaccharides, and myoinositol, after separation on an amine-bonded column [22]; retention was related to the number of hydroxyl groups that could bond to hydrogen and to the calculated hydration number of the molecule.

Hydrophilic interaction chromatography is simi-

lar to normal-phase chromatography in that retention on the column (k') increases as the polarity of the mobile phase decreases [27]. In normal-phase chromatography, a parameter called the solvent-strength weighting factor, S_i, can be used to describe the polarity of the mobile phase [28]. In our study, a linear relationship existed between the k' value of DP 7 and the solvent strength of the mobile phase used for the separation (Fig. 4); this relationship held for all three columns when DP 7 was eluted with mobile phases having acetonitrile concentrations from 50 to 75% (v/v). Increases in the solvent strength of the mobile phase resulted in decreases in the values of k' for the chromatography of DP 7 on all three columns.

Although all three columns were able to function as hydrophilic interaction columns, they exhibited different retention characteristics (Table I) and resolution capabilities (Fig. 5). Although the G-Oligo-PW column retained the oligosaccharides to a far greater degree than did the Protein-Pak 60 column, the resolution of DP 1 to DP 10 was much better on the Protein-Pak 60 column. The TSK-G 2000 SW column could not resolve the mixture even with a more shallow gradient. Gradient elution on the Protein-Pak 60 column (Fig. 5a) eliminated the separation of anomers that was seen when an isocratic mobile phase composed of 65% (v/v) acetonitrile was used in chromatography (Fig. 1b).

Both the Protein-Pak 60 and G-Oligo-PW columns were able to separate certain monosaccharides and to separate mono- from disaccharides, but neither column was suitable for the complete resolution of a mixture of mono- and disaccharides (Table II). Complete resolution did not occur even when 80% (v/v) acetonitrile was used; these columns were better suited to the separation of gluco-oligosaccharides, and the Protein-Pak 60 column gave the best resolution of the three columns tested. Twenty peaks were resolved by the Protein-Pak 60 column when a commercial glucose polymer mixture with added monosaccharides was applied. Although glucooligosaccharides with degrees of polymerization greater than 30 have been separated [16,21], the resolution of 20 peaks in this study was not a matter of separation capability, but probably a consequence of the composition of the starch-derived enzyme hydrolysate. Optimization of the gradient allowed the separation and detection of 33 μg of the Polycose mixture (Fig. 7). The peak widths were narrow and baseline resolution of the oligosaccharides occurred. The chromatography was also applied to the analysis of enzyme-catalyzed starch hydrolysis products (Figs. 8 and 9), and it enables one to see the effect of different conditions on the enzymatic hydrolysis of starch.

A significant feature of the gradient elution is its high degree of reproducibility (Table III); the column was equilibrated with 1.4 column volumes of starting mobile phase before each injection, and the between-run precision (n = 16, 2 days) for the retention times of 18 peaks was less than 0.47% (R.S.D.).

The columns used in this study are polar-bonded supports that can be used either as size-exclusion or hydrophilic interaction columns. Of the three columns used, the Protein-Pak 60 column enabled superior resolution and reproducibility in the separation of glucose polymers. Pulsed amperometric detection allowed gradient elution and sensitive detection. The separations demonstrate the versatility and potential of hydrophilic interaction chromatography.

ACKNOWLEDGEMENTS

We would like to thank Jerry Eastman for his editorial assistance and Adam Gillum for producing the figures.

This work is a publication of the USDA/ARS Children's Nutrition Research Center, Department of Pediatrics, Baylor College of Medicine, Houston, TX. This project has been funded in part with federal funds from the US Department of Agriculture, Agricultural Research Service under Cooperative Agreement number 58-6250-1-003. The contents of this publication do not necessarily reflect the views or policies of the US Department of Agriculture, nor does mention of trade names, commercial products, or organizations imply endorsement from the US Government.

REFERENCES

1 S. A. Barker, B. W. Hatt, J. F. Kennedy and P. J. Somers, *Carbohydrate Res.*, 9 (1969) 327.
2 R. W. Goulding, *J. Chromatogr.*, 103 (1975) 229.
3 K. B. Hicks, P. C. Lim and M. J. Haas, *J. Chromatogr.*, 319 (1985) 159.

4 G. Bonn, *J. Chromatogr.*, 387 (1987) 393.
5 H. Derler, H. F. Hormeyer and G. Bonn, *J. Chromatogr.*, 440 (1988) 281.
6 K. B. Hicks and A. T. Hotchkiss, *J. Chromatogr.*, 441 (1988) 382.
7 N. W. H. Cheetham, P. Sirimanne and W. R. Day, *J. Chromatogr.*, 207 (1981) 439.
8 K. Koizumi and T. Utamura, *J. Chromatogr.*, 436 (1988) 328.
9 R. D. Rocklin and C. A. Pohl, *J. Liq. Chromatogr.*, 6 (1983) 1577.
10 D. C. Johnson and T. L. Polta, *Chromatogr. Forum*, 1 (1986) 37.
11 M. R. Hardy, R. R. Townsend and Y. C. Lee, *Anal. Biochem.*, 170 (1988) 54.
12 R. R. Townsend, M. R. Hardy, O. Hindsgual and Y. C. Lee, *Anal. Biochem.*, 174 (1988) 459.
13 L.-M. Chen, M.-G. Yet and M.-C. Shao, *FASEB J.*, 2 (1988) 2819.
14 M. R. Hardy and R. R. Townsend, *Proc. Natl. Acad. Sci. USA*, 85 (1988) 3289.
15 R. R. Townsend, M. R. Hardy, D. A. Cumming, J. P. Carver and B. Bendiak, *Anal. Biochem.*, 182 (1989) 1.
16 K. Koizumi, Y. Kubota, T. Tanimoto and Y. Okada, *J. Chromatogr.*, 464 (1989) 365.
17 J. C. Linden and C. L. Lawhead, *J. Chromatogr.*, 105 (1975) 125.
18 F. M. Rabel, A. G. Caputo and E. T. Butts, *J. Chromatogr.*, 126 (1976) 731.
19 L. A. Th. Verhaar and B. F. M. Kuster, *J. Chromatogr.*, 234 (1982) 57.
20 C. Brons and C. Olieman, *J. Chromatogr.*, 259 (1983) 79.
21 K. Koizumi, T. Utamura and Y. Okada, *J. Chromatogr.*, 321 (1985) 145.
22 Z. L. Nikolov and P. J. Reilly, *J. Chromatogr.*, 325 (1985) 287.
23 M. Verzele and F. Van Damme, *J. Chromatogr.*, 362 (1986) 23.
24 B. Bendiak, J. Orr, I. Brockhausen, G. Vella and C. Phoebe, *Anal. Biochem.*, 175 (1988) 96.
25 V. Carunchio, A. M. Girelli and A. Messina, *Chromatographia*, B23 (1987) 731.
26 Y.-B. Yang and M. Verzele, *J. Chromatogr.*, 387 (1987) 197.
27 A. J. Alpert, *J. Chromatogr.*, 499 (1990) 177.
28 C. F. Poole and S. A. Schuette, *Contemporary Practice of Chromatography*, Elsevier, Amsterdam, New York, 1984, p. 260.

Journal of Chromatography, 607 (1992) 19–24
Elsevier Science Publishers B.V., Amsterdam

CHROM. 24 273

Rapid and sensitive anion-exchange high-performance liquid chromatographic determination of radiolabeled inositol phosphates and inositol trisphosphate isomers in cellular systems

Luan Tao and Weiye Li

Department of Ophthalmology, Hahnemann University, Broad and Vine Street, Philadelphia, PA 19102 (USA)

(First received November 27th, 1991; revised manuscript received April 9th, 1992)

ABSTRACT

A rapid and sensitive high-performance liquid chromatographic method for the determination of multiple inositol phosphates and inositol trisphosphate isomers was developed. The separation of inositol phosphates was optimized by controlling the ionic strength with stepped gradient programs and the pH of mobile phase. Six inositol phosphates were determined within 22 min or the six compounds plus an inositol trisphosphate isomer within 24 min using a single anion-exchange column containing the quaternary ammonium functional group. This technique was successfully applied to the determination of inositol phosphatide turnover by AlF_4^- stimulation in a small amount ($5 \cdot 10^5$–$1 \cdot 10^6$ cells) of cultured retinal capillary pericytes. Because of its efficiency, accuracy and applicability to the separation of inositol phosphates from biological samples, this method may be useful in signal transduction studies in cellular systems.

INTRODUCTION

Agonists activate phospholipase C which triggers the hydrolysis of phosphatidylinositol, phosphatidylinositol phosphate and phosphatidylinositol bisphosphate with the subsequent formation of 1,2-diacylglycerol and inositol phosphates, including inositol 1,4,5-triphosphate [1,2]. The six hydroxyl groups on the myoinositol ring can be substituted by phosphate groups, yielding multiple inositol phosphate species [3]. These inositol phosphates possess various physiological functions [3]. To study the metabolic pathways of inositol phosphates in cellular systems, a rapid and accurate method for the determination of these compounds in biological samples is required.

Correspondence to: Dr. Weiye Li, Department of Ophthalmology, Hahnemann University, Mail Stop 209, Broad and Vine Street, Philadelphia, PA 19102, USA.

However, most data on inositol phosphatide-mediated signal transduction have been generated either by the low-pressure, anion-exchange technique of Downes and Michell [4], or by a time-consuming anion-exchange high-performance liquid chromatographic (HPLC) method [5–7]. Taylor et al. [8] have recently developed a rapid HPLC method for determining radiolabeled inositol phosphates including inositol 1-phosphate (IP), inositol 1,4-bisphosphate (IP_2), inositol trisphosphate (both isomers) and inositol 1,3,4,5-tetrakisphosphate (IP_4) by using a Vydac nucleotide column. To our knowledge, no rapid assay for the determination of IP–inositol hexakisphosphate (IP_6) plus both inositol trisphosphate isomers has yet been reported.

The aim of this study was to develop an HPLC method that is not only rapid but also as comprehensive as the reported time-consuming anion-exchange HPLC method for determining IP–IP_6 plus both inositol triphosphate isomers in biological samples.

0021-9673/92/$05.00

EXPERIMENTAL

Reagents

Radiolabeled [^{3}H]myoinositol, IP, IP_2, inositol 1,3,4-trisphosphate [I(1,3,4)P_3, inositol 1,4,5-trisphosphate [I(1,4,5)P_3] IP_4 and IP_6 were obtained from New England Nuclear (Boston, MA, USA) Nucleotide standards (GMP, GDP and GTP) were obtained from Sigma (St. Louis, MO, USA). Ammonium phosphate, phosphoric acid and other HPLC-grade reagents were purchased from Fisher Scientific (Philadelphia, PA, USA).

Preparation of radiolabeled inositol 1,3,4,5,6-pentakisphosphate (IP_5) standard

The standard of radioactive IP_5 was prepared by the method of Menniti *et al.* [9]. Cultured retinal capillary pericytes (for culture conditions, see below) with a density of 10^7 cells per 100-mm petri dish were labeled with [^{3}H]myoinositol (20 μCi/ml) for 72 h in M199 medium supplemented with 10% dialyzed serum. Supernatants from trichloroacetic acid-stopped reactions were neutralized by the method of Shears *et al.* [10]. Inositol phosphates, including IP_5 in neutralized samples, were separated on an anion-exchange column (Whatman Partisil SAX 10, 5-μm particle size) according to the method of Balla *et al.* [11]. IP_5 was collected and diluted tenfold with H_2O prior to column calibration.

HPLC analysis

The HPLC system (Waters–Millipore) consists of two Model 501 pumps, a Model U6K injector, a Model 484 UV detector and Baseline 810 computer software. For detection of nucleotide standards the detector was set at 254 nm. All separations were performed with Bio-Gel TSK IC-Anion-PW (PW) and Bio-Gel TSK IC-Anion-SW (SW) columns (50 × 4.6 mm I.D.) (Bio-Rad Labs.), a Vydac nucleotide column (50 × 4.6 mm I.D.) (Rainin) and a Whatman Partisil SAX 10 column (250 × 4.6 mm I.D.), with a guard column (Waters Guard-Pak) precolumn module and IC-PAK anion concentrator).

Rapid separation of inositol phosphates with the PW, SW or Vydac column was carried out by using stepped gradients of 0–0.5 *M* ammonium phosphate and by adjusting the pH of the mobile phase with 85% phosphoric acid (optimum pH as indicated in Fig. 1). Elution was carried out at a flow-rate of 3 ml/min with 1.5 ml per fraction. At the designated pH for elution of each inositol phosphate the ionic strength used in the stepped gradient program was first predetermined using a continuous gradient from 0 to 0.5 *M* ammonium phosphate within 60 min (flow-rate 3 ml/min). Based on the values obtained, we then determined the proper ionic strength empirically (exact concentrations of ammonium phosphate as indicated in Fig. 1). The stepped gradients were programmed over the first 3.5-min period to elute myoinositol with H_2O, followed by a sharp increase in the concentration of ammonium phosphate to elute IP within the 3.5-min period during which IP_2 did not elute from the columns. In the subsequent stepped gradient program, for elution of individual inositol phosphates the period was reduced to 3 min instead of 3.5 min (the required ammonium phosphate concentrations for each inositol phosphate with the difference columns are indicated in the figure captions).

The separation of inositol trisphosphate isomers and other inositol phosphates with a single column was carried out with the same stepped gradient program with modification. After the elution of IP, the concentration of ammonium phosphate was sharply increased to a level at which an 8-min isocratic run was used to elute IP_2, I(1,3,4) P_3 and I(1,4,5) P_3. The ionic strength for this isocratic elution was empirically chosen to be slightly lower (3% lower for the Vydac column, 5% lower for the SW column) than the predetermined ionic strength for IP_2 elution (see above). Subsequently, the stepped gradient program was resumed to elute IP_4, IP_5 and IP_6 as described above.

The radioactivity of each fraction was determined with a liquid scintillation counter (Wallac 1410; Pharmacia–LKB), and the counting data were analysed by the Data Capture Program (Beckman software version 2.8503 B) to obtain each radioactive peak area.

Because inositol phosphates lack UV absorbance, the retention times of guanine mono-, bis- and trisphosphate, which are sufficiently close to inositol monophosphate, bisphosphate and trisphosphate, allow the calibration of these columns periodically.

Metabolic labeling, AlF_4^- stimulation and biological sample preparation

Bovine retinal capillary pericytes were isolated and cultured in six-well plates (final cell number $5 \cdot 10^5$ per well) [12] and 1.0 ml of [^{3}H]myoinositol (5 μCi/ml) was introduced into each well. The incubation lasted 48 h in M199 medium supplemented with 10% dialyzed fetal bovine serum; 10 m*M* LiCl (final concentration) was added and incubated for 30 min before 10 μM $AlCl_3$ and 30 m*M* NaF (final concentration) were introduced. The osmolarity was kept constant by adding NaCl to the control. Incubation (30 min) was terminated by taking out the labeling solution and rapidly washing three times with ice-cold Puck's solution, followed by adding 1.5 ml of ice-cold 15% trichloroacetic acid (TCA) to each well. After a 10-min extraction, the cells were scraped off and centrifuged at 16 000 *g* for 5 min. The supernatant solution was washed five times with water-saturated diethyl ether to remove TCA. The whole aqueous fraction (1.5 ml) was neutralized with ammonia solution prior to PW or Vydac column chromatography.

Precision and recovery

The recovery of radioactive inositol phosphates in cellular samples was determined by comparison with aqueous standard solutions [myoinositol 150 000, IP 80 000, IP_2 50 000, I(1,4,5)P_3 50 000, IP_4 30 000, IP_5 10 000, IP_6 30 000 cpm/ml]. The cellular samples were prepared by using scraped unlabeled cells which were extracted with TCA to a final volume of 1.5 ml, and 1.4 ml of this extract were spiked with 0.1 ml of aqueous standard solutions. A 0.1-ml volume of each aqueous standard was diluted with 1.4 ml of water and the standard solution with total volume of 1.5 ml was injected. The recovery was calculated from the peak-area ratios (cellular sample to aqueous standard solution).

The reproducibility was determined by injecting eight times 1.5 ml of water containing 0.1 ml of the aqueous standard of I(1,4,5)P_3 (50 00 cpm/ml).

RESULTS AND DISCUSSION

Chromatographic conditions

To study the cellular signal transduction which is mediated by inositol phosphatide turnover, handling of a large number of samples is usually required. Hence it is desirable to have a rapid and accurate assay to examine multiple inositol phosphates. Low-pressure chromatography with Dowex ion exchangers is rapid, whereas is not adequate for quantitative or accurate separation [8]. The reported anion-exchange HPLC methods are sensitive and comprehensive, but they are time consuming [5–7]. A recently reported HPLC assay is efficient, but it is unable to detect IP_5 and IP_6 [8]. We applied an HPLC method with any one of three quaternary ammonium anion-exchange columns under optimized chromatographic conditions to separate rapidly multiple inositol phosphates. Fig. 1 shows the chromatograms of standards of radioactive myoinositol and six inositol phosphates obtained with these three columns under optimum pH conditions. By using the stepped gradient program, very sharp elution profiles without carryover of radioactivity between two inositol phosphate peaks were achieved. As this program was designed to obtain a suitable ionic strength for eluting a specific inositol phosphate within a few seconds, each compound was completely eluted within 2 min. The total elution time was *ca.* 22 min including IP_5 and IP_6 elution (Fig. 1).

Fig. 2 shows the effect of pH on the ionic strength for eluting individual inositol phosphates. Because of their phosphate ester linkages, inositol phosphates are charged molecules in the pH range 2–7. Over the pH range 2.0–6.0, in view of these charged molecules from IP_2 to IP_6, the more phosphate residues there are on an inositol ring, the higher is the ionic strength required (Fig. 2). In addition, for elution of an individual inositol phosphate, the higher the pH the higher is the ionic strength of the mobile phase needed (Fig. 2). However, each column has a limit of both pH and ionic strength (indicated in the caption of Fig. 2). Under some conditions, the required high salt concentrations may exceed the limit. In a recent report [8], pH 2.7 of the mobile phase was used for the separation of inositol phosphates with a Vydac nucleotide column. The salt concentration for eluting IP_4 already reached the limit of this column. Under such circumstances it was impossible to separate IP_5 and IP_6 further. In contrast, by using the same column and the same range of molar concentration of salt, we selected a higher pH of the mobile phase (pH 4.0 or 6.0). With such a modification, both IP_5 and IP_6 were detected (Fig.

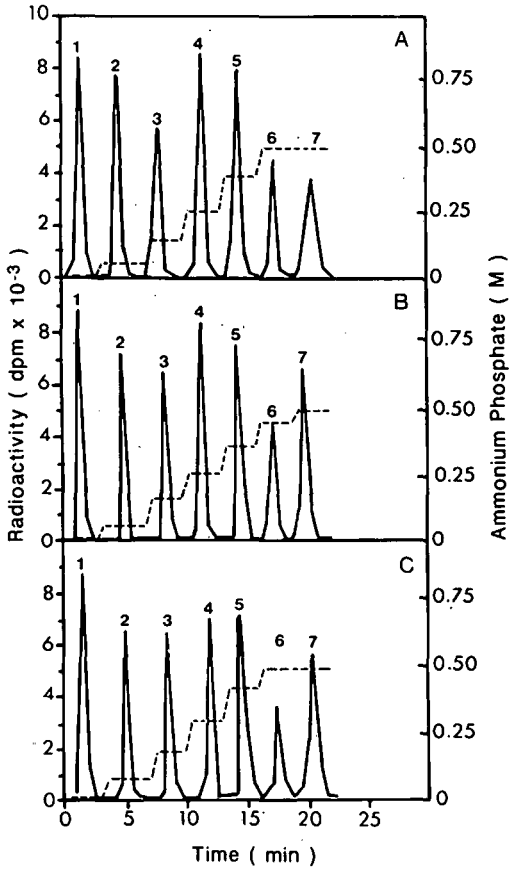

Fig. 1. Chromatogram of aqueous standards of radioactive myoinositol and six inositol phosphates by rapid anion-exchange HPLC. A mixture of labeled (1) myoinositol, (2) IP, (3) IP_2, (4) inositol trisphosphate, (5) IP_4, (6) IP_5 and (7) IP_6 was applied to and resolved by (A) the PW column (50 × 4.6 mm I.D.) (pH 1.0–12.0, maximum salt concentration 0.5 *M*), (B) the SW column (50 × 4.6 mm I.D.) (pH 2.0–8.0, maximum salt concentration 0.5 *M*) and (C) the Vydac column (50 × 4.6 mm I.D.) (pH 2.0–7.0, maximum salt concentration 0.5 *M*). The stepped gradient programs for eluting the six inositol phosphates with column A (pH 2.0), B (pH 2.5) or C (pH 4.0) are as follows: myoinositol, H_2O; IP, 0.060, 0.070, 0.085 *M*; IP_2, 0.150, 0.165, 0.190 *M*; inositol trisphosphate, 0.260, 0.265, 0.300 *M*; IP_4, 0.385, 0.370, 0.415 *M*; IP_5, 0.500, 0.455, 0.500 *M*; IP_6, 0.500, 0.500, 0.500 *M*.

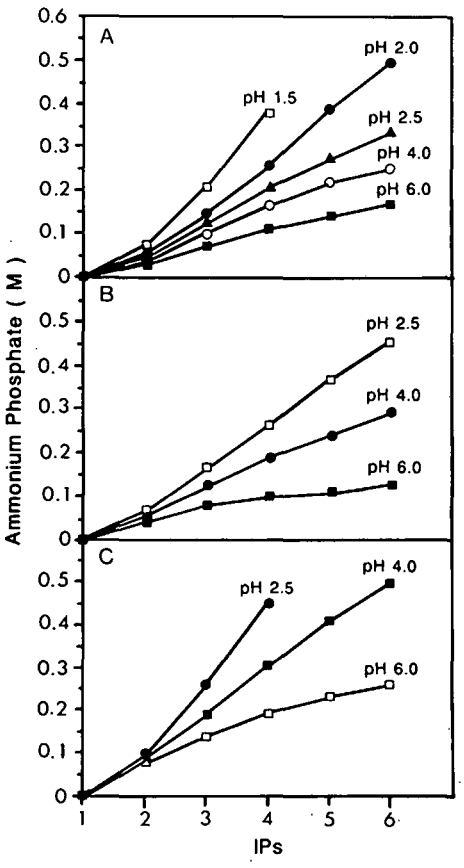

Fig. 2. Effect of pH on ionic strength required for eluting the six inositol phosphates using (A) the PW, (B) the SW and (C) the Vydac column. Compounds numbered on abscissa: 1 = IP; 2 = IP_2; 3 = inositol trisphosphate; 4 = IP_4; 5 = IP_5; 6 = IP_6.

1B). Moreover, because Taylor *et al.*'s study with pH 2.7 buffer [8] failed to elute IP_5 and IP_6, which intrinsically exist in mamalian cells [13,14], these radiolabeled polyphosphates which were retained and degraded in the columns might cause unpredictable radioactive contamination in the subsequent analytical process. Therefore, the use of eluents with pH higher than 2.7 in the Vydac column is recommended in order to avoid this pitfall.

To separate inositol trisphosphate isomers, the chromatographic conditions for the use of the three columns were also examined. Both the SW and Vydac columns were successfully used to separate I[1,3,4)P_3 and I(1,4,5)P_3 (Fig. 3). In order to identify these isomers, a stepped gradient program, with a rapid change of the ionic strength of the mobile phase, is not appropriate. Therefore, an isocratic run (0.165 *M* ammonium phosphate, pH 2.5 for the SW column; 0.175 *M* ammonium phosphate, pH 4.0 for the Vydac column) was inserted in the stepped gradient program after the elution of IP (Fig. 3). With a similar approach, we failed to differentiate I(1,4,5)P_3 and I(1,3,4)P_3 by the PW col-

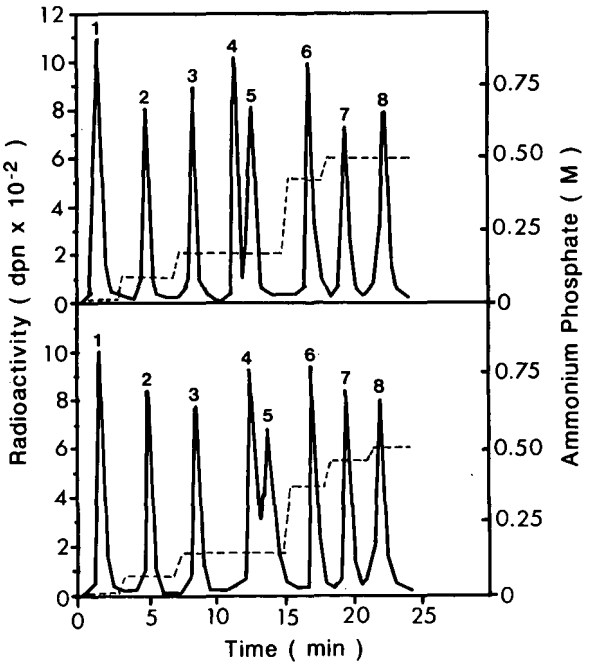

Fig. 3. Separation of radiolabeled I(1,3,4)P_3 and I(1,4,5)P_3 isomers together with myoinositol and five other inositol phosphates using (top) the Vydac column and (bottom) the SW column. Peaks: 1 = myoinositol; 2 = IP; 3 = IP_2; 4 = I(1,3,4)P_3; 5 = I(1,4,5)P_3; 6 = IP_4; 7 = IP_5; 8 = IP_6.

umn. It is possible that because of the much lower theoretical plate (TP) number (TP/column >900) for the PW column in comparison with the Vydac (TP/column >1200) and SW (TP/column >1400) columns, the limited resolution of the PW column was not able to differentiate subtle differences in isomer binding to the exchangers. Although a mobile phase of pH 4.0 was used with the Vydac column in this present study, the separation of I(1,4,5)P_3 and I(1,3,4)P_3 was similar to the results of Taylor *et al.* with an eluent of pH 2.7 [8].

Precision, recovery and detection limit

The reproducibility of the method for the detection of I(1,4,5)P_3 with three different columns resulted in a relative standard deviation of 6% for the PW, 7% for the SW and 9% for the Vydac column.

Recoveries of the six inositol phosphates for cellular media are shown in Table I, indicating high recoveries.

As large volumes (1.5 ml) can be injected on-column, a high sensitivity was achieved with this technique. At an injection volume of 1.5 ml, the method reveals a detection limit of six inositol phosphates and inositol trisphosphate isomers generated from 5 · 10^5 – 1 · 10^6 resting cells.

TABLE I

RECOVERY OF MYOINOSITOL AND SIX INOSITOL PHOSPHATES FROM CULTURED CELLULAR SAMPLES

Results are means of three determinations. The recovery of individual inositol phosphates from cellular samples was calculated as described in the Experimental section.

Column	Recovery of radiolabeled compound (%)						
	MI	IP	IP_2	Inositol trisphosphate	IP_4	IP_5	IP_6
PW	92.5	92.4	95.2	91.3	95.2	93.6	88.4
SW	94.1	97.1	94.0	89.6	95.4	91.7	92.6
Vydac	95.8	91.4	94.4	92.4	91.9	94.3	90.3

Applicability

To confirm the practical utility of the method in the analysis of biological samples, we applied it to the determination of six inositol phosphates in cultured retinal capillary pericytes (10^5 – 10^6 cells) treated with AlF_4^-, a non-specific activator of GTP-binding G proteins [15]. The inositol phosphate profiles of metabolically labeled pericytes treated with or without AlF_4^- are compared in Fig. 4. The results showed a great stimulatory effect of AlF_4^- on IP, IP_2, inositol trisphosphate and IP_4 formation, but little action on IP_5 and IP_6. In comparison, the ratios of stimulated cells to resting cells were 14.8, 14.0, 5.1, 3.9, 1.0 and 0.9, respectively. Because fluoride activates G proteins by mimicking the γ-phosphate of GTP, the increase in the production of IP, IP_2 and inositol trisphosphates indicated that inositol phosphatidylinositol-specific phospholipase C was activated by GTP-binding protein in retinal pericytes [15]. IP_4 was labeled to a steady state after 48 h of incubation with [^{3}H]inositol [9]. The substantial increase in [^{3}H]IP_4 after the stimulation suggests that the inositol trisphosphate–IP_4 pathway was also activated by AlF_4^- (Fig. 4). The levels of both IP_5 and IP_6 in resting or stimulated cells were only slightly changed. Because both IP_5 and IP_6 may not be labeled to a steady state under the present labeling condition [9], the quantitative cor-

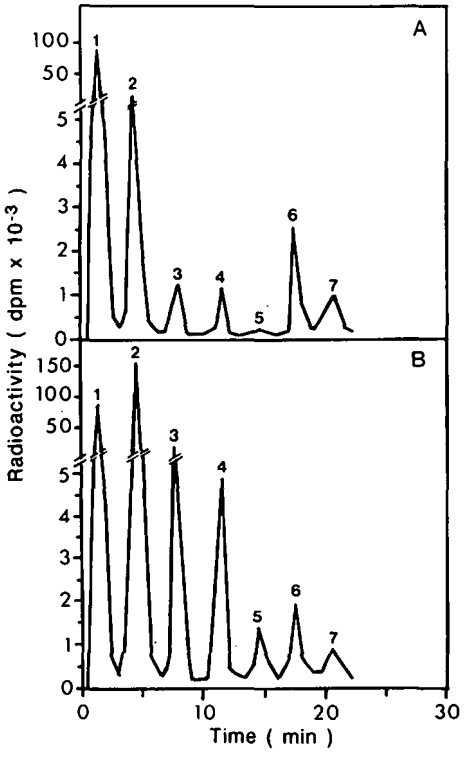

Fig. 4. Comparative chromatograms of inositol phosphate formation in retinal capillary pericytes (A) without and (B) with AlF_4^- treatment. Metabolic labeling, stimulation and TCA extraction are described in the Experimental section. Chromatography with the PW column using a stepped gradient program as described Fig. 1. Peaks: 1 = myoinositol; 2 = IP; 3 = IP_2; 4 = inositol trisphosphate; 5 = IP_4; 6 = IP_5; 7 = IP_6.

relation was not overstated. The above comments are based on assay with the PW column. Similar results were also obtained with the SW and Vydac columns (data not shown).

CONCLUSION

A rapid and sensitive single-column HPLC method has been developed for the determination of radiolabeled inositol phosphates and inositol trisphosphate isomers. Three different anion-exchange columns with the same functional group were tested. Except for the difficulty in detecting inositol trisphosphate isomers with the PW column, the three columns used have similar virtues for examining multiple inositol phosphates. As this method has been applied to evaluate inositol phosphatide turnover of cultured retinal pericytes in the range of $5 \cdot 10^5 - 1 \cdot 10^6$ cells, it is useful for studies of signal transduction in cellular systems.

ACKNOWLEDGEMENTS

The authors thank Dr. John Di Gregorio for providing access to the HPLC system and Drs. Staleny Cohen and Myron Yanoff for consistent support and valuable discussions. The authors are grateful to Zsuasanna and Mary Catherine for excellent photographic work. This study was supported by NIH grant EY06563 and grants from the American Diabetic Association, the Frank Snider Memorial Trust Fund and the Macula Foundation, New York.

REFERENCES

1 S. G. Rhee, P. G. Suh, S. H. Ryu and S. Y. Lee, *Science (Washington, D.C.)*, 244 (1989) 456.
2 H. Deckmyn, B. J. Whiteley and P. W. Majerus, *G Proteins*, Academic Press, New York, 1990.
3 V. S. Bansal and P. W. Majerus, *Annu. Rev. Cell Biol.* 6 (1990) 41.
4 C. P. Downes and R. H. Michell, *Biochem. J.*, 198 (1981) 133.
5 P. T. Hawkins, L. Stephens and C. P. Downes, *Biochem. J.*, 238 (1986) 507.
6 W. R. Mathews, D. M. Guido and R. M. Huff, *Anal Biochem.*, 168 (1988) 63.
7 K. A. Wreggett and R. F. Irvine, *Biochem. J.*, 262 (1989) 997.
8 G. S. Taylor, J. G. N. Garcia, R. Dukes and D. English, *Anal. Biochem.*, 188 (1990) 118.
9 F. S. Menniti, K. G. Oliver, K. Noginori, J. F. Obie, S. B. Shears and J. W. Putney, Jr., *J. Biol. Chem.*, 265 (1990) 11167.
10 S. B. Shears, D. J. Storey, A. J. Morris, A. B. Cubitt, J. B. Parry, R. H. Michell and C. J. Kirk, *Biochem. J.*, 242 (1987) 242.
11 T. Balla, A. J. Baukal, L. Hunyady and K. J. Catt, *J. Biol. Chem.*, 264 (1989) 13605.
12 W. Li, S. Shen, M. Khtami and J. H. Rockey, *Diabetes*, 33 (1984) 785.
13 D. Perrett, *HPLC of Small Molecules. A Practical Approach.* IRL Press, Oxford, 1987.
14 N. M. Dean and J. D. Moyer, *Biochem. J.*, 250 (1988) 493.
15 A. R. Hughes and J. W. Putney, Jr., *J. Biol. Chem.*, 264 (1989) 9400.

Journal of Chromatography, 607 (1992) 25–29
Elsevier Science Publishers B.V., Amsterdam

CHROM. 24 328

Rapid fluorimetric assay for the detection of the peptidyl α-amdating enzyme intermediate using high-performance liquid chromatography

Angelo P. Consalvo, Stanley D. Young and David J. Merkler

Department of Analytical Protein and Organic Chemistry, Unigene Laboratories, Inc., Fairfield, NJ 07004 (USA)

(First received February 25th, 1992; revised manuscript received May 4th, 1992)

ABSTRACT

Peptidylglycine α-amidating enzyme catalyzes the conversion of glycine-extended peptides to their corresponding amidated peptides via a stable α-hydroxyglycine intermediate. Using a new rapid fluorimetric reversed-phase high-performance liquid chromatographic assay, we have demonstrated that the substrate and product of the amidation reaction, as well as both stereoisomers of the α-hydroxyglycine intermediate, can be separated and detected in quantities as low as 1 pmol. The method is highly reproducible and requires less than 11 min for separation and quantification.

INTRODUCTION

Carboxyl terminal amidation is a post-translational modification which is often required for full biological activity of neural peptides and endocrine hormones [1,2]. Peptidylglycine α-amidating enzyme (α-AE) catalyzes the conversion of glycine extended peptides to their corresponding C-terminal amidated peptide products [3,4]. α-AE activity has been identified in and purified from a variety of tissues [5–10]. Early speculation regarding the mechanism of α-amidation suggested that the reaction proceeded through an α-hydroxyglycine intermediate [4,11]. In addition, Young and Tamburini [12] have shown, using a synthetic α-hydroxyglycine tripeptide as a substrate, that α-AE derived from rat medullary thyroid carcinoma cells exhibits a stereobias, where only one stereoisomer of the α-hydroxyglycine peptide is enzymatically converted to amidated product. Recently, an α-hydroxyglycine peptide formed by equine serum α-AE was isolated and characterized [13]. These results support the view that enzymatic amidation proceeds via a two-step mechanism, where formation of a stable peptidyl α-hydroxyglycine intermediate is followed by conversion to a mature α-amidated product. The enzymatic formation of the peptidyl α-hydroxyglycine intermediate by α-AE requires copper, ascorbate [12,13] and molecular oxygen [14]. Conversion of the peptidyl-α-hydroxyglycine intermediate to amidated product is also catalyzed by α-AE, but conversion can occur spontaneously at alkaline pH [13,15,16]. Proteins that possess only one of the two catalytic activities, namely peptidylglycine hydroxylase (PGH) or peptidylamidoglycolate lyase (PAL), have been described recently [13,15–19].

Peptidylglycine α-amidating enzyme

$$\text{R–CONH–CH}_2\text{–CO}_2\text{H} \xrightarrow{\text{PGH}} \text{R–CONH–CH(OH)–CO}_2\text{H} \xrightarrow{\text{PAL}} \text{R–CONH}_2 + \text{OHC–CO}_2\text{H}$$

Correspondence to: Dr. A. P. Consalvo, Department of Analytical Protein and Organic Chemistry, Unigene Laboratories, Inc., Fairfield, NJ 07004, USA.

0021-9673/92/$05.00

Several rapid sensitive assay systems have been described which employ a variety of separation and detection techniques for measuring amidation activity [3,7,20–24]. All of these assays are based on the conversion of a synthetic glycine-extended peptide to its corresponding peptide amide. None of these commonly used assays, however, was specifically designed to detect the formation of the peptidyl-α-hydroxyglycine intermediate; consequently, the PGH activity cannot be measured. There are only two assays presently available which can selectively detect and measure PGH activity [13,15]. Both of these assays utilize a model peptide substrate and employ reversed-phase high-performance liquid chromatography (RP-HPLC) to separate the enzymatically generated products. Briefly, the corresponding enzymatic products of either Phe–Gly–Phe–Gly–OH or trinitrophenyl–Tyr–Val–Gly–OH are separated by RP-HPLC and detected by monitoring the absorbance at 214 and 344 nm, respectively. Both of these assays are time consuming and possess rather poor detection limits.

We have previously reported the use of a fluorescent RP-HPLC assay system, based on the amidation of a dansyl (Dns) peptide substrate, for measuring enzyme activity [20]. In this communication, we report a modification of the assay that also resolves the α-hydroxyglycine intermediate from substrate and product. This new assay is thus capable of measuring peptidylglycine α-hydroxylase and peptidylamidoglycolate lyase activities.

EXPERIMENTAL

Materials

HPLC-grade acetonitrile (ACN) was obtained from EM Science (Gibbstown, NJ, USA). Sequalog-grade trifluoroacetic acid (TFA) was purchased from Schweizerhall (South Plainfield, NJ, USA). Sodium acetate (NaOAc), tris(hydroxymethyl)aminomethane (Tris), 2-(N-morpholino)ethane sulfonic acid (MES), piperazine-N,N′-bis(2-ethanesulfonic acid) (PIPES), N-2-hydroxyethylpiperazine-N′-2-ethane sulfonic acid (HEPES), 4-(2-hydroxyethyl)-1-piperazinepropanesulfonic acid (EPPS), 3-[tris (hydroxymethyl)methylamino]-1-propanesulfonic acid (TAPS) and 3-[(1,1-dimethyl-2-hydroxyethyl)-amino]-2-hydroxy-1-propanesulfonic acid (AMPSO) were purchased from Sigma (St. Louis, MO, USA).

Peptide synthesis

DNS–Tyr–Val–Gly–OH and Dns-Tyr–Val–NH_2 were synthesized as previously described [20,25]. Synthesis of Dns–Tyr–Val–α-hydroxyglycine–OH and purification of the resulting stereoisomers were carried out as previously described [12].

RP-HPLC assay

RP-HPLC assays were performed using a Hewlett-Packard (Paramus, NJ, USA) 1090 liquid chromatograph equipped with a binary solvent system (DR5), heated column compartment, LUSI controller, auto sampler and auto injector. Separations were achieved on a Keystone (Bellefonte, PA, USA) Hypersil ODS column (100 × 4.6 mm; 5 μm particle size) fitted with a Brownlee (Santa Clara, CA, USA) RP-18 guard column. The substrate, Dns–Tyr–Val–Gly–OH, both stereoisomers of α-hydroxyglycine intermediate, Dns–Tyr–Val–α-hydroxyglycine–OH and amidated product, Dns–Tyr–Val–NH_2, were resolved by gradient elution between 200 m*M* NaOAc pH 6.5 (buffer A) and ACN (buffer B). Elution was carried out at 50°C with a shallow linear gradient from 22–27% B over 8 min, followed by a steep linear gradient to 80% B over 3 min. The column was operated at a flow-rate of 1.2 ml/min. Dansylated peptides were detected using a Gilson (Middleton, WI, USA) 121 fluorimeter equipped with an excitation filter of 352–360 nm and emission cut-off filter of 482 nm. Each peptide was quantified by peak height with reference to standards of known concentration using a Hewlett-Packard 3392A integrator.

Preparation of peptidylglycine α-amidating enzyme

Recombinant type A, relative molecular mass, M_r = 75 000 (A75) α-AE was obtained from stably transformed Chinese hamster ovary (CHO) cells [26] and purified as previously described [27].

RESULTS AND DISCUSSION

RP-HPLC based assay systems utilizing dansylated peptides have proven to be extremely valuable for the study of proteolytic enzymes and other post-translational processing events [20,25,28,29]. Our previously reported fluorescent RP-HPLC α-AE assay, measuring the conversion of Dns–Tyr–Val–Gly–OH to Dns–Tyr–Val–NH_2, would not resolve

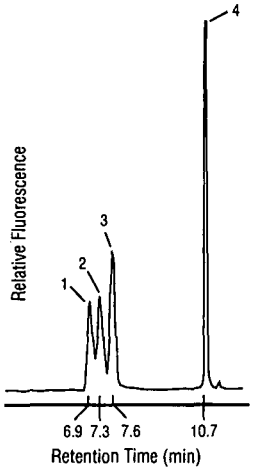

Fig. 1. RP-HPLC separation of dansyl peptides. Each peak represents an equimolar amount (140 pmol) of dansyl peptide. Peaks: 1 = Dns–Tyr–Val–α-hydroxyglycine–OH (stereoisomer No. 1); 2 = Dns–Tyr–Val–α-hydroxyglycine–OH (stereoisomer No. 2); 3 = Dns–Tyr–Val–Gly–OH; 4 = Dns–Tyr–Val–NH_2.

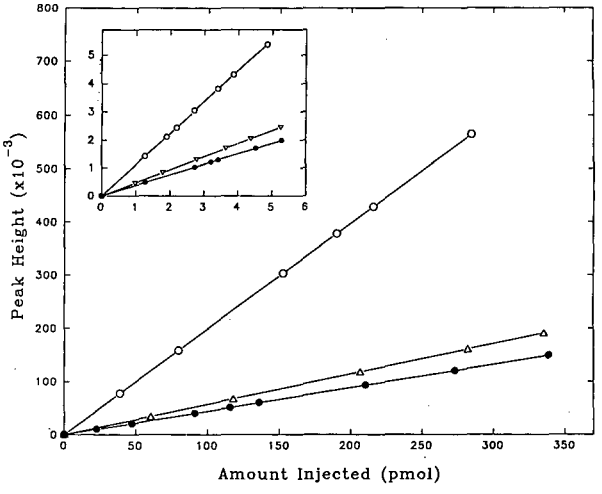

Fig. 2. Typical standard curves for the fluorometric detection of Dns–Tyr–Val–Gly–OH (▽, △), Dns–Tyr–Val–α-hydroxyglycine–OH (●) and Dns–Tyr–Val–NH_2 (○) during RP-HPLC analysis. Each peptide was subjected to analysis in triplicate. Peaks heights are reported in arbitrary units. The inset illustrates the assay sensitivity in the low picomol range.

the substrate from any potential α-hydroxyglycine peptide intermediates. Therefore, we have developed a RP-HPLC assay capable of separating Dns–Tyr–Val–Gly–OH, Dns–Tyr–Val–NH_2 and both stereoisomers of Dns–Tyr–Val–α-hydroxyglycine–OH. Separation of these peptides is achieved by gradient elution between 200 m*M* NaOAc, pH 6.5 and ACN (Fig. 1). The elution is monitored by fluorescence detection and the amount of each dansylated peptide can be quantified by either peak area or peak height. Fluorometric detection allows the direct assay of crude tissue homogenates without interference from other components of the assay mixtures.

Serial dilutions of an equimolar mixture containing both diastereomers of Dns–Tyr–Val–α-hydroxyglycine–OH were analyzed to determine the detection limits of the assay. For either isomer the limit of detection was found to be approximately 1 pmol. A linear relationship between peak height and amount of peptide injected was obtained for each component of the assay (Fig. 2). This relationship allows accurate quantification of the α-hydroxyglycine intermediate, glycine-extended substrate and amidated product in a single assay (Fig. 3). Spontaneous (*i.e.* non-enzymatic) conversion of the peptidyl α-hydroxyglycine compounds, which occurs significantly at alkaline pH [13,15,16], is negligible during the time required for the separation. It should be noted that the RP-HPLC assay reported by Tajima *et al.* [13] employs an ammonium hydrogencarbonate buffer at pH 9.0 to achieve separation of its glycine-extended substrate and α-hydroxyglycine intermediate. Although the α-hydroxyglycine intermediate can be detected using this assay, non-enzymatic conversion of the α-hydroxyglycine intermediate at pH 9.0 precludes the use of this assay for rigorous enzymological studies.

While examining the formation of the α-hydroxyglycine intermediate by A75 α-AE derived from recombinant CHO cells, we noted that the accumulation of intermediate was dependent on assay conditions (Fig. 3). These data show that there is an accumulation of intermediate under both assay conditions, but that the extent of accumulation at pH 5.5 (Fig. 3A) is more than twofold higher than the level attained at pH 7.5 (Fig. 3B). This increase in accumulation occurs despite the fact that the rate of product formation is substantially increased at pH 5.5. The increased formation of amidated peptide in reactions of A75 α-AE at acidic pH has been reported previously [6,27] and is consistent with the

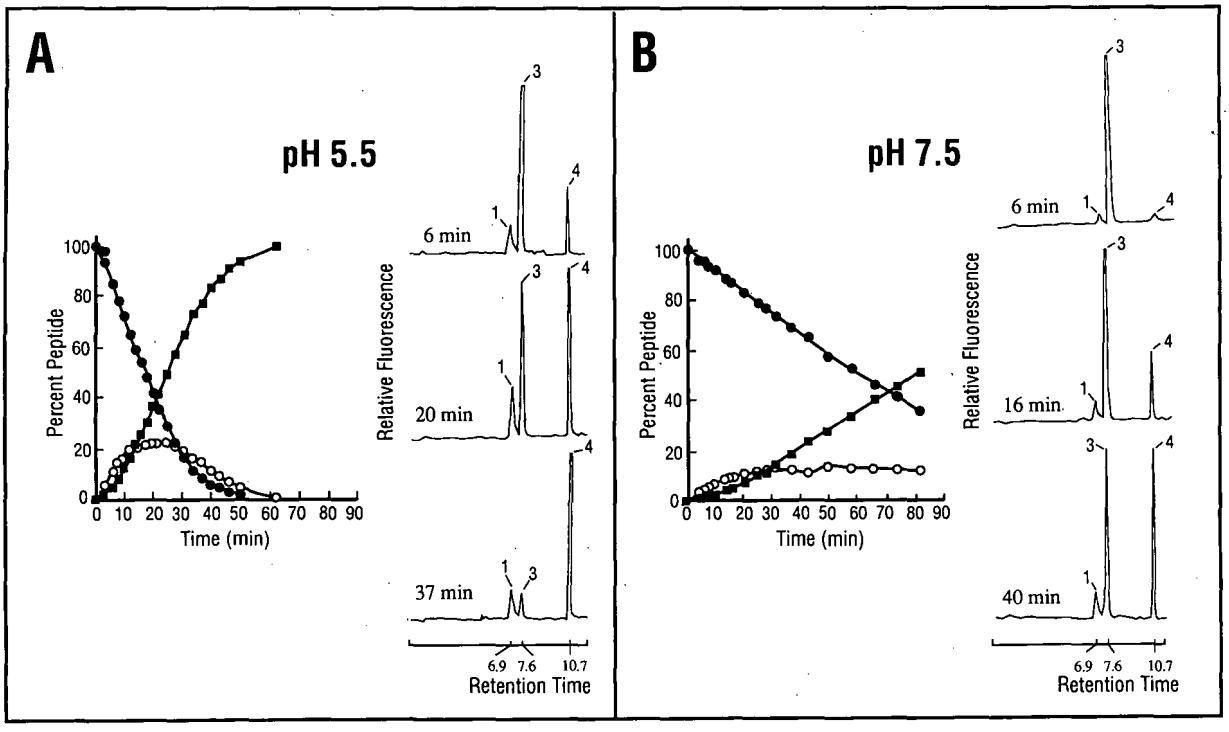

Fig. 3. Time course for the reaction of Dns–Tyr–Val–Gly–OH with A75 α-AE at pH 5.5 and pH 7.5. ● = Dns–Tyr–Val–Gly–OH (substrate); ○ = Dns–Tyr–Val–α-hydroxyglycine–OH (intermediate); ■ = Dns–Tyr–Val–NH_2 (product). Enzyme (0.1 μg, specific activity of $4.6 \cdot 10^6$ pmol/min/mg) was added to 900 μl of 25 m*M* mixed buffers, 0.001% Triton X-100, 1 μ*M* $CuSO_4$, 15 μ*M* Dns–Tyr–Val–Gly–OH, 3 m*M* ascorbate and incubated at 37°C. At the indicated time, an aliquot (10–15 μl) was removed and the reaction was terminated by addition of TFA to a final concentration of 1%. Aliquots were analyzed directly using the RP-HPLC assay. The mixed buffers consisted of MES, PIPES, HEPES, EPPS, TAPS and AMPSO adjusted to pH 5.5 (A) or pH 7.5 (B). In each panel (A and B) the time course of the reaction is shown to the left and selected chromatograms at the indicated time points are shown to the right.

fact that the enzyme functions in acidic secretory granules [30]. The RP-HPLC assay clearly demonstrates the ability to efficiently monitor both the PGH and PAL activities.

In the assay, we have included both stereoisomers of the α-hydroxyglycine intermediate, Dns–Tyr–Val–(*R*,*S*)-α-hydroxyglycine–OH, in order to permit further investigation into the mechanism of α-amidation. As mentioned above, Young and Tamburini [12] have shown that only a single stereoisomer of Dns–Tyr–Val–α-hydroxyglycine–OH is converted to α-amidated product. We further substantiated this result by incubating both stereoisomers (*R*,*S*) of Dns–Tyr–Val–α-hydroxyglycine–OH with A75 α-AE and monitoring the conversion to Dns–Tyr–Val–NH_2 using the RP-HPLC assay (data not shown). In addition, the chromatograms in Fig. 3A and B clearly illustrate the stereospecificity of the A75 α-AE catalyzed amidation. With time, only a single stereoisomer of the α-hydroxyglycine intermediate is detected (Fig. 3, peak 1) and subsequently converted to amidated product. We have isolated the α-hydroxyglycine intermediate catalyzed by the A75 α-AE in an attempt to assign absolute configuration (*R* or *S*). However, crystallization of the isolated intermediate necessary to perform the X-ray experiments has been problematic. Since it has been shown that α-AE abstracts the *pro*-S hydrogen of glycine-extended substrates during oxidation [31], it is likely that the stereospecific α-hydroxylation exhibited by the A75 α-AE yields Dns–Tyr–Val–(*S*)-α-hydroxyglycine–OH. In support of this view, α-AE is unable to catalyze the conversion of peptide substrates when the C-termi-

nal glycine residue is replaced with L-amino acids, but is does amidate substrates terminating with D-alanine [32].

In summary, we have developed a rapid and sensitive assay capable of measuring both the PGH and PAL activities which encompass the catalytic activity contained in bifunctional α-amidating enzymes. The assay is ideally suited for the analysis of a large number of samples and can be used for precise measurements of kinetic parameters. This novel assay is extremely useful for the study of multiple forms of α-AE in order to probe their differences and may help to further elucidate the mechanism of α-amidation. The assay is also being used to evaluate the modification of catalytic domains by site-directed mutagenesis.

ACKNOWLEDGEMENTS

We would like to thank Raviraj Kulathila for the purification of the CHO A75 α-AE and Dr. P. P. Shields for helpful discussions in the preparation of this manuscript.

REFERENCES

1 J. Douglas, O. Civelli and E. Herbert, *Ann. Rev. Biochem.*, 53 (1984) 665–715.
2 D. R. Lynch and S. H. Snyder, *Ann. Rev. Biochem.*, 55 (1986) 773–799.
3 A. F. Bradbury, M. D. Finnie and D. G. Smyth, *Nature (London)*, 298 (1982) 686–688.
4 B. A. Eipper, R. E. Mains and C. C. Glembotski, *Proc. Natl. Acad. Sci. U.S.A.*, 80 (1983) 5144–5148.
5 J. P. Gilligan, S. J. Lovato, S. D. Young, B. N. Jones, J. A. Koehn, L. F. LeSueur, A. M. Sturmer, A. H. Bertelsen, T. G. Warren, R. S. Birnbaum and B. A. Roos, in D. Puett, F. Ahmad, S. Black, D. M. Lopez, M. H. Melner, W. A. Scott and W. J. Whelan (Editors), *Advances in Gene Technology: Molecular Biology of the Endocrine System*, Cambridge University Press, New York, 1986, pp. 38–39.
6 N. M. Mehta, J. P. Gilligan, B. N. Jones, A. H. Bertelsen, B. A. Roos and R. S. Birnbaum, *Arch. Biochem. Biophys.*, 261 (1988) 44–54.
7 K. Mizuno, J. Sakata, A. Kojima, K. Kanagawa and H. Matsuo, *Biochem. Biophys. Res. Commun.*, 137 (1986) 984–991.
8 B. A. Eipper, V. May and K. M. Braas, *J. Biol. Chem.*, 263 (1988) 8371–8379.
9 L. Ouafik, V. May, H. T. Keutmann and B. A. Eipper, *J. Biol. Chem.*, 264 (1989) 5839–5845.
10 R. S. Birnbaum, G. A. Howard and B. A. Roos, *Endocrinology*, 124 (1989) 3134–3136.
11 R. C. Bateman, Jr., W. W. Youngblood, W. H. Busby, Jr. and J. S. Kizer, *J. Biol. Chem.*, 260 (1985) 9088–9091.
12 S. D. Young and P. P. Tamburini, *J. Am. Chem. Soc.*, 111 (1989) 1933–1934.
13 M. Tajima, T. Iidaa, S. Yoshida, K. Komatsu, R. Namba, M. Yanagi, M. Noguchi and H. Okamoto, *J. Biol. Chem.*, 265 (1990) 9602–9605.
14 D. J. Merkler and S. D. Young, *Arch. Biochem. Biophys.*, 289 (1991) 192–196.
15 A. G. Katopodis, D. Ping and S. W. May, *Biochemistry*, 29 (1990) 6115–6120.
16 K. Takahashi, H. Okamoto, H.Seino and M. Noguchi, *Biochem. Biophys. Res. Commun.*, 169 (1990) 524–530.
17 I. Kato, A. Yonekura, M. Tajima, M. Yanagi, H. Yamamoto and H. Okamoto, *Biochem. Biophys. Res. Commun.*, 172 (1990) 197–203.
18 S. N. Perkins, E. J. Husten and B. A. Eipper, *Biochem. Biophys. Res. Commun.*, 171 (1990) 926–932.
19 K. Suzuki, H. Shimoi, Y. Iwasaki, T. Kawahara, Y. Matsuura and Y. Nishikawa, *EMBO J.*, 9 (1990) 4259–4265.
20 B. N. Jones, P. P. Tamburini, A. P. Consalvo, S. D. Young, S. J. Lovato, J. P. Gilligan, A. Y. Yeng and L. P. Wennogle, *Anal. Biochem.*, 168 (1988) 272–279.
21 C. Mollay, J. Wichta and G. Kreil, *FEBS Lett.*, 202 (1986) 251–254.
22 I. Husain and S. S. Tate, *FEBS Lett.*, 152 (1983) 277–281.
23 T. Chikuma, K. Hanaoka, Y. P. Loh, T. Kato and Y. Ishii, *Anal. Biochem.*, 198 (1991) 263–267.
24 N. Miyazaki and T. Uemura, *Anal. Biochem.*, 197 (1991) 108–112.
25 A. P. Consalvo, P. P. Tamburini, W. Stern and S. D. Young, *Tetrahedron Lett.*, 30 (1990) 39–42.
26 D. A. Miller, K. U. Sayad, R. Kulathila, G. A. Beaudry, D. J. Merkler and A. H. Bertelsen, *Arch. Biochem. Biophys.*, in press.
27 G. A. Beaudry, N. M. Mehta, M. L. Ray and A. H. Bertelsen, *J. Biol. Chem.*, 265 (1990) 17694–17699.
28 P. P. Tamburini, R. N. Dreyer, J. Hansen, J. Letsinger, J. Elting, A. Gore-Willse, R. Dally, R. Hanko, D. Osterman, M. E. Kamarck and H. Yoo-Warren, *Anal. Biochem.*, 186 (1990) 363–368.
29 A. P. Consalvo, S. D. Young, B. N. Jones and P. P. Tamburini, *Anal. Biochem.*, 175 (1988) 131–138.
30 H. Gainer, J. T. Russel and Y. P. Loh, *Neuroendocrinology*, 40 (1985) 171–184.
31 S. E. Ramer, H. Cheng, M. M. Palcic and J. C. Vederas, *J. Am. Chem. Soc.*, 110 (1988) 8526–8532.
32 A. E. N. Landymore-Lim, A. F. Bradbury and D. G. Smyth, *Biochem. Biophys. Res. Commun.*, 117 (1983) 289–293.

Journal of Chromatography, 607 (1992) 31–35
Elsevier Science Publishers B.V., Amsterdam

CHROM. 24 281

Rapid determination of sulphonamides in milk using liquid chromatographic separation and fluorescamine derivatization

Nobuyuki Takeda and Yumi Akiyama

Food and Drug Division, Hyogo Prefectural Institute of Public Health, Arata-cho, Hyogo-ku, Kobe 652 (Japan)

(First received January 15th, 1992; revised manuscript received April 14th, 1992)

ABSTRACT

A simple and selective method is presented for the multiple residue determination of eight sulphonamides in consumers' milk. The drugs are sulphisomidine (ID), sulphadiazine (DZ), sulphamerazine, sulphadimidine, sulphamonomethoxine, sulphamethoxazole, sulphadimethoxine and sulphaquinoxaline (SQ). The milk sample was deproteinized with the same volume of 2 *M* hydrochloric acid and filtered. A 1-ml volume of the filtrate was mixed with 1 ml each of 1.25 *M* sodium acetate solution and a buffer (pH 3.0) for derivatization with 0.6 ml of 0.02% fluorescamine solution in acetone. A high-performance liquid chromatographic analysis was carried out on a C_{18} column with a mobile phase of acetonitrile–2% acetic acid (3:5) at 55°C using a fluorescence detector at an excitation wavelength of 405 nm and an emission wavelength of 495 nm. Average recoveries at fortification levels of 2, 5 and 10 ng/ml were 114%, 109% and 106%, respectively. Relative standard deviations were 1–4% at 10 ng/ml. The limit of determination was 10 ng/ml for ID, 5 ng/ml for DZ and SQ and 2.5 ng/ml for the other five sulphonamides. The method was applied to 25 milk samples and all appeared to be free from the drugs.

INTRODUCTION

Residues of sulphonamides, which are commonly used antibacterial agents for livestock, have been found in consumers' milk from Canada and the USA [1,2]. Although Japanese regulations prohibit their use in lactating dairy cows, possible improper use of the drugs has been reported [3]. Daily milk consumption is expected to be greater than that of meat and meat products, particularly in infants, and one of the drugs (sulphamethazine) is suspected to be carcinogenic [4]. Therefore, there is a need for a rapid, sensitive and selective method for monitoring their residual concentration in milk.

Most conventional methods for milk analysis are too tedious and time consuming for a large surveillance, as they include multiple manipulations such as extraction with an organic solvent, evaporation/concentration and clean-up/defatting steps [2,5,6]. Also, UV detection in a high-performance liquid chromatographic (HPLC) analysis seems to have insufficient selectivity for sulphonamides in milk samples, where in some instances two different mobile phases were required for isocratic separation of ten sulphonamide residues [5]. Recently, new methods have been introduced to solve the problems of the conventional technique, including a matrix solid-phase disperson (MPSD) extraction method [7], an immunochemical method [8] and a fully automated on-line dialysis–postcolumn derivatization method [9].

We have successfully introduced a fluorescamine derivatization method in the HPLC determination of residues of eight sulphonamides in meat and meat products [11]. We report here a procedure for the determination of sulphonamides in milk at ng/

Correspondence to: Dr. N. Takeda, Food and Drug Division, Hyogo Prefectural Institute of Public Health, Arata-cho, Hyogo-ku, Kobe 652, Japan.

0021-9673/92/$05.00

ml levels using this highly selective HPLC procedure coupled with a simple isolation method.

EXPERIMENTAL

Samples

A total of 25 samples of consumers' milk from twelve cities in Japan was collected at three retailers in Kobe and stored in a refrigerator until analysis. The samples were analysed within 2 days. The fat contents of the samples were 1.0–4.2%. Nine samples were processed milk, which consisted of raw milk, defatted–powdered milk and cream-butter.

Reagents and apparatus

Sulphisomidine (ID), sulphadiazine (DZ) and sulphamethoxazole (XZ) were purchased from Sigma (St. Louis, MO, USA), sulphamonomethoxine (MX) and sulphadimethoxine (DX) from Daiich-Seiyaku (Tokyo, Japan) and sulphaquinoxaline (SQ) from Dainihon-Seiyaku (Osaka, Japan). Sulfamerazine (MR) and sulphadimidine (DM) were generous gifts from Dr. T. Hamano of the Public Health Institute of Kobe City, Japan. Standard stock solutions (100 μg/ml) were prepared by accurately weighing 10 mg of the individual drugs and dissolving them in 100 ml of methanol. A mixture of the standards (1 μg/ml) was prepared by mixing 1 ml of the individual stock solution and diluting to 100 ml with methanol. The mixture was diluted with methanol for recovery tests. Fluorescamine reagent (0.02%) was prepared by dissolving 10 mg of Fluram (Hoffman-La Roche, Basle, Switzerland) in 50 ml of acetone. A buffer solution of pH 3.0 was prepared by mixing of 3 *M* hydrochloric acid and 3 *M* sodium acetate solution using a Beckman 12pH/ISE meter (Beckman Instruments, Fullerton, CA, USA). HPLC-grade methanol, acetonitrile and acetone and analytical-reagent grade hydrochloric acid, acetic acid and sodium acetate were used (Wako, Osaka, Japan). Water was purified with a Milli-Q SP TOC system (Millipore, Bedford, MA, USA).

The high-performance liquid chromatograph (HPLC) was composed of an LC-6AD pump, an RF-535 fluorescence monitor set at the highest sensitivity, a C-R4A integrator set at attenuation 1 and an Inertsil ODS-2 column (150 mm × 4.6 mm I.D., 5-μm particle size) (GL Sciences, Tokyo, Japan) placed in a CTO-6A column oven set at 55°C (Shimadzu, Kyoto, Japan). Although an unusually high column temperature (55°C) was used for obtaining a better separation in a shorter period, no problems with the column performance were found after separating more than 100 samples. The mobile phase was acetonitrile–2% acetic acid (5:3) at a flow-rate of 1 ml/min.

Deproteinization/extraction and derivatization

A 2-ml sample of milk was placed into a 10-ml test-tube containing 2 ml of 2 *M* hydrochloric acid and mixed thoroughly, then allowed to stand for 5 min. The mixture was filtered through a No. 5A filter-paper (Toyo Roshi Kaisha, Japan). To obtain a clearer filtrate, it is recommended to discard the first 0.5–1 ml of the filtrate or to filter again with the same filter. A 1-ml volume of the filtrate was mixed with 1 ml of 1.25 *M* sodium acetate solution, then 1 ml of 3 *M* buffer (pH 3.0), followed by 0.6 ml of the fluorescamine solution. The mixture was incubated for 20 min at room temperature, then 100 μl were injected into the HPLC system.

RESULTS AND DISCUSSION

Sample pretreatment is often the time-limiting step in most procedures for residue analysis. A number of new techniques for saving time and solvent have already been applied to extract residual sulphonamides from milk, including a solid-phase extraction method (SPE) with a commercially available C_{18} cartridge, a matrix solid-phase dispersion method (MPSD) with C_{18}-bonded phase material [7] and an on-line dialysis/sample enrichment method [9].

Highly selective methods such as enzyme-linked immunosorbent assay (ELISA) [8], postcolumn derivatization [9] and photodiode-array detection [10] have also been developed for determining sulphonamide residues in food. An ELISA system provides excellent rapidity and specifity. However, apart from the difficulty in preparing anti-sulpha drug antibodies for the usual chemical analysis, a multiple sulphonamide residue analysis is impossible. On the other hand, on-line dialysis/concentration in combination with an HPLC separation and a postcolumn derivatization method [9] seemed very promising for the determination of residual sulphona-

mides in milk. However, it required additional apparatus to set up the overall instrumentation.

Therefore, the SPE and MPSD methods were first tried for extracting sulphonamides from milk. However, the former required keeping a high positive pressure for an adequate flow and gave poor recovieres and the latter required time-consuming manipulation to prepare a column containing the C_{18}–milk mixture, making them unattractive methods for the pretreatment of milk samples. In the method development, direct derivatization of the acid-deproteinized milk sample with fluorescamine was considered to be a simple and selective procedure which requires no evaporation/concentration and clean-up steps, because all the sulphonamides having amino groups dissolve in an aqueous acid and the reagent reacts selectively with sulphonamides under acidic conditions to give highly fluorescent products [11–13].

In a preliminary experiment, a milk sample fortified with sulphonamides at 10 ng/ml was deproteinized with 6 *M* hydrochloric acid. A 1-ml volume of the filtrate, with an acid concentration was 3 *M*, was mixed with 1 ml of 3.5 *M* sodium acetate, then incubated with 0.5 ml of the fluorescamine reagent for 20 min [11]. However, no reproducible results were obtained. As the derivatization had been found to be pH dependent [11–13], the pH of the incubation mixture was checked. Some samples that had shown smaller fluorescent peaks on the HPLC trace were found to have a pH of less than 1.0. This result showed that the acid concentration (6 *M*) was too high to keep the pH of the incubation mixture at the optimum value of 3.0 [11]. Therefore, an attempt to obtain an incubation mixture of pH 3.0 was made by mixing 1 ml of 1 *M* hydrochloric acid with 1 ml of sodium acetate solution of concentration ranging from 1.0 tot 1.4 *M* and 0.6 ml of the reagent. The pH of the mixture was checked with and without the addition of 1 ml of 3 *M* hydrochloric acid–sodium acetate buffer (pH 3.0). Fig. 1 shows that 1 *M* hydrochloric acid mixed with 1.2 and 1.3 *M* sodium acetate gave mixtures of pH 3.1 and 3.0 with and without the buffer, respectively. In subsequent milk analyses, 2 *M* hydrochloric acid as a deproteinization agent (the acid concentration of the filtrate was 1 *M*) and 1.25 *M* sodium acetate solution were used. Buffer solution was further added, because the milk extract was expected to contain

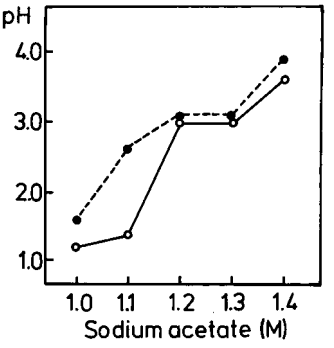

Fig. 1. Effect of sodium acetate concentration on pH of the incubation mixture with (●) and without (○) 3 *M* buffer (pH 3.0).

many components which would affect the pH of the mixture. The pH of the incubation mixture of real samples was found to be 3.0 ± 0.2 [n = 12, relative standard deviation (R.S.D.) = 7.0%]. The dose–response relationship was tested under the optimum reaction conditions and was found to be linear over the range tested, which was equivalent to 2–100 ng/ml sulphonamides in milk.

This method was applied to residual analysis for eight sulphonamides in 25 consumer milk samples. A typical chromatogram and the data for interfering peaks are shown in Fig. 2 and Table I. All the samples showed three large peaks at retention times

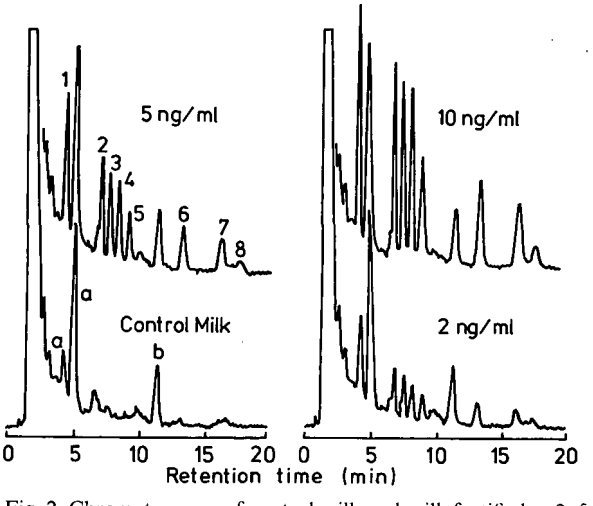

Fig. 2. Chromatograms of control milk and milk fortified at 2, 5 and 10 ng/ml. 1 = ID; 2 = DZ; 3 = MR; 4 = DM; 5 = MX; 6 = XZ; 7 = DX; 8 = SQ. a = Endogenous peak; b = reagent-derived peak.

TABLE I

DATA ON INTERFERING PEAKS AND LIMIT OF DETECTION (LOD), LIMIT OF QUANTIFICATION (LOQ) AND LIMIT OF DETERMINATION (L.Dtm) FOR THE HPLC METHOD FOR SULPHONAMIDE DETERMINATION

Data were obtained from 25 consumer milk samples.

Interfering peaks t_R (min)	Corresponding drugs		ng equivalent/ml milk		LOD[a] (ng/ml)	LOQ[a] (ng/ml)	L.Dtm.[a] (ng/ml)
	Drug	t_R	Av.	S.D.			
4.4	ID	4.4	2.46	0.42	3.7	6.7	10.0
6.7	DZ	7.0	0.96	0.15	1.4	2.5	5.0
7.6	MR	7.7	0.43	0.08	0.7	1.2	2.5
8.2	DM	8.3	0.30	0.05	0.4	0.8	2.5
9.0	MX	9.1	0.48	0.08	0.7	1.3	2.5
13.2	XZ	13.2	0.56	0.11	0.9	1.6	2.5
16.8	DX	16.2	0.47	0.12	0.8	1.7	2.5
17.3	SQ	17.5	1.17	0.12	1.5	2.3	5.0

[a] LOD = Av. + 3S.D.; LOQ = Av. + 10S.D; L.Dtm. ≈ 2LOQ.

t_R of 4.3, 5.1 and 11.3 min. The first two peaks might be endogenous peaks and the last one was derived from the reagent. The first peak interfered with the analysis of ID (t_R 4.4 min), which was equivalent to 2.5 ± 0.4 ng/ml I.D. in milk. The remaining two large peaks were well separated from the drugs of interest. All the chromatograms showed another smaller interfering peak (t_R 6.7 min) which was poorly resolved from DZ (t_R 7.0 min). It was equivalent to 1.0 ng/ml of DZ in milk. More than half of the samples gave slight but positive instrumental readings and nearly the same retention times of other drugs. These interferences were equivalent to 0.3–1 ng/ml of the corresponding sulphonamide in milk (Table I). The limits of detection (LOD) and quantification (LOQ) were determined using the data from the actual analysis ($n = 25$), and the values are summarized in Table I. LOD and LOQ are defined as the average of the background plus three standard deviations and ten standard deviations, respectively [5,14]. The LODs and LOQs of ID and DZ were higher owing to the interfering peaks described above, and those of other drugs were 0.4–2.3 ng/ml. All the milk samples tested were found to contain no sulphonamide above the LOQs.

Recovery studies were done at fortification levels of 2, 5 and 10 ng/ml using milk that had been found free from sulphonamides. The sample was prepared by adding 100 μl of a standard methanolic solution (0.2, 0.5 or 1.0 μg/ml) per 10 ml of the milk. A control sample was prepared similarly by adding 100 μl of methanol. Average recoveries of four replicate analyses, standard deviations (S.D.s), R.S.D.s and retention times (t_R) are presented in Table II. At the 2 ng/ml level DZ had the lowest recovery (61.6%) and the highest R.S.D. (39%), owing to the poorly resolved peak at t_R 6.7 min. The average recoveries were 106–114% for the three fortification levels. These values indicated that all the sulphonamides in milk were completely extracted into the acidic medium but at lower levels the instrumental readings gave slightly higher positive results. The R.S.D.s for the six drugs other than of DZ and SQ were in the range of 0.7–4.9% (average 2.4%). These recoveries and R.S.D.s were satisfactory for the surveillance. Taking the LOQs and visual inspection of the chromatograms into consideration, where SQ gave the smallest peak among the drugs, the limit of determination (L.Dtm.) was set at 10 ng/ml for ID, 5 ng/ml for DZ and SQ and 2.5 ng/ml for other sulphonamides (Table I). The L.Dtm. were set at about twice the LOQs to avoid "false positive" due to the interfering peaks in the actual routine analysis. They are, in other words, practical LOQs.

Compared with published HPLC methods for determining multiple sulphonamide residues in milk [5,7,9], the present method requires less sample manipulation, giving high precision and recovery with

TABLE II

RECOVERIES OF SULPHONAMIDES IN MILK FORTIFIED AT 2, 5 AND 10 ng/ml.

Values represent the averages of four analyses.

Drug	Fortification level								
	2 ng/ml			5 ng/ml			10 ng/ml		
	Av. recovery (%)	S.D. (%)	R.S.D. (%)	Av. recovery (%)	S.D. (%)	R.S.D. (%)	Av. recovery (%)	S.D. (%)	R.S.D. (%)
ID	106.7	2.0	1.9	113.7	5.6	4.9	111.8	2.7	2.4
DZ	61.6	24.2	39.3	93.8	14.1	15.0	98.4	4.0	4.1
MR	117.5	3.0	2.5	113.3	0.8	0.7	108.3	2.2	2.0
DM	126.5	2.7	2.2	115.8	1.2	1.0	109.5	2.6	2.4
MX	148.5	5.4	3.6	113.8	3.2	2.8	109.6	0.9	0.9
XZ	123.7	4.8	3.9	106.5	1.9	1.8	109.6	2.3	2.1
DX	106.1	5.2	4.9	107.9	2.9	2.7	107.5	1.9	1.8
SQ	123.3	3.3	2.7	104.0	14.1	18.5	94.2	1.5	1.6
Average	114.2			108.6			106.1		

lower limits of determination. In conclusion, this simple, rapid and selective method is considered to be applicable to the multiple determination of sulphonamide residues in milk for large surveillance projects.

REFERENCES

1 D. L. Colins-Thompson, D. S. Wood and I. Q. Thomson, *J. Food Protect.*, 51 (1988) 632.
2 L. Larocque, G. Carigman and S. Sved, *J. Assoc. Off. Anal. Chem.*, 73 (1990) 365.
3 *Report on Safety Use of Animal Drugs, Feed and Pesticides* (in Japanese), Administrative Inspection Bureau of Japan, Tokyo, 1991.
4 N. Littlefield, *Technical Report, Chronic Toxicity and Carcinogenicity Studies of Sulfamethazine in B6CF1 Mice*, National Center for Toxicological Research, Jefferson, AR, 1988.
5 M. D. Smedley and J. D. Weber, *J. Assoc. Off. Anal. Chem.*, 73 (1990) 875.
6 F. Tishler, J. L. Sutter, S. N. Bathish and H. F. Hagman, *J. Agric. Food Chem.*, 16 (1968) 50.
7 A. R. Long, C. R. Short and S. A. Barker, *J. Chromatogr.*, 502 (1990) 87.
8 P. Singh, B. P. Ram and N. Sharkov, *J. Agric. Food Chem.*, 37 (1989) 109.
9 M. M. L. Aerts, W. M. J. Beek and U. A. Th. Brinkman, *J. Chromatogr.*, 435 (1988) 97.
10 M. Horie, K. Saito, Y. Hoshino, N. Nose, N. Hamada and H. Nakazawa, *J. Food Hyg. Soc. Jpn.*, 31 (1990) 171.
11 N. Takeda and Y. Akiyama, *J. Chromatogr.*, 558 (1991) 175.
12 T. Sakano, S. Masuda, A. Yamaji, T. Amano, H. Oikawa and K. Nakamoto, *Yakugaku Zasshi*, 97 (1977) 464.
13 J. F. A. de Silva and N. Strojny, *Anal. Chem.*, 47 (1975) 714.
14 M. J. Shepherd, in C. Creaser and R. Purchase (Editors), *Food Contaminants: Sources and Surveillance*, Royal Society of Chemistry, Cambridge, 1991, Ch. 8, p. 109.

Journal of Chromatography, 607 (1992) 37–45
Elsevier Science Publishers B.V., Amsterdam

CHROM. 24 298

Sensitive method for the determination of organophosphorus pesticides in fruits and surface waters by high-performance liquid chromatography with ultraviolet detection

R. Carabias Martinez, E. Rodriguez Gonzalo, M. J. Amigo Moran and J. Hernandez Mendez

Departamento de Química Analítica, Nutrición y Bromatología, Universidad de Salamanca, 37008 Salamanca (Spain)

(First received January 17th, 1992; revised manuscript received April 24th, 1992)

ABSTRACT

A sensitive method for the high-performance liquid chromatographic determination of five organophosphorus pesticides (paraoxon, methyl-parathion, ethyl-parathion, guthion and fenitrothion) in fruits and tap and river water samples is described. For the determination of pesticides in fruits a simple and rapid sample preparation procedure was developed that allowed pesticides to be determined at 50–100 μg/kg levels with recoveries ranging from 83 to 118% and relative standard deviations below 6%. The determination of pesticide residues in surface water samples was also successfully accomplished. Concentrations at sub-ppb levels can be measured by using a solid-phase concentration step, the recoveries being over 80%. In analyses of both fruits and surface waters, the sensitivity levels achieved were 2–10 times lower than legal limits admitted in the European Economic Community.

INTRODUCTION

As a result of their relatively rapid degradation and low accumulation in the biological food chain, organophosphorus pesticides are widely applied to a variety of crops, including green vegetables and fruits. However, their widespread use could be expected to leave residues not only on crops but also in surface waters draining the croplands. Hence, the monitoring of pesticide residues in agricultural and food products and in environmental matrices has become a priority field in pesticide research and analysis.

Gas chromatography has undoubtedly been the most common technique for analysing surface waters and vegetable materials for pesticides [1]. High-performance liquid chromatographic (HPLC) methods for pesticide residue analysis were firstly developed for non-volatile or thermally labile compounds such as carbamate insecticides. As HPLC can offer a simpler and/or faster approach to analyses for a wide number of other compounds [2,3], HPLC methods are continually increasing in acceptance and applications [4–6]. Although applications of HPLC to the formulation analysis of organophosphorus pesticides have been reported [7–10], the literature concerning organophosphorus multiresidues in foodstuff is scarce [11–14]. Clark *et al.* [12] reported a method for parathions using HPLC with series UV–amperometric detection. Detection limits of 2–3 ng of injected pesticide and 0.8–0.9 ng were obtained with UV and electrochemical detectors, respectively. Concentrations less than 10 ng/ml in waters and 50 μg/kg in vegetable materials

Correspondence to: Dr. R. Carabias Martinez, Departamento de Química Analítica, Nutrición y Bromatología, Universidad de Salamanca, 37008 Salamanca, Spain.

0021-9673/92/$05.00

were measured using electrochemical detection, but UV detection could not be applied because of the multiple interferences from plant substances.

The number of HPLC methods for pesticide residue analysis is limited, but extraction and clean-up procedures can readily be found for numerous pesticides [15]. Many of these procedures will no doubt produce sufficiently clean extracts for HPLC, but most of them are laborious and time consuming. Pesticide sample preparation is usually achieved by liquid–liquid extraction or by enrichment of trace compounds of interest by solid-phase extraction (SPE). The latter technique is gaining acceptance [16–18] and will probably be increasingly used as a wider variety of solid-phase supports become available.

This paper deals with the determination of five frequently used organophosphorus pesticides in fruits; extraction with benzene and solvent replacement with methanol provides extracts clean enough to avoid any further clean-up step. The analysis of tap and river water samples, including an SPE concentration step, was also accomplished.

EXPERIMENTAL

Apparatus

A Spectra-Physics chromatograph equipped with an SP 8800 ternary pump, an SP 8450 UV–VIS detector and an SP 4290 integrator was used. Columns were Spheri-5 RP-8 (5 μm) (220 × 4.6 mm I.D.) and Spheri-5 RP-18 (5 μm) (250 × 4.6 mm I.D.) from Brownlee Labs. A Rheodyne injection valve with a 10μl injection loop was used throughout. All solvents and samples were filtered through 0.45-μm pore-size nylon membrane filters (Millipore).

Apple samples were homogenized in an electric mixer (Moulinex).For pesticide extraction and preconcentration from water samples, Sep-Pak C_{18} bonded-phase silica cartridges (Waters) were used; samples were pumped through them by a Gilson Minipuls 2 HP 4 peristaltic pump with vinyl tubing.

Reagents

Paraoxon (99% purity), guthion (99%), methylparathion (97%), fenitrothion (99%) and ethylparathion (99%) were obtained from Riedel-de Haën (Seelze-Hannover, Germany). Ultra-high-quality water used for the preparation of solutions was obtained with an Elgastat UHQ water-purification system. Methanol, benzene and dichloromethane were of HPLC grade (Carlo Erba, Milan, Italy). All other chemicals were analytical-reagent grade.

Samples and standards

Golden-type apples were obtained in area retail markets. River water samples were taken from different rivers of SE Salamanca (Spain). They were collected directly in 1-l glass containers, stored at 4°C in the dark and analysed within 24 h after collection.

Stock solutions containing the five pesticides were prepared in pure methanol and stored at 4°C; working standard solutions were daily prepared by dilution with methanol.

HPLC operating conditions

Separation was accomplished in the Spheri-5 RP-18 column, the mobile phase being methanol–water (70:30, v/v) containing $2.5 \cdot 10^{-2}$ *M* acetic acid–acetate buffer at a flow-rate of 1.25 ml/min. It was degassed by bubbling 99.998% helium through it. The injection volume was 10 μl in all experiments. Detection was carried out at 260 nm and peak areas were used for quantification.

Determination of pesticides in apples

Two or three apples were sliced and homogenized in an electric mixer. An amount of 3.0 *g* of homogenized sample was spiked with 1.0 ml of a methanolic solution of the five pesticides and allowed to stand for at least 24 h at room temperature. Then 8.0 ml of benzene were added and the mixture was stirred in a magnetic device for 30 min to improve the sample–benzene contact and hence, the extraction process. After centrifugation at 1307 *g* for 20 min, a 3.0-ml aliquot of the organic layer was evaporated to dryness at room temperature by passing an air stream. The dry extract was dissolved in 2.0 ml of methanol using an ultrasonic bath and the sample was then ready for analysis. Samples were prepared in triplicate and 10-μl aliquots of each sample were injected into the chromatograph. Quantification was carried out by using the external standard method by taking the mean peak-area value of three injections.

Determination of pesticides in waters

Tap water samples were used without any further treatment. All river water samples were filtered through sintered glass filters (No. 5) to remove suspended particulate matter before use. Pesticides were added to water samples by placing 1 ml of pesticide mixture solution in a volumetric flask and making up to 1 l with the water sample. Analytes were adsorbed on the Sep-Pak C_{18} cartridge by a single pass through the cartridge at a flow rate of about 5 ml/min. Desorption was effected by elution with 2.0 ml of a solution with the same composition as the mobile phase and 7.0 ml of methanol and the eluate was collected into a 10-ml volumetric flask, diluting to the mark with mobile phase solution. These samples were then analyzed immediately by triplicate injections of 10-μl aliquots. In addition, non-spiked water samples were analysed following the same procedure to check for the presence of pesticides under study.

The cartridges were equilibrated with 5.0 ml of methanol and 5.0 ml of UHQ-purified water before use for pesticide preconcentration.

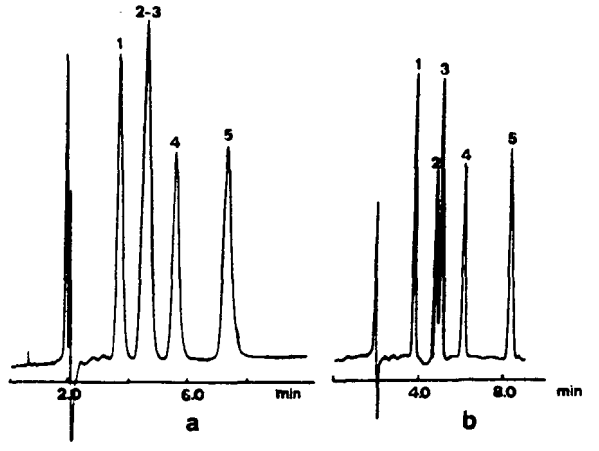

Fig. 1. Representative chromatograms obtained with (a) RP-8 and (b) RP-18 columns. Peaks: 1 = paraoxon; 2 = guthion; 3 = methyl-parathion; 4 = fenitrothion; 5 = ethyl-parathion. Experimental conditions: (a) methanol–water (70:30, v/v) + $2.5 \cdot 10^{-2}$ *M* acetic acid–acetate buffer as mobile phase, flow-rate 1.25 ml/min; (b) methanol–water (75:25, v/v) + $2.5 \cdot 10^{-2}$ *M* acetic acid–acetate buffer as mobile phase, flow-rate 1.0 ml/min.

RESULTS AND DISCUSSION

Two reversed-phase columns (C_8 and C_{18}) were tried for pesticide separation. Using methanol–water (75:25, v/v) as the mobile phase, the C_8 column was unable to resolve guthion and methyl-parathion with retention times of 4.39 and 4.56 min, respectively, when injected alone, the chromatogram showing a single broad peak at 4.45 min (Fig. 1). As further modifications of mobile phase composition were not successful in improving the resolution, the RP-18 column appeared to be more suitable than the RP-8 column for these pesticide separations.

To find suitable conditions for pesticide separation, the HPLC operating conditions, such as mobile phase constituents and flow rate, were optimized. A mobile phase of methanol–water (70:30, v/v) was found to give a good resolution and a reasonable analysis time. Methanol concentrations higher than 80% (v/v) gave poor peak resolution and with concentrations lower than 70% long analysis times were obtained.

The addition of acetate buffer to the mobile phase was found to be an easy way to shorten the analysis time with no decrease in resolution. Buffer concentrations in the range $0.5 \cdot 10^{-2}$–0.1 *M* were tested; concentrations up to $2.5 \cdot 10^{-2}$ *M* produced an earlier elution of the less polar pesticides, such as fenitrothion and ethyl-parathion, the retention times of the other peaks remaining unmodified. For buffer concentrations higher than $2.5 \cdot 10^{-2}$ *M*, no further modifications were found.

Flow-rate was studied in the range 0.5–2.0 ml/min. As expected, shorter analysis times were obtained at higher flow-rates but guthion and methyl-parathion were not well resolved at flow-rates higher than 1.5 ml/min.

Under the optimum conditions described under Experimental, linear relationships were found between peak area or height and pesticide concentration in the studied range, between 2.90 and 210 ng of each pesticide injected. The detection limits, calculated as the ratio between twice the noise and the calibration slope, are given in Table I, together with data from the calibration fittings and standard deviations obtained from ten replicate analyses at a concentration level of 12 ng of each pesticide. A chromatogram corresponding to a standard solution near the detection limit (about 0.30 ng of each pesticide injected) is shown in Fig. 2.

TABLE I

CALIBRATION FITTINGS

Concentration range between *ca.* 2.90 and 210 ng of each pesticide injected.

Pesticide	Intercept	Slope (l/mol)	Correlation coefficiënt	RSD[a] (%)	DL[b] (ppb)
Paraoxon	$(1.0 \pm 0.8) \cdot 10^3$	$(8.78 \pm 0.03) \cdot 10^9$	0.997	3.55	26
Guthion	$(6.3 \pm 3.7) \cdot 10^2$	$(6.59 \pm 0.02) \cdot 10^9$	0.999	2.11	53
Methyl-parathion	$(4.5 \pm 2.3) \cdot 10^2$	$(9.55 \pm 0.04) \cdot 10^9$	0.999	2.74	30
Fenitrothion	$(6.4 \pm 7.7) \cdot 10^2$	$(7.76 \pm 0.02) \cdot 10^9$	0.999	2.95	49
Ethyl-parathion	$(1.6 \pm 0.6) \cdot 10^2$	$(9.79 \pm 0.04) \cdot 10^9$	0.999	2.99	57

[a] Relative standard deviation ($n = 10$); amount injected, 12 ng of each pesticide.
[b] Detection limit, $2s/m$, where s is the blank standard deviation and m is the slope of the calibration graph.

Determination of pesticides in fruits

For the development of an appropriate procedure for the determination of pesticide residues in fruits, benzene, methanol and dichloromethane were tested as organic solvents for the extraction of the pesticides; no spiked apple samples were used in studies on the possible interferences from crop components.

Samples spiked at about 10 μg/g were used in comparative recovery experiments (Fig. 3); the pesticides were allowed to equilibrate with the sample matrix for at least 24 h but no longer than 48 h before extraction. Studies on the pesticide–matrix contact time showed that with maceration times longer than 48 h, the pesticide recoveries were dramatically decreased.

The blanks obtained using methanol as extraction solvent showed a large peak early in the chromatogram, whereas dichloromethane and benzene extracts gave only small peaks. Conversely, at high retention times, several peaks were observed in these extracts with benzene and dichloromethane but not in the methanolic extract.

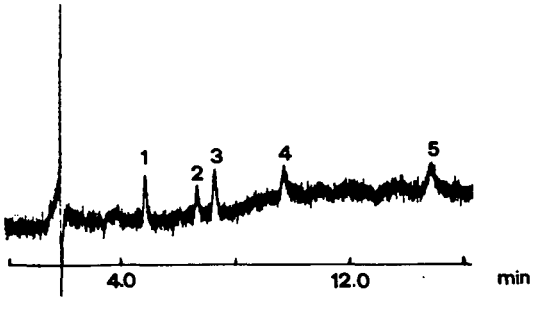

Fig. 2. Chromatogram obtained for a standard solution near the estimated detection limit. Amounts injected: (1) paraoxon, 0.30 ng; (2) guthion, 0.29 ng; (3) methyl-parathion, 0.30 ng; (4) fenitrothion, 0.30 ng; (5) ethyl-parathion, 0.30 ng. Experimental conditions as given under Experimental.

Regarding extraction percentages (Fig. 3), organophosphorus pesticides are not well extracted with methanol (about 70%). If it is considered that for a correct determination of pesticide residues, the recoveries should be within the range 70–110%, with a mean value greater than 80% [19]; adequate recoveries for all five pesticides were obtained with benzene (98–108%) and dichloromethane (86–99%) as extraction solvents, the former giving cleaner chromatograms.

Although both solvents were adequate, benzene was chosen for pesticide extraction from apple samples. Fig. 4 shows a representative chromatogram of a benzene extract where several peaks can be seen; no interferences with relevant analytes were observed. This solvent minimizes co-extractives from the vegetable matrix as vegetables are relatively polar in their matrix profile. The analysis time should be prolonged to allow the elution of less polar matrix compounds, with retention times longer than 25 min.

After extraction, the next step was evaporation to dryness of a 3.0-ml aliquot of the organic extract. The dry residue was then dissolved in 2.0 ml of a solution whose composition was also studied: (a) 2.0 ml of methanol, (b) 2.0 ml of mobile phase and (c) 1.0 ml of methanol + 1.0 ml of mobile phase

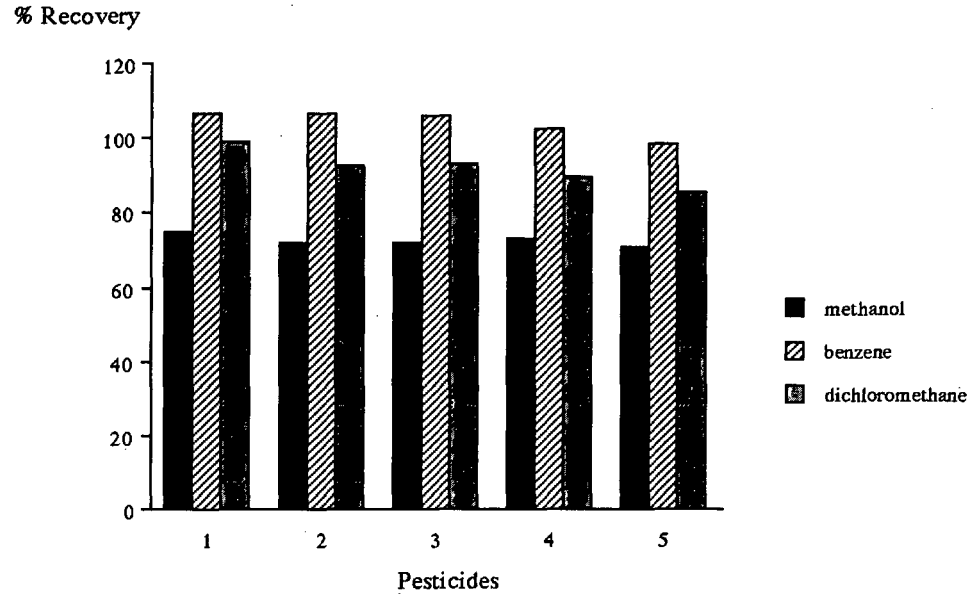

Fig. 3. Influence of the extraction solvent on the percentage extraction of pesticides from apple samples spiked with *ca.* 10 μg/g of each pesticide. Numbers 1–5 as in Fig. 1.

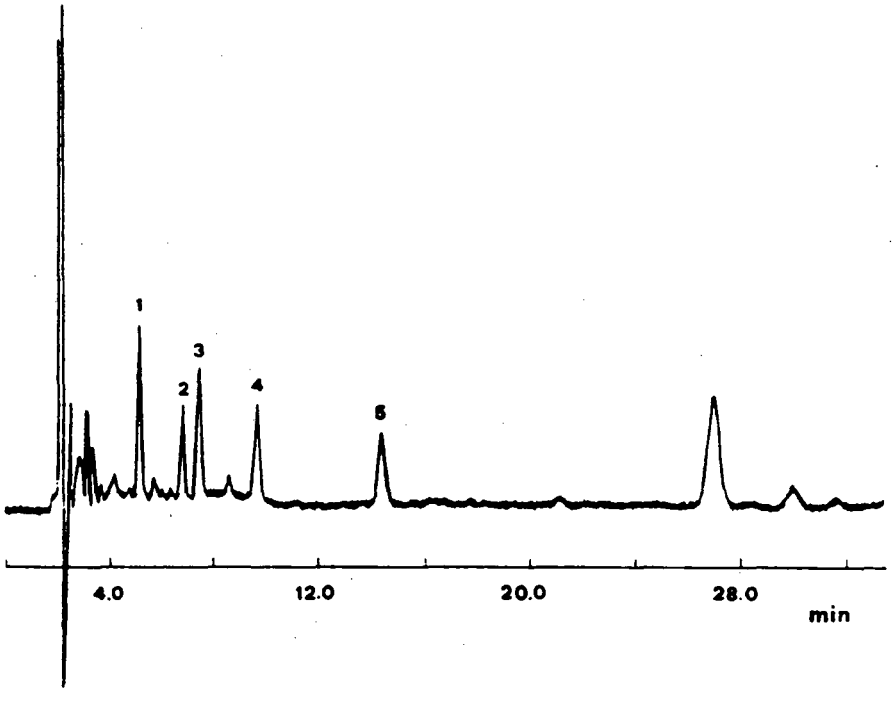

Fig. 4. Representative chromatogram of an apple sample spiked at the 0.46 μg/g level using benzene as solvent for pesticide extraction. Peaks as in Fig. 1.

TABLE II

PESTICIDE RECOVERIES FROM APPLE SAMPLES

Pesticide	Added (μg/g)	Recovery (%)	RSD[a] (%)	DL[b] (μg/g)
Paraoxon	1.17.	95.4	6.0	0.046
	9.88	94.9	2.5	
Guthion	1.15	101.6	3.9	0.094
	9.75	98.8	3.7	
Methyl-parathion	1.16	98.5	4.0	0.053
	10.02	100.6	2.2	
Fenitrothion	1.17	93.3	4.6	0.085
	10.03	100.0	1.4	
Ethyl-parathion	1.16	86.3	3.7	0.099
	10.19	98.3	1.4	

[a] $n = 4$

[b] Detection limit ($2s/m$) calculated with peak-area data from experiment in Fig. 5

solution were tested. Good recoveries, between 97 and 109%, were found for paraoxon, guthion, methyl-parathion and fenitrothion no matter which solution was used for dissolving the dry residue. Ethyl-parathion was quantitatively recovered [19] only when solution (a) was used.

The selectivity of the overall process can be explained as follows: as the non-polar solvent benzene is used to achieve an efficient extraction of organophosphates, most of the polar components of the sample are eliminated in this extraction step. In the next step, benzene is replaced with the polar solvent methanol, evaporating the former and dissolving the dry residue. As methanol is a weak solvent for low polarity compounds, pesticides are dissolved in solution whereas less polar impurities remain mainly in the solid residue. At this point, the sample is relatively clean and no interferences from the fruit

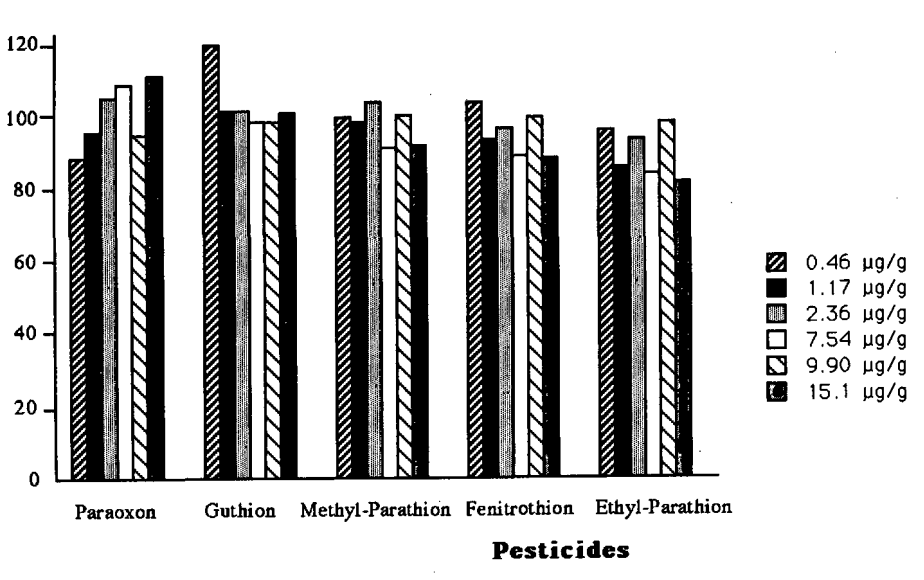

Fig. 5. Recovery from apple samples as a function of pesticide concentration in the original samples.

TABLE III

PESTICIDE RECOVERIES FROM DISTILLED WATER SAMPLES

Fortification level (ng/ml)	Recovery (%)				
	Paraoxon	Guthion	Methyl-parathion	Fenitrothion	Ethyl-parathion
1.40	90.5	88.7	84.3	78.6	76.3
2.80	86.3	88.0	85.7	80.8	78.7
27.9	100.7	102.5	101.1	98.2	89.6
46.1	104.4	101.3	97.8	98.1	91.6
69.2	104.3	101.1	101.7	98.1	91.2
DL (ng/ml)	0.26	0.53	0.30	0.49	0.57

matrix were observed in the elution range of interest, so no further residue clean-up step was required. Quantitative recovery results and relative standard deviations were calculated on the average percentage recovery of four replicate samples injected in triplicate and bracketed with injections of the standards (Table II). In the range of fortification levels tested (0.46–15.1 μg/g) the recoveries were found to be independent of concentration and similar for the five pesticides assayed, ranging from 83 to 118% (Fig. 5). By using the peak-area data obtained for the concentration range displayed in Fig. 5, detection limits were calculated (Table II). Values as low as 50–100 μg/kg for only 3.0 g of homogenized sample were obtained. These levels are 5–10 times lower than the legal limits admitted in the European Economic Community (EEC) for fruits and vegetables [20].

Determination of pesticides in tap and river waters

To determine pesticide residues in water samples at levels below the legal limits, trace enrichment on commercially available Sep-Pak C_{18} cartridges was chosen because it facilitates simultaneous extraction and analyte preconcentration.

Pesticide adsorption on the cartridges was carried out as described under Experimental. For pesticide desorption from the cartridge, good recoveries (81–90%) were found on eluting the pesticides with 2.0 ml of mobile phase solution and 7.0 ml of methanol.

The overall procedure was checked for samples at fortification levels between 1.4 and 69.2 ng/ml (Ta-

TABLE IV

PESTICIDE RECOVERIES FROM TAP AND RIVER WATER SAMPLES

Pesticide	Tap water			River water		
	Added (ng/ml)	Recovery (%)	RSD[a] (%)	Added (ng/ml)	Recovery (%)	RSD[a] (%)
Paraoxon	14.1	86.4	0.88	1.5	91.2	8.4
	45.3	100.3	1.12	33.1	94.9	1.6
Guthion	14.0	87.2	0.97	1.7	84.4	3.3
	46.7	97.4	0.71	34.2	91.5	1.7
Methyl-parathion	13.7	88.2	0.77	1.6	86.4	3.9
	45.6	98.1	0.70	33.4	94.0	2.3
Fenitrothion	14.0	83.8	1.25	1.7	86.3	5.9
	46.6	94.8	0.60	34.1	90.6	2.1
Ethyl-parathion	13.9	79.3	1.28	1.6	81.7	7.2
	46.5	88.4	1.28	34.0	82.0	1.6

[a] $n = 4$.

ble III), the recoveries being over 76%. Based on these results and bearing in mind the enrichment factor of 100 achieved in the preconcentration step, it should be possible to determine pesticides in water samples at sub-ppb levels (Table III), which is 2–5 times less than levels admitted in the EEC for surface waters destined for drinking water production [21].

Tap water analysis. None of the blank tap water samples gave peaks that interfered with the determinations of the pesticides of interest. Recovery determinations were made on pesticide-fortified tap water samples ($n = 4$) at two different concentration levels, 14 and 45 ng/ml (Table IV).

River water analysis. For the analysis of river water samples, six different points in the agricultural area SE of Salamanca (Spain) were sampled. Unspiked aliquots of each sample were analysed to quantify ambient levels of pesticide concentration. Each water sample showed several peaks but none of them corresponded to the studied pesticides except one (Fig. 6a), where a small peak with a retention time (9.54 min) similar to that of fenitrothion was observed. As this peak is below the calculated limit value for fenitrothion, no further conclusions can be drawn. Recovery results for a river water sample spiked at 1.6 and 33 ng/ml are given in Table IV and a chromatogram of a river water at the 1.6 ng/ml fortification level is shown in Fig. 6b.

CONCLUSIONS

Conditions have been established for the HPLC determination of trace levels of paraoxon, guthion, methyl-parathion, ethyl-parathion and fenitrothion residues in fruits and surface waters. The UV detec-

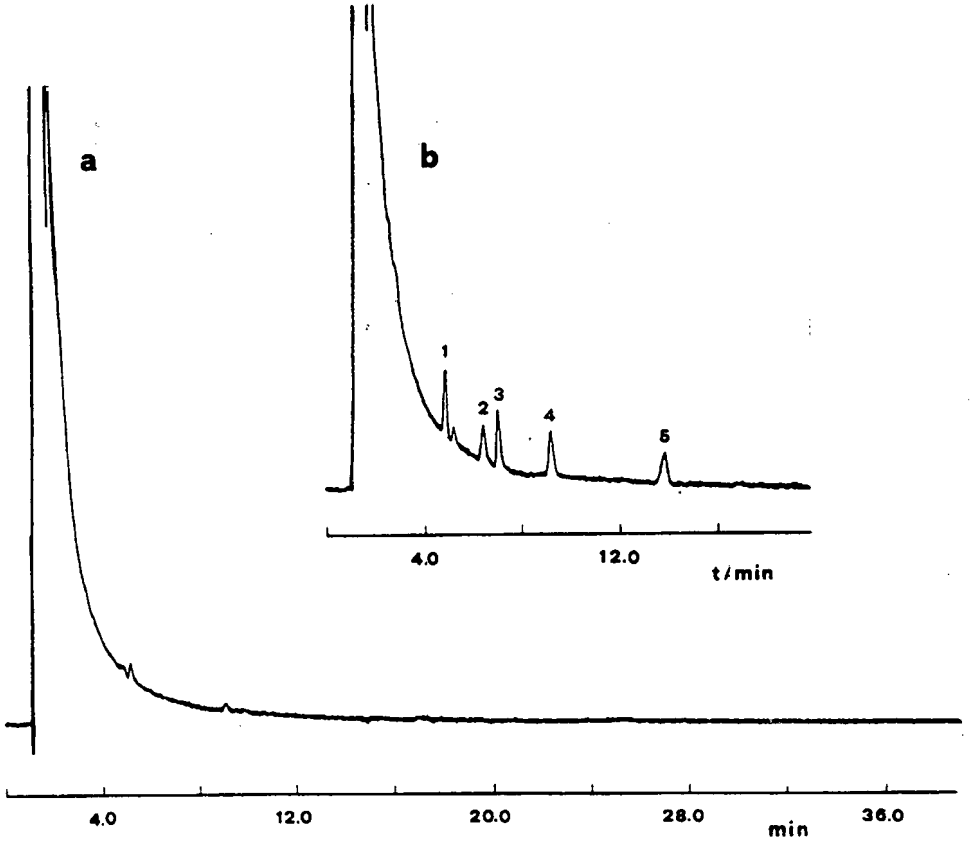

Fig. 6. Chromatogram of a river water sample (P.io Portillo, Salamanca, Spain) (a) before and (b) after being spiked at the 1.6 ng/ml level. Peaks as in Fig. 1.

tion limits are 0.2–0.6 ng of pesticide injected, which compare well with results reported by Clark *et al.* [12] for electrochemical detection and represent some improvement on the results obtained by the same authors with a UV detector.

The sample preparation scheme proposed for fruits is simple and rapid and gives clean extracts without the need for further clean-up steps of the residues, generally required for analyses of real samples. Analysis of river water samples allows pesticide concentrations at sub-ppb levels to be monitored. In both instance the detection limits found are sufficiently low for the method to be applied to crop extracts and river waters at levels 2–10 times lowers than the legal limits admitted in the EEC for these types of samples.

ACKNOWLEDGEMENT

The authors thank the Dirección General de Investigación Científica y Técnica (DGICYT, Spain) for the financial support of this work (project No. PB89-0397)

REFERENCES

1 R. R. Watts (Editor), *Manual of Analytical Methods for the Analysis of Pesticides in Humans and Environmental Samples*, US Environmental Protection Agency, Environmental Toxicology Division, Health Effects Research Laboratory, Research Triangle Park, NC, 1980, EPA-600/8-80-038.
2 J. F. Lawrence and D. Turton, *J. Chromatogr.*, 157 (1978) 207.
3 E. Rodríguez Gonzalo, M. J. Sánchez Martín and M. Sánchez Camazano, *J. Chromatogr.*, 585 (1991) 324.
4 A. R. Hanks and B. M. Colvin, in K. G. Das (Editor), *Pesticide Analysis*, Marcel Dekker, New York, 1981, pp. 99–174.
5 J. Sherma, *Anal. Chem.*, 59 (1987) 18R.
6 D. Barceló, *Chromatographia*, 25 (1988) 928.
7 E. R. Jackson, *J. Assoc. Off. Anal. Chem.*, 60 (1977) 724.
8 E. R. Jackson, *J. Assoc. Off. Anal. Chem.*, 61 (1978) 495.
9 W. P. Cochrane, M. Lanouette and R. Greenhalgh, *J. Assoc. Off. Anal. Chem.*, 62 (1979) 1222.
10 S. C. Slahck, *J. Assoc. Off. Anal. Chem.*, 71 (1988) 988.
11 X. -D. Ding and I. S. Krull, *J. Agric. Food Chem.*, 32 (1984) 622.
12 G. J. Clark, R. R. Goodin and J. W. Smiley, *Anal. Chem.*, 57 (1985) 2223.
13 J. C. Gluckman, G. Barceló, G. J. DeJong, J. W. Frei, F. A. Maris and U. A. Th. Brinkman, *J. Chromatogr.*, 367 (1986) 35.
14 A. Farran and J. De Pablo, *Int. J. Environ. Anal. Chem.*, 30 (1987) 59.
15 G. J. Sharp, J. G. Brayan, S. Dilli, P. R. Haddad and J. M. Desmarchelier, *Analyst (London)*, 113 (1988) 1493.
16 J. J. Richard and G. A. Junk, *Mikrochim. Acta*, I (1986) 387.
17 G. A. Junk and J. J. Richard, *Anal. Chem.*, 60 (1988) 451.
18 D. A. Hinckley and T. F. Bidleman, *Environ. Sci. Technol.*, 23 (1989) 995.
19 G. M. Telling, *Proc. Anal. Div. Chem. Soc.*, 20 (1979) 38.
20 *Off. J. Eur. Communities*, No. L 340/26 of 12/09/76 (Council Directive 76/895/EEC).
21 *Off. J. Eur. Communities*, No. L 194/34 of 7/25/75 (Council Directive 75/440/EEC).

Journal of Chromatography, 607 (1992) 47–53
Elsevier Science Publishers B.V., Amsterdam

CHROM. 24 344

Complementary use of counter-current chromatography and preparative reversed-phase high-performance liquid chromatography in the separation of a synthetic mixture of brominated tetrachlorofluoresceins☆

Adrian Weisz and Alan L. Scher

Division of Colors and Cosmetics, US Food and Drug Administration, Washington, DC 20204 (USA)

Denis Andrzejewski

Division of Contaminants Chemistry, US Food and Drug Administration, Washington, DC 20204 (USA)

Yoichi Shibusawa and Yoichiro Ito

Laboratory of Biophysical Chemistry, National Heart, Lung, and Blood Institute, National Institutes of Health, Bethesda, MD 20892 (USA)

(First received February 12th, 1992; revised manuscript received May 4th, 1992)

ABSTRACT

A synthetically prepared mixture of brominated 4,5,6,7-tetrachlorofluoresceins was separated by a combination of preparative reversed-phase high-performance liquid chromatography and high-speed counter-current chromatography. Two new lower-brominated subsidiary colors of D&C Red Nos. 27 and 28 (phloxine B), 4′,5′-dibromo-4,5,6,7-tetrachlorofluorescein and 2′,4′,5′-tribromo-4,5,6,7-tetrachlorofluorescein, were isolated and characterized by ^{1}H NMR and chemical ionization mass spectrometry.

INTRODUCTION

D&C Red No. 27 (mainly 2′,4′,5′,7′-tetrabromo-4,5,6,7-tetrachlorofluorescein, **1**, Colour Index No. 45410:1) and its disodium salt, D&C Red No. 28 (mainly phloxine B, **2**, Colour Index No. 45410), are xanthene color additives that are listed in the US Code of Federal Regulations (CFR) for use in drugs and cosmetics [1]. D&C Red No. 27 is manufactured by bromination of 4,5,6,7-tetrachlorofluorescein, **3**, and D&C Red No. 28 is manufactured by alkaline hydrolysis of **1** [1], as shown in Fig. 1. Among the impurities expected to be present in the color additives are lower-brominated subsidiary

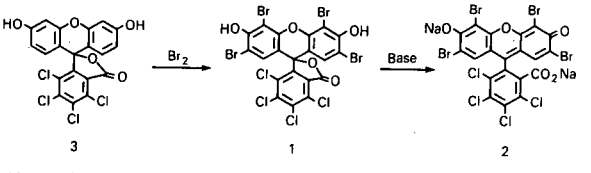

Fig. 1. Manufacture of D&C Red Nos. 27 (**1**) and 28 (**2**) from 4,5,6,7-tetrachlorofluorescein (**3**).

Correspondence to: Adrian Weisz, Food and Drug Administration, Division of Colors and Cosmetics (HFF-445), Center for Food Safety and Applied Nutrition, 200 C St., S.W., Washington, DC 20204, USA.

☆ Presented at *Chromexpo '91, Washington, DC, May 21, 1991.*

colors of **1** and **2** that are formed by substitution of **3** with fewer than four bromine atoms. Before they may be used as color additives, **1** and **2** are subject to batch certification by the US Food and Drug Administration (FDA) to assure compliance with the specifications set forth in the CFR. The current specifications for D&C Red Nos. 27 and 28 limit the total amount of lower-halogenated subsidiary colors, including the lower-brominated subsidiary colors, to $\leqslant 4\%$ (w/w) [1]. In the development and validation of a reversed-phase high-performance liquid chromatographic (RP-HPLC) method for the analysis of **1** and **2** that are submitted to the FDA for certification, pure lower-brominated subsidiary colors were needed as reference materials. An attempt to prepare 4′,5′-dibromotetrachlorofluorescein by partial bromination of **3** yielded a complex mixture shown by analytical RP-HPLC to contain four main components. This mixture was separated by preparative RP-HPLC into fractions containing pure 4′,5′-dibromotetrachlorofluorescein and other fractions containing multiple components. Fractions containing a mixture that included one of the major products were combined and further separated by high-speed counter-current chromatography (HSCCC) [2,3]. HSCCC was chosen for this separation because it was previously used successfully to purify the tetrabrominated analogues, **1** and **2** [4].

This paper describes the application of HSCCC as a complement to preparative RP-HPLC in the separation of a complex mixture containing various brominated tetrachlorofluoresceins.

EXPERIMENTAL

Materials

Ammonium acetate (NH_4OAc), methanol, water, ethyl acetate and *n*-butanol were chromatography grade. Deuterium oxide (99.9%, MSD Isotopes, Montreal, Canada), sodium deuteroxide (99.9%, *ca.* 40% in ^2H_2O, Fluka, Buchs, Switzerland), bromine (99.5%, Aldrich, Milwaukee, WI, USA), and 4,5,6,7-tetrachlorofluorescein (Thomasset Colors, now Hilton Davis Co., Cincinnati, OH, USA) were used as received.

Synthesis of the brominated tetrachlorofluorescein mixture

A crude mixture of brominated tetrachlorofluoresceins was prepared by brominating tetrachlorofluorescein following the preparation of 4′,5′-dibromofluorescein [5]. Thus, a *ca.* 5°C solution of sodium hypobromite (from 3.84 g, 24 mmol of bromine in 50 ml of 1 *M* NaOH) was added to a stirred *ca.* 5°C solution (cooled in an ice–water bath) of the disodium salt of tetrachlorofluorescein (from 4.7 g, 10 mmol of tetrachlorofluorescein and 100 ml of 0.4 *M* NaOH) over 10 min. After 10 min of additional stirring, the solution was acidified with 3 *M* HCl until no further precipitate formed. The precipitate was filtered, washed (5 × 30 ml water), and dried (130 mmHg, 100°C, 5 h), yielding an orange powder (7.25 g).

Preparative RP-HPLC

Preparative RP-HPLC was performed using a Waters Delta Prep 3000 system and a Waters Delta-Pak C_{18} preparative cartridge column (15 μm particle size, 100 Å pore size, 300 × 47 mm I.D.) in a Waters 1000 PrepPAK module. Detection was at 254 nm with a Linear UVIS 204 detector and a variable-pathlength preparative flow cell adjusted to 0.05 mm. The eluents, A = water, B = methanol and C = 1.00 *M* aqueous NH_4OAc, were sparged with helium. The column was washed with methanol and equilibrated at 40 ml/min with A–B–C (55:40:5) for 6 min and then with A–B–C (45:50:5) for 5 min. A solution of the diammonium salt prepared from 2 g of the crude brominated tetrachlorofluoresceins in 74 ml of water, 5 ml of 5% NH_4OH, 1.5 g of NH_4OAc, and 31 ml of methanol was syringe-filtered through a Millipore Millex-HV 0.45-μm pore size, 25-mm diameter filter unit. The filtrate was pumped onto the column at 15 ml/min and the column was eluted at 40 ml/min with a 90-min linear gradient from A–B–C (45:50:5) to B–C (95:5). Over 46 fractions were collected with volumes of *ca.* 20 ml when there were major peaks, *ca.* 50 ml when there were weaker and tailing peaks, and *ca.* 100 ml or more when there was little detector response. Diluted aliquots of these fractions were analyzed by analytical RP-HPLC.

Analytical RP-HPLC

The system consisted of a Model 8800 ternary pump, Model 8500 dynamic mixer, Model 8780 autosampler and Model 4270 integrator (all Spectra-Physics, San Jose, CA, USA), and a Model 490 dual-wavelength UV–VIS detector set at 254 and

546 nm (Waters Assoc., Milford, MA, USA). The autosampler was equipped with a Model 7010 injector (Rheodyne, Cotati, CA, USA) with a 200-μl sample loop. A Hypersil MOS-1 RPC-8 column (5 μm particle size, 250 × 4.6 mm I.D., Keystone Scientific, Bellefonte, PA, USA) was used throughout.

Eluents were 0.1 *M* aqueous NH_4OAc and methanol. The column was eluted using consecutive linear gradients of 25 to 90% methanol in 25 min, 90 to 100% methanol in 5 min, and 100% methanol for 5 min. The column was re-equilibrated with 25% methanol for 15 min. Other conditions were injection volume 20 μl, full scale response 0.128 absorbance, and flow-rate 1 ml/min.

An aliquot of each desired fraction from the preparative RP-HPLC and HSCCC separations was diluted with approximately 3 ml of methanol–0.1 *M* aqueous NH_4OAc (50:50, v/v). The solution was filtered through a LID/X glass microfiber syringeless filter unit AQOR.45 (Genex, Gaithersburg, MD, USA) prior to chromatography.

Isolation of fluorescein dyes from preparative RP-HPLC and HSCCC fractions

The dyes were isolated in the lactone form as the following example shows. Fractions 30–33 from the preparative RP-HPLC separation were combined and concentrated to *ca.* 1 ml on a rotary evaporator at 25 and 30 mmHg at *ca.* 50°C. The residue was acidified with 10–15 ml of 10% HCl and the precipitated lactones were extracted into ethyl acetate. The organic layer was washed (2 × 10 ml water) and dried (anhydrous Na_2SO_4), and the solvent was evaporated, yielding *ca.* 100 mg orange solid.

Preparative high-speed counter-current chromatography

The commercial high-speed counter-current chromatograph (P.C. Inc., Potomac, MD, USA) [6] holds an Ito multilayer-coil separation column and a counterweight whose centers revolve 10 cm around the centrifugal axis. The column consists of approximately 150 m × 1.6 mm I.D. polytetrafluoroethylene tubing with a total capacity of approximately 300 ml. The β value [7] ranges from 0.5 at the internal terminal to 0.85 at the external terminal.

The two-phase solvent system, composed of ethyl acetate–*n*-butanol–(0.01 *M* aqueous NH_4OAc adjusted to pH 8.6 with ammonium hydroxide) (1:1:2), was selected on the basis of previous experience with HSCCC purification of **2** [4]. The solvent system was thoroughly equilibrated in a separatory funnel and the two phases were separated shortly before use.

The column was completely filled with the stationary (upper) phase by using a metering pump (Milton Roy minipump; LDC Analytical, Riviera Beach, FL, USA). The lactone mixture (*ca.* 100 mg, isolated from fractions 30–33 of the preparative RP-HPLC separation as described above) was dissolved in a mixture of 10 ml solvent system (5 ml each of the upper and lower phases) and 100 μl of 30% ammonium hydroxide. This solution was injected into the column by syringe. The mobile (lower) phase was then pumped into the column at 2 ml/min while the column was rotated at 800 rpm. The column effluent was monitored with a UV detector (Uvicord S; LKB Instruments, Stockholm, Sweden) at 280 nm, and 4-ml fractions were collected (Ultrorac, LKB Instruments).

Mass spectrometry

The positive ion chemical ionization (PICI) mass spectra were obtained on a Finnigan Mat TSQ-46 instrument interfaced to an INCOS 2300 data system with TSQ software (Revision D). The spectrometer had a source temperature of 100°C, emission of 0.35 mA at 70 eV, 0.25 Torr methane, pre-

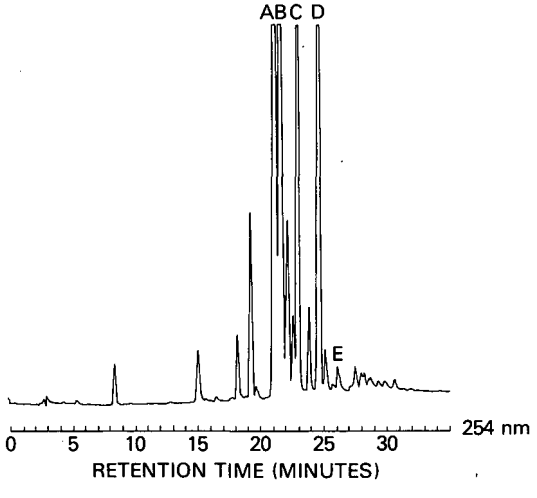

Fig. 2. Analytical RP-HPLC of the crude brominated tetrachlorofluorescein. See text.

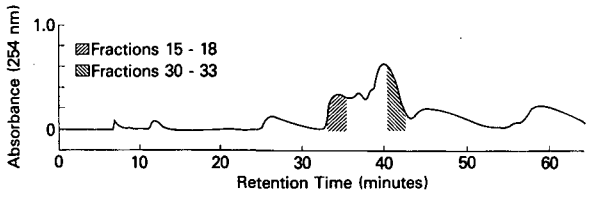

Fig. 3. Overloaded preparative RP-HPLC separation of the crude brominated tetrachlorofluorescein.

amplifier setting of 10^{-8} A/V, and conversion dynode of -5 kV, and was scanned from m/z 65 to 765 in 1.0 sec. The fluoresceins (lactone form, obtained as described above) were dissolved in either ethyl acetate or methanol and were introduced via the direct chemical ionization (DCI) probe at a heating rate of 20 mA/s. Fragmentation patterns m/z (relative intensity): peak A (Fig. 4b): 625 (26.2, MH^+), 580 [2.6, $(M-CO_2)^{+}\cdot$], 545 [0.7, $(M-CO_2-Cl)^+$]; peak B (Fig. 8b): 469 (74.1, MH^+), 424 [11.8, $(M-CO_2)^{+}\cdot$], 389 [5.6, $(M-CO_2-Cl)^+$]; peak C (Fig. 7b): 703 (12.4, MH^+), 658 [1.1, $(M-CO_2)^{+}\cdot$], 623 [0.4, $(M-CO_2-Cl)^+$].

^1H Nuclear magnetic resonance

^1H NMR spectra were obtained on a Varian XL 200 Fourier transform NMR spectrometer at 200 MHz. Typical concentrations were 4 mg compound (lactone form, see above) in 0.5 ml of 0.5% NaO^2H in ^2H_2O. Peak A (Fig. 4c): 7.19 ppm (d, H-a), 6.81 ppm (d, H-b). Peak B (Fig. 8c): 7.18 ppm (d, H-a), 6.72 ppm (d, H-b), 6.68 ppm (s, H-c). Peak C (Fig. 7c) 7.50 ppm (s, H-a), 7.10 ppm (d, H-b), 6.80 ppm (d, H-c).

RESULTS AND DISCUSSION

In adapting the published method for the preparation of 4′,5′-dibromofluorescein by bromination of fluorescein [5], it was expected that 4′,5′-dibromotetrachlorofluorescein would be the single major product of bromination of 4,5,6,7-tetrachlorofluorescein. Instead, the reaction resulted in a complex mixture as shown by analytical RP-HPLC (Fig. 2). B and D, two of the four major peaks, had retention times matching those of the unbrominated and tetrabrominated dyes, **3** and **2** (Fig. 1), respectively. Because the two other major peaks were probably

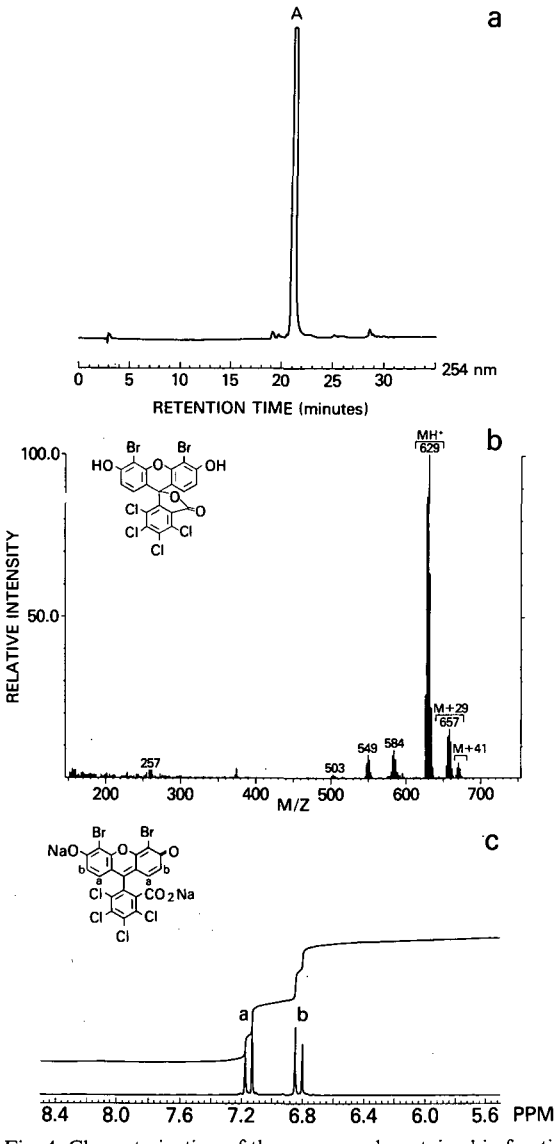

Fig. 4. Characterization of the compound contained in fractions 15–18 of the preparative RP-HPLC separation (see Fig. 3). (a) Analytical RP-HPLC of fraction 17, (b) positive ion chemical ionization (methane) mass spectrum of fraction 17, (c) ^1H NMR spectrum of fraction 17 (in $NaO^2H/^2H_2O$, 200 MHz).

lower-brominated subsidiary colors of D&C Red Nos. 27 and 28, separation of 2 g of the mixture by preparative RP-HPLC was attempted. This overloaded separation yielded several peaks (Fig. 3), and the eluate corresponding to two of these peaks was collected in fractions 15–18 and 30–33.

Fractions 15–18 contained a single component

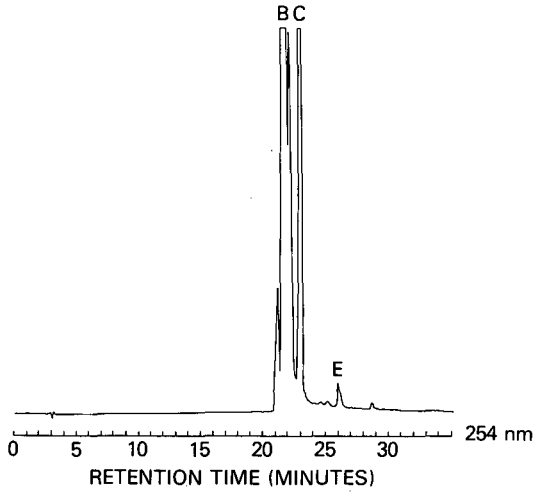

Fig. 5. Analytical RP-HPLC of combined fractions 30–33 (see Fig. 3).

whose HPLC peak (Fig. 4a) corresponded to peak A in Fig. 2. This component was isolated as the lactone (94 mg) and identified, by MS and ^{1}H NMR, as 4′,5′-dibromotetrachlorofluorescein (Fig. 4b and c).

The analytical RP-HPLC of fractions 30–33 (Fig. 5) produced two main peaks that corresponded to peaks B and C in Fig. 2. To separate this mixture (approximately 100 mg), the counter-current chromatographic method developed previously to purify the tetrabrominated dye [4] was chosen over the

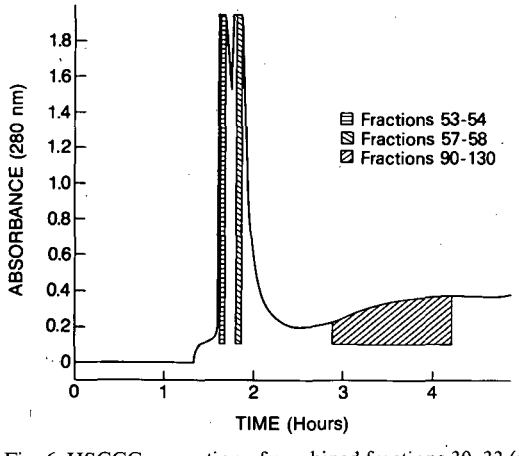

Fig. 6. HSCCC separation of combined fractions 30–33 (see Fig. 3).

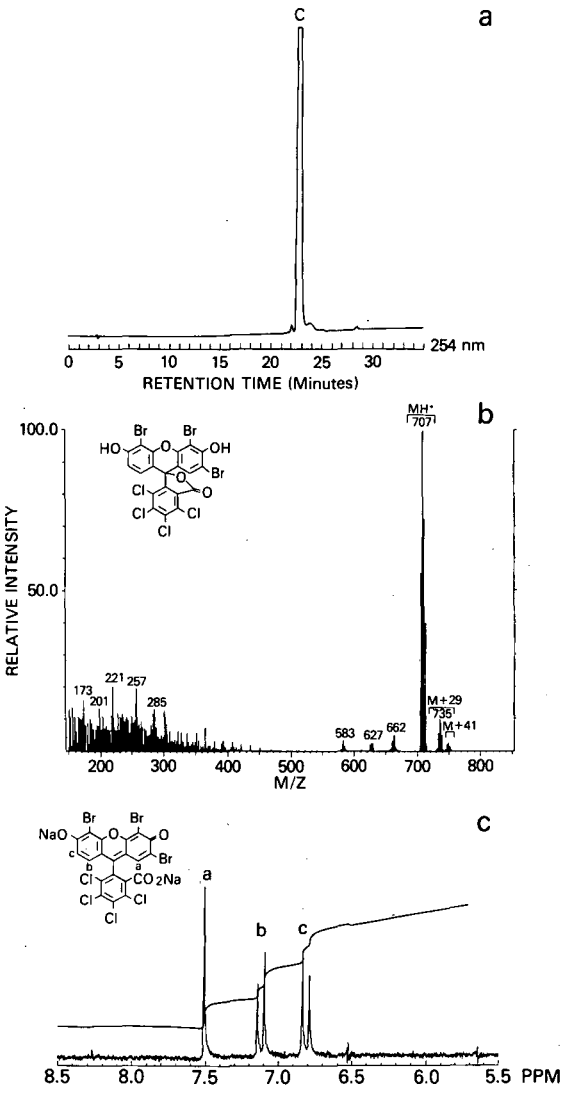

Fig. 7. Characterization of the compound contained in fractions 57–58 of the HSCCC separation (see Fig. 6). (a) Analytical RP-HPLC of HSCCC fraction 58, (b) positive ion chemical ionization (methane) mass spectrum of fraction 58, (c) ^{1}H NMR spectrum of fraction 58 (in $NaO^2H/^2H_2O$, 200 MHz).

feasible alternative of using the preparative HPLC procedure with the lower load. The HSCCC separation of the mixture resulted in three peaks, and the corresponding eluate was collected in fractions 57–58, 90–130, and 53–54 (Fig. 6).

HSCCC fractions 57–58 contained a single component whose HPLC peak (Fig. 7a) corresponded

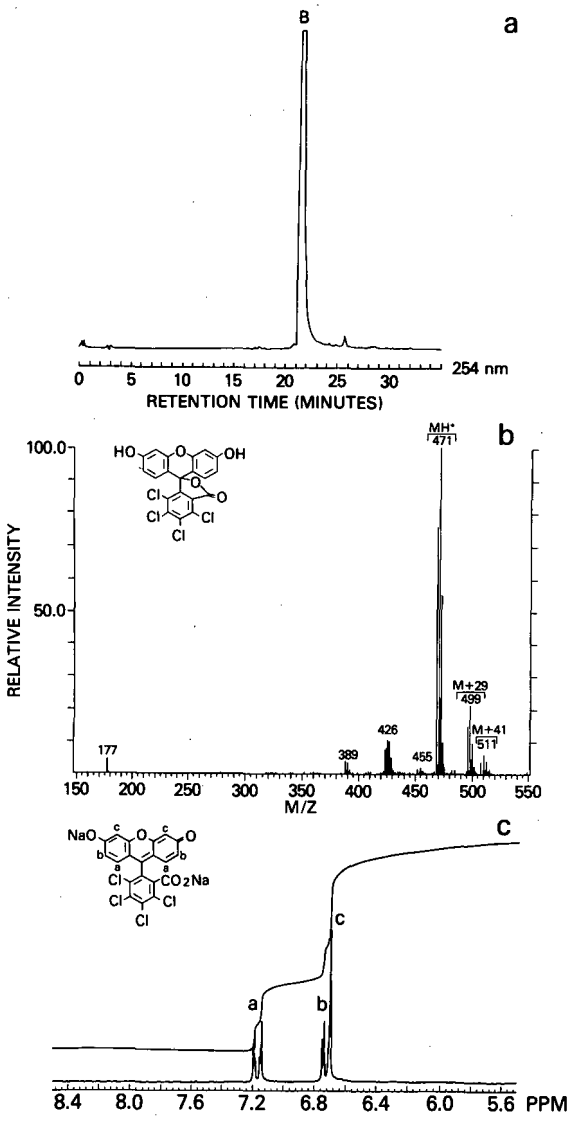

Fig. 8. Characterization of the compound contained in fractions 90–130 of the HSCCC separation (see Fig. 6). (a) Analytical RP-HPLC of combined fractions 90–130, (b) positive ion chemical ionization (methane) mass spectrum of combined fractions 90–130, (c) ^1H NMR spectrum of combined fractions 90–130 (in $NaO^2H/^2H_2O$, 200 MHz).

to peak C in Fig. 2. The compound was isolated as the lactone (20 mg) and identified by MS and ^1H NMR as 2′,4′,5′-tribromotetrachlorofluorescein (Fig. 7b and c).

HSCCC fractions 90–130 contained one compound whose HPLC peak (Fig. 8a) corresponded to peak B in Fig. 2. The compound was isolated as the lactone (12 mg) and identified by MS and ^1H NMR as the unbrominated starting material, 4,5,6,7-tetrachlorofluorescein (Fig. 8b-c).

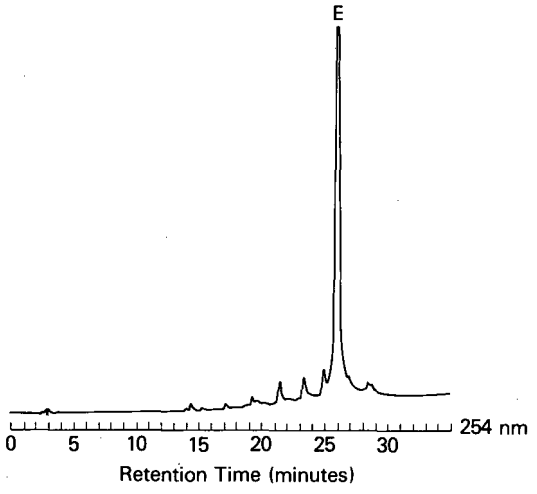

Fig. 9. Analytical RP-HPLC of HSCCC fraction 53 (see Fig. 6).

HSCCC fractions 53–54 contained a major component, whose HPLC peak (Fig. 9) corresponded to the minor peak E in Fig. 2, and several minor components. To date, peak E remains unidentified.

CONCLUSIONS

This work demonstrates that HSCCC can be used in combination with other chromatographic techniques to successfully separate complex mixtures. The use of silica gel HPLC followed by HSCCC [8] and the use of HSCCC followed by RP-HPLC [9], both on an analytical scale, to substantially improve purification of various compounds has been previously reported. To our knowledge, this work represents the first reported coupling of HSCCC and RP-HPLC for purification on a preparative scale. Two new lower-brominated subsidiary colors of D&C Red Nos. 27 and 28 (phloxine B), 4′,5′-dibromo-4,5,6,7-tetrachlorofluorescein and 2′,4′,5′-tribromo-4,5,6,7-tetrachlorofluorescein, were isolated and characterized by ^1H NMR and chemical ionization MS.

ACKNOWLEDGEMENT

The authors are indebted to Dr. Robert J. Highet, National Institutes of Health, Bethesda, MD, USA, for valuable advice and assistance in producing and interpreting the NMR spectra.

REFERENCES

1 *Code of Federal Regulations*, Title 21, Part 74, US Government Printing Office, Washington, DC, 1991.
2 Y. Ito, J. Sandlin and W. G. Bowers, *J. Chromatogr.*, 244 (1982) 247–258.
3 Y. Ito, *CRC Crit. Rev. Anal. Chem.*, 17 (1986) 65–143.
4 A. Weisz, A. J. Langowski, M. B. Meyers, M. A. Thieken and Y. Ito, *J. Chromatogr.*, 538 (1991) 157–164.
5 C. Graichen and J. C. Molitor, *J. Assoc. Off. Anal. Chem.*, 42 (1959) 149–160.
6 Y. Ito, in N. B. Mandava and Y. Ito (Editors), *Countercurrent Chromatography: Theory and Practice*, Marcel Dekker, New York, 1988, p. 823.
7 Y. Ito, *J. Chromatogr.*, 301 (1984) 387–403.
8 I. Hanbauer, A. G. Wright, Jr. and Y. Ito, *J. Liq. Chromatogr.*, 13 (1990) 2363–2372.
9 J. A. Apud and Y. Ito, *J. Chromatogr.*, 538 (1991) 177–185.

Journal of Chromatography, 607 (1992) 55–67
Elsevier Science Publishers B.V., Amsterdam

CHROM. 24 329

Studies on the methanolysis of small amounts of purified phospholipids for gas chromatographic analysis of fatty acid methyl esters

K. Eder, A. M. Reichlmayr-Lais and M. Kirchgessner

Institut für Ernährungsphysiologie, Technische Universität München, 8050 Freising-Weihenstephan (Germany)

(First received January 7th, 1992; revised manuscript received April 22nd, 1992)

ABSTRACT

The methanolysis of small amounts of purified phosphoglycerides and sphingomyelin was studied and a quantitative comparison of five methods for the methanolysis of standard phosphoglycerides was made. These methods were based on methanolysis with boron trifluoride–methanol, methanolic sodium methoxide (at ambient temperature and with heating) and methanolic sulphuric acid. A further method was based on saponification with methanolic sodium hydroxide and subsequent esterification with boron trifluoride–methanol. Under the experimental conditions, only the sodium methoxide-catalysed method at ambient temperature gave complete methanolysis of phosphoglycerides. For methanolysis of sphingomyelin, boron trifluoride–methanol, methanolic sulphuric acid and methanolic hydrochloric acid were used. It was found that complete methanolysis of sphingomyelin takes 15 h at 90°C. Based on these results, procedures for the methanolysis of phosphoglycerides and sphingomyelin separated by high-performance liquid chromatography are presented.

INTRODUCTION

For the quantification of phospholipid classes in biological materials, thin-layer chromatographic separation with subsequent densitometric or spectrophotometric measurement of phospholipid phosphorus is the most widely used procedure [1–4]. Newer methods often measure phospholipids, which have been separated by thin-layer chromatography or high-performance liquid chromatography (HPLC), by determining total phospholipid-bound fatty acids by gas chromatography (GC) [5,6]. This procedure allows a more precise measurement of phospholipid classes than phosphorimetry, because the molecular mass of bound fatty acids is taken into consideration.

For the quantification of phospholipid classes by fatty acid analysis, a complete conversion of phospholipid-bound fatty acids into fatty acid methyl esters (FAMEs) is necessary. For methanolysis of phospholipids, many methods have been published. Most of them use boron trifluoride–methanol [7–10], diazomethane [11,12], methanolic sulphuric or hydrochloric acid [13,14], methanolic sodium methoxide [15–18] and quaternary ammonium hydroxides [19–21]. Other reagents for methanolysis, seldom used, include methanolic acetyl chloride [22], methanolic aluminium chloride [23] and methanolic methyl iodide [24]. There are also methods involving saponification with subsequent esterification [25,26]. All these methods for preparing FAMEs have been reviewed [27,28]. Moreover, studies comparing different methods have been published [12,29,30]. However, most of these methods have been applied to standards or samples containing milligrams to grams of triacylglycerols [27], and there is little information about the methanolysis of very small amounts of phospholipids. Therefore, in

Correspondence to: Dr. M. Kirchgessner, Institut für Ernährungsphysiologie, Technische Universität München, 8050 Freising-Weihenstephan, Germany.

0021-9673/92/$05.00

this work various methods were applied to the methanolysis of phospholipid standards in small amounts in order to check the rate of conversion of bound fatty acids into FAMEs. In the first part of the study, various methods were used for the methanolysis of standard phosphoglycerides. In the second part, methanolysis of sphingomyelin was investigated by using various reagents and experimental conditions. This paper also presents methods for the methanolysis of phosphoglycerides and sphingomyelin from erythrocyte membranes in microgram amounts separated by high-performance liquid chromatography (HPLC).

EXPERIMENTAL

Materials

All chemicals were purchased from Merck (Darmstadt, Germany) with the exception of boron trifluoride–methanol reagent (100 g/l, puriss.), which was from Fluka (Buchs, Switzerland), and fatty acid and phospholipid standards, which were from Sigma (Taufkirchen, Germany). Phospholipid standards were phosphatidylcholine (PC, from egg yolk, hydrogenated), phosphatidylethanolamine (PE, synthetic, dipalmitoyl; and PE, from bovine brain, containing *ca.* 60% plasmalogen); phosphatidylserine (PS, from bovine brain), lyso-phosphatidylcholine (LPC, from egg yolk), lyso-phosphatidylethanolmine (LPE, from egg yolk) and sphingomyelin (SM, from bovine brain). A "phospholipid standard from egg" purchased from Merck was also used. Blood samples were taken from adult female Sprague–Dawley rats.

FAMEs were analysed using a GC system which consists of a Siemens (Karlsruhe, Germany) Sichromat 2 gas chromatograph equipped with a temperature-programmed vaporizing (PTV) injection system, a Chrompack (Middelburg, Netherlands) wall-coated open-tubular fused-silica (CP-Sil 88) column (50 m × 0.25 mm I.D., film thickness 0.2 μm), a flame ionization detector (FID) and a Merck–Hitachi D-2500 integrator. HPLC separation of erythrocyte membrane phospholipids was carried out with a Merck–Hitachi HPLC system (L-6200 intelligent pump, L-3000 multi-channel photodetector, D-2000 integrator) with a 25 cm × 0.4 cm I.D. Si 60 (5 μm) cartridge (LiChroCART, Merck) and a Model 201 fraction collector (Gilson, Villiers-le-Bel, France).

Extraction and separation of erythrocyte membrane phospholipids

Extraction and separation of erythrocyte membrane phospholipids were carried out as described by Eder *et al.* [6,31]. Erythrocytes were washed three times with physiological saline, lysed by addition of distilled water and freezing. Erythrocyte membranes were washed three times according to Hanahan and Ekholm [32]. Phospholipids were extracted by the method of Peuchant *et al.* [33] using isopropanol as solvent. Erythrocyte membrane phospholipid classes were separated by HPLC using a gradient system based on the mobile phases (a) acetonitrile, (b) acetonitrile–H_3PO_4 (99.8:0.02) and (c) methanol–H_3PO_4 (99.8:0.02). Using this separation method, the major phospholipid classes of erythrocyte membranes (PS, PE, PC and SM) could be separated. Moreover, plasmalogens could be separated from diacyl phosphoglycerides, as plasmalogens were hydrolysed by the acidic mobile phase and hence eluted as 2-acyl lyso analogues [34–36]. Therefore, all the phosphoglycerides mentioned were purified phospholipids, which exist either as diacylphosphoglycerides or as plasmalogens. A 100-μl aliquot of the lipid extract containing phospholipids from *ca.* 170 μl of packed erythrocytes was injected manually. Phospholipid classes which were detected at 205 nm were collected automatically with a fraction collector. The mobile phase was evaporated and phospholipids were dissolved in chloroform–methanol (1:1) for methanolysis.

Methanolysis procedures

Methanolysis of phosphoglyceride standards

Standard solutions of each of the phospholipids PC, PE, PS, LPC and LPE were prepared in chloroform–methanol (1:1), containing butylated hydroxytoluene (BHT) at similar concentrations (0.5–1 mg/ml). A solution of "phospholipids from egg" was prepared in the same solvent at a concentration of 4.6 mg/ml. For investigation of methanolysis of each of these preparations, test tubes with PTFE-lined caps were used. Prior to methanolysis, a

known amount of methyl heptadecanoate (dissolved in *n*-hexane), as internal standard, was pipetted into the test-tube and the solvent removed by vacuum. After addition of the sample to be methanolysed, and before closing, the tubes were flushed with nitrogen. Methanolysis was carried out by one of the procedures A–E detailed below. On completion of the methanolysis reaction, 0.5 ml of water was added to the reaction mixture and the FAMEs were extracted twice with 0.5-ml amounts of *n*-hexane. After separation from the aqueous phase, the pooled hexane layers contained the FAMEs, which were then suitable for GC analysis.

Procedure A was a modification of the method of Morrison and Smith [7]: 1 ml of phospholipid solution and 2 ml of boron trifluoride–methanol reagent were added to the tubes containing methyl heptadecanoate. The solution was heated at 90°C for 30 min, cooled and the FAMEs were extracted.

Procedure B was a modification of the method of Butte [20]: 1 ml of phospholipid solution and 1 ml of 1 *M* methanolic sodium methoxide solution were added to the tubes containing methyl heptadecanoate. The tubes were heated at 75°C for 20 min, cooled and the FAMEs were extracted.

Procedure C was a modification of the method of Olegard and Svennerholm [37]: 1 ml of phospholipid solution and 1 ml of 1 *M* methanolic sodium methoxide solution were added to the tubes containing methyl heptadecanoate and the tubes were shaken at ambient temperature for 1 h, then the FAMEs were extracted.

Procedure D: 1 ml of phospholipid solution and 2 ml of 6% methanolic sulphuric acid were added to the tubes containing methyl heptadecanoate. The tubes were heated at 90°C for 2 h, cooled and the FAMEs were extracted.

Procedure E was a modification of the method of Slover and Lanza [25]: 1 ml of phospholipid solution and 1 ml of 1 *M* methanolic sodium hydroxide solution were added to the tubes containing methyl heptadecanoate. The tubes were heated at 90°C for 15 min. After the tubes had cooled, 2 ml of boron trifluoride–methanol reagent were added and the tubes were heated at 90°C for 15 min. The tubes were cooled and the FAMEs were extracted.

Methanolysis of plasmalogens

A standard solution of "PE from bovine brain", which contained *ca.* 60% plasmalogens, was prepared in chloroform–methanol (1:1), containing BHT, at a concentration of *ca.* 1 mg/ml. For methanolysis of this standard, boron trifluoride–methanol (according to procedure A above), methanolic sodium methoxide (according to procedure C) and methanolic sulphuric acid (according to procedure D) were used.

Methanolysis of sphingomyelin standard

A standard was prepared by dissolving sphingomyelin in chloroform–methanol (1:1), containing BHT, at a concentration of *ca.* 1 mg/ml. For investigation of methanolysis, tubes with PTFE lined caps were used. After addition of the sample to be methanolysed, and before closing, the tubes were flushed with nitrogen. On completion of the methanolysis reaction, 0.3 ml of water was added to the reaction mixture and FAMEs were extracted twice with 0.3-ml amounts of *n*-hexane. After separation from the aqueous phase, the pooled hexane layers contained the FAMEs, which were then suitable for GC analysis.

Time and concentration studies

Boron trifluoride–methanol methanolysis. Into each test-tube, 0.5 ml of sphingomyelin solution, 0.2 ml of *n*-hexane containing methyl heptadecanoate and 1 ml of boron trifluoride–methanol reagent were pipetted. The tubes were heated at 90°C for 1, 2, 6 or 15 h.

Sulphuric acid–methanol methanolysis. Into each test-tube, 0.5 ml of sphingomyelin solution, 0.2 ml of *n*-hexane containing methyl heptadecanoate and 1 ml of 6% or 15% methanolic sulphuric acid were pipetted (giving sulphuric acid concentrations of 1 and 2.5 *M*). To obtain a one-phase system, 0.5 ml of chloroform was added. Into other test-tubes, 0.2 ml of *n*-hexane containing methyl heptadecanoate was pipetted and the solvent was evaporated. A 0.5-ml volume of sphingomyelin solution, 0.5 ml of chloroform and 2 ml of 30% methanolic sulphuric acid were added (giving a sulphuric acid concentration of *ca.* 7.5 *M*). The tubes were heated at 90°C for 1, 2, 6 or 15 h.

In a further experiment, the effect of water on the rate of conversion was tested. For this, part of the

methanol (10% and 20%) was replaced with water. Methanolic hydrochloric acid was also used for methanolysis.

Methanolysis of erythrocyte membrane phospholipids separated by HPLC

Phospholipids separated by HPLC were collected, the solvent was evaporated and phospholipids were dissolved in 1 ml of chloroform–methanol (1:1). The phosphoglycerides were methanolysed with either methanolic sodium methoxide or boron trifluoride–methanol reagent. In the former instance, 4 ml of 0.5 *M* methanolic sodium methoxide solution were added to the test-tubes containing phosphoglyceride classes and the tube was shaken for 1 h. FAMEs were extracted twice by adding 2 ml each of *n*-hexane and water. The hexane phases were collected. In the latter instance, 2 ml of boron trifluoride–methanol reagent were added to the test-tubes, which were closed and heated at 90°C for 2 h. FAMEs were extracted twice by adding 0.5 ml each of *n*-hexane and water. Sphingomyelin was methanolysed using boron fluoride reagent. A 2-ml volume of boron trifluoride–methanol reagent was added to the test-tubes containing the sphingomyelin fraction. The tubes were closed and heated at 90°C for 15 h. FAMEs were extracted twice by adding 0.5 ml each of *n*-hexane and water.

Gas chromatographic analysis of FAMEs

FAMEs were analysed as described by Eder *et al.* [38]. A 0.5-μl portion of the FAME extract was injected manually into the GC system using a PTV system. For injection of FAMEs from phospholipid standards the splitting ratio was 1:20 and for injection of FAMEs from rat erythrocyte membranes it was 1:2. Hydrogen was used as the carrier gas at a flow-rate of 2.0 ml/min. The PTV programme was as follows: initial temperature, 40°C, held for 1 min, then increased at 800°C/min to 300°C, which was maintained for 10 min. The flame ionization detector temperature was 300°C. After an initial temperature of 50°C for 1 min, the oven temperature was increased at 25°C/min to 160°C, then at 15°C/min to 200°C, held at that temperature for 1.5 min, and subsequently increased at 10°C/min to 225°C, which was then maintained for a further 10 min. The amount of each FAME was calculated using C_{17} FAME as internal standard. As an example, the GC separation of FAMEs from phospholipids from egg is shown in Fig. 1.

Calculation of conversion rates

Conversion rates were calculated from the ratio between fatty acids converted into FAMEs and total phospholipid-bound fatty acids. The amounts of total phospholipid-bound fatty acids were calculated by determining the average molecular mass of the fatty acids, the molecular mass of the phospholipid core, the mass of total phospholipids and the amount (in percent) of fatty acids in the phospholipid molecule.

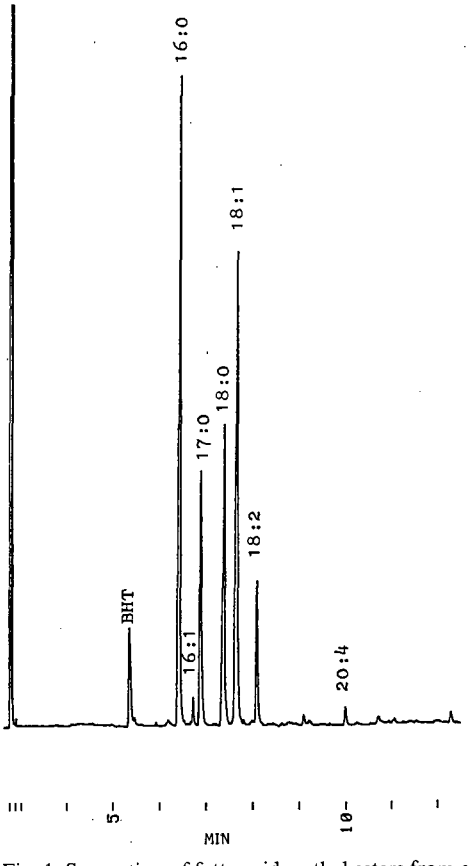

Fig. 1. Separation of fatty acid methyl esters from egg phospholipids obtained by methanolysis with methanolic sodium methoxide. Splitting ratio 1:20; 17:0 = internal standard; time scale in minutes.

RESULTS AND DISCUSSION

Methanolysis of phosphoglycerides

Various methods were applied to the methanolysis of small amounts of standard phospholipids and phospholipids from rat erythrocyte membranes separated by HPLC. In the first experiment, the rate of conversion of standard phospholipid bound fatty acids into FAMEs was checked using various methods based on methanolysis with (A) boron trifluoride–methanol (90°C, 30 min), (B) methanolic sodium methoxide (75°C, 20 min), (C) methanolic sodium methoxide (ambient temperature, 60 min) and (D) methanolic sulphuric acid (90°C, 2 h). Method E was based on saponification with methanolic sodium hydroxide and subsequent esterification with boron trifluoride–methanol. Rates of phospholipid-bound fatty acids converted into FAMEs using various methods are shown in Table I.

Of the methods investigated, only reaction with sodium methoxide at ambient temperature gave results that could be considered to be reasonable. For the other four methods, the yields of FAMEs from individual phospholipid classes were so variable and so lacking in reproducibility that they cannot be considered to be viable quantitative methods. Even in the case of reaction with sodium methoxide at ambient temperature, the yields were scattered to the extent that it would appear that there is still the need to improve control over the experimental conditions. Table II shows that methods A, B, D and E gave lower rates of conversion of both saturated and unsaturated fatty acids into FAMEs than the method based on sodium methoxide at ambient temperature. This indicates that the low yields of FAMEs produced by methods A, B, D and E are not due to oxidation of polyunsaturated fatty acids during heating, but to unreasonable experimental conditions in general. Similar results were obtained in the methanolysis of phospholipids from egg. The method based on sodium methoxide at ambient temperature gave the highest yields of FAMEs, whereas the yields of FAMEs obtained by methanolysis using the boron trifluoride method were smaller (Table III).

In a further experiment, phospholipids from rat erythrocyte membranes separated by HPLC were methanolysed using either methanolic sodium methoxide at ambient temperature for 1 h or boron

TABLE I

RATES OF PHOSPHOLIPID-BOUND FATTY ACIDS CONVERTED INTO FAMEs USING VARIOUS METHODS

Results are given in means ($n = 3$) and ranges (%)

Pl class[a]	Method				
	A[b]	B[c]	C[d]	D[e]	E[f]
PC	88	96	99	79	91
	(86–89)	(96–97)	(98–100)	(71–86)	(90–91)
PE	84	99	103	82	98
	(81–87)	(98–101)	(101–106)	(81–83)	(94–101)
PS	70	102	97	74	85
	(64–75)	(100–103)	(96–98)	(68–82)	(84–86)
LPC	83	93	98	80	83
	(82–86)	(93–94)	(96–99)	(79–82)	(81–84)
LPE	91	99	101	91	90
	(89–92)	(97–101)	(100–102)	(90–92)	(90–91)

[a] Phospholipid classes in amounts of 0.5–1 mg.
[b] A: boron trifluoride–methanol (30 min at 90°C).
[c] B: 0.5 *M* methanolic sodium methoxide (20 min at 75°C).
[d] C: 0.5 *M* methanolic sodium methoxide (1 h at ambient temperature).
[e] D: 6% methanolic sulphuric acid (2 h at 90°C).
[f] E: saponification with subsequent esterification.

TABLE II

AMOUNTS OF THE MOST IMPORTANT PHOSPHOLIPID-BOUND FATTY ACIDS CONVERTED INTO FAMEs USING VARIOUS METHODS

Results are mean (n = 3) μg FAMEs per mg of phospholipid.

Pl class	Fatty acid	Method				
		A[b]	B[c]	C[d]	D[e]	E[f]
PC	16:0	196	218	231	185	205
	18:0	353	423	438	350	402
	20:0	28	34	32	25	35
PE	16:0	617	729	759	597	716
PS	18:0	239	335	319	255	286
	18:1	170	231	218	177	192
	22:6	36	82	75	48	68
LPC	16:0	288	322	334	280	302
	18:0	118	135	145	112	102
	18:1	16	18	19	15	14
LPE	16:0	208	218	218	214	190
	18:0	298	336	345	290	310

[b–f] See Table I.

trifluoride–methanol at 90°C for 2 h. Both methods gave similar yields of fatty acids converted into FAMEs (Table IV). This result, showing that for methanolysis of erythrocyte membrane phospholipids the boron trifluoride method is equivalent to the sodium methoxide method, contrasts with the results of methanolysis of standard phosphoglycerides, showing that the sodium methoxide method is superior to the boron trifluoride method. The reason for this inconsistency might be that both methods used for methanolysis of standard phospholipids were modified in the experimental conditions for methanolysis of erythrocyte membrane phospholipids. Using the boron trifluoride method the period of heating used was 30 min for methanolysis of standard phospholipids whereas it was 2 h for methanolysis of erythrocyte membrane phospholipids. Hence it seems that 30 min are not sufficient for completion of methanolysis of phospholipids using boron trifluoride at 90°C. This result is in contrast to the results of Morrison and Smith [7], which showed that phosphoglycerides can be methanolysed completely at 100°C in 10 min. Surprisingly, methanolysis with methanolic sulphuric acid under conditions often used [39,40] also gave incomplete conversion of fatty acids from standard phospholipids into FAMEs. The incompleteness of methanolysis might be due to the period of heating, as Freedman *et al.* [41] found that complete methanolysis of vegetable oils using 1% methanolic sulphuric acid takes over 50 h at 65°C. Saponification with sodium hydroxide and subsequent esterification with boron trifluoride–methanol also gave incomplete methanolysis. In this instance the incompleteness might be due to the short period of saponification (15 min) and might not be due to the short period of esterification (15 min), as Morrison and

TABLE III

METHANOLYSIS OF PHOSPHOLIPIDS FROM EGG USING VARIOUS METHODS

Results are mean μg fatty acids converted into FAMEs per mg of phospholipids from egg, with ranges.

FAME	Method		
	A[a] (n=4)	B[b] (n=3)	C[c] (n=3)
16:0	187 (185–193)	264 (255–269)	258 (255–261)
16:1	9 (7–10)	11 (7–14)	12 (11–13)
18:0	73 (71–78)	94 (92–95)	107 (105–110)
18:1	125 (119–131)	173 (169–178)	185 (183–187)
18:2	46 (43–50)	62 (60–64)	65 (64–67)
20:4	6 (6–7)	8 (6–10)	9 (9–10)
Sum	447 (437–459)	611 (597–620)	636 (633–638)

[a] A: boron trifluoride–methanol (30 min at 90°C).
[b] B: 0.5 *M* methanolic sodium methoxide (20 min at 75°C).
[c] C: 0.5 *M* methanolic sodium methoxide (1 h at ambient temperature).

TABLE IV

METHANOLYSIS OF RAT ERYTHROCYTE MEMBRANE PHOSPHOLIPID CLASSES USING EITHER BORON TRIFLUORIDE OR SODIUM METHOXIDE

Results are μg phospholipid-bound fatty acids converted into FAMEs per 170 μl of packed erythrocytes (duplicate results).

Reagent	Sample No.	Phospholipid class				
		PS	PE	PE plasmalogens	PC	Sum
$NaOCH_3$[a]	1	44.2	58.7	51.8	192.1	346.8
	2	45.0	63.1	52.5	196.6	357.1
BF_3[b]	1	50.0	65.1	48.4	194.5	358.0
	2	47.6	61.7	51.7	189.0	350.0

[a] Ambient temperature, 1 h.
[b] 90°C, 2 h.

Smith [7] found that esterification of free fatty acids using boron fluoride is complete within 2 min. On the other hand, there are studies showing that phospholipids cannot be saponified completely [27].

Although in this study methods A, C and D did not give complete methanolysis of phosphoglyceride standards, it should be noted that this does not mean that the reagents used are not useful for methanolysis but rather that the experimental conditions used in this study did not allow complete methanolysis. In fact, many studies have shown that methods using boron trifluoride–methanol [7,8,27,28] or methanolic sulphuric acid [14,27], as well as the saponification–esterification procedure [26,42], are suitable for the complete methanolysis of glycerides, provided that the reaction conditions are optimized.

The results using standard phospholipids indicate that methanolic sodium methoxide might be the most useful reagent for the methanolysis of phospholipids in small amounts. Many investigators have also shown that methanolic sodium methoxide might be more useful for the methanolysis of fats and oils than the widely used boron fluoride and other reagents [17]. On the other hand, in this study methanolysis of erythrocyte membrane phosphoglycerides with boron trifluoride–methanol reagent for 2 h gave similar yields of FAMEs to those obtained by methanolysis with sodium methoxide. However, methanolysis with sodium methoxide is faster and simpler than methanolysis with boron trifluoride and can be applied at ambient temperature, so that simple tubes such as centrifuge tubes can be used. This offers the possibility of the use of a one-vial procedure. In the method described, phospholipid classes were separated by HPLC. The eluate containing phospholipid classes was collected in 10-ml centrifuge tubes and the solvent was evaporated under vacuum at ambient temperature. Then methanolysis of phospholipids and extraction of FAMEs were carried out using the same tubes. Hence losses of phospholipids during transfer from one tube to another can be completely avoided. Therefore, the recoveries of phospholipids were *ca.* 100% (98.9% for PE, 101.8% for PC). Moreover, methanolysis at ambient temperature did not require BHT. This is undoubtedly advantageous because in some instances, in the GC analysis of FAMEs, methyl myristate or palmitoleate and BHT and its derivatives cannot be separated [43]. In Fig. 2 a typical GC separation of FAMEs from rat erythrocyte membrane PE obtained by methanolysis with the method described is shown.

Methanolysis of plasmalogens

The major phospholipids, namely PC and PE, exist in plasmalogen and non-plasmalogen subfractions [43,44]. In this study, a PE standard from bovine brain which contains *ca.* 60% plasmalogen was methanolysed using boron trifluoride–methanol reagent, methanolic sulphuric acid and methanolic sodium methoxide. Methanolysis of PE plasmalogen with boron trifluoride–methanol and methanol-

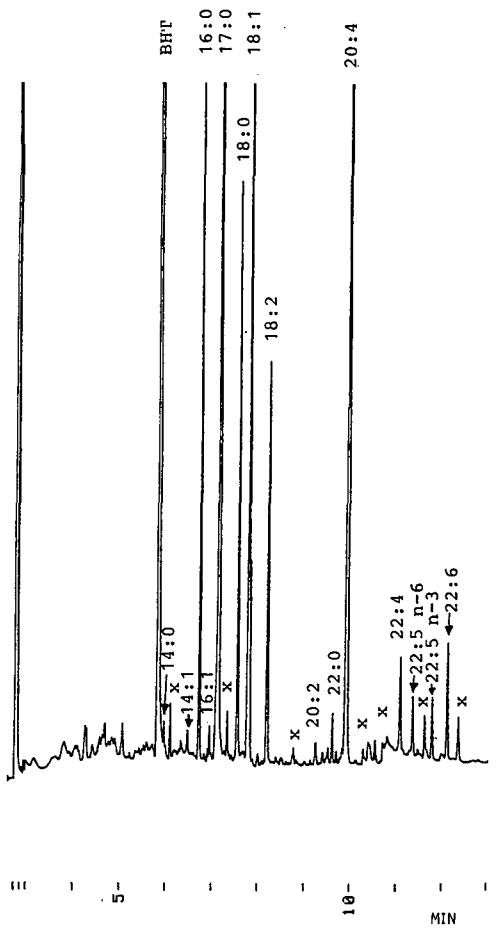

Fig. 2. Separation of fatty acid methyl esters from rat erythrocyte membrane phosphatidylethanolamine obtained by methanolysis with methanolic sodium methoxide. Splitting ratio 1:2; 17:0 = internal standard; time scale in minutes; x = unidentified peak.

ic sulphuric acid resulted in the formation of dimethylacetals (DMAs), which interfered with the GC separation of FAMEs (Fig. 3a and b). Using the conditions described, peaks of FAME 17:0 and DMA 18:0 could not be separated. However, the formation of DMAs was prevented if PE plasmalogen was methanolysed with sodium methoxide (Fig. 3c). This observation is in agreement with the results of other studies [45], also showing that DMA formation from plasmalogen aldehydes can be prevented by base-catalysed methanolysis. Hence, methanolic sodium methoxide is a useful reagent for the methanolysis of plasmalogens.

Another possibility for preventing DMA formation from plasmalogens is to hydrolyse the labile enol–ether binding prior to methanolysis by treatment of plasmalogens with concentrated HCl fumes [5] or 90% acetic acid [36,43]. If plasmalogens are injected into an HPLC system using a mobile phase containing phosphoric or sulphuric acid they are also hydrolysed during their passage through the column [5,34–36]. Thus plasmalogens elute as their 2-acyl lyso analogues. In this study, phospholipids from rat erythrocyte membranes were separated using a mobile phase containing 0.2% of orthophosphoric acid (85%). GC determination of the methylated fatty acids showed that the lyso-PE fraction eluted corresponds to the PE plasmalogen injected into the HPLC system as there is a large portion of polyunsaturated fatty acids with 20 and 22 carbon atoms which is typical of erythrocyte plasmalogens [43] (Fig. 4). Moreover, the chromatogram shows that there were no DMAs formed during methanolysis with boron trifluoride–methanol reagent.

Methanolysis of sphingomyelin

Sphingomyelin is extremely resistant to alkali treatment because fatty acids exist as amides rather than as esters. Therefore, methanolic inorganic acids such as hydrochloric and sulphuric acid and also boron trifluoride–methanol are the most often used catalysts for the methanolysis of sphingomyelin [7,46–49]. However, in the literature there is little information about experimental conditions that ensure complete methanolysis of sphingomyelin. Moreover, the published results are not consistent. For example, Morrison and Smith [7] found that when using boron trifluoride–methanol, methanolysis of sphingomyelin is complete within 75 min. In studies by MacGee and Williams [50], the rate of conversion of fatty acids from sphingomyelin into FAMEs using boron trifluoride–methanol reagent was only 25% within 2 h. Therefore, in this study, methanolysis was carried out using boron trifluoride and methanolic sulphuric acid in order to investigate the effect of the period of heating on the rates of conversion of sphingomyelin fatty acids. Our results are in agreement with those of MacGee

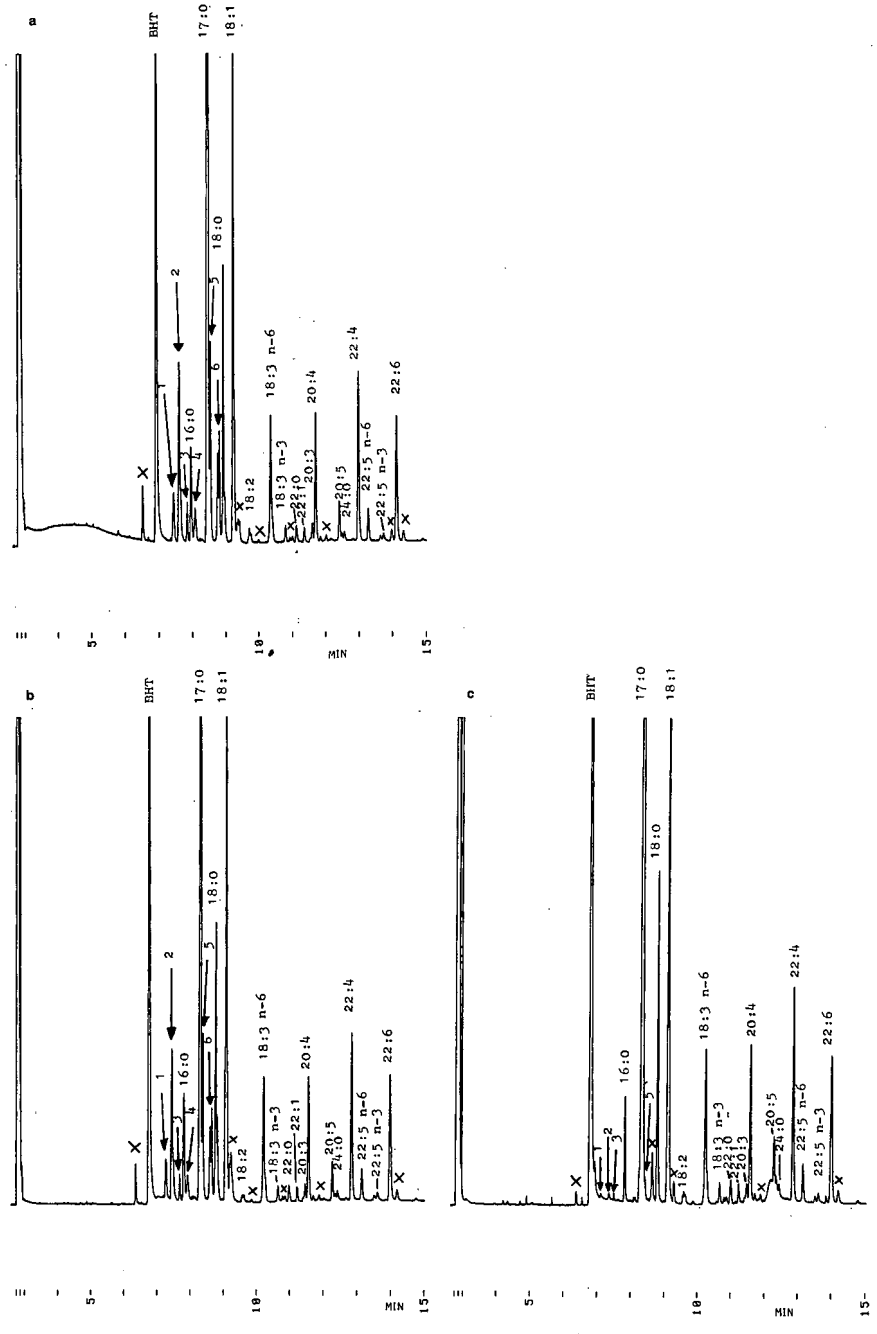

Fig. 3. Separation of fatty acid methyl esters from bovine brain phosphatidylethanolamine containing 60% plasmalogens. Fatty acid methyl esters were prepared using (a) boron trifluoride–methanol reagent, (b) methanolic sulphuric acid and (c) methanolic sodium methoxide. Arrows indicate dimethylacetals formed during methanolysis; 17:0 = internal standard; time scale in minutes; x = unidentified peak.

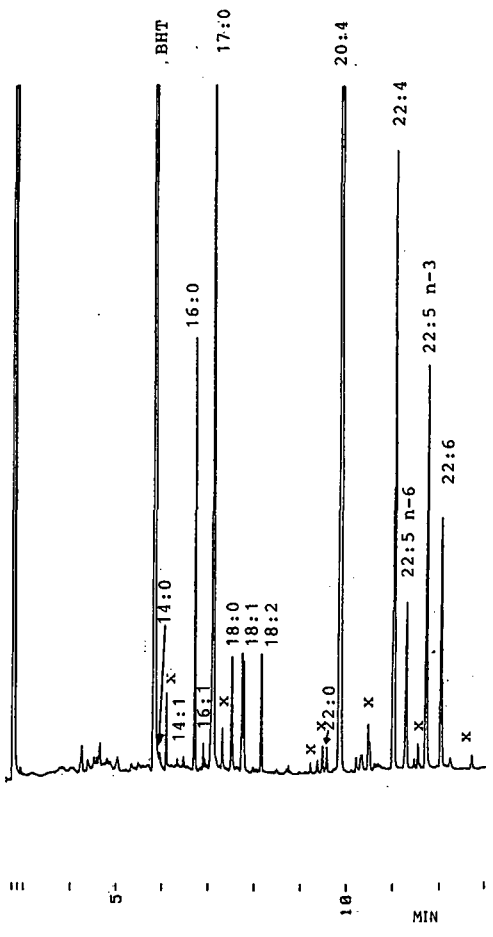

Fig. 4. Separation of fatty acid methyl esters from rat erythrocyte membrane phosphatidylethanolamine plasmalogen obtained by methanolysis with boron trifluoride–methanol reagent. Splitting ratio = 1:2; 17:0 = internal standard; time scale in minutes; x = unidentified peak.

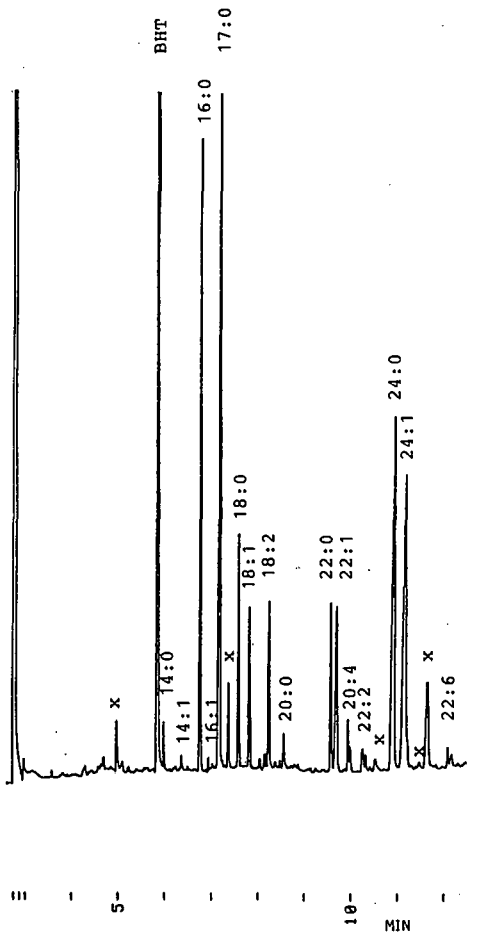

Fig. 5. Separation of fatty acid methyl esters from rat erythrocyte membrane sphingomyelin obtained by methanolysis with boron trifluoride–methanol reagent. Splitting ratio = 1:2; 17:0 = internal standard; time scale in minutes; x = unidentified peak.

and Williams [50], showing that very long periods of heating are necessary for complete conversion of sphingomyelin fatty acids into FAMEs using both boron trifluoride and methanolic sulphuric acid (1 and 2.5 *M*) (Table V).

Using methanolic sulphuric acid and boron trifluoride–methanol, complete methanolysis was achieved after heating at 90°C over a period of 15 h. However, the rates of conversion for periods of 1, 2 and 6 h were higher for methanolic sulphuric acid than for boron trifluoride. Moreover, the period of heating required for complete methanolysis could not be shortened by increasing the concentration of sulphuric acid. Using 7.5 *M* methanolic sulphuric acid, the rate of conversion decreased with an increase in heating time. This phenomenon is due to oxidation of unsaturated fatty acids caused by high temperature and high concentration of sulphuric acid.

Although a large amount of BHT (100 μg) was added to each test-tube, the amounts of polyunsaturated FAMEs decreased with an increase in heating time (Table VI). On the other hand, the fatty acid composition of sphingomyelin standard ob-

TABLE V

EFFECT OF PERIOD OF HEATING ON RATES OF CONVERSION OF SPHINGOMYELIN FATTY ACIDS INTO FAMEs USING BORON TRIFLUORIDE OR METHANOLIC SULPHURIC ACIDS AT VARIOUS CONCENTRATIONS

Results are means ($n = 3$) and ranges (%)

Reagent	Period of heating (h)			
	1	2	6	15
BF_3	35.5 (32.6–37.3)	60.4 (58.1–63.1)	82.7 (82.0–83.2)	99.1 (98.6–99.4)
1.0 *M* H_2SO_4	53.5 (52.7–54.2)	81.4 (79.4–83.0)	94.6 (93.0–96.0)	97.6 (96.3–99.6)
2.5 *M* H_2SO_4	75.5 (73.9–76.9)	87.6 (86.4–89.0)	92.4 (90.2–94.8)	100.3 (96.0–103.4)
7.5 *M* H_2SO_4	74.8 (73.5–76.2)	84.8 (83.6–85.5)	73.1 (71.5–74.4)	65.6 (64.8–66.2)

tained by methanolysis with boron trifluoride–methanol reagent and using various periods of heating was similar (Table VII). Moreover, the fatty acid composition of sphingomyelin standard obtained by methanolysis was similar using 1 and 2.5 *M* methanolic sulphuric acid and boron trifluoride (Table VIII).

Methanolic hydrochloric acid is also often used for the methanolysis of sphingomyelin [46–48]. In the present experiments, the rates of conversion of sphingomyelin fatty acids into FAMEs using 2.4 *M* methanolic hydrochloric acid and 2.25 *M* methanolic sulphuric acid were similar. Moreover, the addition of small amounts of water (200–400 μl, representing 10–20% of the total volume) did not influence the rate of conversion. On adding 0, 10 and 20% of water, the rates of conversion of sphingomyelin standard fatty acids into FAMEs using 2.25 *M* methanolic sulphuric acid were 97.9, 98.9 and 97.1% respectively, and using 2.4 *M* methanolic hydrochloric they were 99.9, 100.8 and 101.7% respectively. This indicates that methanolic acids are also useful for the methanolysis of sphingomyelin from extracts containing small amounts of water. However, 10% or more of water disturbs the methanolysis of sphingomyelin using methanolic acetyl chloride [22].

The method for the determination of fatty acid composition of sphingomyelin from rat erythrocyte membranes described used boron trifluoride as catalyst. The separation of FAMEs from rat erythrocyte membrane sphingomyelin obtained by this method is shown in Fig. 5.

TABLE VI

CONVERSION OF SPHINGOMYELIN FATTY ACIDS INTO FAMEs USING 7.5 *M* SULPHURIC ACID AND VARIOUS PERIODS OF HEATING

Results are mean μg sphingomyelin-bound fatty acids converted into FAMEs per mg of sphingomyelin ($n = 3$).

Fatty acid	Period of heating (h)			
	1	2	6	15
16:0	10.1	11.8	12.6	12.6
18:0	113.3	136.9	144.3	134.7
20:0	3.6	3.7	5.5	5.3
22:0	12.9	15.2	16.0	15.0
24:0	30.2	36.6	35.0	38.2
20:4	21.0	24.9	19.9	13.4
22:1	2.9	2.9	3.0	2.3
22:2	6.3	7.4	4.2	1.9
24:1	110.1	109.2	51.5	37.2

CONCLUSION

For the methanolysis of small amounts of phosphoglycerides, sodium methoxide is the most useful reagent. Sodium methoxide methanolysis of phosphoglycerides from rat erythrocyte membranes, separated by HPLC, can be carried out at ambient temperature using a one-vial procedure. This meth-

TABLE VII

FATTY ACID COMPOSITION OF SPHINGOMYELIN STANDARD OBTAINED BY METHANOLYSIS WITH BORON TRIFLUORIDE USING VARIOUS PERIODS OF HEATING

Results are mean mol% ($n = 3$) and ranges

Fatty acid	Period of heating (h)			
	1	2	6	15
16:0	4.6 (4.2–5.0)	4.7 (4.6–4.8)	4.6 (4.3–5.0)	3.9 (3.6–4.1)
18:0	43.1 (41.4–44.7)	44.5 (41.8–47.6)	41.1 (40.7–41.5)	42.7 (41.0–43.9)
20:0	1.3 (0.6–1.7)	0.9 (0.8–0.9)	1.1 (0.9–1.3)	0.9 (0.8–1.0)
20:4	7.4 (7.1–7.9)	7.4 (6.7–8.0)	8.9 (8.6–9.3)	7.6 (7.2–8.0)
22:0	3.6 (3.4–3.9)	3.9 (3.5–4.2)	4.3 (3.8–4.7)	3.7 (3.3–4.0)
22:1	1.2 (0.5–1.8)	1.1 (0.9–1.3)	1.2 (1.0–1.4)	0.9 (0.6–1.2)
22:2	1.8 (1.7–2.0)	1.7 (1.5–2.0)	1.3 (1.2–1.3)	1.9 (1.8–2.0)
24:0	6.7 (6.0–7.2)	6.3 (6.0–6.6)	6.8 (6.7–7.0)	7.9 (7.5–8.1)
24:1	30.3 (25.4–35.6)	29.5 (25.7–31.6)	30.7 (29.1–32.1)	30.5 (30.0–31.5)

TABLE VIII

FATTY ACID COMPOSITION OF SPHINGOMYELIN STANDARD OBTAINED BY METHANOLYSIS WITH BORON TRIFLUORIDE AND 1 AND 2.5 *M* METHANOLIC SULPHURIC ACID

Period of heating 15 h in each instance. Results are mean mol% ($n = 3$) and ranges

Fatty acid	Reagent for methanolysis		
	BF_3	1 *M* H_2SO_4	2.5 *M* H_2SO_4
16:0	3.9 (3.6–4.1)	4.3 (4.1–4.6)	4.2 (4.2–4.4)
18:0	42.7 (41.0–43.9)	42.2 (41.9–42.4)	41.5 (40.4–43.4)
20:0	0.9 (0.8–1.0)	0.9 (0.9–1.0)	0.9 (0.8–1.0)
20:4	7.6 (7.2–8.0)	6.8 (5.3–8.4)	7.5 (6.5–9.1)
22:0	3.7 (3.3–4.0)	3.9 (3.7–4.3)	4.3 (4.3–4.5)
22:1	0.9 (0.6–1.2)	1.0 (0.8–1.0)	0.9 (0.9–1.1)
22:2	1.9 (1.8–2.0)	1.5 (1.4–1.6)	1.3 (1.1–1.3)
24:0	7.9 (7.5–8.1)	8.0 (7.8–8.4)	9.0 (8.4–10.0)
24:1	30.5 (30.0–31.5)	31.4 (30.8–32.4)	30.4 (29.1–32.1)

od is simple and gives complete methanolysis, as was demonstrated by using phospholipid standards. For the methanolysis of sphingomyelin, boron trifluoride and also methanolic sulphuric and hydrochloric acid can be used. The study presented shows that complete methanolysis of sphingomyelin takes about 15 h.

REFERENCES

1 R. M. Broekhuyse, *Clin. Chim. Acta*, 23 (1969) 457.
2 W. W. Christie, *Z. Lebensm.-Unters.-Forsch.*, 181 (1985) 171.
3 C. Leray, X. Pelletier, S. Hemmendinger and J. P. Cazenave, *J. Chromatogr.*, 420 (1987) 411.
4 G. Freyburger, A. Heape, H. Gin, M. Boisseau and C. Cassagne, *Anal. Biochem.*, 171 (1988) 213.
5 M. Seewald and H. M. Eichinger, *J. Chromatogr.*, 469 (1989) 271.
6 K. Eder, A. M. Reichlmayr-Lais and M. Kirchgessner, *J. Chromatogr.*, 598 (1992) 33.
7 W. R. Morrison and L. M. Smith, *J. Lipid Res.*, 5 (1964) 600.
8 C. D. Bannon, J. D. Craske, N. T. Hai, N. L. Harper and K. L. O'Rourke, *J. Chromatogr.*, 247 (1982) 63.
9 L. D. Metcalfe and A. A. Schmitz, *Anal. Chem.*, 33 (1961) 363.
10 D. Firestone and W. Horowitz, *J. Assoc. Off. Anal. Chem.*, 62 (1979) 710.

11 H. Schlenk and J. L. Gellerman, *Anal. Chem.*, 32 (1960) 1412.
12 B. M. Craig and N. L. Murty, *J. Am. Oil. Chem. Soc.*, 36 (1959) 549.
13 I. Hornstein, J. A. Alford, L. E. Elliot and P. F. Crowe, *Anal. Chem.*, 32 (1960) 540.
14 W. Stoffel, F. Chu and E. H. Ahrens, Jr., *Anal. Chem.*, 31 (1959) 307.
15 S. W. Christopherson and R. L. Glass, *J. Dairy Sci.*, 52 (1969) 1289.
16 F. E. Luddy, R. A. Barford, S. F. Herb and P. Magidman, *J. Am. Oil Chem. Soc.*, 45 (1968) 549.
17 C. D. Bannon, G. J. Breen, J. D. Craske, N. T. Hai, N. L. Harper and K. L. O'Rourke, *J. Chromatogr.*, 247 (1982) 71.
18 A. Y. Shehata, J. M. de Man and J. C. Alexander, *Can. Inst. Food Technol. J.*, 3 (1970) 85.
19 L. D. Metcalfe and C. N. Wang, *J. Chromatogr. Sci.*, 19 (1981) 530.
20 W. Butte, *J. Chromatogr.*, 261 (1983) 142.
21 R. Misir, B. Laarveld and R. Blair, *J. Chromatogr.*, 331 (1985) 141.
22 G. Lepage and C. C. Roy, *J. Lipid Res.*, 27 (1986) 114.
23 R. Segura, *J. Chromatogr.*, 441 (1988) 99.
24 K. G. Allen, J. MacGee, M. E. Fellows, P. A. Tornheim and K. R. Wagner, *J. Chromatogr.*, 309 (1984) 33.
25 H. T. Slover and E. Lanza, *J. Am. Oil. Chem. Soc.*, 56 (1979) 933.
26 L. D. Metcalfe, A. A. Schmitz and J. R. Pelka, *Anal. Chem.*, 38 (1966) 514.
27 A. J. Sheppard and J. L. Iverson, *J. Chromatogr. Sci.*, 13 (1975) 448.
28 R. G. Ackman, *Methods Enzymol.*, 14 (1969) 329.
29 M. L. Vorbeck, L. R. Mattick, F. A. Lee and C. S. Pederson, *Anal. Chem.*, 33 (1961) 1512.
30 G. R. Jamieson and E. H. Reid, *J. Chromatogr.*, 17 (1965) 230.
31 K. Eder, A. M. Reichlmayer-Lais and M. Kirchgessner, submitted for publication.
32 D. J. Hanahan and J. E. Ekholm, *Methods Enzymol.*, 31 (1974) 168.
33 E. Peuchant, R. Wolff, C. Salles and R. Jensen, *Anal. Biochem.*, 181 (1989) 341.
34 J. R. Yandrasitz, G. Berry and S. Segal, *J. Chromatogr.*, 225 (1981) 319.
35 T. L. Kaduce, K. C. Norton and A. A. Spector, *J. Lipid Res.*, 24 (1983) 1398.
36 E. B. Hoving, J. Prins, H. M. Rutgers and F. A. J. Muskiet; *J. Chromatogr.*, 434 (1988) 411.
37 R. Olegard and L. Svennerholm, *Acta Paediatr. Scand.*, 59 (1970) 637.
38 K. Eder, A. M. Reichlmayr-Lais and M. Kirchgessner, *J. Chromatogr.*, 588 (1991) 265.
39 L. Ciccoli, Y. Hayek, D. Berti and R. Bracci, *Biol. Neonate*, 40 (1981) 187.
40 L. A. Piche and V. G. Mahadevappa, *J. Nutr.*, 120 (1990) 444.
41 B. Freedman, E. H. Pryde and T. L. Mounts, *J. Am. Oil. Chem. Soc.*, 61 (1984) 1638.
42 D. van Wijngaarden, *Anal. Chem.*, 39 (1967) 848.
43 V. Rogiers, *J. Chromatogr.*, 182 (1980) 27.
44 G. J. Nelson, in E. G. Perkins (Editor), *Analysis of Lipids and Lipoproteins*, American Oil Chemists Society, Campaign, IL, 1975, pp. 1–70.
45 M. D. Laryea, P. Cieslicki, E. Dickmann and U. Wendel, *Clin. Chim. Acta*, 171 (1988) 11.
46 J. S. O'Brien, D. L. Fillerup and J. F. Mead, *J. Lipid Res.*, 5 (1964) 109.
47 C. C. Sweeley and E. A. Moscatelli, *J. Lipid Res.*, 1 (1959) 40.
48 R. C. Gaver and C. C. Sweeley, *J. Am. Oil. Chem. Soc.*, 42 (1965) 294.
49 R. F. Lee and F. Gonsoulin, *Comp. Biochem. Physiol. B*, 64 (1979) 375.
50 J. MacGee and M. G. Williams, *J. Chromatogr.*, 205 (1981) 281.

Journal of Chromatography, 607 (1992) 69–77
Elsevier Science Publishers B.V., Amsterdam

CHROM. 24 286

Direct measurement of the inverse secondary isotope effects of Rh(I)–C_2H_4 and Rh(I)–C_2H_3D utilizing gas chromatography

Dae Young Youn, Kwang Bum Hong and Kyung-Hoon Jung

Centre for Molecular Science and Department of Chemistry, Korea Advanced Institute of Science and Technology, Taedok Science Town, Taejon 305-701 (South Korea)

Dongho Kim

Spectroscopy and Color Laboratory, Korea Standard Research Institute, Taedok Science Town, Taejon 305-606 (South Korea)

Kyoung-Rae Kim

College of Pharmacy, Sungkyunkwan University, Suwon 440-746 (South Korea)

(First received January 8th, 1992; revised manuscript received April 24th, 1992)

ABSTRACT

The inverse secondary equilibrium isotope effects of Rh(I)–C_2H_4 and Rh(I)–C_2H_3D were directly measured using a gas chromatographic column of dicarbonyl-rhodium(I)-3-trifluoroacetyl-1*R*-camphorate in squalane solution at 283–333 K. Statistical isotope effects were also obtained from a reduced partition function using harmonic vibrational frequencies of RHC–C_2H_4 complexes and normal-mode analysis. The observed isotope effects were in good agreement with those deduced from the reduced partition function. Thermodynamic data of the inverse isotope effect were $\Delta_{D,H}\Delta H = -469 \pm 12$ J mol^{-1} and $\Delta_{D,H}\Delta S = -0.975 \pm 0.017$ J mol^{-1} K^{-1}, where $\Delta_{D,H}\Delta H = \Delta H_D - \Delta H_H$ = the difference of the enthalpy changes of the deuterated and non-deuterated compounds (see refs. 1 and 22) and $\Delta_{D,H}\Delta S = \Delta S_D - \Delta S_H$ = the difference of the entropy changes of the deuterated and non-deuterated compounds. The detailed analysis of the force constant most affected, $F_{C-C} = 8.39$ mdyn/Å, by metal complexation was closer to that of the carbon–carbon double bond (9.1 mdyn/Å) than to that of the carbon–carbon single bond (4.3 mdyn/Å).

INTRODUCTION

The selective separation of olefin isomers by complexation gas chromatography (GC) [1], involving a π-coordination equilibrium complex of metal with substrates (solute), was demonstrated by Bradford *et al.* [2], and extension of its usage for the separation of enantiomers [1,3], and constitutional [4–6] and isotopic isomers has also been reported.

The application of the technique to isotopic ethylene isomers, $C_2H_{4-n}D_n$, has been tested extensively using stationary systems such as silver nitrate–ethylene glycol [7,8], silver nitrate–water [9] and dicarbonyl-rhodium(I)-β-ketoenolates–squalane [1]. In conventional gas–liquid chromatography (GLC), the elution of isotopic samples usually occurs in order of decreasing volatility [10–12], but the order of elution in complexation GC is reversed [1,7–9]. Since this anomaly results from a large inverse

Correspondence to: Dr. K.-H. Jung, Centre for Molecular Science and Department of Chemistry, Korea Advanced Institute of Science and Technology, Taedok Science Town, Taejon 305-701, South Korea.

0021-9673/92/$05.00

secondary equilibrium isotope effect between complexes, we considered it a logical extension to measure this anomaly using GC and to correlate it with the inverse isotope effects, K_D/K_H, of metal–olefin complexes, where K_D and K_H are the equilibrium constants of the deuterated and non-deuterated systems, respectively [1,13,14]. It is also worth noting that some of existing data are rather inadequate to correlate the anomaly with the equilibrium phenomena owing to a lack of information regarding the structural properties of the equilibrium complexes.

In this paper we report on the inverse secondary isotope effects of Rh(I)–C_2H_4 and Rh(I)–C_2H_3D determined from the retention data obtained by GC and on the correlation of the measured values with the structural properties of equilibrium complexes obtained from their vibrational characteristics. Differences in the separation factors of Rh(I) and Ag(I) complexes are also correlated in terms of rehybridization of C_2H_4 for metal complexation in conjunction with our previous studies [14].

EXPERIMENTAL

Materials

Ethylene (Matheson), ethylene-d_1 (Merck Sharpe and Dohme, Canada) and methane (Matheson) were used after several freeze–pump–thaw cycles at liquid nitrogen temperature until traceable impurities were no longer detected by GC. For ethylene-d_1 no isotopic purification was attempted. Dicarbonyl-rhodium(I)-3-trifluoroacetyl-1*R*-camphorate (RHC) was purchased from Johnson Matthey.

Gas chromatography

An HP 5880A gas chromatograph equipped with two flame ionization detectors was used to measure K_D/K_H. Sample injection was done using a 1.0-ml internal loop six-port gas sampling valve (Valco) attached to a high-vacuum sampling system line. The GC oven temperature was maintained at the operating temperature of 283–333 K to within ± 0.1 K by a built-in liquid nitrogen cryogenic system.

The separation column for isotopic samples was a 30 m × 2 mm I.D. PTFE column packed with 60–80 mesh Chromosorb P AW DMCS coated with squalane containing 0.06 *M* RHC. The newly prepared column was conditioned by passing helium through at a low flow-rate (*ca.* 5 ml/min) for more than 3 days at room temperature. The freshly made column lasted more than 3 months with minimum change in its activity by preventing unnecessary exposure to air, water or organics.

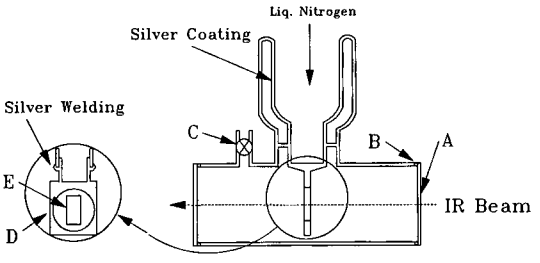

Fig. 1. Low-temperature IR cell for the measurements of solid–gas and liquid–gas interface phenomena. A = window; B = O-ring; C = stopcock; D = copper tip; and E = KBr pellet.

Infrared spectroscopy

Infrared spectra of Rh(I)–olefin complexes were obtained using a Bomen MB 100 spectrometer (Fourier transform infrared FT-IR). Since RHC–olefin complex formation processes are known to be fast reversible reactions, a low-temperature IR cell was used to obtain IR spectra of the equilibrium π-complexes. The IR cell was composed of a 10-cm gas cell with KRS-5 windows (Yanus), 36 mm diameter and 5 mm thickness, at both ends and a copper tip located in the middle of the cell which intersected the IR beam path perpendicularly. A detailed configuration is shown in Fig. 1. The tip had a circular hole in the middle to hold a KBr pellet containing stationary phase in order to form an equilibrium chemical complex with its environment gas, *i.e.* olefins at liquid nitrogen temperature. The potassium bromide/squalane ratio of the pellet was 20:1 and it was mounted on the copper tip using Torr-Seal (Varian). On top of the cell a liquid nitrogen Dewar was attached to chill the pellet through the copper tip heat-transmitting medium. An external blow fan was installed near the cell to prevent deposition of water vapour on the window surface.

Experimental procedures

Gas chromatographic and IR spectroscopic measurements in conjunction with the normal-mode

analyses were made to obtain the equilibrium and statistical isotope effects, respectively.

The equilibrium isotope effect was obtained from retention data of both C_2H_4 and C_2H_3D in an RHC–squalane stationary phase system. The retention data were observed by injecting a sample mixture of C_2H_4–C_2H_3D–CH_4 (10:10:1) into the gas chromatograph at a flow-rate of 14.6 ml/min at 283–333 K. Sample pressures for GC injection were kept at <1 Torr to prevent column overloading, which causes lowering of retention time and peak tailing [15]. Methane gas was used as an internal reference to measure the dead volume of the instrument and the relative corrected retention volumes of the olefins.

The statistical isotope effect was deduced from the experimentally observed IR spectra and the vibrational frequencies calculated by normal-mode analyses of the olefins and the complex molecules. Since the vibrational frequencies of both olefins have been well studied [16–18], the normal-mode analyses of these compounds, checked against the literature values, were utilized to obtain transfer force constants for the analysis of the complex molecules. However, the vibrational frequencies of RHC–olefin equilibrium complexes have not been available up until now. We have obtained IR spectra of the complexes using the low-temperature IR cell and performed the analysis utilizing our calculated force constants as well as literature values [19] for similar compounds such as $[RhCl(C_2H_4)_2]_2$ or $[RhBr(C_2H_4)_2]_2$. To obtain IR spectra, gas samples were introduced into the gas cell, prechilled with liquid nitrogen and evacuated. The temperature of the tip or pellet was not monitored but was assumed to be that of liquid nitrogen since the system was continuously pumped and cooled long enough for it to reach equilibrium temperature with the cooling system. The sample pressure was varied to obtain the best IR spectrum. These pressures were *ca.* 1 atm at liquid nitrogen temperature owing to condensation of samples around the upper part of the tip but they were *ca.* 20 Torr at room temperature where condensation did not occur. To accomplish complete normal-mode analysis of the complexes, one should have complete knowledge of the geometrical structures of the complexes. However, since the structures of neither RHC nor RHC–olefins are well known [20], we have treated the complexes as free Rh–olefin complex molecules for the calculations. This simplified calculation is further justified by the fact that the interaction between the vicinal group CO, which is covalently bound to Rh, and Rh–olefin is not so prominent and hence the complete calculation is impractical.

The free Rh(I)–olefin spectra were acquired by subtracting the free RHC spectra from the RHC–olefin spectra using the spectra subtraction function, Bomen program. The spectra obtained by subtraction contained high background noise. This noise was eliminated by averaging 10–20 repeated runs of the same spectra.

RESULT AND DISCUSSION

Determination of isotope effect, K_D/K_H, using complexation GC

The retention volumes of C_2H_4 and C_2H_3D were obtained from chromatograms of these compounds by analysing on an RHC–squalane stationary phase. The retention volumes were expressed as a product of the partition equilibrium between the gas phase and the liquid phase of the olefin of interest, and the thermodynamic association equilibrium between the olefin and the metal complex [21]. The expression can be approximated with an equilibrium constant (K_H or K_D) when the relative corrected retention volume of the olefin with respect to methane as an inert reference standard on RHC–squalane (r_H or r_D) is larger than that on pure squalane ($r_{\circ H}$ or $r_{\circ D}$). Consequently, the inverse secondary isotope effect, K_D/K_H, is reduced to [1]:

$$K_D/K_H \approx (r_D/r_H) \times (r_{\circ H}/r_{\circ D}) \quad (1)$$

where r_D/r_H and $r_{\circ H}/r_{\circ D}$ are the relative corrected retention volume ratios or the separation factor on RHC–squalane and on pure squalane, respectively, using methane as an inert reference material. r_D/r_H is directly measured from the retention data, while the direct measurement of $r_{\circ H}/r_{\circ D}$ is impractical since it requires a long squalane column causing peak broadening too large to handle. Alternatively, $r_{\circ H}/r_{\circ D}$ can be obtained from the relationship $r_{\circ H}/r_{\circ D} \approx P_D/P_H$, where P_D and P_H are the vapour pressures of deuterated and non-deuterated solutes on an apolar stationary phase, respectively [22]; the ratio of retention volumes is inversely proportional to that of the vapour pressures of constituents on an apolar

TABLE I

GAS CHROMATOGRAPHIC PROPERTIES OF ETHYLENE AND ETHYLENE-D_1 ON THE RHC–SQUALANE STATIONARY SYSTEM

Temperature (K)	K_D/K_H	r_D/r_H	$r_{\circ H}/r_{\circ D}$[a]
283	1.087	1.078	1.0080
293	1.076	1.068	1.0079
303	1.070	1.062	1.0078
313	1.065	1.057	1.0077
323	1.060	1.052	1.0076
333	1.053	1.045	1.0074

[a] $r_{\circ H}/r_{\circ D}$ is calculated from the relationship $r_{\circ H}/r_{\circ D} \approx P_D/P_H$ and $\ln(P_H/P_D) = 406/T^2 - 3.687/T$ [23].

stationary phase and can be expressed by a simple empirical relationship [23]. The deduced inverse secondary isotope effects, the ratios of relative corrected retention volume on both RHC-squalane and neat squalane at a set of temperatures, are listed in Table I. A typical chromatogram is displayed in Fig. 2. The separation factors measured on the 30-m packed column used for this study were approximately the same as those on a 200-m stainless-steel capillary column in the literature [1]. Average thermodynamic values deduced from the partition equilibrium secondary isotope effects $\Delta_{D,H}\Delta H$ and $\Delta_{D,H}\Delta S$, obtained at different temperatures, by

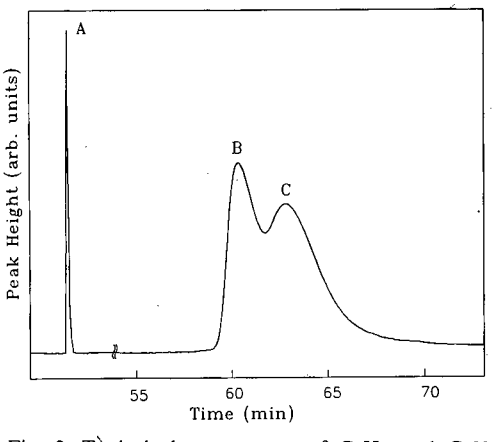

Fig. 2. Typical chromatogram of C_2H_4 and C_2H_3D on an RHC–squalane stationary phase system. GC conditions: oven temperature, 323 K; carrier gas flow-rate, 14.6 ml/min. A, B and C refer to internal standard CH_4 (retention time = 13.0 min), C_2H_4 (60.5 min) and C_2H_3D (63.1 min), respectively.

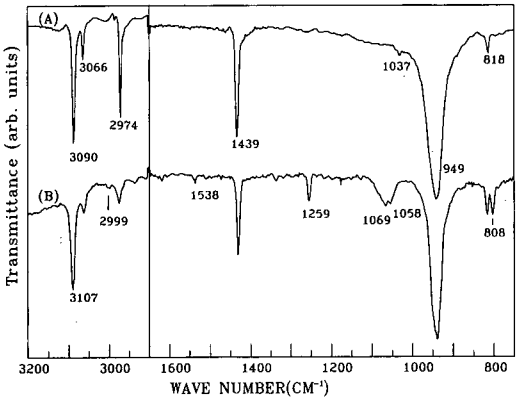

Fig. 3. IR spectra of free ethylene (A) and the ethylene portion in of the RHC–C_2H_4 complex (B).

Gibbs–Helmholz plot are -469 ± 12 J mol^{-1} and -0.975 ± 0.017 J mol^{-1} K^{-1}, respectively, where $\Delta_{D,H}\Delta H = \Delta H_D - \Delta H_H$ = the difference of the enthalpy changes of the deuterated and non-deuterated compounds (see refs. 1 and 22) and $\Delta_{D,H}\Delta S = \Delta S_D - \Delta S_H$ = the difference of the entropy changes of the deuterated and non-deuterated compounds.

The bonding structures of metal–olefin π-complexes can be explained well by the two-way donor–acceptor model known as the Dewar–Chatt–Duncanson model [24,25], in which the bondings are composed of a dative σ-bond [π(olefin) $\rightarrow$ metal] and a π-back-bond [metal $\rightarrow$ π^*(olefin)]. The quantitative contributions of the two bonds in Ag(I)–C_2H_4 and in Rh(I)–C_2H_4 complexes are not well understood, but the dative σ-bond is known to be relatively more dominant than the π-back-bond for both complexes [1,26,27]. Consequently, one would expect the more electronegative Rh(I) to form a stronger Rh(I)–C_2H_4 bond than Ag(I)–C_2H_4 and hence the separation factor on an Rh(I) column to be larger than that on an Ag(I) column. These phenomena are supported by our observed secondary isotope effect for Rh(I), *e.g.* 1.087 on RHC–squalane at 283 K is larger than 1.047 on silver nitrate–ethylene glycol at 273 K [14].

Infrared spectroscopic studies

An IR spectroscopic study was undertaken to determine the vibrational characteristics of Rh(I)–C_2H_4 and the structural changes occurring during the complexation. The ethylene portion of the

spectrum was obtained by subtracting the free RHC spectrum from that of RHC–C_2H_4. By scanning the RHC–squalane solution at liquid nitrogen temperature, we obtained shifted ethylene bands in the ethylene portion of the spectrum (shown in Fig. 3) together with the band of free C_2H_4 adsorbed on KBr surface, which we compared with that obtained at room temperature and that of the RHC–C_2H_4–KBr pellet. The observed frequencies of free C_2H_4 are similar to those of a thick film (a few microns) of C_2H_4 obtained by Dows [28] at 65 K. The ethylene portion of the spectra demonstrated two types of spectra, *i.e.* one composed of uncomplexed C_2H_4 bands and the other composed of shifted bands caused by complexation. The uncomplexed C_2H_4 bands in the scan showed less than ± 2 cm^{-1} shift of line frequencies except for 3107 cm^{-1}. The large shift for the 3107 cm^{-1} band, *ca.* 17 cm^{-1}, is interpreted as a cause of the convolution of the 3090 cm^{-1} free C_2H_4 band and the hidden complexed band around 3107 cm^{-1}. In the C_2H_4 portion of the spectrum, we could identify seven frequencies among fifteen fundamental frequencies of Rh(I)–C_2H_4 complex ranging from 400 to 4000 cm^{-1}. In the 1650–750 cm^{-1} range, like other transition metal complexes [29–31], we also observed several relatively high-intensity peaks. The 1538 and 1259 cm^{-1} peaks are assigned to C=C stretching and CH_2 in-phase scissoring motion, respectively, by reference to other metal complexes. These bands play key roles in predicting the degree of C=C bond rehybridization on metal–olefin complexes [29–32]. Stuve and Madix [32] proposed the $\pi\sigma$-parameter as a measure of the degree of C_2H_4 rehybridization in adsorption. This parameter takes into account the vibrational coupling of these two bands and ranges from 0 to 1, *i.e.* 0 for gaseous C_2H_4, 0.38 for Zeise's salt, a model for π-bonded C_2H_4 and 1 for $C_2H_4Br_2$, a model for di-σ-bonded C_2H_4. The calculated $\pi\sigma$-parameter of Rh(I)–C_2H_4, 0.31, obtained from 1538 and 1259 cm^{-1}, is larger than that of Ag(I)–C_2H_4, 0.12, obtained from 1579 and 1320 cm^{-1} bands [33] of $[Ag(C_2H_4)]BF_4$. Since C_2H_4 in Rh(I)–C_2H_4 is rehybridized more than that in Ag(I)–C_2H_4, one would expect the separation factor to be larger in an Rh(I) column than in an Ag(I) column. Though the simplified calculation given above predicts the $\pi\sigma$-parameters reasonably well, it requires further information on coupling parameters such as

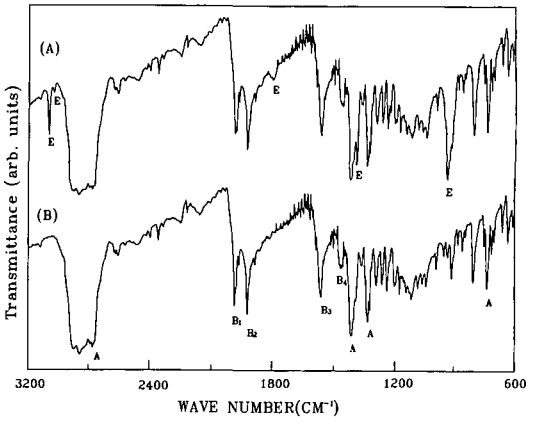

Fig. 4. IR peak assignments for RHC–C_2H_4 peaks (A) and neat RHC peaks (B). The letters A, B_1, B_2, B_3, B_4 and E on both IR spectra refer to squalane, C≡O asymmetric stretching, C≡O symmetric stretching, C=O asymmetric stretching, C=O symmetric stretching and ethylene peaks, respectively.

the geometry, the magnitude of force constants and the degree of coupling between each mode for more precise calculation. These are discussed in some detail in the normal-mode analysis section.

Both 1069 and 1058 cm^{-1} bands can be assigned as either dimer bands or CH_2 wagging bands (A_1 and B_1) because of their broad nature [28]. We assigned these bands to the waggings on the experimental ground that stoichiometrically different species other than the 1:1 complex were not found during all our observations and the shift to higher frequencies agrees with the generally increasing trend of the wagging frequency by complexation [31]. The 808 cm^{-1} band is assigned to CH_2 bending mode shifted from 819 cm^{-1} of free C_2H_4. Though our observed weak band at 2999 cm^{-1} and a hidden band around 3107 cm^{-1} are well within the 3200–2900 cm^{-1} range of the CH stretching region, CH stretching motions attributed to Rh(I)–C_2H_4 are difficult to assign on the basis of IR spectra alone because of their weak absorption and strong tendency to overlap free C_2H_4 bands. These are, therefore, assigned to CH stretching bands with less confidence.

Fig. 4 displays the strong characteristic peaks at 2089, 2021, 1628 and 1519 cm^{-1} in full spectra of RHC and RHC–C_2H_4. The first two bands are assigned to C≡O asymmetric and symmetric stretchings, and the last two are C=O asymmetric and symmetric stretchings. The observation of frequency

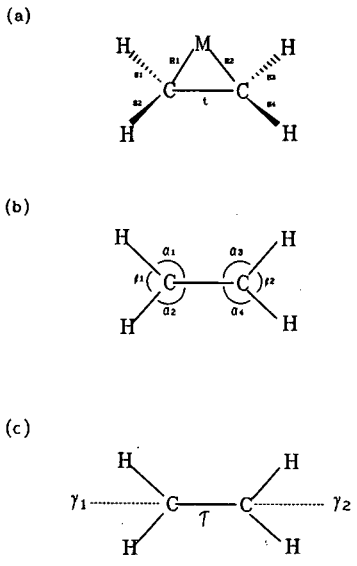

Fig. 5. Internal coordinate assignments for Rh(I)–C_2H_4 complex. (a) The stretching coordinates; (b) the bending coordinates; and (c) the wagging and torsional coordinates. Adapted from ref. 16.

shift of these bands from RHC to RHC–C_2H_4 may give a good idea of structural changes in the RHC skeleton. Schurig and Gil-Av [20] have proposed that the square planar shape of uncomplexed RHC is changed to trigonal bipyramid by olefin complexation with the CO groups in apical, and the olefin and β-diketonate in equatorial, positions. In our system, however, no considerable band shifts were observed from RHC to RHC–C_2H_4, and these findings indicate that there are very few structural changes between the four coordinates of RHC and the intermediate five coordinates of RHC–C_2H_4. Consequently, we suggest that the structure of the intermediate five coordinates of RHC–C_2H_4 complexes is closer to the square pyramid geometry. It is also likely that there is no structural change in RHC during the reaction with C_2H_4 since the IR spectra of both fresh RHC and used RHC are almost identical.

Normal-mode analysis

Normal-mode analysis was used to compare quantitatively the molecular parameters of the Rh(I)–C_2H_4 complex and those of other π-complexes and to assign vibrational frequencies of Rh(I)–C_2H_3D. We used valence force fields [34] obtained from the seven observed frequencies of the C_2H_4 portion of the spectrum of the RHC–C_2H_4 complex and its assumed geometry. The geometries of the complexes are assumed on the basis of X-ray data of Rh-containing compounds [35,36], and these are Rh(I)–C = 2.2, C–C = 1.38, C–H = 1.09 Å and <HCH = 120°, with the C_2H_4 group held in a planar structure as shown in Fig. 5. For the choice of internal coordinates, a factor to bear in mind was facilitation of the quantitative comparison with other metal–ethylene complexes within the same framework [29,30,37]. The calculations and discussions are emphasized, in particular the coupling parameters, which are responsible for the degree of C_2H_4 rehybridization of metal–C_2H_4 complexes in complexation GC, and vibrational frequencies re-

TABLE II

CALCULATED FUNDAMENTAL FREQUENCIES OF Rh(I)–C_2H_4 AND Rh(I)–C_2H_3D AND THE OBSERVED VALUES OF THE ETHYLENE PORTION IN THE SPECTRUM OF RHC–C_2H_4 COMPLEX

F_{Rh-C} = 1.13 mdyn/Å, F_{C-C} = 8.39 mdyn/Å, F_{C-H} = 5.09 mdyn/Å, $F_{<CCH}$ = 0.54 mdyn Å, $F_{<CCH,<CCH}$ = −0.01 mdyn Å, $F_{<HCH}$ = 0.39 mdyn Å, $F_{<HCH,<HCH}$ = 0.07 mdyn Å, F_{wag} = 0.186 mdyn Å, $F_{wag,wag}$ = 0.06 mdyn Å, F_{twist} = 0.175 mdyn Å and $F_{C-C,<HCH}$ = −0.375 mdyn.

Mode characteristics	Observed value	Calculated value	
		Rh(I)–C_2H_4	Rh(I)–C_2H_3D
A_1			
ν_1: CH stretch		3010	2263
ν_2: C=C stretch	1539	1538	1517
ν_3: CH_2 scissor	1259	1259	1231
ν_4: CH_2 wag	1058	1058	913
ν_5: Rh–C stretch		393	388
A_2			
ν_6: CH stretch		3121	3115
ν_7: CH_2 rock		1212	1089
ν_8: CH_2 twist		1150	1122
B_1			
ν_9: CH stretch	2999	2991	3001
ν_{10}: CH_2 scissor		1423	1371
ν_{11}: CH_2 wag	1069	1068	1063
ν_{12}: Rh–C stretch		324	311
B_2			
ν_{13}: CH stretch	3107	3107	3063
ν_{14}: CH_2 rock	808	809	714

$$K_D/K_H = \frac{(s_1/s'_1)\prod_i (U'_{1i}/U_{1i})\exp[(U_{1i} - U'_{1i})/2][1 - \exp(-U_{1i})/1 - \exp(-U'_{1i})]}{(s_2/s'_2)\prod_i (U'_{2i}/U_{2i})\exp[(U_{2i} - U'_{2i})/2][1 - \exp(-U_{2i})/1 - \exp(-U'_{2i})]} \quad (2)$$

sponsible for the inverse secondary isotope effect. The present model includes fourteen out of fifteen vibrations for Rh(I)–C_2H_4 and does not take into account a B_1 tilting motion, since it is expected to have a very low frequency and hence very small isotopic shift [29,30]. Two Rh–C stretching modes, causing relatively large isotopic shifts, were obtained from the normal-mode analysis, and these are 393 and 324 cm^{-1}. For the calculation, we used a transferred force constant, F_{Rh-C} = 1.13 mdyn/Å from similar systems. The transferred force constant was deduced from known Rh–C stretching frequencies of other Rh-containing molecules such as 399 cm^{-1} in $[RhCl(C_2H_4)_2]_2$ [19], 393 cm^{-1} in $[RhBr(C_2H_4)_2]_2$ [19], 355 cm^{-1} in adsorbed C_2H_4 on Rh(111) [31] and two peaks at 325 and 395 cm^{-1} in adsorbed C_2H_4 on Rh(100) [31]. The same geometrical parameters and force constants were assumed for Rh(I)–C_2H_3D). The observed and calculated frequencies are listed in Table II for both Rh(I)–C_2H_4 and Rh(I)–C_2H_3D.

For general trends of metal–olefin complexes, Bent *et al.* [31] have suggested a method of predicting the correlation of the degree of the rehybridization with the mode frequencies of C_2H_4. The trends are that the CC and CH stretching and CH_2 bending mode frequencies are decreased but the wagging and twisting are increased by complexation. For all calculation force constant F_{C-C} is clearly the most affected by metal complexation. Compared with free C_2H_4 F_{C-C} is reduced from 9.1 to 8.39 mdyn/Å and found to be closer to that of a double bond than to that of a single bond, 4.3 mdyn/Å [29,30], in cyclopropane. Comparative studies with other metal complexes were also made. These are 6.14 mdyn/Å [37] for $(C_2H_4)Fe(CO)_4$ and 4.23 mdyn/Å [37] for $K[PtCl_3(C_2H_4)]H_2O$, which suggest CC single-bond characters in both Fe and Pt complexes, while the 8.91 mdyn/Å value for $[Ag(C_2H_4)]BF_3$ is quite similar to that of RHC–C_2H_4 and CC double-bond character. The reduction in F_{C-C} represents a higher degree of rehybridization of C_2H_4 in metal complexes. Both Ag(I)–C_2H_4 and Rh(I)–C_2H_4 show double-bond character, form reversible equilibrium complexes and can be used as stationary phases in complexation GC, whereas both Fe–C_2H_4 and Pt–C_2H_4, show single-bond character and form the stable complexes at room temperature. From the foregoing discussion, we conclude that the degree of rehybridization of C_2H_4 in metal complexes is greatly affected by the chemical and physical properties of the metal–olefin complex. The higher separation factor in Rh(I) than in Ag(I) columns is also responsible for the higher degree of rehybridization of C_2H_4 in Rh(I)–C_2H_4 than in Ag(I)–C_2H_4.

Statistical isotope effect

The statistical inverse secondary isotope effect was calculated from the reduced partition functions, expressed in terms of the normal-mode vibrations of the molecules involved. It can be expressed in terms of the reduced partition function, $(s/s')f$, the ratio of the uncomplexed and the complexed molecules, *i.e.* $(s_1/s'_1)f[C_2H_3D/C_2H_4]/(s_2/s'_2)f[Rh(I)–C_2H_3D/Rh(I)–C_2H_4]$. A more comprehensive expression using the complete set of normal-mode frequencies, ν_i, is as in eqn. 2 [38,39], where subscripts 1 and 2 represent the complex and free C_2H_4, respectively. The primed quantities refer to the deuterated molecules. U_i has its usual meaning, $h\nu_i/kT$. The symmetry number, s, for C_2H_4, C_2H_3D, Rh(I)–C_2H_4 and Rh(I)–C_2H_3D is 4, 2, 2 and 1, respectively. For simplicity, eqn. 2 can be resolved into three terms:

$$K_D/K_H = (VP)(ZPE)(EXC) \quad (3)$$

where $VP = (s_1/s'_1)\prod_i (U'_{1i}/U_{1i})/(s_2/s'_2)\prod_i (U'_{2i}/U_{2i})$,

$ZPE = \prod_i \exp[(U_{1i} - U'_{1i})/2]/\prod_i \exp[(U_{2i} - U'_{2i})/2]$

and $EXC = \prod_i [1 - \exp(-U_{1i})/1 - \exp(-U'_{1i})]/\prod_i [1 - \exp(-U_{2i})/1 - \exp(-U'_{2i})]$ and where VP, ZPE and EXC represent the vibrational product, the zero-point energy and the vibrational excitation

TABLE III

CALCULATED AND OBSERVED VALUES OF K_D/K_H AND VP, ZPE, AND EXC TERMS AS A FUNCTION OF TEMPERATURE

Temperature (K)	K_D/K_H[a]	VP	ZPE	EXC
283	1.086 (1.087)	0.921	1.158	1.018
293	1.078 (1.076)	0.921	1.148	1.019
303	1.070 (1.070)	0.921	1.140	1.019
313	1.064 (1.065)	0.921	1.133	1.020
323	1.059 (1.060)	0.921	1.127	1.020
333	1.054 (1.053)	0.921	1.121	1.021

[a] The observed values in the RHC–squalane column are in parentheses.

terms, respectively. The VP term comes from the classical translational and rotation partition function, given by the Redlich–Teller product rule for the isotopically substituted compounds. The ZPE and EXC terms are from the classical vibrational partition function. The calculated values of K_D/K_H at different temperatures together with the observed values are shown in Table III. The calculated $\Delta_{D,H}\Delta H$ and $\Delta_{D,H}\Delta S$ values are -469 J mol^{-1} and -0.975 J mol^{-1} K^{-1}, respectively. The calculated values are in good agreement with those obtained experimentally by GC. Investigation of the data in Table III reveals several interesting points. The positive contributions are mainly attributable to the ZPE and EXC terms, whereas the negative contribution comes from the VP term. The temperature dependence of each term also shows some interesting phenomena. The VP term is temperature-independent and the slight positive effect of EXC cancels the negative dependency of ZPE; thus, the overall effect shows little temperature dependency.

CONCLUSIONS

In this paper we report on the successful achievement of a method to correlate the equilibrium isotope effect with the statistical isotope effect of Rh(I)–C_2H_4 and Rh(I)–C_2H_3D. The equilibrium isotope effect is directly measured by the GC technique using RHC–squalane as the stationary phase. The statistical isotope effect is deduced from the reduced partition function based on the RHC–C_2H_4 vibrational frequencies acquired from IR spectroscopic data. The larger separation factor of Rh(I)–olefins compared with that of Ag(I)–olefins is caused by their greater rehybridization capabilities. Both the $\pi\sigma$-parameter and F_{C-C} are useful to the degree of rehybridization of C_2H_4 in metal–olefin complexes, which can be used to predict the physical and chemical properties of metal–olefin complexes. The procedures used in this study provided insight into the physical separation of olefinic isotopes in complexation GC and clarification of the molecular properties of metal–olefin complexes.

ACKNOWLEDGEMENTS

This work was carried out with financial assistance from the Korea Standards Research Institute and the Korea Science and Engineering Foundation, which is gratefully acknowledged.

REFERENCES

1 V. Schurig, *Chromatographia*, 13 (1980) 263 and earlier references therein.
2 B. W. Bradford, D. Harvey and D. E. Chalkley, *J. Inst. Petrol., London*, 41 (1955) 80.
3 V. Schurig, *Angew. Chem., Int. Ed. Engl.*, 16 (1977) 110.
4 E. Gil-Av and V. Schurig, *Anal. Chem.*, 43 (1971) 2030.
5 V. Schurig, R. C. Chang, A. Zlatkis, E. Gil-Av and F. Mikes, *Chromatographia*, 6 (1973) 223.
6 A. M. Soto, N. Yanagihara and T. Ogura, *Anal. Chem.*, 63 (1991) 1178.
7 R. J. Cvetanovic, F. J. Duncan and W. E. Falconer, *Can. J. Chem.*, 41 (1963) 2095.
8 J. G. Atkinson, A. A. Russell and R. S. Stuart, *Can. J. Chem.*, 45 (1967) 1963.
9 S. P. Wasik and W. Tsang, *J. Phys. Chem.*, 74 (1970) 2970.
10 K. E. Wilzbach and P. Riesz, *Science*, 126 (1957) 748.
11 W. E. Falconer and R. J. Cvetanovic, *Anal. Chem.*, 34 (1962) 1064.
12 F. Bruner, P. Ciccioli and A. Di Corcia, *Anal. Chem.*, 44 (1972) 894.
13 R. J. Cvetanovic, F. J. Duncan, W. E. Falconer and R. S. Irwin, *J. Am. Chem. Soc.*, 87 (1965) 1827.
14 K. B. Hong, K.-H. Jung and S. H. Kang, *Bull. Korea Chem. Soc.*, 3 (1982) 79.
15 D. Y. Youn, S. J. Yun and K.-H. Jung, *J. Chromatogr.*, 591 (1992) 19.
16 K. Machida, *J. Chem. Phys.*, 44 (1966) 4186.
17 B. L. Crawford, Jr., J. E. Lancaster and R. G. Inskeep, *J. Chem. Phys.*, 21 (1953) 678.
18 P. Pulay and W. Meyer, *J. Mol. Spectrosc.*, 40 (1971) 59.
19 M. A. Bennett, R. J. H. Clark and D. L. Milner, *Inorg. Chem.*, 6 (1967) 1647.
20 V. Schurig and E. Gil-Av, *Chem. Commun.*, (1971) 650.
21 V. Schurig, R. C. Chang, A. Zlatkis and B. Feibush, *J. Chromatogr.*, 99 (1974) 147.

22 F. Bruner, G. P. Cartoni and A. Liberti, *Anal. Chem.*, 38 (1966) 298.
23 M. J. Stern, W. A. Van Hook and M. Wolfsberg, *J. Chem. Phys.*, 39 (1963) 3179.
24 J. Chatt and L. A. Duncanson, *J. Chem. Soc.*, (1953) 2939.
25 M. J. S. Dewar, *Bull. Soc. Chim. Fr.*, 18 (1951) C79.
26 H. Basch, *J. Chem. Phys.*, 56 (1972) 441.
27 M. J. S. Dewar and G. P. Ford, *J. Am. Chem. Soc.*, 101 (1979) 783.
28 D. A. Dows, *J. Chem. Phys.*, 36 (1962) 2833.
29 L. Manceron and L. Andrews, *J. Phys. Chem.*, 94 (1990) 3513.
30 L. Manceron and L. Andrews, *J. Phys. Chem.*, 93 (1989) 2963.
31 B. E. Bent, C. M. Mate, L.-T. Kao, A. J. Slavin and G. A. Somorjai, *J. Phys. Chem.*, 92 (1988) 4720.
32 E. M. Stuve and R. J. Madix, *J. Phys. Chem.*, 89 (1985) 3183.
33 D. B. Powell, J. G. V. Scott and N. Sheppard, *Spectrochim. Acta*, 28A (1972) 327.
34 E. B. Wilson, Jr., J. C. Decius and P. C. Cross, *Molecular Vibrations*, McGraw-Hill, New York, 1955.
35 M. Herberhold, *Metal π-Complexes*, Vol. 2, Elsevier, Amsterdam, 1974.
36 H. W. Quinn and J. H. Tsai, *Adv. Inorg. Chem. Radiochem.*, 12 (1969) 217.
37 D. C. Andrews, G. Davidson and D. A. Duce, *J. Organometal. Chem.*, 101 (1975) 113.
38 J. Bigeleisen and M. G. Mayer, *J. Chem. Phys.*, 15 (1947) 261.
39 R. F. Hout, Jr., M. Wolfsberg and W. J. Hehre, *J. Am. Chem. Soc.*, 102 (1980) 3296.

Journal of Chromatography, 607 (1992) 79–89
Elsevier Science Publishers B.V., Amsterdam

CHROM. 24 278

Efficiency in supercritical fluid chromatography as a function of linear velocity, pressure/density, temperature and diffusion coefficient employing *n*-pentane as the eluent

A. Hütz and E. Klesper

Lehrstuhl für Makromolekulare Chemie, Aachen University of Technology, Worringerweg 1, D(W)-5100 Aachen (Germany)

(First received January 22nd, 1992; revised manuscript received April 22nd, 1992)

ABSTRACT

The effect of the physical factors linear velocity, pressure/density, and temperature on the efficiency expressed in terms of effective plate number, N_{eff}, or height equivalent to a theoretical plate, H_{eff}, were studied for supercritical fluid chromatography using *n*-pentane as the mobile phase modified with a small amount of methanol (0.5%, v/v), unbonded silica gel as the stationary phase, and a mixture of polycyclic aromatic hydrocarbons as the analytes on a packed analytical column (4.6 mm I.D.). The results are presented as three-dimensional graphs which, on plotting N_{eff} of chrysene, N_{eff}(C), *versus* column average pressure, $\bar{p}$, and temperature, T, at different constant linear velocities, $\bar{u}$, show movement of the maxima of N_{eff} to higher temperatures when $\bar{u}$ increases. Moreover, the maxima are highest at medium $\bar{u}$, *i.e.*, at $\bar{u}_{opt}$. An analogous behaviour is found when N_{eff}(C) is plotted *versus* the average density in the column, $\bar{\rho}$. On replacing N_{eff}(C) with the capacity factor of chrysene, k'(C), and again plotting *versus* $\bar{p}$ and T, the k'(C) values do not change greatly with increasing $\bar{u}$. If the customary Van Deemter plots of H_{eff}(C) *versus* $\bar{u}$ are combined with $\bar{p}$ or $\bar{\rho}$ as a third axis, keeping T = constant, the dependence of $\bar{u}_{opt}$ on $\bar{p}$ or $\bar{\rho}$ becomes obvious. As expected, $\bar{p}$ and $\bar{\rho}$ should be kept as low as possible in order to obtain low H_{eff}(C). Employing T as the third dimension for the Van Deemter plots and keeping p = constant, it is seen that only specific ranges of T yield the low H_{eff}(C). The graphs are explained in terms of the interdiffusion coefficient, $D_{1,2}$. Three-dimensional graphs for the dependence of $D_{1,2}$ or of the viscosity on pressure and temperature are shown. The three-dimensional plots of N_{eff}(C) and H_{eff}(C) can be rationalized with respect to their dependence on the average linear velocity, pressure/density and temperature.

INTRODUCTION

In supercritical fluid chromatography (SFC) many and, in part, very early studies have been reported on the dependence of the capacity factor, k', and the selectivity, α, on pressure/density, p/ρ, or on temperature, T, for different single mobile phases, stationary phases and analytes (*e.g.*, [1–10]). Many studies are also concerned with k' and α for binary mobile phases (*e.g.*, [11–18]). There are, in addition, a number of reports dealing with the dependence of the efficiency, either in terms of plate numbers, N, or of height equivalent to a theoretical plate, H, and with the dependence of the resolution, R, on pressure/density and on temperature [2,4,5,8, 10,16–23]. In a number of these studies, particularly with packed columns, the volume flow-rate of the pump, and therefore approximately the mass flow-rate, was kept constant during the measurement of a chromatogram. In other studies, particularly with microcolumns, the volume flow-rate of the pump was changed to obtain some desired pressure or density. Therefore, with both packed columns and microcolumns, the linear velocity of the mobile phase in the column was not constant during a separation and hence was not changed in a way generally suitable for optimizing this velocity with the aim of optimizing the chromatographic parameters. Moreover, the dependence of the chromatographic parameters on the average linear velocity, $\bar{u}$,

Correspondence to: Dr. E. Klesper, Lehrstuhl für Makromolekulare Chemie, Aachen University of Technology, Worringerweg 1, D(W)-5100 Aachen, Germany.

0021-9673/92/$05.00

has not received sufficient attention in publications, although the velocity should be considered more closely on account of its large influence on the chromatographic parameters [8,10,24–28]. The linear velocity in conjunction with the dynamic viscosity, η, of the mobile phase also determines the pressure drop, Δp, over a given column which, in turn, may influence the chromatographic parameter s by means of solubility and peak compression. Often lacking in previous work is a systematic investigation of the simultaneous influence of all independent physical parameters of the mobile phase on the chromatographic parameters. Because of the large experimental effort required for this type of study, it may be practical only for some selected and typical chromatographic system. This is even more the case if it is considered that, for obtaining a complete set of information, the stationary phase should also be changed over an appropriate range of physical and chemical properties. The same applies to the chemical nature of the substrate.

In this work, the influence of the average linear velocity, pressure/density and temperature on efficiency and retention was simultaneously studied for a specific chromatographic system. The system consisted on *n*-pentane as the mobile phase, unbonded silica gel as the stationary phase, a mixture of four polycyclic aromatic hydrocarbons as the analytes and an analytical wide-bore (4.6 mm I.D.) packed column. The influence of the four physical properties $\bar{u}$, p/ρ and T on the three chromatographic parameters effective plate number, N_{eff}, effective plate height, H_{eff}, and capacity factor, k', is presented in the form of three-dimensional graphs and explained by the interdiffusion coefficients. The graphs allow an immediate overview of the interrelations between physical and chromatographic parameters. The influence of $\bar{u}$, p/ρ and T on the chromatographic parameters resolution, R, and capacity factor, k', for the same chromatographic system will be the subject of a forthcoming paper [29].

In this and in previous studies (*e.g.*, [8–10,21]) the chromatographic experiments were standardized to simplify comparisons. First, the standardization applies to the stationary phase for which unbonded (naked) silica gel was used because this is both the simplest and an often employed phase which was (and still is to some extent) more stable toward temperature and solvolysis than many bonded phases. The polycyclic aromatic hydrocarbons used as the analytes are also employed by many investigators and range from those possessing considerable vapour pressure at the temperatures at which the chromatography is carried out to those with only a low vapour pressure. When there is no or negligible vapour pressure, movement through the column is due only to the dissolution power of the mobile phase. In this work with naphthalene, anthracene, pyrene and chrysene as the analytes and *n*-pentane as the mobile phase, some vapour pressure exists even for chrysene because separations with this mobile phase required temperatures up to 300°C. Another standardization applied to the feed rate of the pump and the column with a length of 25 cm and an I.D. of 4.6 mm. Either a constant pump feed rate of 1 ml min^{-1} at ambient temperature in the liquid state was chosen, or else, as in this work, a varied pump feed rate which was adjusted to yield a constant average linear velocity in the separation column. A constant pump feed rate has the advantage of being conveniently obtainable with simple present-day hardware. Specifically, the rate of 1 ml min^{-1} is in the general range of $\bar{u}_{\text{opt}}$ with the present mobile phase and column (bare silica gel; 4.6 mm I.D.) whereby it is to be understood that $\bar{u}_{\text{opt}}$ depends on the nature of the mobile phase, stationary phase, p and T.

EXPERIMENTAL

The eluent, *n*-pentane, containing a small amount of the modifier methanol (0.5%, v/v), was supplied from a container pressurized by helium. Between the container and a piston-driven membrane pump (Type MF 65; Orlita, Germany) a filter of stainless-steel frits (2-μm pore size) and between the pump and the column a membrane-type pulse damper (Type 3.350; Orlita) were installed. The analytical column (25 cm × 0.46 cm I.D.) was packed with unbonded silica gel (LiChrosorb Si 100, 10 μm; Merck, Germany) using a slurry method, the column being placed in an air-circulated oven (Type UT 5042, Heraeus, Germany). The column inlet and outlet pressures were measured with Bourdon-type manometers (class 0.6 VDO; Wika, Germany). For each chromatogram, 20 μl of a sample solution of naphthalene, anthracene, pyrene and chrysene, dis-

solved in *n*-heptane (0.13, 0.07, 0.13 and 0.03 mg, respectively, in 1 ml of heptane), were introduced by a loop injector (Type 7125; Rheodyne, USA) and monitored at the column exit by a UV detector (Type LC-75; Perkin-Elmer, USA). The outlet pressure downstream of column and detector was controlled by an adjustable back-pressure valve (Type 26-3200; Tescom, USA). To measure the flow-rate, the eluted mobile phase was collected with cooling. The apparent average linear velocity in the column was determined using $\bar{u} = L/t_0$ (L = column length, t_0 = dead time), whereby an injection of *n*-heptane was employed to determine t_0.

The four polycyclic aromatic hydrocarbons were purified by crystallization or sublimation. The *n*-pentane was dried over sodium, distilled, filtered and degassed. The methanol used as the modifier was of spectroscopic grade. The effective plate number, N_{eff}, and the effective plate height, H_{eff}, were obtained from the chromatogram according to

$$N_{eff} = 5.54\,(t'_r/w')^2 \quad (1)$$

and

$$H_{eff} = L/N_{eff} \quad (2)$$

where $t'_r = t_r - t_0$ is the net retention time, t_r the retention time, w' the width of the peak at half-height and L the column length. The capacity factors were obtained from $k' = (t_r - t_0)/t_0$.

For collecting chromatographic data, the physical parameters for the necessary isobaric–isothermal runs at constant linear velocity were varied between chromatograms as follows: at a given constant temperature, chromatograms were obtained for each average linear velocity and for each average pressure, whereby only one of the two physical parameters was changed at a time. Then the temperature was changed and enough time was allowed for the system to reach equilibrium before the velocity and pressure were changed in steps again. In all, chromatograms were obtained from 210 to 300°C and at apparent average velocities from 0.1 to 0.5 cm s^{-1} and at pressures from 20 to 70 bar.

Most of the N_{eff} data thus obtained correspond to a regular data grid of pressure and temperature, at a given constant linear velocity. Another part of the data, which were not obtained at regular intervals of pressure or density, and therefore did not fit the desired regular grid, were first drawn as curves *versus* pressure or density and then interpolated to obtain data which conformed to the grid. All the N_{eff} data were then used to calculate also the H_{eff} according to eqn. 2. Fig. 1a shows the directly measured lines of the pressure–temperature grid (solid lines) and the lines obtained by interpolation (dashed lines), whereby the pressures are average column pressures $\bar{p} = (p_i + p_o)/2$ (i, o = inlet and outlet, respectively). From theoretical considerations it is known that the arithmetic mean pressure $\bar{p}$ is about two thirds of the way down the column and is only reached after about two thirds of the total residence time of the mobile phase in the column [30]. The p–T pairs were converted into ρ–T pairs using published tables [31,32]. The calculations assumed pure *n*-pentane, neglecting the effect of the

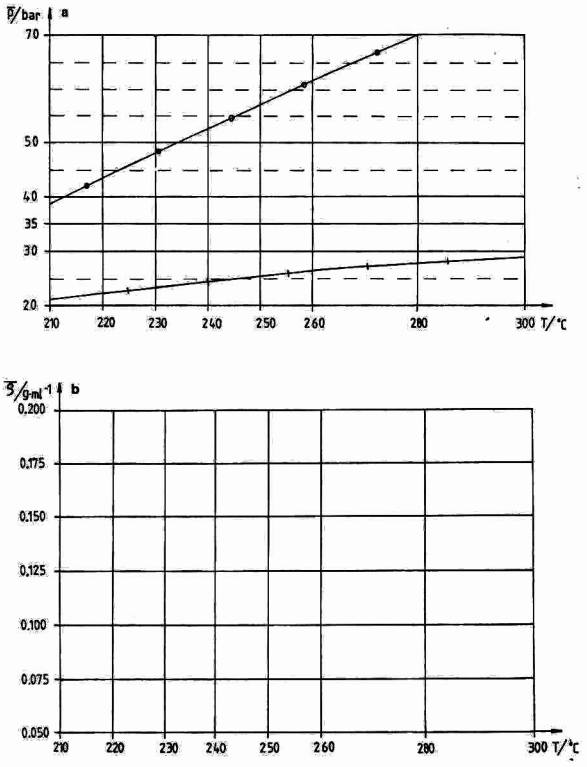

Fig. 1. (a) Two-dimensional grid of direct and interpolated experimental data (*e.g.*, of effective plate number, N_{eff}, or of capacity factor, k') at average column pressures, $\bar{p}$, temperatures, T, and constant average linear velocity. Sloping lines represent isochores of (+) $\rho = 0.050$ g cm^{-3} and (○) $\rho = 0.200$ g cm^{-3}. (b) Two-dimensional grid of experimental data (*e.g.*, N_{eff} or k') at average densities in the column, $\bar{\rho}$, temperatures, T, and constant average linear velocity. Grid is derived from the $\bar{p}$–T data in (a).

0.5% (v/v) modifying methanol on density. The density–temperature grid derived in this way from the original pressure–temperature grid in Fig. 1a is shown in Fig. 1b; the densities, $\bar{\rho}$, are average column densities corresponding to the average column pressures, $\bar{p}$. The isochores at the highest (0.20 g cm^{-3}) and the lowest density (0.05 g cm^{-3}) occurring in Fig. 1b are seen as two sloping lines in Fig. 1a. In order to obtain for Fig. 1b a rectangular grid, essentially only those data of Fig. 1a which are situated between the two isochores appear in Fig. 1b. Therefore, Fig. 1b contains less data than Fig. 1a and the same applies to plots seen later which show $\bar{\rho}$ instead of $\bar{p}$. For each average linear velocity a separate grid is established both for the type of grid in Fig. 1a and that in Fig. 1b. Each intersection or tee in Fig. 1a and b represents one data point for one of the chromatographic parameters (N_{eff}, H_{eff} or k'). From the grids three-dimensional graphs were obtained using a personal computer and graphics software as described previously [33].

RESULTS AND DISCUSSION

The data for N_{eff} are plotted as the third axis in three-dimensional plots and also as the hatching of the three-dimensional surfaces in these plots in Figs. 2 and 3. In Fig. 2a, b and c the other two axes are $\bar{p}$ and T and in Fig. 3a, b and c they are $\bar{\rho}$ and T, with the linear velocity, $\bar{u}$, being kept constant for a given plot. From the five linear velocities actually employed ($\bar{u}$ = 0.1, 0.2, 0.3, 0.4 and 0.5 cm s^{-1}), only three ($\bar{u}$ = 0.1, 0.3 and 0.5 cm s^{-1}) are shown in Figs. 2 and 3. Moreover, only the N_{eff} for chrysene, N_{eff}(C), is shown, chrysene being the last-eluting analyte in the mixture of polycyclic aromatic hydrocarbons used as a test substrate. Remarkably, all the plots presented in Figs. 2 and 3 are of similar shape, at least in principle. Particularly at a given low pressure or at a given low density, N_{eff}(C) passes through pronounced maxima with changing temperature. When the pressure increases, the maxima are found at higher temperatures than at lower pressures (Fig. 2). However, when the density increases this effect is hardly present any longer (Fig. 3). In both instances, the maxima decrease strongly in height with increasing pressure or increasing density. With increasingly linear velocity, *i.e.*, going from a to b to c, the maxima are shifted to higher

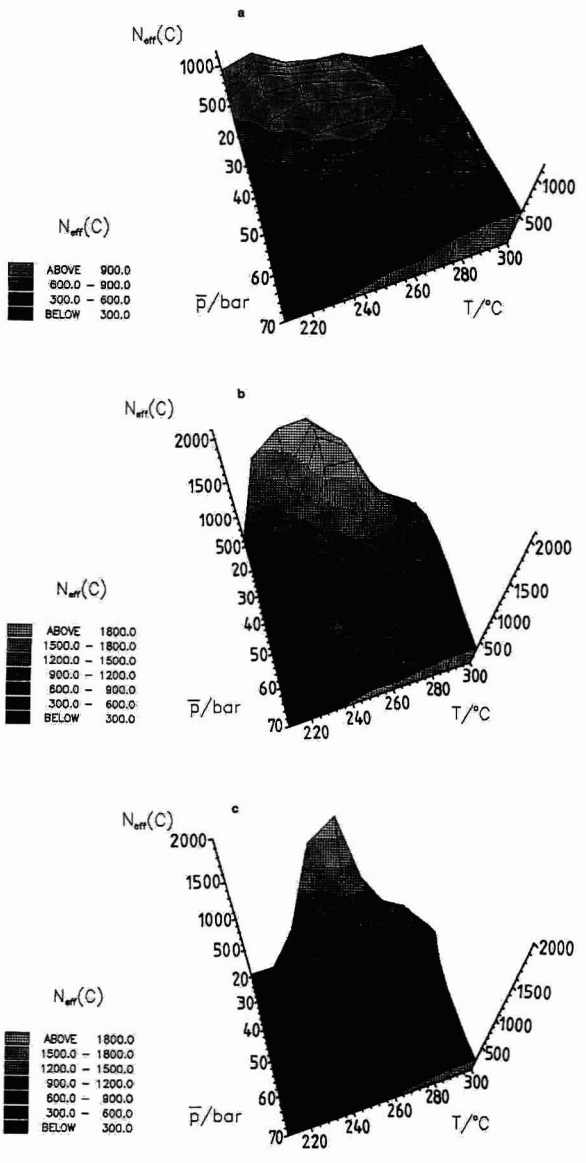

Fig. 2. Effective plate numbers of chrysene, N_{eff}(C), *versus* average column pressure, $\bar{p}$, and temperature, T, at three constant average linear velocities, $\bar{u}$: (a) 0.1; (b) 0.3; (c) 0.5 cm s^{-1}. The N_{eff}(C) are plotted on the z-axis as a three-dimensional surface, but they are also indicated as shadings on the surface of the graph. The data were obtained with *n*-pentane as mobile phase and unbonded silica gel as stationary phase.

temperatures. Thereby, the heights of the maxima appear to reach their greatest height at some intermediative velocity. With increasing velocity, the areas of low N_{eff}(C) become larger. Therefore, it becomes less easy to select $\bar{p}$–T or $\bar{\rho}$–T regions

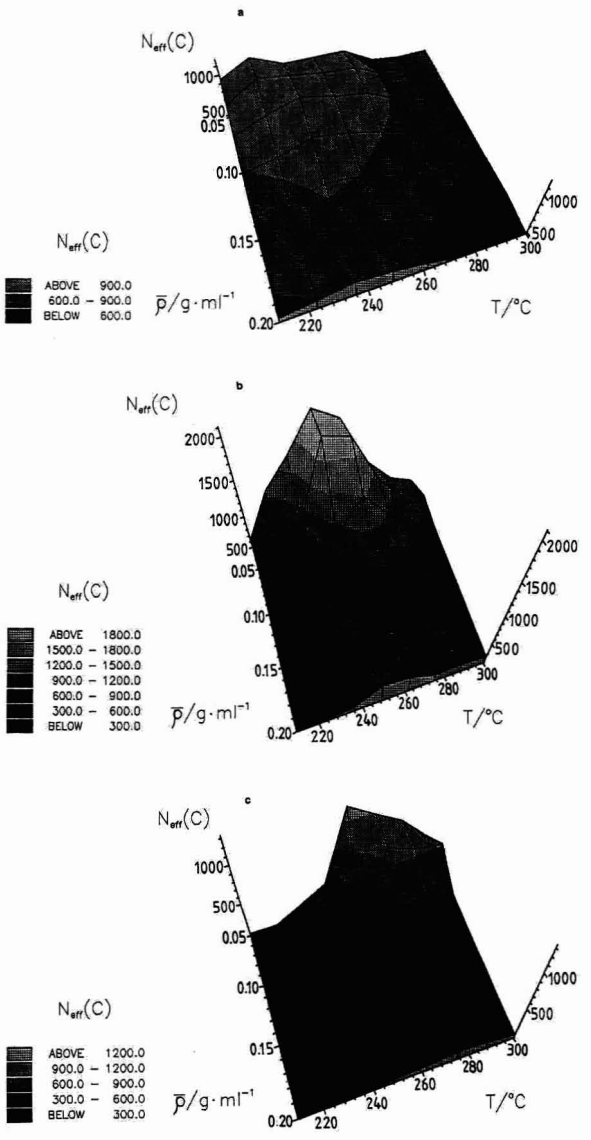

Fig. 3. Effective plate numbers of chrysene, $N_{eff}(C)$, *versus* average density of the mobile phase in the column, $\bar{p}$, and temperature, T, at three constant average linear velocities, $\bar{u}$: (a) 0.1; (b) 0.3; (c) 0.5 cm s^{-1}. Other details as in Fig. 2.

possessing an acceptable $N_{eff}(C)$ at higher than at lower velocity. Summarizing, in Figs. 2 and 3 strong decreases in $N_{eff}(C)$ from their maxima are seen when proceeding to higher pressures and higher or lower temperatures. Also, the highest $N_{eff}(C)$ are obtained at medium velocities in Figs. 2 and 3, which are closer to the optima of the velocity, $\bar{u}_{opt}$.

The results in Figs. 2 and 3 may be qualitatively explained by the Van Deemter equation and its modifications [34,35]:

$$H = A + B/\bar{u} + C\bar{u} + D\bar{u} \tag{3}$$

with H_{eff} being derived from H by

$$H \cdot \frac{(1 + k')^2}{k'^2} = H_{eff} \tag{4}$$

and

$$A = 2\lambda d_p \tag{5}$$

$$B = 2\gamma D_{1,2} = B' D_{1,2} \tag{6}$$

$$C = \frac{\Theta(k_0 + k' + k_0 k')^2 d_p^2}{30 k_0 (1 + k_0)^2 (1 + k')^2 D_{1,2}} = \\ = \frac{C'(k_0 + k' + k_0 k')^2}{D_{1,2} k_0 (1 + k_0)^2 (1 + k')^2} = \frac{C''}{D_{1,2}} \tag{7}$$

$$D = \frac{2k'}{(1 + k_0)(1 + k')^2 k_d} = \frac{D'}{k_d} \tag{8}$$

where

λ = eddy diffusion factor for the dispersion of size, direction, and velocity of the mobile phase streams in the interstitial flow channels between particles;

γ = obstruction factor for longitudinal diffusion;

Θ = tortuosity factor for impeding the diffusion within the intraparticulate pores of the particles;

k_0 = ratio of the intraparticulate void volume to the interstitial void volume;

k_d = velocity constant of desorption of analyte from the outside surface and from the pore surface of the particles;

$D_{1,2}$ = interdiffusion coefficient of the analyte molecules in the mobile phase.

λ, γ and Θ may be tentatively considered as independent of $\bar{p}$, T and $\bar{u}$ for a given chromatographic system, *i.e.*, for a given mobile and stationary phase, column geometry and analyte. The same may apply to k_0, but k', k_d and $D_{1,2}$ will depend strongly on p and T, although not on $\bar{u}$. It should be noted, however, that it may be expected that with greatly increasing $\bar{u}$ the pressure drop along the column, Δp, may reach levels such that k', k_d, and

$D_{1,2}$ start to depend to a considerable extent on $\bar{u}$ via Δp. This may arise if k', for instance, in the first half of the column decreases considerably less on account of higher density than it will increase in the second half of the column owing to lower density.

Turning now to the capacity factor instead of N_{eff}, the behaviour of the capacity factor of chrysene, k'(C), with respect to $\bar{p}$, T and $\bar{u}$ can be seen in the plots in Fig. 4. There is the usual strong decrease in k' with increasing $\bar{p}$ and also with increasing T, provided that one has passed already the maximum value of k' as a function of T, as is the case here. At velocities $\bar{u}$ between 0.1 and 0.4 cm s^{-1} little if any change in k' with $\bar{u}$ can be observed, but some decrease in k' may, in fact, be present with $\bar{u}$ = 0.5 cm s^{-1} at low $\bar{p}$ and T. On the whole, and over a moderate range of $\bar{u}$, one finds a k' which depends strongly on $\bar{p}$ and T but not on $\bar{u}$. If one desires to quantify the behaviour of k' it should be considered that a pressure drop over the column changes the k' along the column. One may start with the concept of an infinite number of equally long, identical sections over the total column length, each of these sections having its own k'. If there exists a significant pressure drop Δp at T = constant along the column, for instance, the sections closer to the inlet of the column will exhibit a lower k', whereas the sections closer to the outlet of the column will show a larger k', all relative to the k' measured experimentally for the total column length. This total k' will be composed of the k' of the individual sections. Assuming for simplicity that the total column is composed of only three sections, 1, 2 and 3, of equal length, one may start from the additivity of the retention times:

$$t_{r,1} + t_{r,2} + t_{r,3} = t_r(\text{total}) \quad (9)$$

where $t_{r,i}$ is the retention time of the analyte in the ith section. Similarly, one may write for the corresponding dead times

$$t_{0,1} + t_{0,2} + t_{0,3} = t_0(\text{total}) \quad (10)$$

If the same p–T conditions exist for all sections of the column,

$$t_{r,1} = t_{r,2} = t_{r,3} = 1/3\, t_r(\text{total}) \quad (11)$$

$$t_{0,1} = t_{0,2} = t_{0,3} = 1/3\, t_0(\text{total}) \quad (12)$$

If the p–T conditions are different, then eqns. 11 and 12 do not hold. Subtracting eqn. 10 from eqn. 9 and dividing by eqn. 10 yields

$$\frac{t_{r,1} - t_{0,1}}{t_{0,1} + t_{0,2} + t_{0,3}} + \frac{t_{r,2} - t_{0,2}}{t_{0,1} + t_{0,2} + t_{0,3}} + \frac{t_{r,3} - t_{0,3}}{t_{0,1} + t_{0,2} + t_{0,3}} = \frac{t_r(\text{total}) - t_0(\text{total})}{t_0(\text{total})} = k'(\text{total}) \quad (13)$$

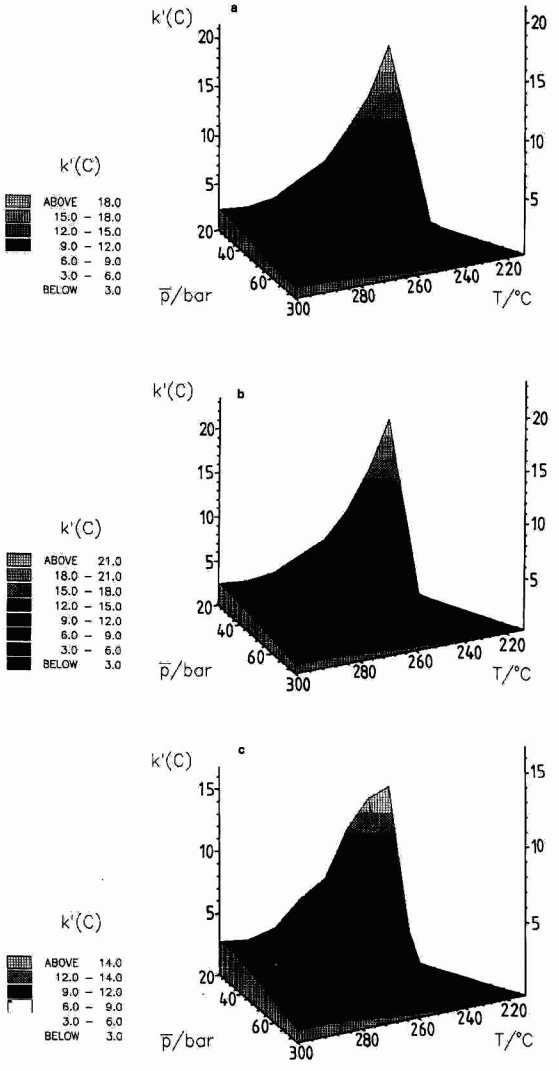

Fig. 4. Capacity factors of chrysene, k'(C), *versus* average column pressure, $\bar{p}$, and temperature, T, at three constant average linear velocities, $\bar{u}$: (a) 0.1; (b) 0.3; (c) 0.5 cm s^{-1}. The k'(C) are plotted on the z-axis as a three-dimensional surface and also shown by shading of this surface.

Considering that the density will be proportional to the dead time, provided that the mass flow-rate is not changed, it is obvious that the $t_{0,i}$ can be transformed into each other by a ratio of densities:

$$t_{0,1} = (\rho_1/\rho_2)t_{0,2} \quad (14a)$$

$$t_{0,1} = (\rho_1/\rho_3)t_{0,3} \quad (14b)$$

$$t_{0,2} = (\rho_2/\rho_3)t_{0,3} \quad (14c)$$

where the ρ_i are the densities in the ith section of the column, as counted from the column inlet. Substitution of eqns. 14 in eqn. 13 leads to

$$\frac{t_{r,1} - t_{0,1}}{(1 + \rho_2/\rho_1 + \rho_3/\rho_1)t_{0,1}} + \frac{t_{r,2} - t_{0,2}}{(\rho_1/\rho_2 + 1 + \rho_3/\rho_2)t_{0,2}} + \frac{t_{r,3} - t_{0,3}}{(\rho_1/\rho_3 + \rho_2/\rho_3 + 1)t_{0,3}} = k'(\text{total}) \quad (15)$$

or

$$\frac{k'_1}{1 + \rho_2/\rho_1 + \rho_3/\rho_1} + \frac{k'_2}{\rho_1/\rho_2 + 1 + \rho_3/\rho_2} + \frac{k'_3}{\rho_1/\rho_3 + \rho_2/\rho_3 + 1} = k'(\text{total}) \quad (16)$$

whereby the denominators with their ρ_i can be considered as weighting factors for the k' in the individual sections. Eqn. 13 can be generalized for n column sections, as in fact has been written before [36]:

$$\frac{\sum_{i=1}^{n} t_{r,i} - \sum_{i=1}^{n} t_{0,i}}{\sum_{i=1}^{n} t_{0,i}} = \frac{\sum_{i=1}^{n} (t_{0,i}k'_i)}{\sum_{i=1}^{n} t_{0,i}} = k'(\text{total}) \quad (17)$$

Eqn. 16 can also be rewritten as

$$\frac{k'_1}{\frac{\rho_1 + \rho_2 + \rho_3}{\rho_1}} + \frac{k'_2}{\frac{\rho_1 + \rho_2 + \rho_3}{\rho_2}} + \frac{k'_3}{\frac{\rho_1 + \rho_2 + \rho_3}{\rho_3}} = k'(\text{total}) \quad (18)$$

which becomes in general

$$\frac{\sum_{i=1}^{n} (k'_i\rho_i)}{\sum_{i=1}^{n} \rho_i} = \frac{\sum_{i=1}^{n} \frac{k'_i}{u_i}}{\sum_{i=1}^{n} \frac{1}{u_i}} = k'(\text{total}) \quad (19)$$

where u_i is the linear velocity in the ith column section. The u_i are inversely proportional to the ρ_i, other conditions being equal.

Inspecting Fig. 5, where the experimental pressure drop Δp is plotted *versus* $\bar{p}$ and T at $\bar{u}$ = constant, the expected strong decrease in Δp with decreasing $\bar{u}$ is seen. In fact, a graph for $\bar{u} = 0.1$ cm s^{-1} is not shown in Fig. 5 on account of the small Δp, leading with our experimental set-up to large relative errors in measurement. However, one can conclude from the data that Δp at $\bar{u} = 0.1$ cm s^{-1} is too small to cause significant differences between the k'_i along the column. Therefore, one may take the results of k'(total) in Fig. 4a ($\bar{u} = 0.1$ cm s^{-1}) as the results one will obtain not only at some average $\bar{p}$ but also at $\bar{p}$ = p(inlet) = p(outlet), *i.e.*, $\Delta p = 0$, that is, without pressure drop over the entire column. One may then read the approximate k'_i for individual sections of the column which possess different p from Fig. 4a. Assuming higher Δp, it is seen from Fig. 4a, b and c that the k'_i of the sections of the first

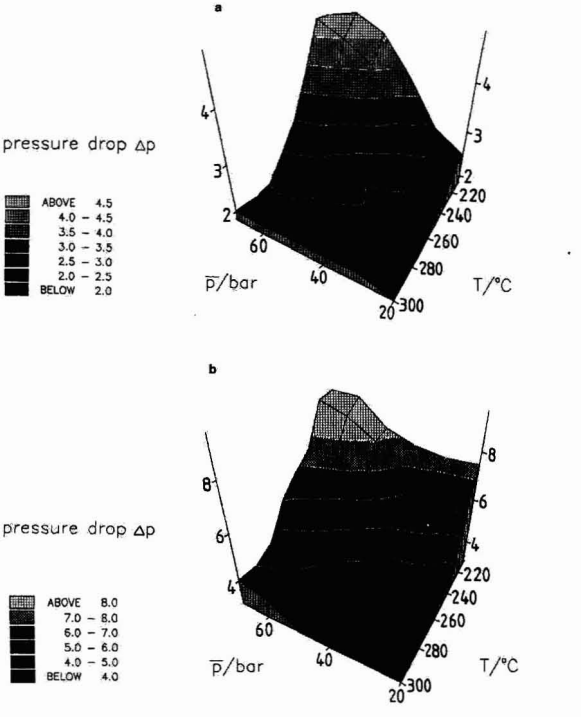

Fig. 5. Pressure drop over the total column, Δp (bar), *versus* average column pressure, $\bar{p}$, and temperature, T, at two constant velocities, $\bar{u}$: (a) 0.3; (b) 0.5 cm s^{-1}. The Δp are presented both on the z-axis and by shading.

half of the column will be compensated in part by the k'_i of the second half. This is the case whenever the k'_i of a p(inlet) is connected to the k'_i of p(outlet) by a sloping, more or less straight line in the graph. One may expect that within the range of the present pressure drops Δp, the k'(total) are roughly independent of $\bar{u}$, as in fact is found experimentally.

The p–T dependence of the interdiffusion coefficient $D^{\circ}_{1,2}$ at infinite dilution for chrysene in n-pentane is presented in Fig. 6, together with the viscosity data [37] needed for its calculation. The $D^{\circ}_{1,2}$ values were calculated according to the Wilke–Chang equation [38]:

$$D^{\circ}_{1,2} = 7.4 \cdot 10^{-8} \frac{(\phi M_2)^{\frac{1}{2}} T}{\eta_2 V_1^{0.6}} = K \cdot \frac{T}{\eta_2} \qquad (20)$$

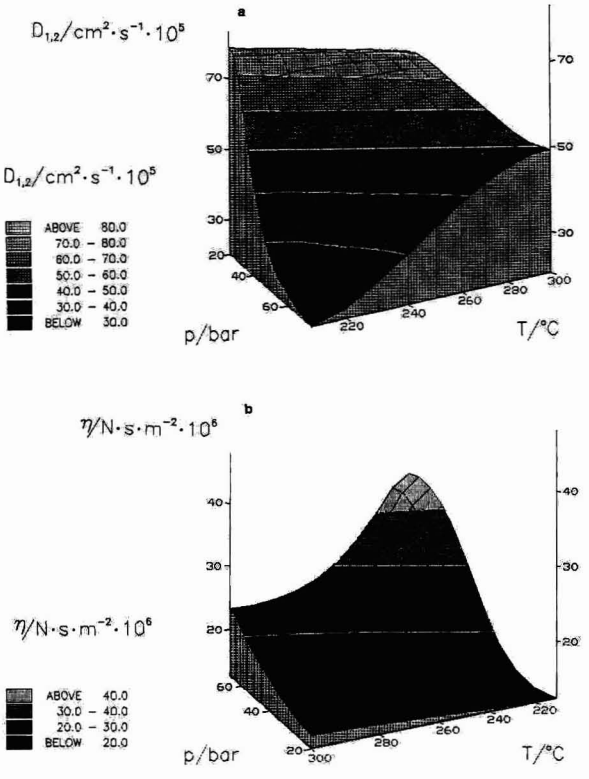

Fig. 6. (a) Interdiffusion coefficient, $D_{1,2}$, of chrysene in n-pentane at different pressures, p, and temperatures, T. $D_{1,2}$ calculated by the Wilke–Chang equation. Data are presented both on the z-axis and by shading. (b) Dynamic viscosity, η, of n-pentane at different pressures, p, and temperatures, T. Data are presented both on the z-axis and by shading.

where 1 and 2 refer to the analyte and the supercritical fluid, respectively, ϕ = dimensionless association factor (1.0 for unassociated supercritical fluids such as n-pentane), M_2 = molecular weight of the fluid, η_2 = dynamic viscosity of the fluid (cP), V_1 = molar volume of the analyte at its normal boiling temperature ($cm^3\ g\ mol^{-1}$) and K the combination of constants which is valid for a given solvent and solute. Although the Wilke–Chang equation is intended for liquid solvents, it is expected to yield reasonable values also for dense supercritical fluids well above T_c. The η_2 in Fig. 6b follow expectations in as much as an increasing pressure increases the viscosity particularly at lower temperature. It may be noted in passing that at a given density the temperature has only a negligible influence on viscosity [38], which means that lines of equal η in Fig. 6b have p–T pairs that lead to equal ρ.

The interdiffusion coefficient $D_{1,2}$ in Fig. 6a shows, as expected, a pronounced drop at the highest pressure and lowest temperature. This is also the location of highest η_2, the η_2 exerting a larger influence than temperature on $D_{1,2}$ (eqn. 20) because the relative ranges studied here are larger for η than for T. Obviously, a large $D_{1,2}$ may be obtained at low pressure over the entire temperature range. To obtain a sizeable $D_{1,2}$ at higher pressures, however, a higher temperature is required.

The viscosity, η, is not only connected to $D_{1,2}$ but also to the pressure drop, Δp. The viscosity and the average linear velocity, $\bar{u}$, of the fluid are the variables to determine the pressure drop for a given chromatographic column. According to Darcy's law,

$$\frac{dp}{dx} = -\frac{\bar{u}\eta}{B} \qquad (21)$$

where B is the specific permeability coefficient of a given column. Because $\bar{u}$ and η are in general functions of the distance travelled in the column, x, eqn. 21 is written in differential form. The experimental column pressure drop, Δp, in Fig. 5 increases with η and $\bar{u}$, as expected, although a non-trivial dp/dx must actually hold because of non-linear functions $u(x)$ and $\eta(x)$, and possibly also on account of partially non-laminar flow.

Plotting H_{eff} *versus* $\bar{u}$ at constant pressure and temperature would yield Van Deemter-type graphs.

In Figs. 7a, b and c pressure or density is employed as an additional third axis, showing the Van Deemter plots of H_{eff} of chrysene, $H_{eff}(C)$, as a function of $\bar{p}$ or $\bar{\rho}$ at T = constant. In Fig. 7a, which present the Van Deemter plot as a function of $\bar{p}$ at T = 220°C, the location of $\bar{u}_{opt}$ is shown as the dark black area. The movement of $\bar{u}_{opt}$ to lower $\bar{u}$ with increasing pressure becomes obvious, in addition to the very unfavourable $H_{eff}(C)$ with larger $\bar{u}$, *i.e.*, on the high velocity part of the graph. When the temperature is raised to 280°C, other conditions being equal, as in Fig. 7b, the higher temperature yields in almost all areas of the graph lower H_{eff} than in Fig. 7a. When $\bar{\rho}$ is used as the third axis instead of $\bar{p}$, T remaining at 280°C, as in Fig. 7c, the graph remains similar to Fig. 7b. Again, the $\bar{u}_{opt}$ move to lower $\bar{u}$ as pressure or density is increased, whereby at the highest pressure and densities the $H_{eff}(C)$ apparently have left the useful range. Fig. 8 shows the dependence of the Van Deemter plots on temperature at a constant pressure of p = 30 bar (Fig. 8a) and 50 bar (Fig. 8b). There is a tendency for $\bar{u}_{opt}$

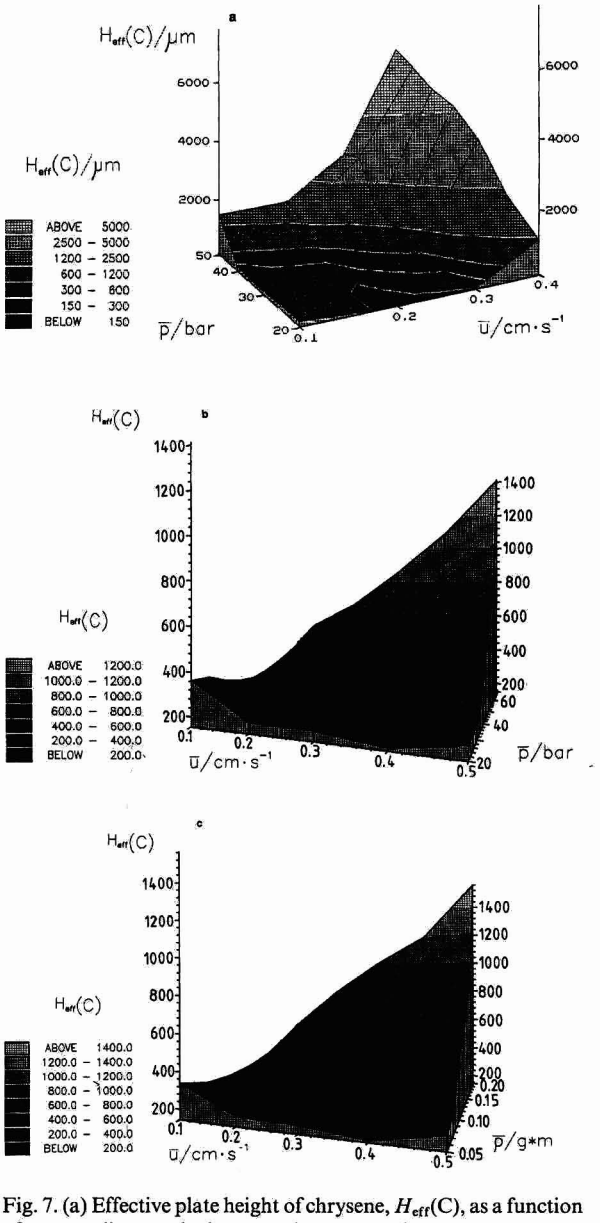

Fig. 7. (a) Effective plate height of chrysene, $H_{eff}(C)$, as a function of average linear velocity, $\bar{u}$, and average column pressure, $\bar{p}$, at 220°C. This is a Van Deemter-type plot with the additional feature of exhibiting the dependence on $\bar{p}$ on a third axis. (b) As (a), but at 280°C. (c) As (b), but replacing $\bar{p}$ with the average density, $\bar{\rho}$.

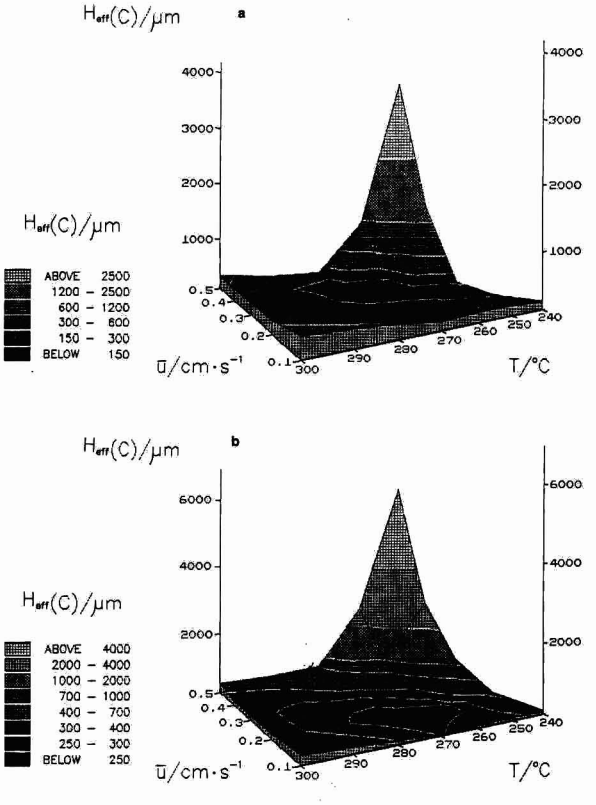

Fig. 8. Effective plate height of chrysene, $H_{eff}(C)$, as a function of average linear velocity, $\bar{u}$, and temperature, T, at a constant pressure. This is a Van Deemter-type plot with the additional feature of exhibiting the temperature dependence on a third axis. $\bar{p}$ = (a) 30 and (b) 50 bar.

to move to higher $\bar{u}$ when the temperature is raised. Comparing Fig. 8a and b, the range of $\bar{u}_{opt}$ is located at higher velocities when the pressures are lower and the H_{eff} are generally smaller. Both Figs. 7 and 8 lead to analogous conclusions.

The appearance of a minimum in H or H_{eff} at $\bar{u}_{opt}$ is, of course, a consequence of the validity of Van Deemter-type equations such as eqn. 3. Because the A term in eqn. 3 does not usually change much with $\bar{u}$ in gas chromatography, it is taken in eqn. 3 as independent of $\bar{u}$. The minimum in H or H_{eff} appears because of the counteracting influence of the $B/\bar{u}$ term *versus* the high-velocity terms $C\bar{u}$ and $D\bar{u}$. When the pressure increases in Fig. 7a and b, $D_{1,2}$ becomes smaller, particularly at lower temperature (Fig. 6a). At the same time the k' values decrease with increasing pressure and, therefore, the factor C'' decreases (eqn. 7), whereas k_d increases (eqn. 8). As Fig. 7a and b show, the overall result is an increase in H_{eff} and a moving of its minimum, $H_{eff,min}$, to lower $\bar{u}$. When the temperature, instead of the pressure or density, is increased, as plotted in Fig. 8a and b, $D_{1,2}$ increases strongly, particularly at higher pressure (Fig. 6a). The k' values mostly decrease with increasing temperature in the temperature range investigated (Fig. 4). This leads to a similar behaviour of C'' and k_d, as before, with increasing pressure. As Fig. 8a and b show, the overall result with increasing temperature is an increase in H_{eff} at velocities around $\bar{u}_{opt}$ or lower in the plateau region, but a strong decrease in H_{eff} at higher velocities. Generally, a movement of $H_{eff,min}$ to higher $\bar{u}$ is observed at higher temperatures. The latter is just the opposite of the effect of increasing pressure in Fig. 7a and b.

ACKNOWLEDGEMENTS

We thank B. Lorenschat for able technical assistance and the Deutsche Forschungsgemeinschaft for financial support.

REFERENCES

1 S. T. Sie, W. van Beersum and G. W. A. Rijnders, *Sep. Sci.*, 1 (1966) 459.
2 S. T. Sie and G. W. A. Rijnders, *Sep. Sci.*, 2 (1967) 729.
3 S. T. Sie and G. W. A. Rijnders, *Sep. Sci.*, 2 (1967) 755.
4 M. Novotny, W. Bertsch and A. Zlatkis, *J. Chromatogr.*, 61 (1971) 17.
5 B. P. Semonian and L. B. Rogers, *J. Chromatogr. Sci.*, 16 (1978) 49.
6 J. E. Conaway, J. A. Graham and L. B. Rogers, *J. Chromatogr. Sci.*, 16 (1978) 102.
7 U. van Wasen, I. Swaid and G. M. Schneider, *Angew. Chem.*, 92 (1980) 585.
8 D. Leyendecker, F. P. Schmitz and E. Klesper, *J. Chromatogr.*, 315 (1984) 19.
9 F. P. Schmitz, D. Leyendecker and E. Klesper, *Ber. Bunsenges. Phys. Chem.*, 88 (1984) 912.
10 D. Leyendecker, F. P. Schmitz, D. Leyendecker and E. Klesper, *J. Chromatogr.*, 321 (1985) 273.
11 J. M. Levy and W. M. Ritchey, *J. High Resolut. Chromatogr. Chromatogr. Commun.*, 8 (1985) 503.
12 C. R. Yonker and R. D. Smith, *J. Chromatogr.*, 361 (1986) 25.
13 J. M. Levy and W. M. Ritchey, *J. Chromatogr. Sci.*, 24 (1986) 242.
14 B. W. Wright and R. D. Smith, *J. Chromatogr.*, 355 (1986) 367.
15 S. M. Fields, K. E. Markides and M. L. Lee, *J. Chromatogr.*, 406 (1987) 223.
16 C. R. Yonker, D. G. McMinn, B. W. Wright and R. D. Smith, *J. Chromatogr.*, 396 (1987) 19.
17 S. M. Fields, K. E. Markides and M. L. Lee, *J. High Resolut. Chromatogr. Chromatogr. Commun.*, 11 (1988) 25.
18 J. L. Venthey, J. L. Janicot, M. Caude and R. Rosset, *J. Chromatogr.*, 499 (1990) 637.
19 S. T. Sie and G. W. A. Rijnders, *Sep. Sci.*, 2 (1967) 699.
20 J. A. Graham and L. B. Rogers, *J. Chromatogr. Sci.*, 18 (1980) 75.
21 F. P. Schmitz, H. Hilgers, D. Leyendecker, B. Lorenschat, U. Setzer and E. Klesper, *J. High Resolut. Chromatogr. Chromatogr. Commun.*, 7 (1984) 590.
22 S. M. Fields and M. L. Lee, *J. Chromatogr.*, 349 (1985) 305.
23 R. C. Simpson, J. R. Gant and P. R. Brown, *J. Chromatogr.*, 371 (1986) 109.
24 D. R. Gere, R. Board and D. McManigill, *Anal. Chem.*, 54 (1982) 736.
25 S. Shah and L. T. Taylor, *Chromatographia*, 29 (1990) 453.
26 P. A. Mourier, M. H. Caude and R. H. Rosset, *Chromatographia*, 23 (1987) 21.
27 H. Engelhardt, A. Gross, R. Mertens and M. Petersen, *J. Chromatogr.*, 477 (1989) 169.
28 M. Ashraf-Khorassani, S. Shah and L. T. Taylor, *Anal. Chem.*, 62 (1990) 1173.
29 A. Hütz and E. Klesper, in preparation.
30 D. E. Martire, *J. Chromatogr.*, 461 (1989) 165.
31 H. J. Löffler, *Thermodynamische Eigenschaften binärer Gemische leichter gesättigter Kohlenwasserstoffe im kritischen Gebiet*, Verlag C. F. Müller, Karlsruhe, 1962.
32 *Zahlenwerte und Funktionen, Landolt–Börnstein*, Bd. 52 II, 1. Teil, 6. Auflage, Springer, Berlin, 1971, p. 167.
33 A. Hütz, D. Leyendecker, F. P. Schmitz and E. Klesper, *J. Chromatogr.*, 505 (1990) 99.
34 L. R. Snyder and J. J. Kirkland (Editors), *Introduction to Modern Liquid Chromatography*, Wiley, New York, 2nd ed., 1979.
35 E. Heftmann (Editor), *Chromatography, Fundamentals, and Application of Chromatographic and Electrophoretic Methods, part A: Fundamentals and Techniques (Journal of Chromatography Library*, Vol. 22A), Elsevier, Amsterdam, 1983.

36 H. G. Janssen, H. M. J. Snijders, J. A. Rijks, C. A. Cramers and P. J. Schoenmakers, *J. High Resolut. Chromatogr.*, 14 (1991) 439.
37 K. Stephan and K. Lucas, *Viscosity of Dense Fluids*, Plenum Press, New York, 1979.
38 R. C. Reid, J. M. Prausnitz and T. K. Sherwood (Editors), *The Properties of Gases and Liquids*, McGraw-Hill, New York, 3rd ed., 1977, p. 567.

Journal of Chromatography, 607 (1992) 91–95
Elsevier Science Publishers B.V., Amsterdam

CHROM. 24 288

Molecular topology and chromatographic retention parameters for benzodiazepines

R. M. Soler Roca, F. J. García March, G. M. Antón Fos, R. García Doménech, F. Pérez Giménez and J. Gálvez Alvarez

Unidad de Investigación de Diseño de Fármacos y Conectividad Molecular, Departamento de Química-Física, Facultad de Farmacia, Universidad de Valencia, Valencia (Spain)

(First received January 28th, 1992; revised manuscript received April 15th, 1992)

ABSTRACT

The relationship between gas–liquid chromatographic (GLC) retention properties and R_F values in thin-layer chromatography (TLC) with molecular connectivity indices, ${}^m\chi_t$, was investigated for a series of benzodiazepines using multiple correlation coefficients, standard errors of estimate, *F*-Snedecor function values and Student's *t*-test as the criteria for best equation selection. Regression analyses show that the molecular connectivity model predicts the retention properties in GLC with the polar stationary phase OV-17 at 280°C and the R_F values in TLC with the stationary phase silica gel. However, zero- or second-order connectivity indices alone are not sufficient; higher-order indices are shown to be necessary. The effect of the polarity of the mobile phases in TLC was also investigated.

INTRODUCTION

Quantitative structure–activity relationship (QSAR) studies are used to explain or predict the physicochemical [1,2] or pharmacological [3–6] behaviour of drug molecules. Attempts have been made to develop a numerical description of a molecule derived not from experimental measurements of a property but from knowledge of the molecular structure itself [7]. Molecular topology transcribes molecular structure into a topological graph from which a number is derived, the topological index. Topological parameters, such as the molecular connectivity indices [8], can be used to quantify these properties.

The degree of retention in a chromatographic experiment depends on the structure and properties of the stationary phase and the molecular characteristics of the solute (volume, temperature, partition coefficient of each molecule, etc.). Experimental retention data of several groups of molecules on a given stationary phase can be correlated with parameters describing the molecular structure [9]. Unfortunately, the only criterion used to test the relationship between the observed and calculated retention properties in these experiments is the statistical correlation coefficient. This criterion is insufficient for predicting retention properties since a high correlation coefficient does not necessarily imply a correct elution sequence [10]. Other results indicate that the empirical additive scheme will not be able to reproduce adequately the retention indices of chlorinated benzenes unless a large number of parameters are employed [11,12].

Kier and Hall [13] have established that chromatographic behaviour depends on both topological and non-topological molecular structural characteristics. It seems that, for polar columns, the topological characteristics are more important. Other, later studies [14–16] have established that chromatographic parameters in a polar stationary phase system correlate better with the valence connectivity indices, whilst Kovat's parameters, obtained from

Correspondence to: Dr. Jorge Gálvez Alvarez, C/Ciscar 40, 46005 - Valencia, Spain.

0021-9673/92/$05.00

the apolar phase interaction, show best correlation with the non-valence connectivity terms.

In this study, the connectivity indices of nineteen benzodiazepines with different chromatographic properties were compared: retention times (t_R) in seconds, retention indices (RI) and R_F values are those reported in ref. 17.

Some reports correlating the chromatographic behaviour of drugs with molecular connectivity, for example the barbiturates [18] and the neuroleptics [19], have been published. However, the benzodiazepines have not been investigated.

METHOD OF CALCULATION

Connectivity indices are calculated from a hydrogen-suppressed formula or graph of the molecule, following the method of Kier and Hall [20]. The general form of the indices, ${}^m\chi_t$, is found by assigning to each vertex (non-hydrogen atom) in the molecular graph a value (δ) which is the number of edges (bonds) to that atom, bonds to hydrogen being ignored. Thus, for a graph of m edges and s subgraphs (binding between $m+1$ atoms), ${}^m\chi_t$ is calculated according to eqn. 1.

$$ {}^m\chi_t = \sum_{s=1}^{n_m} \prod_{i=1}^{m+1} (\delta_i)_s^{-1/2} \quad (1) $$

where n_m is the number of paths. Connectivity indices describing non-linear arrangements of bonds, such as clusters of three bonds, ${}^3\chi_c$, and path clusters of four bonds, ${}^4\chi_{pc}$, are calculated in the same way.

The vertex valences, δ^v, of the unsaturated carbon atoms and the heteroatoms (N or O) can be calculated using eqn. 2.

$$ \delta^v = Z^v - N_H \quad (2) $$

where Z^v is the number of valence electrons of the atom and N_H is the number of hydrogen atoms attached to it. The empirically derived values for the halogens were also used [21].

Single and multiple regression analyses were used to find the relationship between the gas chromatographic properties and the connectivity indices, and are calculated from eqn. 3.

$$ P = A_0 + \sum_{m,t} A_{m,t}\,{}^m\chi_t \quad (3) $$

where P is a property, and A_0 and $A_{m,t}$ represent the regression coefficients of the obtained equation.

Eqn. 3 was obtained by multilinear regression with 9R and 5R programs of the biostatistic package BMDP (Biomedical Computer Programs) [22]. To test the quality of the regression equations, the following statistical parameters were used: multiple correlation coefficient (r), standard error of estimate (s), F-Snedecor function values (F) and Student's t-test (statistical significance).

The retention time (t_R) in seconds and the retention index (RI) values in gas–liquid chromatography (GLC) used in this study, reported by Schütz [17], were obtained at 280°C with a 1.5 m × 2 mm I.D. glass column packed with 3% OV-17 on Chromosorb G AW DMCS (80–100 mesh) as the polar stationary column and nitrogen as the carrier gas at a flow-rate of *ca.* 15 m/min. The R_F values in thin-layer chromatography (TLC) were obtained with precoated TLC plates, silica gel 60 F_{254}, 20 cm × 20 cm, layer thickness 0.25 mm, activated for 1 h (110°C), saturated chamber, ascending method, length of run 10 cm, 20°C, and two solvent systems: chloroform–acetone (90:10, v/v) and benzene–isopropanol–25% ammonia solution (85:15:1, v/v/v).

RESULTS AND DISCUSSION

The connectivity indices and experimental chromatographic properties of nineteen benzodiazepines examined in this study are shown in Tables I and II, respectively.

Essentially, all these parameters represent the degree of affinity between the solute considered and the two phases, namely stationary and mobile. This affinity is closely related to the molecular solubility in both phases, and it is quantified by the distribution coefficient value for the solute in the two phases. This solubility, in turn, basically depends on two factors: first, the polar character of the solute (evaluated by its dipolar moment value) and, second, the solvent's capacity for solute solvation.

The selected equations for the retention times and retention indices in GLC of the compounds studied were, respectively:

$$ t_R = 1047.2\,{}^2\chi - 797.0\,{}^2\chi^v - 556.7\,{}^4\chi_{pc} + 461.7\,{}^4\chi^v_{pc} - 1402.7 \quad (4) $$

$$ n = 19 \quad r = 0.946 \quad s = 87.54 \quad F = 29.66 $$

TABLE I

CONNECTIVITY INDICES USED IN THE CORRELATIONS OF A GROUP OF BENZODIAZEPINES

Compound	$^0\chi$	$^2\chi$	$^2\chi^v$	$^3\chi_p$	$^3\chi_c^v$	$^4\chi_p$	$^4\chi_p^v$	$^4\chi_{pc}$	$^4\chi_{pc}^v$
Chlordiazepoxide	13.110	5.945	5.198	4.273	0.556	3.176	2.641	1.530	1.050
Demoxepam	12.240	5.786	4.966	3.980	0.556	3.109	2.535	1.468	0.985
3-Desmethylchlordiazepoxide	12.403	5.780	5.082	3.913	0.647	3.072	2.513	1.446	1.126
Diazepam	12.188	5.659	5.122	4.231	0.541	2.912	2.739	1.697	1.063
Nordiazepam	12.163	5.285	4.568	3.554	0.485	2.497	2.147	1.278	0.746
3-Hydroxydiazepam	13.058	6.122	5.201	4.608	0.577	3.191	2.724	2.029	1.106
Oxazepam	12.188	5.731	5.139	4.118	0.655	2.828	2.480	1.614	1.175
Nitrazepam	12.179	5.496	4.566	3.981	0.430	2.884	2.262	1.201	0.887
7-Aminonitrazepam	11.317	5.275	4.384	3.676	0.452	2.684	2.135	1.195	0.849
7-Acetamidonitrazepam	13.232	6.240	5.021	4.090	0.541	3.076	2.399	1.326	0.928
Medazepam	11.688	5.553	5.039	4.063	0.443	2.967	2.815	1.419	0.914
Lorazepam	13.110	6.180	5.697	4.469	0.818	3.068	2.768	1.894	1.522
Prazepam	13.886	6.303	5.751	4.589	0.745	3.431	3.093	1.702	1.117
3-Hydroxyprazepam	14.757	6.766	5.882	4.977	0.791	3.652	3.108	2.047	1.192
Clonazepam	13.102	5.945	5.125	4.331	0.593	3.123	2.549	1.481	1.233
7-Aminoclonazepam	12.240	5.724	4.943	4.026	0.615	2.923	2.422	1.475	1.196
7-Acetamidoclonazepam	14.154	6.689	5.247	4.441	0.602	3.315	2.612	1.606	1.230
Clobazam	12.895	6.191	5.304	4.627	0.533	3.386	2.029	2.005	0.966
Norclobazam	12.025	5.808	4.928	4.071	0.549	3.180	2.570	1.503	0.864

TABLE II

EXPERIMENTAL VALUES FOR SEVERAL CHROMATOGRAPHIC PROPERTIES OF BENZODIAZEPINES USING THE MOLECULAR CONNECTIVITY METHOD

Compound	GLC		TLC	
	t_R (s)	RI	R_{F_A}	R_{F_B}
Chlordiazepoxide	180	3160	0.07	0.47
Demoxepam	169	3142	0.10	0.30
3-Desmethylchlordiazepoxide	474	3590	0.02	0.30
Diazepam	127	3020	0.52	0.74
Nordiazepam	162	3124	0.26	0.52
3-Hydroxydiazepam	194	3200	0.42	0.51
Oxazepam	93	2888	0.16	0.26
Nitrazepam	335	3455	0.24	0.48
7-Aminonitrazepam	369	3475	0.08	0.30
7-Acetamidonitrazepam	823	3815	0.04	0.18
Medazepam	71	2775	0.56	0.85
Lorazepam	115	2979	0.16	0.30
Prazepam	230	3178	0.63	0.79
3-Hydroxyprazepam	358	3375	0.56	0.61
Clonazepam	435	3518	0.27	0.48
7-Aminoclonazepam	470	3560	0.08	0.30
7-Acetamidoclonazepam	1200	3970	0.04	0.19
Clobazam	232	3170	0.52	0.59
Norclobazam	316	3297	0.22	0.45

and

$$RI = 1129.3\,{}^{2}\chi - 1210.0\,{}^{2}\chi^{v} + 1447.7\,{}^{3}\chi_{c}^{v} - 477.5\,{}^{4}\chi_{pc} + 2705.9 \quad (5)$$

$$n = 19 \quad r = 0.911 \quad s = 124.12 \quad F = 17.05$$

Statistically, eqns. 4 and 5 are significant above the 99.9% level, while the ${}^{2}\chi$, ${}^{2}\chi^{v}$ and ${}^{4}\chi_{pc}$ indices are significant above the 99.9% level and ${}^{3}\chi_{c}^{v}$ and ${}^{4}\chi_{pc}^{v}$ indices are significant above the 95% level. In both cases, there is dependence on the ${}^{2}\chi$ and ${}^{2}\chi^{v}$ indices and typically branching parameters such as ${}^{3}\chi_{c}^{v}$, ${}^{4}\chi_{pc}$ and ${}^{4}\chi_{pc}^{v}$ occur. The size of benzodiazepines is described and quantified by the ${}^{2}\chi$ indices, the numerical values of which are directly proportional to the number of bonds in a molecule, and by the substitution pattern given by structural parameters. The difference ${}^{2}\chi - {}^{2}\chi^{v}$ somehow measures the polar character of the molecule, whilst the branching indices, *i.e.* cluster and path cluster, take into account the solvation effects, closely related to steric aspects.

Graphical representations of the experimental and theoretical values for these properties following equns. 4 and 5 are given in Figs. 1 and 2, respectively.

For the R_F values (with high polar mobile phase, R_{F_A}, or lower polar mobile phase, R_{F_B}) in TLC, the best regression equations and their statistical parameters are as follows:

$$R_{F_A} = 0.47\,{}^{3}\chi_{p} - 0.78\,{}^{4}\chi_{p} + 0.80\,{}^{4}\chi_{p}^{v} - 0.66\,{}^{4}\chi_{pc}^{v} - 0.74 \quad (6)$$

$$n = 19 \quad r = 0.927 \quad s = 0.07 \quad F = 21.31$$

and

$$R_{F_B} = 0.23\,{}^{0}\chi - 0.87\,{}^{2}\chi + 0.85\,{}^{4}\chi_{p}^{v} + 0.54 \quad (7)$$

$$n = 19 \quad r = 0.906 \quad s = 0.08 \quad F = 22.94$$

Eqns. 6 and 7 are statistically significant above the 99.9% level and 99% level, respectively. ${}^{2}\chi$, ${}^{4}\chi_{p}$, ${}^{4}\chi_{p}^{v}$ and ${}^{4}\chi_{pc}^{v}$ are significant above the 99.9% level and ${}^{0}\chi$ and ${}^{3}\chi_{p}$ are significant at the 99% level. The dependence on the ${}^{4}\chi_{p}$, ${}^{4}\chi_{p}^{v}$ and ${}^{4}\chi_{pc}^{v}$ indices should be emphasized; it occurs when polar eluents [chloroform–acetone mixture (90:10, v/v)] are used. However, when mixtures with a lower polar character are

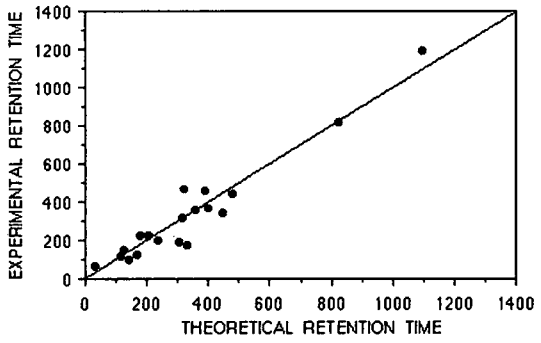

Fig. 1. Correlation between experimental (GLC with polar stationary phase, OV-17) and calculated (eqn. 4) retention times of nineteen benzodiazepines.

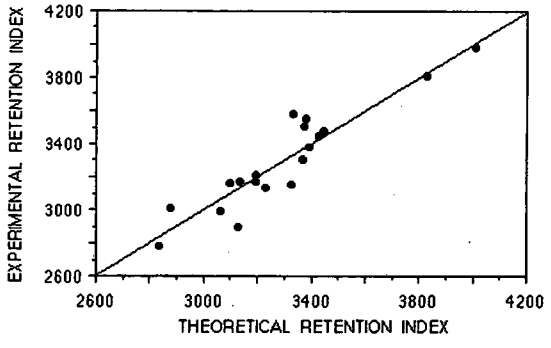

Fig. 2. Correlation between experimental (GLC with polar stationary phase, OV-17) and calculated (eqn. 5) retention indices of nineteen benzodiazepines.

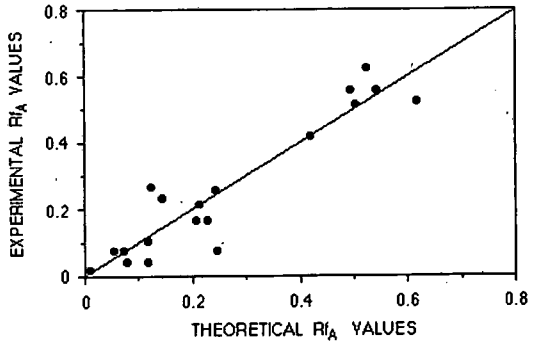

Fig. 3. Correlation between experimental (TLC with stationary phase silica gel and high polar mobile phase) and calculated (eqn. 6) R_{F_A} values of nineteen benzodiazepines.

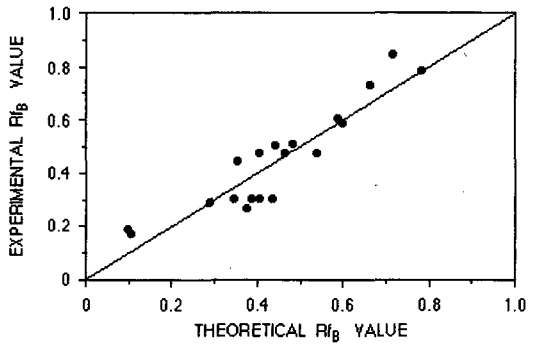

Fig. 4. Correlation between experimental (TLC with stationary phase silica gel and lower polar mobile phase) and calculated (eqn. 7) R_{F_B} values of nineteen benzodiazepines.

used, such as benzene–isopropanol–25% ammonia solution (85:15:1, v/v/v), these indices do not appear.

These results suggest that these indices, particularly $^4\chi^v_{pc}$, are a measure of the eluent's polar character. The comparison between experimental and theoretical R_F values is illustrated in Figs. 3 and 4.

This report demonstrates that a relationship exists between molecular connectivity and chromatographic retention parameters for a group of benzodiazepines. Generally a three or four-variable model is necessary to obtain a good degree of correlation.

CONCLUSION

The molecular connectivity model has been shown to be a useful tool for predicting and interpreting the different chromatographic retention parameters of benzodiazepines on different polarity phases. Statistical analyses show that the size of molecules and the structural terms control the drugs' chromatographic behaviour. In those cases concerning a system containing one polar phase, the dependence on the $^2\chi$, $^2\chi^v$ or $^4\chi_p$, $^4\chi^v_p$, together with a cluster or path cluster index, indicates that the three somehow evaluate the molecular dipolar moment, while the last estimates the solvent's solvation effects on the solute molecules.

REFERENCES

1 D. Hadzi and B. Jerman-Blazic, *QSAR in Drug Design and Toxicology*, Elsevier, Amsterdam, 1987.
2 R. Soler, R. García and J. Gálvez, *An. Real Acad. Farm.*, 57. (1991) 563–580.
3 J. F. Narbonne, P. Cassand, P. Alzieu, P. Grolier, G. Mrlina and J. P. Calmon, *Mutation Res.*, 191 (1987) 21.
4 C. Pandey, K. P. Dwivedi, G. D. Yadava, V. K. Singh, A. K. Srivastava and V. K. Agrawal, *Ind. J. Biochem. Biophys.*, 26 (1989) 405.
5 B. W. Blake, K. Enslein, V. K. Gombar and H. H. Borgstedt, *Mutat. Res.*, 241 (1990) 261.
6 R. García, J. Gálvez, R. Moliner and F. J. García, *Drug Invest.*, 3 (1991) 344.
7 D. H. Rovray and S. El-Basil, *J. Molec. Struct. (Theochem.)*, 165 (1988) 9.
8 J. Ciudad, R. García and J. Gálvez, *An. Quim.*, 83 (1987) 385.
9 M. Gassiot-Matas and G. Firpo-Pamies, *J. Chromatogr.*, 187 (1980) 1.
10 A. Sabljić, *J. Chromatogr.*, 314 (1984) 1.
11 A. Sabljić, *J. Chromatogr.*, 319 (1985) 1.
12 J. K. Haken and I. O. O. Korhonen, *J. Chromatogr.*, 265 (1983) 323.
13 L. B. Kier and L. H. Hall, *J. Pharm. Sci.*, 68 (1979) 120.
14 J. S. Millership and A. D. Woolfson, *J. Pharm. Pharmacol.*, 32 (1980) 610.
15 Gy. Szász, K. Valkó, O. Papp and J. Hermecz, *J. Chromatogr.*, 243 (1982) 347.
16 Gy. Szász, O. Papp, J. Vámos, K. Hankó-Novák and L. B. Kier, *J. Chromatogr.*, 269 (1983) 91.
17 H. Schütz, *Benzodiazepines*, Springer, New York, 1982.
18 R. Kaliszan, *J. Chromatogr.*, 220 (1981) 71.
19 L. Buydens, D. L. Massart and P. Geerlings, *J. Chromatogr. Sci.*, 23 (1985) 304.
20 L. B. Kier and L. H. Hall, *Molecular Connectivity in Chemistry and Drug Research*, Academic Press, New York, 1976.
21 L. B. Kier and L. H. Hall, *Molecular Connectivity in Structure–Activity Analysis*, Research Studies Press, Letchworth, 1986.
22 W. J. Dixon, *BMD Manual: Biomedical Computer Programs*, University of California Press, Los Angeles, CA, 1982.

Journal of Chromatography, 607 (1992) 97–104
Elsevier Science Publishers B.V., Amsterdam

CHROM. 24 361

Separation of polyunsaturated and saturated lipids from marine phytoplankton on silica gel-coated Chromarods☆

Christopher C. Parrish

Ocean Sciences Centre and Department of Chemistry, Memorial University of Newfoundland, St. John's, Newfoundland A1C 5S7 (Canada)

Guy Bodennec and Patrick Gentien

Département Environnement Littoral, IFREMER, Centre de Brest, 29280 Plouzané (France)

(First received February 7th, 1992; revised manuscript received May 18th, 1992)

ABSTRACT

Observations of peak splitting in Chromarod separations of extracts of marine samples led to an in-depth study of this phenomenon. By co-spotting standards with lipids from the phytoplankton *Gyrodinium aureolum* and developing in hexane-based solvent systems it was determined that triacylglycerol and free fatty acid peaks were split due to the presence of high levels of polyunsaturated species. The content of formic acid in the solvent system controlled the separation of saturated and polyunsaturated free fatty acids from each other and from triacylglycerols. The amount of diethyl ether controlled the separation of saturated and polyunsaturated triacylglycerols from each other and from more polar components. It was possible to quantify individual components of split peaks provided loads were kept below 3 μg to maximize separations between species. Iatroscan-measured calibration curves revealed a slightly lower response for polyunsaturated species when developed in hexane-based solvent systems. The proportion of polyunsaturated species determined by Iatroscan compared well with the proportion of polyunsaturated fatty acids determined by gas chromatography.

INTRODUCTION

Silica gel chromatography on Chromarods followed by flame ionization detection (FID) in an Iatroscan has been used extensively in the analysis of lipid classes in environmental samples (*e.g.* refs. 1–4). The attractiveness of this thin-layer chromatographic (TLC)–FID technique lies in the rapidity and simplicity with which samples can be prepared for analysis, the number of different sets of Chromarods that can be processed by a single Iatroscan in a day, and the synoptic type of information that it provides. In studies involving dynamic situations it is often better to obtain totals for classes in a large number of samples than it would be to obtain details of the molecular composition of each class in just a few samples. Different lipid classes may be used as indicators of different processes, *e.g.* anthropogenic inputs, energy storage in organisms, membrane synthesis, etc.

In samples from the marine environment, chromatographic peaks for a single-compound class are sometimes split [2,5–7] as a result of the partial separation of molecular species within that class [8,9]. Hydrogenation has been proposed as a means of eliminating peak splitting in marine samples [7,9]. An alternative approach that avoids this considerable increase in sample handling might be to accept that peak splitting occurs in some classes in some marine samples and to calibrate the components of such classes as individual entities. Indeed, in many

Correspondence to: Dr. C. C. Parrish, Ocean Sciences Centre and Department of Chemistry, Memorial University of Newfoundland, St. John's, Newfoundland A1C 5S7, Canada.

☆ O.S.C. Contribution 167.

0021-9673/92/$05.00

studies involving marine lipids it may be important to know the proportion of polyunsaturated constituents within a class. Currently, there is considerable interest in lipids containing marine polyunsaturated fatty acids in biomedical research [10], aquaculture [11,12], and most recently in the study of toxic algae [13–15]. Some algae are thought to cause fish kills by producing lipid compounds containing polyunsaturated fatty acids [13]. TLC–FID analyses may provide a rapid screening method for marine samples to evaluate their potential toxicity due to the presence of polyunsaturated lipid classes.

EXPERIMENTAL

The Chromarod–Iatroscan procedures used previously for saturated lipid classes [16] were the starting point for this investigation into the separation and calibration of lipids containing significant proportions of polyunsaturated fatty acids. Standards (Sigma, St. Louis, MO, USA) and samples were spotted on Chromarods-SIII (Iatron Labs., Tokyo, Japan) using a Hamilton syringe fitted into a Hamilton repeating dispenser (Hamilton, Reno, NV, USA). Chromarods-SIII are reusable quartz rods coated with silica gel particles of uniform shape and size [17]. Solute was applied near one end of each of ten rods held in a metal frame. The solute was focused twice using acetone to produce a narrow band of lipid near the lower end of the rods. The rods were then dried and conditioned over saturated sodium chloride at 22°C for 5 min before development in a hexane-based solvent system. After separation of classes, the rods were scanned at 0.4 cm/s in an Iatroscan MK IV analyzer (Iatron) with a hydrogen flow-rate of 160 ml/min and an air flow-rate of 2000 ml/min. The scanning direction of the rods was the opposite of the development direction in the TLC tanks. Data acquisition from the FID system and calibration were performed with BOREAL software (FLOTEC, La Queue lez Yvelines, France).

The marine phytoplankton samples were taken from cultures of the toxic dinoflagellate *Gyrodinium aureolum*. The algae were grown in batch culture as described previously [18] at 13 and 18°C [15]. The particulate material in the samples was separated from that material dissolved in the culture medium by centrifugation at 13 200 *g* (12 000 rpm) and the dissolved and particulate fractions were extracted using large-scale extraction procedures [15]. For fatty acid analysis of the neutral lipids in the extracts, a portion of each extract was placed on a Florisil column and eluted with chloroform. TLC–FID analysis of an eluate revealed only 8% contamination of the neutral lipid classes by polar lipids. Fatty acid methyl esters were analyzed in a Hewlett-Packard 5890 Series II gas chromatograph (Hewlett-Packard, Palo Alto, CA, USA) containing a 60 m × 0.25 mm I.D. capillary column coated with Supelcowax-10 (Supelco, Bellefonte, PA, USA). Samples were injected in the splitless mode at 200°C.

RESULTS AND DISCUSSION

Optimization of separations of polyunsaturated and saturated lipids

Lipid class separations were attempted using various standards in various developing systems to optimize the separation between polyunsaturated and more saturated neutral lipids within classes while maintaining the basic class separations according to functional groups. Since non-polar solvent systems are more effective at separating lipids according to the degree of unsaturation [9], Chromarods were developed in solvent systems ranging in polarity from hexane–diethyl ether–formic acid (H–D–F) 95:4:1 to 100% hexane. The use of non-polar solvent systems also minimizes separations according to chain-length [9].

Multicomponent standards containing free fatty acids (FFAs) and triacylglycerols (TGs) with different degrees of unsaturation were spotted onto Chromarods-SIII so that the load of each class was 3–4 μg. We were unable to separate any pair of oleic acid, palmitic acid and lauric acid in any of our hexane-based non-polar solvent systems. In order to be able to separate FFA on Chromarods the degree of unsaturation must differ by more than one double bond [9]. Thus, palmitic acid and linolenic acid were well separated in all solvent systems, provided they contained a minimum of 0.5% formic acid.

The level of formic acid was important in determining the extent to which saturated and unsaturated FFAs were separated from each other and from TGs. In solvent systems containing H–D–F

99.6:0.2:0.2, or less polar, neither saturated nor unsaturated FFAs separated from each other nor from TG. In H–D–F 99:0.5:0.5, linolenic acid and palmitic acid separated from each other and from TGs, but TGs were not well separated from more polar components. The amount of diethyl ether was important in determining the extent to which polyunsaturated and saturated TGs were separated from each other and from more polar components. To separate TGs from all other components requires a system more polar than H–D–F 98:1:1.

Fig. 1 shows the separations obtained in four solvent systems ranging in polarity from H–D–F 97:2:1 to H–D–F 95:4:1. It can be seen that small changes (1% or less) in the proportion of diethyl ether produce large changes in the efficiency of separations between polyunsaturated and saturated species. Tripalmitin and trilinolein are not separated at this load in H–D–F 97:2:1 (Fig. 1a) but are partially separated in 97:3:1 (Fig. 1b). The best separation of all four standards was obtained in 96:3:1 (Fig. 1c). In H–D–F 95:4:1 saturated TGs (TG_s) are too mobile with respect to polyunsaturated FFAs

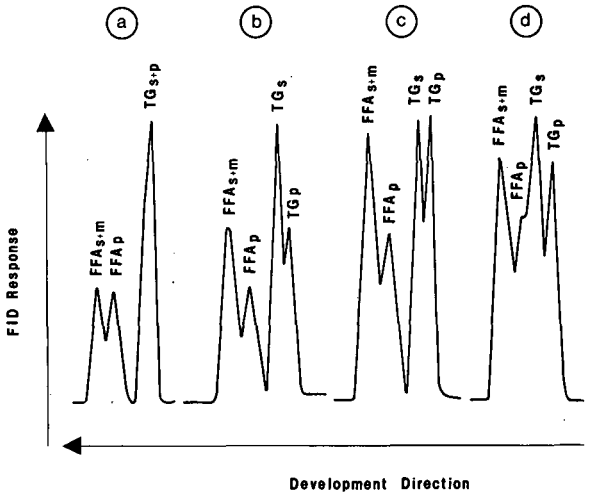

Fig. 1. Separations of saturated (s), monounsaturated (m) and polyunsaturated (p) free fatty acid (FFA) and triacylglycerol (TG) standards on Chromarods-SIII after 40-min developments in (a) hexane–diethyl ether–formic acid (H–D–F) 97:2:1, (b) H–D–F 97:3:1, (c) H–D–F 96:3:1, and (d) H–D–F 95:4:1. The attenuation in each chromatogram has been adjusted according to the size of the major peak.

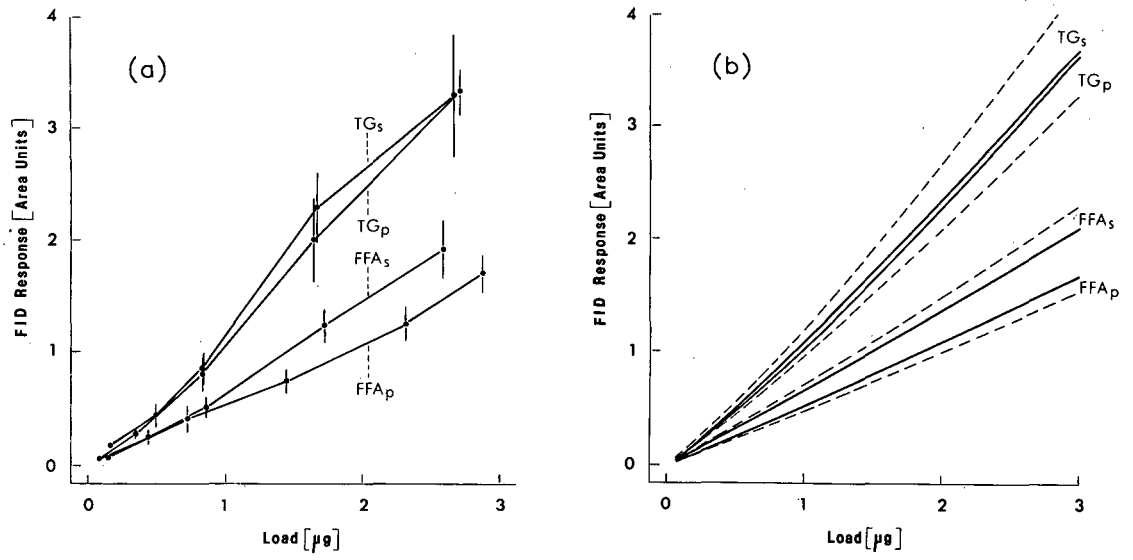

Fig. 2. Iatroscan FID responses to saturated (s) and polyunsaturated (p) triacylglycerol (TG) and free fatty acid (FFA) standards on Chromarods-SIII after 40-min developments in hexane–diethyl ether–formic acid (96:3:1, v/v/v). (a) Calibration data: error bars extend 1 standard deviation from the means. (b) Calibration curves and 95% confidence intervals. Solid lines are power law regressions through raw data points. Broken lines are the upper 95% confidence intervals for the regression lines of the saturated species and the lower 95% confidence intervals for the polyunsaturated species.

(FFA_p) and the separation of linolenic acid and tripalmitin is lost (Fig. 1d). This was also the case in another relatively polar system: H–D–F 97:1:2 (not shown). In systems more polar than this, even the separation between saturated FFAs and TGs would be lost as they run together in H–D–F 92:7:1 [1]. In systems containing more than 7% diethyl ether the elution order of FFAs and TGs is reversed [1].

Quantification of neutral acyl lipid standards

Quantitative mixtures of standard tripalmitin, trilinolenin, palmitic acid and linolenic acid dissolved in chloroform were used for calibration (Fig. 2). Calibration data were obtained at five levels between 0.08 and 2.89 μg with, on average, six analyses per level on different rods within a single set. The average coefficient of variation was 16% (Fig. 2a). These calibration curves show that polyunsaturated species give a slightly lower response as was found with a fish oil developed in a hexane-based solvent system [19].

Regression analysis with the raw calibration data suggested that linear regressions were adequate for calibration (r^2 values in the range 94.1–97.3%); however, power law regressions (Fig. 2b) gave an even better fit (r^2 = 96.6–98.2%). The power law exponents ranged from 1.05 ± 0.03 to 1.11 ± 0.05 for all regressions except that for trilinolenin where the exponent was 1.15 ± 0.03.

Linear regressions through the raw data gave intercepts that were not significantly different from zero for all except the trilinolenin data, suggesting the response for three of these standards was truly linear. This is confirmed by the proximity to 1.0 of the power law exponent for these three components. These exponents are similar to those obtained previously for tripalmitin and palmitic acid on Chromarods-SII [20].

The polyunsaturated standards were monitored for breakdown by looking for build-up of oxidized material at the origin of the Chromarods after development [7]. With normal precautions against oxidation the standards appeared quite stable: there was no evidence for breakdown in a 1-month period.

Separation of neutral acyl lipids in marine phytoplankton samples

G. aureolum is thought to produce polyunsaturated lipids which cause lysis of mouse and trout red blood cells [13,18] and which retard growth in other marine phytoplankton [18,21]. Fig. 3 shows the lipid class composition in extracts of extracellular (dissolved) and intracellular (particulate) lipids of this

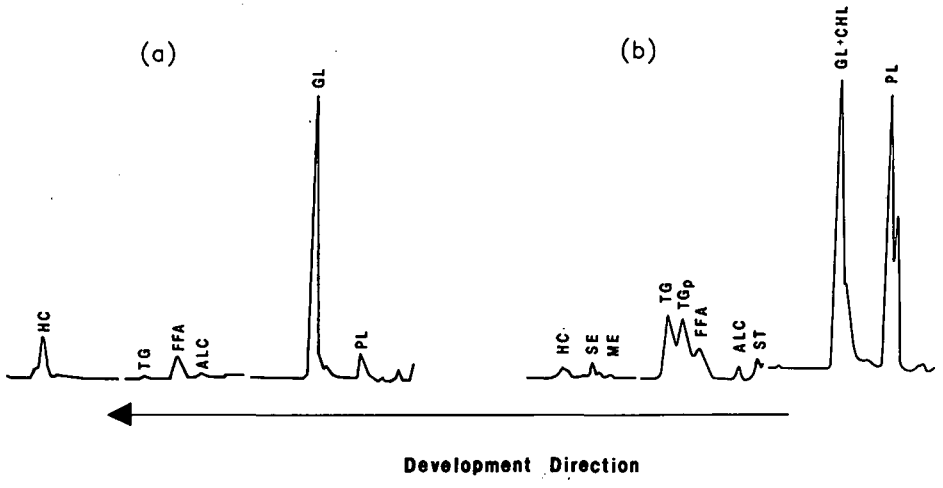

Fig. 3. Multi-step separations of extracts of (a) extracellular lipids and (b) intracellular lipids in a batch culture of *Gyrodinium aureolum* grown at 13°C. Polarity increases from left to right: HC (hydrocarbon), SE (sterol ester), ME (methyl ester), TG (triacylglycerol), TG_p (polyunsaturated triacylglycerol), FFA (free fatty acid), ALC (free alcohol), ST (free sterol), GL (glycolipid), CHL (chlorophyll), PL (phospholipid). Neutral lipid classes were separated by developing twice in hexane–diethyl ether–formic acid (99:1:0.05, v/v/v) partially scanning, and then developing for 40 min in H–D–F (80:20:0.1, v/v/v).

toxic marine dinoflagellate. These chromatograms are composites of three scans of the same sample on the same rod obtained in a multi-step procedure involving several developments with partial scanning in between [15]. It can be seen that glycolipids (identified by co-spotting with galactosyl diglyceride) are the major components in the extracellular lipids (Fig. 3a) and that TGs and phospholipids are proportionally more important within the cells (Fig. 3b). It can also be seen that the TG peak is split into two suggesting that there is a significant proportion of polyunsaturated species (TG_p) in this class. Note that TG runs ahead of FFA in the multi-step procedure because these acyl lipids are eluted in a system containing 20% diethyl ether (Fig. 3).

Figs. 4 and 5 show single-step separations of dissolved and particulate lipid samples from an 18°C culture of *G. aureolum*. The lower two panels of

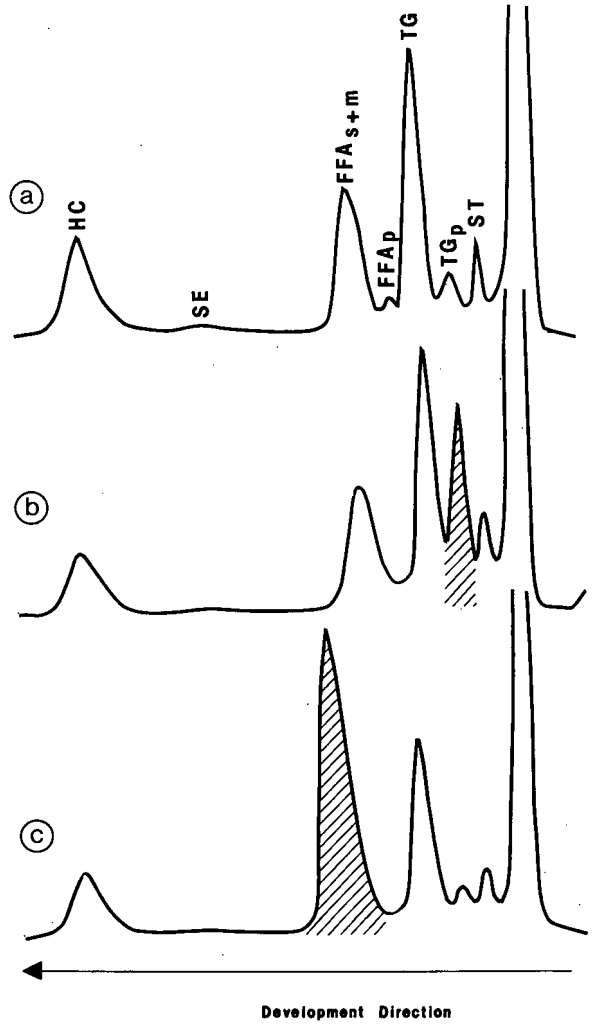

Fig. 4. Separations of extracellular lipids from an 18°C culture of *Gyrodinium aureolum* after a single 40-min development in hexane–diethyl ether–formic acid (97:2:1, v/v/v). (a) Water extract alone. (b) Water extract co-spotted with trilinolein (hatched peak). (c) Water extract co-spotted with palmitic acid and oleic acid (hatched peak).

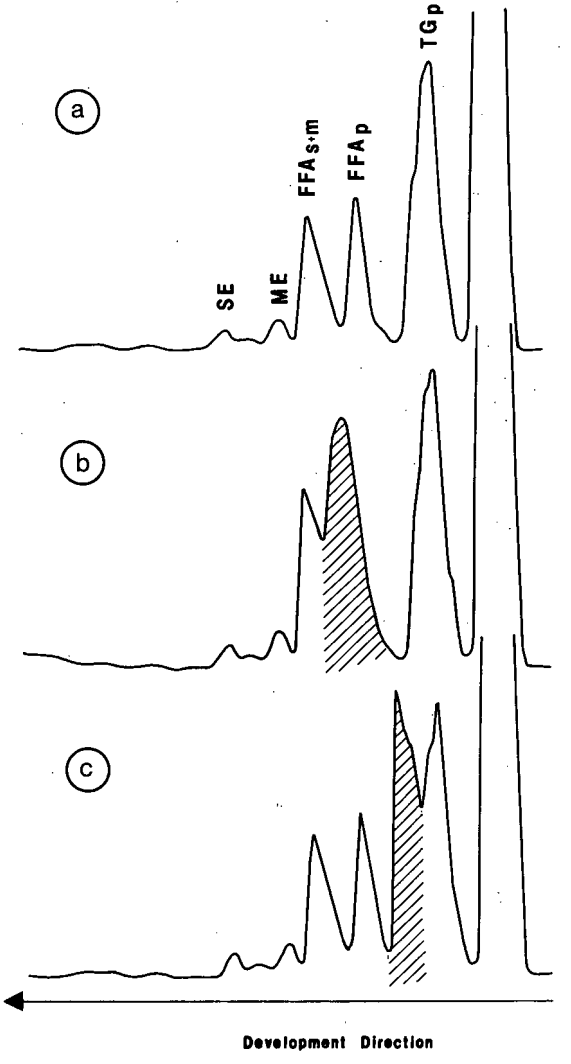

Fig. 5. Separations of intracellular lipids from an 18°C culture of *Gyrodinium aureolum* after a single 40-min development in hexane–diethyl ether–formic acid (97:2:1, v/v/v). (a) Cell extract alone. (b) Cell extract co-spotted with linolenic acid (hatched peak). (c) Cell extract co-spotted with tripalmitin (hatched peak).

these figures show how peak identities were confirmed. The 13°C particulate samples were similar to the 18°C particulate samples in that baseline separations were obtained between an FFA peak containing predominately polyunsaturated fatty acids and a peak containing more saturated species. Likewise for intracellular TGs, separations were obtained between polyunsaturated species and more saturated species in the 13°C samples. However, the 18°C samples appeared to be more strongly dominated by less saturated components (Table I, Fig. 5).

While the particulate samples clearly had a high proportion of polyunsaturated fatty acids in the neutral lipids, the dissolved samples were strongly dominated by saturated species as evidenced by the lack of TG peak splitting in Fig. 3a and the very small peaks for polyunsaturated FFAs and TGs in Fig. 4. Co-spotting with authentic standards showed that the major FFA peak in the dissolved samples resulted from more saturated species.

A single-step separation in H–D–F 96:3:1 is preferable to a multi-step separation in the determination of polyunsaturated neutral lipids as a more strongly bimodal distribution in the degree of unsaturation is necessary for separation in the multi-step procedure. Polyunsaturated and saturated FFA hardly separate in the multi-step procedure and they run close to polyunsaturated TGs so that it was difficult to separate FFAs and polyunsaturated TGs at loads higher than 2 μg using this procedure. Fewer species appear to be included in the TG_p peak as the proportion of the total TGs in this peak was lower when measured in a multi-step procedure. With six analyses, the 13°C culture gave a proportion of 38 ± 5% for TG_p and the 18°C culture gave a value of 68 ± 10% (*cf.* Table I).

While the optimum separation of standards was obtained in H–D–F 96:3:1 (Fig. 1), it should be noted that excellent separations were also obtained with these samples in 97:3:1 and even 97:2:1 (Figs. 4

TABLE I

RELATIVE PROPORTIONS OF SATURATED AND POLYUNSATURATED SPECIES WITHIN THE TRIACYLGLYCEROLS AND FREE FATTY ACIDS IN EXTRACTS OF *GYRODINIUM AUREOLUM* CELLS

Intracellular lipids were separated in a single 40-min development in hexane–diethyl ether–formic acid (96:3:1, v/v/v); data are means ± S.D., n = 6.

	Relative proportion (%)	
	13°C Culture	18°C Culture
Polyunsaturated species in TGs	50 ± 5	88 ± 10
Polyunsaturated species in FFAs	45 ± 8	46 ± 6

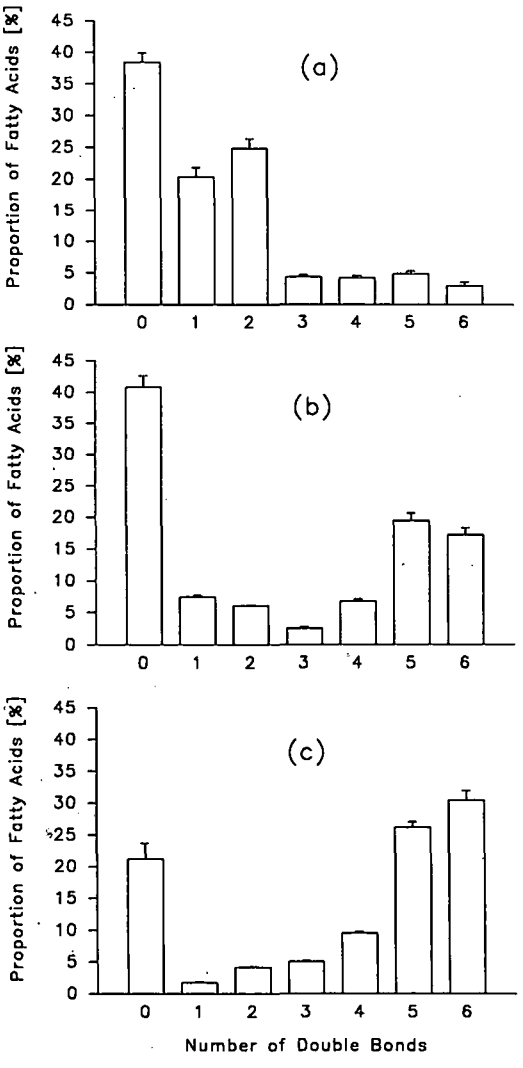

Fig. 6. Distribution of fatty acids with respect to unsaturation in dissolved and particulate matter from an 18°C culture of *Gyrodinium aureolum* sampled after 41 days. (a) Dissolved total lipids. (b) Particulate total lipids. (c) Particulate neutral lipids. Fatty acids were measured as their methyl esters by capillary gas chromatography.

and 5), suggesting the differences in unsaturation between peaks was greater in the samples than in the standards. For quantitation, however, samples and standards were routinely developed in H–D–F 96:3:1 (Table I) to maximize the range over which calibration curves could be obtained (Fig. 2). Nonetheless, overlapping of peaks made it difficult to perform analyses beyond loads of 3 μg. Accurate integration of peak areas in shouldering peaks depends on the integrator's ability to recognize the exact location of the trough between the peaks. The more the peaks overlap, the greater is the effect on accuracy and precision of any error in determining the base of the trough. As loads were lowered the degree of overlapping was reduced but the signal-to-noise ratio decreased so that, although it was possible to detect peaks of both saturated and polyunsaturated lipid classes below 100-ng load, calibration below 100 ng was unreliable.

The comparison between TLC–FID (Figs. 4 and 5) and gas chromatographic (Fig. 6) analyses of extracts of *G. aureolum* further validates the use of Chromarod separations for determining polyunsaturated lipids. The distribution of fatty acids in the total dissolved lipid extracts was biased towards the less unsaturated fatty acids with over half of the fatty acids being saturated or monounsaturated and less than 20% having three or more double bonds (Fig. 6a). The distribution of fatty acids in the total particulate lipid extracts was more bimodal with most of the fatty acids being saturated or highly unsaturated and less than a quarter containing one to four double bonds (Fig. 6b). The low levels of dienoic and trienoic fatty acids would also permit separation of the methyl esters on silica gel coated plates [22]. The distribution of fatty acids in the neutral lipids was biased towards polyunsaturation (Fig. 6c): 77% of the fatty acids in the neutral lipids contained two or more double bonds. This figure compares well with the value of 88 ± 10% obtained in TLC–FID analyses of TG (Table I) which were the major neutral lipid class present in the extracts (Fig. 5).

CONCLUSIONS

It is possible to calibrate split peaks in Chromarod analyses of marine phytoplankton lipids provided loads are kept low. Polyunsaturated standards gave lower responses but the difference in response was small by comparison with the error of repeat analyses at any one level or the error in regression equations obtained from calibration data. This is especially true in the case of TG standards where a single TG calibration curve would suffice for most applications in which a non-polar hexane-based solvent system was used. Thus the components of a split TG peak may be calibrated with a single standard and the sum of these two components would be close to the total TG load on the rod. Quantification of split chromatographic TG peaks in multi-step developments and of TG and FFA peaks in single-step developments may be a very useful way to rapidly determine the degree of polyunsaturation within these marine lipid classes.

ACKNOWLEDGEMENTS

This work is part of the IFREMER programme "Effloresences Algales Toxiques". C.C.P. received partial funding through the Canada–France Science and Technology Cooperation Programme. We are grateful to M. Lunven for looking after the algal cultures.

REFERENCES

1 C. C. Parrish and R. G. Ackman, *J. Chromatogr.*, 262 (1983) 103.
2 D. Emdadi and B. Berland, *Mar. Chem.*, 26 (1989) 215.
3 M. Goutx, C. Gerin and J. C. Bertrand, *Org. Geochem.*, 16 (1990) 1231.
4 J. K. Volkman and P. D. Nichols, *J. Planar Chromatogr.*, 4 (1991) 19.
5 R. P. Delmas, C. C. Parrish and R. G. Ackman, *Anal. Chem.*, 56 (1984) 1272.
6 C. C. Parrish and R. G. Ackman, *Lipids*, 20 (1985) 521.
7 N. C. Shantha and R. G. Ackman, *Lipids*, 25 (1990) 570.
8 J. K. G. Kramer, R. C. Fouchard and E. R. Farnworth, *Lipids*, 20 (1985) 617.
9 T. Ohshima, W. M. N. Ratnayake and R. G. Ackman, *J. Amer. Oil Chem. Soc.*, 64 (1987) 219.
10 R. K. Chandra, *Health Effects of Fish and Fish Oils*, ARTS, St. John's, 1989.
11 T. van Vliet and M. B. Katan, *Am. J. Clin. Nutr.*, 51 (1990) 1.
12 S. Sigurgisladottir, S. P. Lall, C. C. Parrish and R. G. Ackman, *Lipids*, 27 (1992), in press.
13 T. Yasumoto, B. Underdal, T. Aune, V. Hormazabal, O. M. Skulberg and Y. Oshima, in E. Graneli, B. Sundstrom, L. Edler and D. M. Anderson (Editors), *Toxic Marine Phytoplankton, Proceedings of the 4th International Conference on Toxic Marine Phytoplankton, Lund, June 1989*, Elsevier, New York, 1990, pp. 436–440.

14 C. C. Parrish, A. S. W. deFreitas, G. Bodennec, E. J. Macpherson and R. G. Ackman, *Phytochemistry*, 30 (1991) 113.
15 C. C. Parrish, G. Bodennec, J.-L. Sebedio and P. Gentien, *Phytochemistry*, in press.
16 C. C. Parrish, *Can. J. Fish. Aquat. Sci.*, 44 (1987) 722.
17 W. M. Indrasena, A. T. Paulson, C. C. Parrish and R. G. Ackman, *J. Planar Chromatogr.*, 4 (1991) 182.
18 P. Gentien and G. Arzul, *J. Mar. Biol. Assoc. U.K.*, 70 (1990) 571.
19 A. J. Fraser, D. R. Tocher and J. R. Sargent, *J. Exp. Mar. Biol. Ecol.*, 88 (1985) 91.
20 C. C. Parrish, X. Zhou and L. R. Herche, *J. Chromatogr.*, 435 (1988) 350.
21 P. Gentien and G. Arzul, in E. Graneli, B. Sundstrom, L. Edler and D. M. Anderson (Editors), *Toxic Marine Phytoplankton, Proceedings of the 4th International Conference on Toxic Marine Phytoplankton, Lund, June 1989*, Elsevier, New York, 1990, pp. 161–164.
22 N. C. Shantha and R. G. Ackman, *Can. Inst. Sci. Technol. J.*, 24 (1991) 156.

Journal of Chromatography, 607 (1992) 105–111
Elsevier Science Publishers B.V., Amsterdam

CHROM. 24 356

Chromatographic isolation of insecticidal amides from *Piper guineense* root

W. S. K. Gbewonyo* and D. J. Candy

School of Biochemistry, University of Birmingham, Birmingham B15 2TT (UK)

(First received January 14th, 1992; revised manuscript received April 7th, 1992)

ABSTRACT

Fractionation of a light petroleum (b.p. 40–60°C) extract from the male roots of *Piper guineense* Schum and Thonn was carried out by thin-layer chromatography (TLC) followed by reversed-phase high-performance liquid chromatography (HPLC). Fractions were monitored by their insecticidal activity, and five different active amides were purified. The amides were identified by spectral and chemical methods as N-isobutyl-11-(3,4-methylenedioxyphenyl)-2*E*,4*E*,10*E*-undecatrienamide (**1**), N-pyrrolidyl-12-(3,4-methylenedioxyphenyl)-2*E*,4*E*,9*E*,11*Z*-dodecatetraenamide (**2**), N-isobutyl-13-(3,4-methylenedioxyphenyl)-2*E*,4*E*,12*E*-tridecatrienamide (**3**), N-isobutyl-2*E*,4*E*-decadienamide (**4**) and N-isobutyl-2*E*,4*E*-dodecadienamide (**5**). Some of these (**4** and **5**) have not hitherto been identified in *P. guineense*, and one (**2**) appears to be novel from any plant source. TLC–HPLC is suggested to be more suitable than other chromatographic methods used earlier for isolating minor insecticidal components from *Piper* plants.

INTRODUCTION

Most of the earlier work on *Piper* species seem to suggest that the major insecticidally active components are alkamides [1–3]. The isolation of one of these amides (pellitorine) by gas chromatography (GC) from a light petroleum extract of the root of *Piper guineense* was reported earlier [4]. However, GC was found to be unsuitable for the separation and isolation of some of these amides which appear to be unstable at the high temperatures used. There have been few reports on the use of high-performance liquid chromatography (HPLC) for the separation and isolation of amides from *Piper* plant [3,5]. In this study we have used reversed-phase HPLC, preceded by thin-layer chromatography (TLC) for the fractionation of insecticidal amides from a plant extract and for the isolation of these components in sufficient quantities for chemical identification.

EXPERIMENTAL

The male root of *P. guineense* was used. Details of the origin, processing and extraction of the plant material were described earlier [4]. Briefly, 25 g of dried, powdered root was extracted with 250 ml of light petroleum (b.p. 40–60°C) for 6 h at 20°C and was then filtered.

Bioassays

A Petri dish contact method described earlier [4] was used with adult *Musca domestica* as test insects. Eluents of the TLC and HPLC fractions to be bioassayed were introduced into glass Petri dishes (radius = 4.6 cm; area = 67 cm^2), 2.0 ml of olive oil–light petroleum (0.03%, v/v) were added and the mixture was dried. The olive oil served as carrier to facilitate transfer of test materials to the insects. At least two replicates of ten insects were used at each concentration tested and a set of controls was

Correspondence to: Dr. D. J. Candy, School of Biochemistry, University of Birmingham, Birmingham B15 2TT, UK.

* Present address: Department of Biochemistry, University of Ghana, Legon, Ghana.

0021-9673/92/$05.00

included with each group of bioassays. The insects were supplied with sucrose and water and maintained at 26–28°C. Knockdown (proportion of insects no longer able to upright themselves) was recorded at 2 h and lethal effects (proportion of insects showing no movement even after stimulation by contact) at 24 h.

TLC fractionation of the total extract for insecticidal activity

Silica gel chromatoplates (250 μm, 20 cm × 10 cm, spread on glass plates using Kieselgel 60G, Merck, Darmstadt, Germany) were used for analytical separation and identification of active bands. For quantitative separation of active fractions, however, preparative silica gel chromatoplates (approximately 400 μm, 20 cm × 20 cm of Kieselgel 60G) were used. During a preliminary analytical separation, bands were located both with ultraviolet light at 254 and 365 nm and by iodine staining. In all subsequent TLC separations, bands were only located with UV light. The use of UV light at two wavelengths allowed the borders of the bands to be better defined. The sequence of TLC fractionation of the *Piper* root extract is summarized in Fig. 1. First (TLC I) the concentrated extract was run for 50 min. using chloroform–methanol (10:1, v/v) as developing solvent. The individual fractions obtained from this were eluted and run for 40 min using *n*-hexane–ethyl acetate (3:1, v/v) (TLC II). Each fraction was eluted and re-run under the same conditions as for TLC II, *i.e.* using *n*-hexane–ethyl acetate as solvent (TLC III). In general, R_f values for components after TLC II were lower than after TLC III, presumably because of differences in loading. When monitoring the activity of TLC bands, samples of the extract (4.0 mg dry weight) and the subsequent fractions (0.4 mg) were tested. Bands were recovered by scraping off the appropriate region of silica gel and eluting with acetone–light petroleum (2:1). The eluents were centrifuged at 1000 *g* for 15 min to remove suspended silica gel particles, and then evaporated under partial vacuum and taken up in chloroform. Larger amounts of each of the active crude fractions A, B and C were obtained by separating aliquots (100 mg) of the extract on preparative silica gel chromatoplates (Fig. 1). It should be noted that additional components were obtained during TLC fractionation but were not further examined because of their low insecticidal activity.

Isolation and purification of active components from TLC fractions by HPLC

Three active fractions (A, B and C, recovered by TLC) were further separated by reversed-phase HPLC. An LDC Milton Roy (Stone, UK) MP300 multi-processor, consisting of two Constametric III metering pumps, a Spectromonitor III variable-wavelength detector and a printer, all of which were linked to a computer, was used for HPLC separations. A semi-preparative (250 mm × 10 mm I.D.) 5-μm Spherisorb ODS2 C_{18} column (Phase Separa-

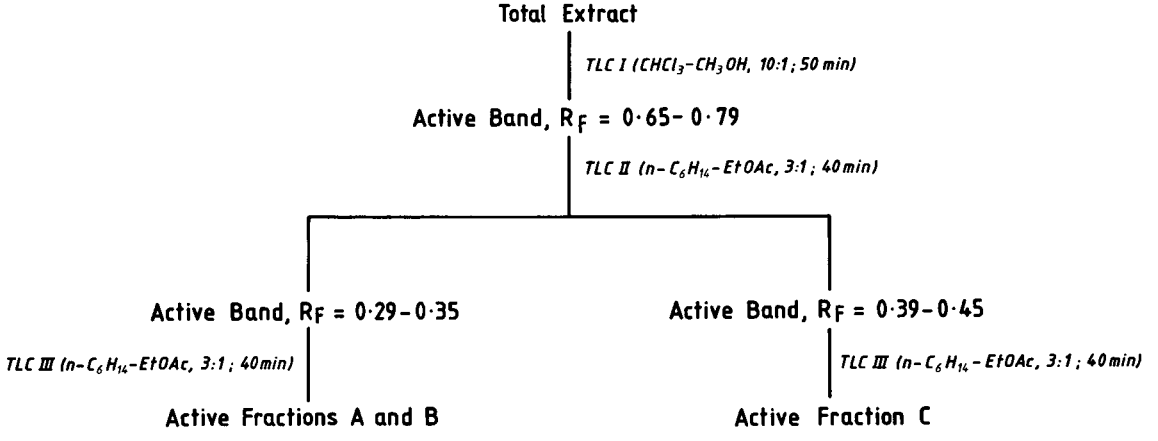

Fig. 1. TLC separation of insecticidal components from *Piper guineense* root extract. For R_F values of active fractions A, B and C after TLC III, see Table I. A, B and C were further separated by HPLC to give components **1, 2, 3, 4** and **5**. EtOAc = Ethyl acetate.

tions, Deeside, UK) was used. The separations were monitored at 254 nm, and the flow-rate was 4.0 ml. A two-solvent gradient elution was carried out using as mobile phase methanol–ammonium acetate buffer (0.05 *M*, pH 5.6). The solvent programme was: 70.0–99.9% methanol over a 15-min period, then 99.9% methanol for another 5 min. Aliquots (50 μg) of each TLC fraction were analysed, and the results were then used to guide in the HPLC fractionation of larger quantities of the TLC fractions. Aliquots of the TLC fractions (0.4 mg) were separated by HPLC and fractions were collected as groups of peaks together (T_1, T_2, T_3, T_4, T_5 and T_6) as shown for the chromatogram in Fig. 2. These HPLC fractions were dried under partial vacuum, taken up in chloroform (1 ml) and bioassayed for insecticidal activity. In order to identify the actual peaks responsible for activity, the HPLC separations of the TLC fractions were repeated and selected individual peaks (areas >8% of the total at 254 nm) were isolated and bioassayed. The active peaks 1, 2, 3, 4 and 5, the elution times for which are shown in Table II, were isolated in sufficient quantities (and then further purified) to allow subsequent structural analysis. For further purification two isocratic solvent systems were used: (i) acetonitrile–ammonium acetate buffer (55:45) for components with elution times of less than 15.0 min during component isolation; (ii) acetonitrile–ammonium acetate buffer (62:38) for components with elution times greater than 15.0 min during component isolation.

Structure determination

The chemical identities of the isolated compounds were determined by spectral and chemical analysis. The details of these procedures were as outlined earlier [4], except that ^{1}H NMR spectra of components B and F were determined with a JEOL JNM-GX 270 FT NMR spectrometer.

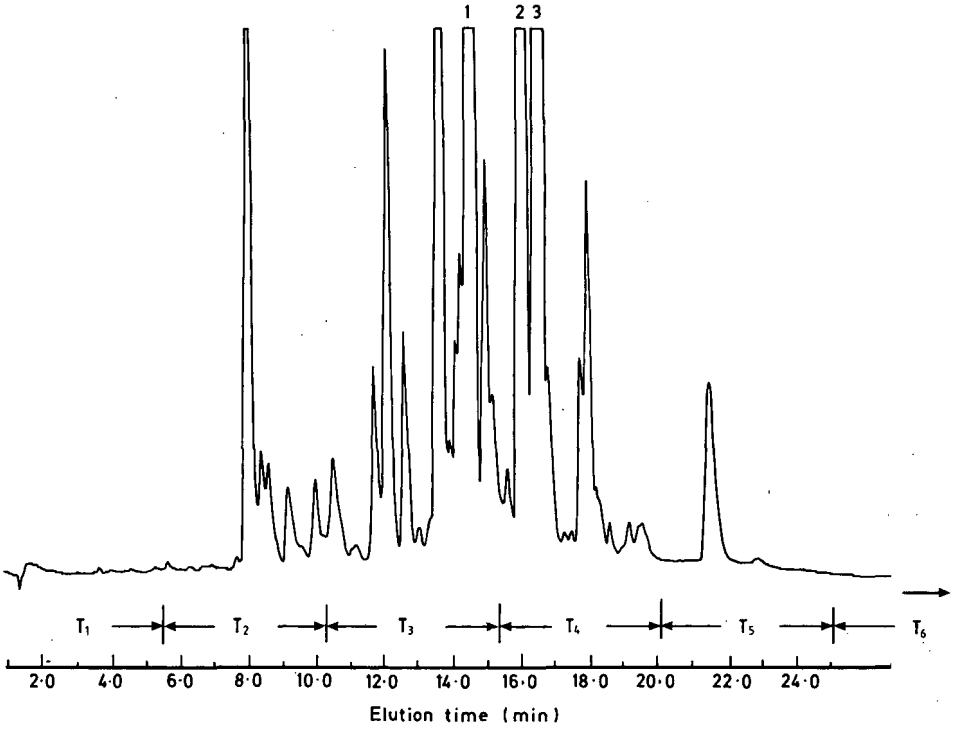

Fig. 2. HPLC separation of components **1, 2** and **3** from TLC fraction A. Elution times (min) are indicated for the various peaks. Peaks marked 1, 2, 3 were the active components isolated. T_1–T_6 represent groups of peaks collected as fractions for bioassay. Column: Spherisorb 50DS2; solvent: methanol–ammonium acetate buffer, gradient; flow-rate: 4.0 ml/min; detector: UV, 254 nm.

RESULTS AND DISCUSSION

Many TLC bands with activity were obtained (Fig. 1). However, the main bands recovered in substantial quantities (recovery > 0.005% dry weight of plant material) and which also showed dissimilar activities on bioassay are shown in Table I. Fraction A showed both good knockdown and good lethal toxicity, B showed moderate lethal toxicity but good knockdown whilst C showed poor lethal toxicity but good knockdown.

The chromatograms obtained by reversed-phase HPLC separation of fractions A, B and C, showed that all the fractions contained several closely related components which absorbed at 254 nm. The areas of the integrated peaks of individual active components in each chromatogram were all greater than 15% of the total absorbance for fractions A, B or C (Table II). The peak eluting at approximately 12.0 min constituted nearly 50% of the total, and the peaks eluting at about 15.0–17.0 min constituted between 15 and 23% of the total (Table II). HPLC peaks 1, 2 and 3, which eluted between approximately 15.0 and 17.0 min, were found to cause knockdown and lethal toxicity to 75% or more of the treated insects (Table II). Peak 4, which eluted at about 12.0 min from TLC fraction B, but formed as much as 50.0% of the total integrated peak area, was also found to cause knockdown to over 75% and lethal toxicity to 50% or more of insects when bioassayed. Peak 5 from TLC fraction C on the other hand had an elution time around 14.0 min but showed only moderate activity, with only up to 50% of treated insects being killed in 24 h or being knocked down in 2 h. All the active peaks contained impurities resulting from overlapping of minor

TABLE I

R_F VALUES, RECOVERY AND TOXICITY OF MAIN ACTIVE FRACTIONS OBTAINED FROM THE SEPARATION OF TLC III FRACTIONS

TLC III, dose = 6.0 μg/cm²; solvent, *n*-hexane-ethyl acetate (3:1, v/v). Degree of activity (percentage of test insects responding: + + + + = 100–95%; + + + = 95–75%; + + = 75–50%; + = 50–25%; − = 0–25%. Each fraction was tested on twenty insects. KD = Knockdown after 2 h; M = mortality after 24 h. The proportion recovered was expressed relative to total dry weight of plant material (710 g).

TLC fraction	R_F of band	Proportion recovered (%)	Degree of activity	
			KD	M
A	0.23–0.37	0.018	+ + + +	+ + + +
B	0.37–0.42	0.005	+ + +	+
C	0.51–0.69	0.022	+ + + +	−

TABLE II

ELUTION TIMES AND ACTIVITIES OF PEAKS ISOLATED FROM TLC FRACTIONS BY REVERSED-PHASE HPLC

Percentage % total int. peaks = % total absorbance for fractions A/B/C (= 100) detected at 254 nm. A 0.4-mg amount of each TLC fraction was separated. Twenty insects were used for the bioassays. Degree of activity (percentage of test insects responding): + + + = 95–75%; + + = 75–50%; + = 50–25%. KD = knockdown after 2 h; M = mortality after 24 h.

TLC fractions	Active HPLC peak(s)	Elution time (min)	Percentage % total int. peaks	Degree of activity	
				KD	M
A	1	14.6	17.4	+ + +	+ + +
	2	16.1	15.3	+ +	+ + +
	3	16.8	22.8	+ + +	+ + +
B	4	11.9	49.6	+ + +	+ +
C	5	14.3	15.3	+	+

peaks adjacent to the major peaks (Fig. 2). On changing from methanol–ammonium acetate buffer to acetonitrile–ammonium acetate buffer as eluting solvent and rechromatography, much better resolution was obtained enabling large quantities of material to be purified. For example, components **2** and **3**, which were isolated together (Fig. 2) and were barely separable with methanol–ammonium acetate buffer, were completely resolved when acetonitrile–ammonium acetate buffer (62:38) was used (Fig. 3). The peaks were therefore purified isocratically using acetonitrile–ammonium acetate buffer of appropriate strength. In this way pure components **1, 2, 3, 4** and **5** were obtained for determination of their chemical identities. The components were identified as follows.

*N-Isobutyl-11-(3,4-methylenedioxyphenyl)-2E,4E,10E-undecatrienamide (component **1**, 2.1 mg)*. Mass spectrum (*m/z*, % intensity): 355 (M^+, 68), 220 (56), 161 (15), 135 (100), 57 (42), 40 (65). ^{1}H NMR (δ, deuterochloroform, 270 MHz): 0.93 (d, J = 6.7 Hz, 6H), 1.47 (m, 4H), 1.80 (m, 1H), 2.18 (m, 4H), 3.17 (t, J = 6.4 Hz, 2H), 5.44 (br s, 1H), 5.74 (d, J = 15.6 Hz, 1H), 5.94 (s, 2H), 6.01 (dt, J = 15.9, 7.0 Hz, 1H), 6.07 (m, 1H), 6.12 (dd, J = 15.3, 9.8 Hz, 1H), 6.28 (d, J = 15.6 Hz, 1H), 6.73 (br s, 2H), 6.87 (br s, 1H), 7.19 (dd, J = 10.1, 15.0 Hz, 1H). IR (γ, NaCl flat, neat, cm^{-1}): 3305, 2930, 1660, 1630, 1620, 1550, 1260, 1000, 925. UV (λ_{max}, methanol): 260, 305 nm.

*N-Pyrrolidyl-12-(3,4-methylenedioxyphenyl)-2E,4E,9E,11Z-dodecatetraenamide (component **2**, 3.4 mg)*. Mass spectrum (m/z, % intensity): 367 (M^+, 56), 232 (50), 192 (30), 164 (70), 135 (100), 98 (25), 70 (43). ^{1}H NMR (δ, deuterochloroform, 270 MHz): 1.48 (m, 2H), 1.55–1.64 (m, 4H), 2.17 (m, 4H, 3.61 (br, 4H), 5.95 (s, 2H), 5.95 (d, J = 10.9 Hz, 1H), 6.02 (m, 2H), 6.09 (m, 1H), 6.18 (dd, J = 15.1, 10.6 Hz, 1H), 6.24 (dd, J = 16.0, 7.7 Hz, 1H), 6.30 (d, J = 8.6 Hz, 1H), 6.75 (br s, 2H), 6.88 (br s, 1H), 7.25 (dd, J = 10.1, 14.6 Hz, 1H). IR (γ, NaCl flat, neat, cm^{-1}): 2920, 1650, 1620, 1595, 1500, 1440, 1245, 1033, 1000, 925. UV (λ_{max}, methanol): 259, 296 nm (inflexion).

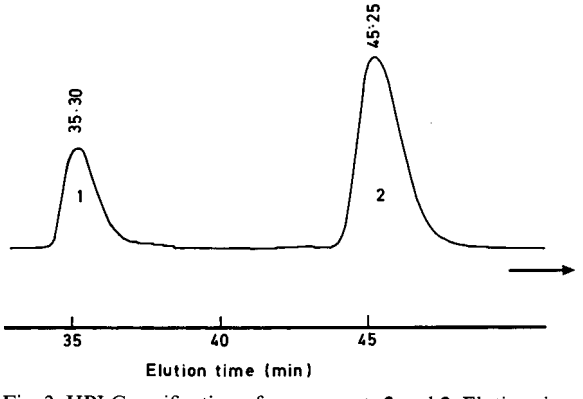

Fig. 3. HPLC purification of components **2** and **3**. Elution times (min) are indicated for the active peaks (1 and 2). Column: Spherisorb 50DS2; solvent: acetonitrile–ammonium acetate (62:38), isocratic; flow-rate: 4.0 ml/min; detector: UV, 254 nm.

*N-Isobutyl-13-(3,4-methylenedioxyphenyl)-2E,4E,12E-tridecatrienamide (component **3**, 7.8 mg)*. Mass spectrum (m/z, % intensity): 383 (M^+, 100), 369 (35), 248 (39), 180 (21), 152 (38), 135 (70), 57 (12). ^{1}H NMR (δ, deuterochloroform, 270 MHz): 0.93 (d, J = 6.7 Hz, 6H), 1.30 (m, 4H), 1.42 (m, 4H), 1.80 (m, 1H), 2.14 (m, 4H), 3.17 (t, J = 6.4 Hz, 2H), 5.45 (br, 1H), 5.74 (d, J = 14.7 Hz, 1H), 5.92 (s, 2H), 6.01 (dt, J = 15.6, 7.7 Hz, 1H), 6.07 (m, 1H), 6.14 (dd, J = 15.3, 9.9 Hz, 1H), 6.28 (d, J = 15.6 Hz, 1H), 6.73 (br s, 2H), 6.88 (br s, 1H), 7.20 (dd, J = 15.0, 10.1 Hz, 1H). IR (NaCl flat, neat, cm^{-1}): 3305, 2920, 1645, 1630, 1605, 1545, 1250, 1030, 1000, 920. UV (λ_{max}, methanol): 260, 304 nm.

*N-Isobutyl-2E,4E-decadienamide (component **4**, 15 mg)*. The spectral data obtained were identical to those reported earlier for the component isolated by gas–liquid chromatography [4]. The identity of this compound was also confirmed by ^{3}H reduction followed by hydrolysis and identification of the hydrolysis product [4].

*N-Isobutyl-2E,4E-dodecadienamide (component **5**, 2.1 mg)*. Mass spectrum (m/z, % intensity): 251 (M^+, 40), 179 (100), 166 (12), 152 (36), 96 (34), 57 (8), 41 (8). ^{1}H NMR (δ, deuterochloroforum, 270 MHz): 0.87 (t, J = 7.7 Hz, 3H), 0.93 (d, J = 6.7, 6H), 1.26-1.30 (m, 8H), 1.42 (m, 2H), 1.83 (m, 1H), 2.10–2.18 (q, 2H), 3.17 (t, J = 6.4 Hz, 2H), 5.44 (br, 1H), 5.74 (d, J = 15.1 Hz, 1H), 6.06–6.14 (m, 2H), 7.19 (dd, J = 10.1, 15.8 Hz, 1H). IR (γ, NaCl flat, neat, cm^{-1}): 3295, 2950, 2920, 1645, 1625, 1605, 1550, 1530, 990. UV (γ_{max}, methanol): 258 nm.

On ^{3}H reduction and hydrolysis [4], component **5** gave as its main hydrolysis product a fatty acid which eluted from HPLC at 22.5 min compared

with the elution times of 4.0, 10.0 and 16.0 min for hexanoic acid, octanoic acid and decanoic acid, respectively, which were run as standards. Thus hydrolysed reduced **5** probably contained twelve carbon atoms and was dodecanoic acid. The λ_{max} from the UV spectrum of **5** suggests the presence of a conjugated diene system adjacent to an amide carbonyl in the molecule, and the IR spectral data is characteristic to the system, $-CH_2-CH=CH-CH=CH-CONHR$ [6]. The fact that the UV and IR spectra of component **5** suggests it is a 2*E*,4*E*-dienamide, the presence of dodecanoic acid as a major component of its reduced hydrolyzed products, and the spectral data from mass spectrometry (MS) and ^{1}H NMR, shows that component **5** is *N*-isobutyl-2*E*,4*E*-dodecadienamide which is being named here kalecide after one of the local Ghanaian names of *P. guineense*, Kale. This compound has not been previously isolated from *P. guineense*. The only reported isolation of this compound from a plant source (*P. peepuloides)* was by Dhar and Raina [7]. The spectral data of component **3** are consistent with those reported for guineensine from *P. attenuatum* by Dasgupta and Ray [8]. The isolation of guineensine from *P. guineense* has been reported previously by Okogun and Ekong [9]. The spectral data of component **1** were consistent with those obtained for pipercide isolated from *P. nigrum* [3]. However, pipercide has so far only been detected in *P. guineense* as a lower homologue and a contaminant in the mass spectrum of guineensine [9]. The present work is the first report of the actual isolation of pipercide in a reasonably pure form from *P. guineense*. The isolation of N-pyrrolidyl-12-(3,4-methylenedioxphenyl)-2*E*,4*E*,9*E*,11*Z*-dodecatetraenamide, *i.e.* component **2**, has not been previously reported. This amide is being given the trivial name guineensinamide. Okogun and Ekong [9] suggested from GC–MS of a hydrogenated mixture of amides, the presence of an amide with M^+ 367, which was indicated to be an isobutylamide of eicosanoic acid. The IR and ^{1}H NMR spectral data obtained for the pure compound isolated with M^+ 367 in the present work shows this compound lacked an –NH group and hence could not be an isobutyl amide. Furthermore, the fragmentation pattern obtained from the mass spectrum was not compatible with the structure of the compound being an isobutylamide of eicosanoic acid. The UV (λ_{max}) at 259 and 296 nm obtained for component **2** is also indicative of the presence of a *Z*-configuration [10].

Isolation procedures involving solvent extraction, column chromatography, TLC and preparative TLC have so far been employed in phytochemical work on *P. guineense*. Most of the studies undertaken which were aimed at the isolation of insecticidal principles from *Piper* species have concentrated on extracts from the fruit. The fact that the isolation of guineensinamide, kalecide and pellitorine from *P. guineense* has hitherto not been reported (pipercide was only reported as a contaminant of guineensine) may partly be due to the relatively low content of these compounds in the plant materials examined. The use of HPLC enabled such components to be isolated in the present work. It must be noted, however, that Addae-Mensah *et al.* [11] did not report the presence of pellitorine in the light petroleum extracts of the root, though the present work shows it is present in the root extract in substantial quantities. Considering the extensive phytochemical work done on *P. guineense*, the absence of any reports on the isolation of pellitorine, kalecide and guineensinamide is significant since unlike previous work on this plant, the present work involved bioactivity-directed isolation of the compounds. The two pairs of homologues isolated and the presence of several successive peaks in all the HPLC chromatograms may suggest the presence of several homologous series of compounds. TLC–HPLC has therefore facilitated the isolation of a number of amides which have hitherto not been reported in *P. guineense*, hence may be the most suitable method for isolating components, particularly the minor yet insecticidally active components from *P. guineense* and related species.

ACKNOWLEDGEMENTS

We thank Dr. N. Janes of the Rothamsted Experimental Station for assistance in obtaining and analysing some of the ^{1}H NMR data. We also thank Mr. D. K. Abbiw of the Department of Botany, University of Ghana, for identification of the plant. The financial support given to W.S.K.G. by the Commonwealth Commission (UK) is gratefully acknowledged.

REFERENCES

1 M. Miyakado, I. Nakayama, N. Ohno and H. Yoshioka, in D. L. Whitehead and W. S. Bowers (Editors), *Natural Products for Innovative Pest Management*, Pergamon Press, Oxford, 1983, p. 369.
2 M. G. Nair, A. P. Mansingh and B. A. Burke, *Agric. Biol. Chem.*, 50 (1986) 3053.
3 H. C. F. Su and R. Hovart, *J. Agric. Food Chem.*, 29 (1981) 115.
4 W. S. K. Gbewonyo and D. J. Candy, *Toxicon*, (1992) in press.
5 M. Rathnawathie and K. A. Buckle, *J. Chromatogr.*, 204 (1983) 316.
6 L. Crombie, *J. Chem Soc.*, (1955) 999.
7 K. L. Dhar and M. L. Raina, *Planta Med.*, 23 (1973) 295.
8 S. Dasgupta and A. B. Ray, *Indian J. Chem.*, 17B (1974) 538.
9 J. I. Okogun and E. U. Ekong, *J. Chem. Soc. Perkin Trans. 1*, (1974) 2195.
10 M. Windholz (Editor), Merck Index, Merck and Co. Inc., Rahway, NJ, 1983, p. 751.
11 I. Addae-Mensah, F. G. Torto, C. I. Dimonyeka, I. Baxter and J. K. M. Sanders, *Phytochemistry*, 16 (1977) 757.

Journal of Chromatography, 607 (1992) 113–118
Elsevier Science Publishers B.V., Amsterdam

CHROM. 24 327

Transport of solutes across aqueous phase interfaces by electrophoresis. Mathematical modeling

Mark L. Levine, Heriberto Cabezas, Jr. and Milan Bier

Center for Separation Science, University of Arizona, Tucson, AZ 85721 (USA)

(First received February 3rd, 1992; revised manuscript received April 29th, 1992)

ABSTRACT

Polarizations of solutes undergoing electrophoresis occur at the interfaces of aqueous two-phase systems. The first mathematical model of this situation is presented, and is shown to predict results qualitatively similar to our experimental work. The numerical simulation of electrophoresis is based on an earlier single-phase model, extended with additional equations and boundary conditions needed in the two-phase case. Results from the simulation of some simple model systems are presented and discussed.

INTRODUCTION

We have previously shown that the electrophoresis of solutes across the interface in aqueous two-phase systems could be strongly influenced by the partitioning of the solutes in the systems [1]. Unexpected polarization was noted as proteins or certain dyes were transported across the interface from preferred to non-preferred phase. The polarization was directional, in that movement from non-preferred to preferred phase appeared unaffected by the phase boundary. The problem is of considerable importance. Similar phenomena were reported by Maxwell in 1892 [2] for organic–organic interfaces. Nernst and Riesenfeld [3] noted the occurrence of polarizations at organic–aqueous interfaces in 1902. We believe our investigations to be the first report on these polarizations in aqueous–aqueous phase systems. This sort of behavior at interfaces can be used as the basis for novel separations. It can also help clarify other examples of interphase transport in aqueous systems, such as transport across cell membranes or within an electrochromatography column. Modeling was undertaken because of this practical importance, and also since these results were not accounted for by any current theory of electrophoresis. Using simple systems, our model demonstrates some of the essential characteristics of the experimental results.

The framework of our theory for electrophoretic transport is provided by Bier and co-workers [4–8], which we expand to account for the special case of a two-phase system. The model for electrophoresis in single phase systems is based on a set of unsteady state mass balances for each species i composing the complete system. The system is assumed isothermal with transport in one dimension only. A generation term R_i (mol/m^3 · s) enables the interconversion between neutral and charged species of a given molecule,

$$\frac{\partial c_i}{\partial t} = -\frac{\partial F_i}{\partial x} + R_i \tag{1}$$

where c_i is the concentration of i (mol/m^3) and t is time (s). F_i represents the flux of i in mol/m^2 · s given by

$$F_i = -c_i z_i \Omega_i \frac{\partial \Phi}{\partial x} - \frac{RT}{e}\Omega_i \frac{\partial c_i}{\partial x} \tag{2}$$

Correspondence to: Milan Bier, Center for Separation Science, Building 20, Room 157, University of Arizona, Tucson, AZ, 85721, USA.

0021-9673/92/$05.00

Flux by both electrophoresis and diffusion is allowed, all other mechanisms are neglected. The left hand term in the flux equation describes electrophoretic motion, with z_i representing the charge on i, Ω_i a mobility factor in $m^2/V \cdot s$, and $\partial\Phi/\partial x$ the gradient in applied potential (V/m). The right hand term in this equation characterizes diffusion. R is the gas constant in V · Coulombs/K · mol, T the absolute temperature in K and e the molar charge of 96 500 Coulomb/mol.

The generation term R_i is assumed to follow mass action kinetics, represented by equations of the form

$$R_{A^-} = k_f c_{HA} - k_r c_{H^+} c_{A^-} \quad (3)$$

where k_f and k_r are forward and reverse reaction rate constants, respectively, in appropriate units. They describe an illustrative reaction such as, for example

$$HA \rightleftharpoons H^+ + A^- \quad (4)$$

In addition to the set of partial differential equations (PDEs) resulting from describing the transport of each species i, a system of algebraic relationships must be simultaneously solved in order to fully describe the problem. Certain elementary species are conserved. For example, the rate at which water disappears from the system must be matched by the rate at which hydroxyl ion appears. Linear combinations of other species yield similar relationships. These may be summed to yield

$$\sum_i z_i R_i \doteq 0 \quad (5)$$

The rate of charge generation within the system must be zero everywhere except at the electrodes. Therefore, the divergence of the sum of the fluxes of charged species is zero,

$$-\nabla \cdot \sum_i e z_i F_i = 0 \quad (6)$$

Also, we assume that electroneutrality prevails on the scale of interest,

$$\sum_i e z_i c_i = 0 \quad (7)$$

It is generally necessary to solve the equations numerically, because of the complex nature of the system. All the classically known modes of electrophoresis could be described with this model, by proper choice of initial and boundary conditions for the PDEs [4].

MODEL FOR ELECTROPHORESIS IN TWO-PHASE SYSTEMS

Our model for two-phase electrophoresis begins with similar equations written for each phase of the two-phase system. Two additional boundary conditions are required at the interface in order to complete the description of this system. The work of Davies [9] and the text of Crank [10] involving diffusion only across the interface of two-phase systems suggested two different possibilities.

One assumption is instantaneous equilibrium across the phase boundary. If the two-phase system is considered infinite in extent with the interface at $x = 0$, phase a encompasses $x < 0$ and phase b extends from $x > 0$. Then

$$K = \frac{c_{i,b}}{c_{i,a}} \quad \text{for} \quad x = 0 \quad (8)$$

where K is the equilibrium partition coefficient of solute i.

The second alternative for this boundary condition is to assume that there is significant resistance to transport. Then, a mass transfer expression best defines the flux at the interface

$$F_i = \alpha(K c_{i,a} - c_{i,b}) \quad \text{for} \quad x = 0 \quad (9)$$

where α is the mass transfer coefficient (m/s).

For either possibility, the second boundary condition at the interface states that all mass flowing out of phase a must flow into phase b. The fluxes across the phase boundary must match

$$F_{i,a} = F_{i,b} \quad \text{for} \quad x = 0 \quad (10)$$

To complete either description of the two-phase system, the remaining boundary and initial conditions must be stated

$$c_{i,a} = c_{i,-\infty} \quad \text{for} \quad x = -\infty \quad (11)$$

$$c_{i,b} = c_{i,+\infty} \quad \text{for} \quad x = +\infty \quad (12)$$

$$c_{i,a} = c_{i,-\infty} \quad \text{for} \quad t = 0 \quad (13)$$

$$c_{i,b} = c_{i,+\infty} \quad \text{for} \quad t = 0 \quad (14)$$

The new boundary conditions at the interface must be substituted into the finite difference approx-

imations for the PDEs at the appropriate spacial grid points. For example, consider an illustrative 50-point grid. Concentrations are estimated at the grid points from fluxes, which are calculated between grid points. The interface is located at the center of the grid, between points 25 and 26. The flux associated with transport across the interface is defined as flux 25.

All concentrations in the model, except those on either side of the interface (25 and 26) are calculated by the normal finite difference approximation

$$\frac{c_i' - c_i}{\Delta t} = -\left(\frac{F_i - F_{i-1}}{\Delta x}\right) \tag{15}$$

where the subscript i now refers to position in the grid. The prime (') indicates a quantity being calculated at the next time point in the simulation from current time point data.

To model the case of equilibrium across the interface, eqn. 15 must be written for grid points 25 and 26:

$$\frac{c_{25}' - c_{25}}{\Delta t} = -\left(\frac{F_{25} - F_{24}}{\Delta x}\right) \tag{16}$$

$$\frac{c_{26}' - c_{26}}{\Delta t} = -\left(\frac{F_{26} - F_{25}}{\Delta x}\right) \tag{17}$$

By use of the boundary condition given by eqn. 10, the common flux 25 is eliminated between these equations. The equilibrium expression across the interface, eqn. 8, is then used to substitute for the new concentration at grid point 26:

$$\frac{\Delta x}{\Delta t}(c_{25} - c_{25}') + F_{24} = \frac{\Delta x}{\Delta t}(Kc_{25}' - c_{26}) + F_{26} \tag{18}$$

This can be solved for the new concentration at point 25

$$c_{25}' = \frac{c_{25} + c_{26}}{1 + K} + \frac{\Delta t}{\Delta x}\left(\frac{F_{24} - F_{26}}{1 + K}\right) \tag{19}$$

The equilibrium equation is then used once more to obtain

$$c_{26}' = Kc_{25}' \tag{20}$$

These last two equations replace eqn. 15 at grid points 25 and 26 for simulations where instantaneous equilibrium is assumed across the interface. Calculation for concentration values at all other spacial grid points are made with eqn. 15.

Alternatively, one may assume there is mass transfer resistance at the interface, not instantaneous equilibrium. To model this case, the mass transfer expression, eqn. 9, is substituted for eqn. 2 for flux 25 at the interface. Eqn. 2 is retained to calculate all other fluxes.

The solution of the models for two-phase systems now follows easily from the single-phase model. All equations are put into non-dimensional form. The dimensionless form of eqn. 6 for conservation of charge is integrated to yield

$$\sum_i z_i F_i = \theta \tag{21}$$

where F_i is now a dimensionless flux and θ is the dimensionless current. An initial component distribution is input into the simulation package. Equilibrium expressions derived from equations of the type shown by eqn. 3 are combined with the requirement for electroneutrality, eqn. 7. From this, pH and concentrations for ionizable species are obtained. Conductivity can then be calculated, which when combined with the applied current, yields the gradient in the potential between pairs of grid points. Fluxes for species are figured from eqn. 2 or 9, as appropriate. Eqn. 1, 19, or 20 is finally solved, as needed, to obtain concentrations at the new step forward in time. The Runga–Kutta–Fehlberg method was used for integration in the examples which follow. The process is then essentially repeated, until the simulation time is finished. Complete details regarding the solution are available in the previously cited references [4–8].

RESULTS

The results presented here are from models in which the following simplifying assumptions are made. Only one component, the one of interest, is considered to be partitioned at the interface. All the other components in the simulation behave as though electrophoresis is taking place in a bulk phase. Furthermore, unless specified otherwise, each component has the same electrophoretic mobility in either phase. Although this is not generally true in reality, it simplifies the interpretation of results since a change in mobility at the interface in and of itself will cause other polarization effects. We have previously demonstrated experimentally that for the

special case of equal electrophoretic velocity in either phase, polarizations still occur at the interface of two-phase systems [1].

The two models, with either instantaneous equilibrium or mass transfer resistance at the interface, have been run for a number of cases. To verify that each was working correctly, the limiting cases for bulk transport by diffusion only with a single solute was tested. Both models were found to be in excellent agreement with the analytical solutions published by Crank [10]. Also, as a further check of the reliability of numerical solution, the amount of solute which accumulates at the interface with electrophoresis in the complete model compares well with the amount calculated for the case of an impermeable wall at the interface.

The simulations used either hemoglobin or a strong base as the partitioned component of interest. The base simplifies the interpretation of results. The values for the partition coefficient and the mass transfer coefficient were those given by Shanbhag [11], for hemoglobin in a system similar, but not identical, to the two-phase system examined experimentally. The partitioned solute was present as a minor component of the system, over 3000 times more dilute than the next most dilute component. This reduces the interaction between the components. The remainder of the system was a buffer, to minimize the effect of pH. The system initially begins at its equilibrium distribution and the figures show a concentration profile calculated after the electric field has been applied for 1 min. Pertinent data for the simulations are summarized in Table I.

TABLE I

PARAMETERS FOR SIMULATIONS

Concentration profiles are shown 1 min after electrophoresis begins from equilibrium conditions.

Simulation space = 0.005 m divided into 200 grid points

Initial current density = 20 A/m^2

For equilibrium model simulations

Run assuming constant current

Supporting Buffer

0.01 M acetate ion, pK = 4.76, $\Omega = 4.12 \cdot 10^{-8}$ m^2/V · s.

0.0063 M ammonium ion, pK = 9.25, $\Omega = 6.39 \cdot 10^{-8}$ m^2/V · s.

pH = 5.0

Hemoglobin, diffusion coefficient = $6.8 \cdot 10^{-7}$ cm^2/s

pH	Charge
3.0	68.5
3.5	43.5
4.5	25.5
6.0	10.25
8.0	−10.25
9.0	−20.5
10.0	−30.75
11.0	−50.0
11.5	−63.5

For mass transfer model simulations

Run assuming constant voltage drop across separation space

Supporting buffer

0.01 M cacodylate ion, pK = 6.21, $\Omega = 2.31 \cdot 10^{-8}$ m^2/V · s.

0.0086 M Tris ion, pK = 8.30, $\Omega = 2.41 \cdot 10^{-8}$ m^2/V · s.

pH = 7.0

Fig. 1 reports the results of a simulation with instantaneous equilibrium at the interface. Two differet values of the equilibrium partition coefficient K are examined. In both cases, phase a is the preferred phase, so that electrophoresis is from preferred into non-preferred phase. Material in both these simulations tends to concentrate on the left side of the interface. As the partitioning between the phases becomes greater (the partition coefficient decreases from a value of 1), the observed polarization increases.

Fig. 2 also demonstrates the results of simulations

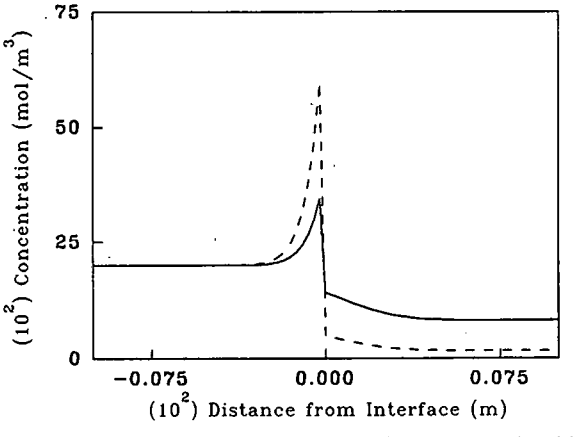

Fig. 1. Concentration profile after 1 min of electrophoresis, with equilibrium for two different partition coefficients. For K = 0.41 (———), $c_{i,-\infty} = c_{i,a,t=0}$ = 0.20 mol/m^3; $c_{i,\infty} = c_{i,b,t=0}$ = 0.082 mol/m^3. For K = 0.082 (— — —), $c_{i,\infty} = c_{i,b,t=0}$ = 0.0164 mol/m^3. The partitioned species is a strong base, with $\Omega = 1.0 \cdot 10^{-8}$ m^2/V · s.

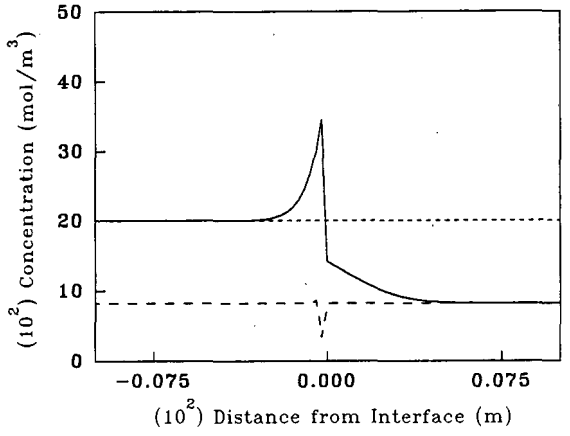

Fig. 2. Concentration profile after 1 min of electrophoresis, for the equilibrium model for three cases of directional transport. Transport from preferred to non-preferred phase (———), K = 0.41; $c_{i,-\infty} = c_{i,a,t=0} = 0.20$ mol/m^3; $c_{i,\infty} = c_{i,b,t=0} = 0.082$ mol/m^3. Transport from non-preferred to preferred phase (– – –), K = 2.439; $c_{i,-\infty} = c_{i,a,t=0} = 0.082$ mol/m^3; $c_{i,\infty} = c_{i,b,t=0} = 0.20$ mol/m^3. Neither phase preferred (-----), K = 1; $c_{i,-\infty} = c_{i,a,t=0} = c_{i,\infty} = c_{i,b,t=0} = 0.20$ mol/m^3. Partitioned species is a strong base, as in Fig. 1.

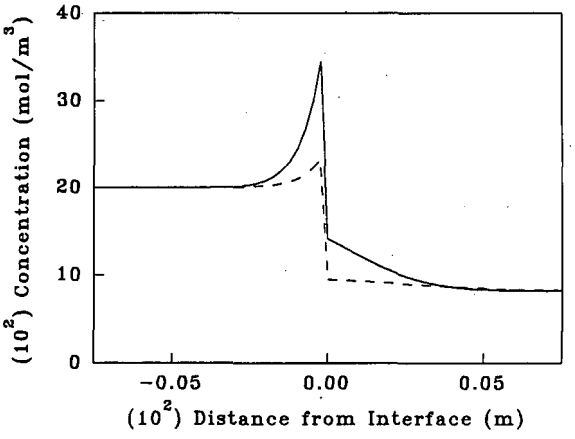

Fig. 3. Concentration profile after 1 min of electrophoresis for equilibrium model; effect of a mobility difference. With the same mobility in either phase (———), $\Omega = 1 \cdot 10^{-8}$ m^2/V · s. For differing mobility (– – –), $\Omega = 1 \cdot 10^{-8}$ m^2/V · s in phase a; $2 \cdot 10^{-8}$ m^2/V · s in phase b. For both simulations, K = 0.41; $c_{i,-\infty} = c_{i,a,t=0} = 0.20$ mol/m^3; $c_{i,\infty} = c_{i,b,t=0} = 0.082$ mol/m^3. Partitioned species is a strong base.

with equilibrium at the interface. For the simulation where K is 0.41, the solute is being transported from preferred to non-preferred phase, and concentration occurs at the interface. If K is changed to 2.439 (1/0.41), the solute is electrophoresed from non-preferred to preferred phase. In this case, this model predicts a small dilution to occur at the interface. Finally, if K is set equal to 1, neither phase is preferred, and the solute is evenly distributed between the phases at equilibrium. The model predicts that the interface has no observable effect on the transport of the solute under these conditions and no polarization is calculated for the interface.

Fig. 3 examines a more complex situation, where the partitioned species has two times the mobility in phase b compared with phase a. This is compared with a similar simulation, with the same mobility in both phases. Equilibrium is assumed at the interface, with K = 0.41. The amount of polarization at the interface decreases with increased mobility in phase b.

Behavior of the protein hemoglobin is examined in Fig. 4, in a simulation with equilibrium assumed at the interface. A comparison run is made with a strong base. For both simulations, K is set at 0.41. The protein is also predicted to concentrate at the interface, when electrophoresis is from preferred to non-preferred phase. The irregularity to the left of the concentrated zone is due to the difficulty in numerically simulating the sharp gradient in concentration in that neighborhood.

In Fig. 5, concentration profiles from simulations

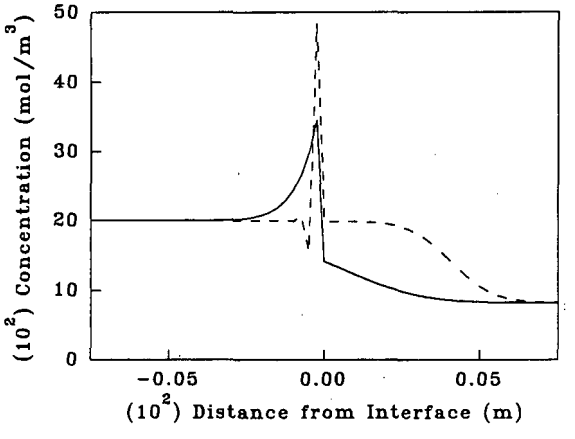

Fig. 4. Concentration profile after 1 min of electrophoresis for equilibrium model; effect of the nature of the partitioned solute. Strong base (———), $\Omega = 1 \cdot 10^{-8}$ m^2/V · s; hemoglobin (– – –). For both simulations, K = 0.41; $c_{i,-\infty} = c_{i,a,t=0} = 0.20$ mol/m^3; $c_{i,\infty} = c_{i,b,t=0} = 0.082$ mol/m^3.

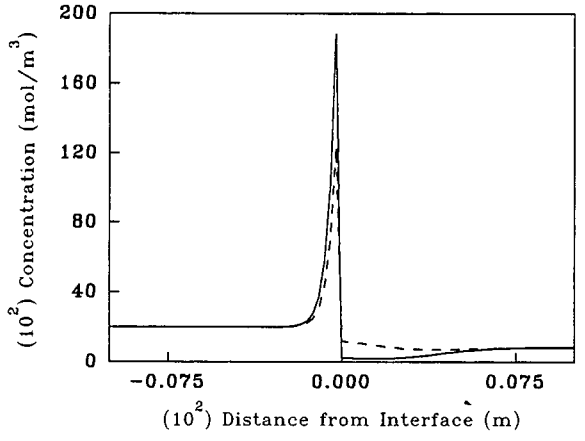

Fig. 5. Concentration profile after 1 min of electrophoresis for mass transfer model for two different mass transfer coefficients. For low mass transfer case (———), $\alpha = 2.29 \cdot 10^{-7}$ m/s, for high mass transfer case (— — —), $\alpha = 2.29 \cdot 10^{-6}$ m/s. For both cases, $K = 0.41$; $c_{i,-\infty} = c_{i,a,t=0} = 0.20$ mol/m^3; $c_{i,\infty} = c_{i,b,t=0} = 0.082$ mol/m^3. Partitioned species is a strong base, as in Fig. 1.

which use a mass transfer resistance model at the interface are shown. Two sets of values for these coefficients are compared, a low interfacial mass transfer rate and a high rate. As expected, the case with a lower mass transfer rate demonstrates a greater concentration of the strong base at the interface for equivalent electric fields applied for the same amount of time.

DISCUSSION

Both models presented here qualitatively demonstrate the most startling effect of our electrophoresis experiments in two-phase systems, the polarization at the interface when electrophoresis is from preferred to non-preferred phase.

The equilibrium model predicts dilution at the interface when transport is from non-preferred to preferred phase. It also calculates no observable polarizations when $K = 1$. Both of these results were observed experimentally, as reported in our earlier work. The polarization increases as the distribution of the solute between the phases at equilibrium becomes more dissimilar.

Similar results can also be obtained from the resistance model. However, few experimental values are available for mass transfer coefficients at these interfaces, and our attempts at measuring them proved unsuccessful. We have concentrated on the equilibrium model, as it provides a simpler explanation of the phenomenon.

The versatility of the model is demonstrated by the simulation which contains protein and the simulation with the change in solute mobility at the interface. Weak electrolytes, peptides, and other amphoteric substances may also be studied. It also allows modeling of a number of other situations, such as partitioning of the buffer salts in addition to the solute partitioning. The behavior of all these systems is made more complex as the concentrations of solute and buffer become comparable and the system is rendered more interactive. Further numerical simulations are underway to explore these situations.

Comparisons of these numerical solutions to our experimental work are limited because of the difficulties in measuring concentration as a function of position in two-phase systems. As noted above, both models are qualitatively in agreement with the experiments in some respects. However, the width of the polarized zone is calculated to be narrower than that observed in our experiments.

ACKNOWLEDGEMENTS

The authors wish to thank Dr. R. A. Mosher, Dr. D. A. Saville and Dr. G. O. Roberts, as well as the reviewers, for their advice. This work was supported in part by the NASA Graduate Student Researchers Program, grant NGT-50270.

REFERENCES

1 M. L. Levine and M. Bier, *Electrophoresis*, 11 (1990) 605–611.
2 J. C. Maxwell, *A Treatise on Electricity and Magnetism*, Vol. 1, Clarendon Press, Oxford, 1892, p. 452.
3 W. Nernst and E. H. Riesenfeld, *Ann. Physik*, 8 (1902) 600–608.
4 M. Bier, O. A. Palusinski, R. A. Mosher and D. Saville, *Science (Washington, D.C.)*, 219 (1983) 1281–1287.
5 D. A. Saville and O. A. Palusinski, *AIChE J.*, 32 (1986) 207–214.
6 O. A. Palusinski, A. Graham, R. A. Mosher, M. Bier and D. A. Saville, *AIChE J.*, 32 (1986) 215–223.
7 R. A. Mosher, D. Dewey, W. Thormann, D. A. Saville and M. Bier, *Anal. Chem.*, 61 (1989) 362.
8 R. A. Mosher, D. A. Saville and W. Thormann, *The Dynamics of Electrophoresis*, VCH, New York, 1992.
9 J. T. Davies, *J. Phys. Coll. Chem.*, 54 (1950) 185–204.
10 J. Crank, *The Mathematics of Diffusion*, Clarendon Press, Oxford, 2nd ed., 1975, pp. 38–40
11 V. P. Shanbhag, *Biochim. Biophys. Acta*, 320 (1973) 517–527.

Journal of Chromatography, 607 (1992) 119–125
Elsevier Science Publishers B.V., Amsterdam

CHROM. 24 326

Noise and detection limits of indirect absorption detection in capillary zone electrophoresis

Tiansong Wang and Richard A. Hartwick

Department of Chemistry, State University of New York at Binghamton, Binghamton, NY 13902 (USA)

(First received March 6th, 1992; revised manuscript received May 6th, 1992)

ABSTRACT

The factors which contribute to the noise and signal in indirect absorption detection in capillary zone electrophoresis are studied. Two independent noise sources, the visualization agent and the detector, are distinguished. The noise from the visualization agent can be affected by the applied voltage, the surface modification of capillaries and the concentration of the visualization agent. A new factor named the "noise coefficient" is found which represents the contribution to the noise from the visualization agent. The physical interpretation of the noise coefficient is the ratio of the concentration fluctuation to the concentration of the visualization agent. A new equation that correlates detection limits with molar absorptivity and concentration of the visualization agent, noise coefficient and instrument noise is proposed, and the functions of those factors are discussed.

INTRODUCTION

Capillary zone electrophoresis (CZE) is a separation technique characterized by high efficiency and small sample volume, and great progress has been made in instrumentation and applications in the last several years. In principle, CZE is very suitable for the analysis of small ionic compounds such as aliphatic carboxylic acids, amino acids and inorganic acids. However, many of these classes of compounds lack chromophores at useful wavelengths, or have such low molar absorptivities as to preclude sensitivity by absorption detection. Conductivity detectors [1–7] and amperometric detectors [7–9] have been developed for CZE analysis of these compounds. The performance of conductivity and amperometric detectors are generally excellent, with detection limits of 10^{-6}–10^{-7} M for carboxylic acids or amino acids. However, these detectors are more difficult to fabricate than absorption detectors, and are not yet commercially available.

Correspondence to: Dr. R. A. Hartwick, Department of Chemistry, State University of New York at Binghamton, Binghamton, NY 13902, USA.

An alternative strategy to detect UV-transparent compounds in CZE is that of indirect fluorescence of indirect absorption detection. To achieve such indirect detection, an ion with either fluorescence or UV absorption properties, which is called the visualization agent, is added to the mobile phase in order to create a high background signal. The analyte ions that have the same sign of charge as the visualization agent but have no fluorescence or absorption are observed from the reduction of the background signal. Indirect fluorescence detection was first introduced to CZE by Kuhr and Yeung [10], and has been applied to the analysis of amino acids, nucleotides, inorganic anions and sugars [10–13]. Impressive detection limits can be achieved, with concentration limits of $2 \cdot 10^{-7}$ M for $H_2PO_4^-$ being reported [12].

Indirect absorption detection in CZE was first reported by Hjertén *et al.* [14]. Foret *et al.* [15] presented more details about indirect absorption detection in CZE. They observed the effect of ion mobility on the peak shape and found that higher sensitivity could be obtained by selecting visualization agents which have high molar absorptivity and effective mobilities similar to those of sample ions.

0021-9673/92/$05.00

More recently, indirect UV detection has successfully been applied to the detection of 30 anions separated by CZE [16], demonstrating great advantages over ion chromatography in terms of speed and peak capacity.

In this paper, the factors which contribute to the noise and signal in indirect absorption detection were studied, and a factor named the "noise coefficient" was defined as one of important parameters to estimate detection limit and to select operating conditions.

EXPERIMENTAL

Instrumentation

A Spectra Phoresis 1000 with SP4400 integrator (Spectra-Physics, Reno, NV, USA) was used. The fused-silica capillary (Polymicro Technologies, Phoenix, AZ, USA) was 75 μm I.D. × 360 μm O.D. with an effective length of 35.0 cm and a total length 42.5 cm. The column temperature was 25.0°C. The detector wavelength was set according to the maximum absorption position of each visualization agent. Sample was injected by 1.0-s hydrodynamic injection. A laboratory-constructed CZE apparatus was employed to conduct the noise measurement with a Pyrex rectangular capillary (0.05 × 0.5 mm, Wilmad Glass, Buena, NJ, USA). The rectangular capillary was glued to a modified cell on a Spectra 100 detector (Spectra-Physics), and an aperture of about 1.2 × 0.4 mm was created. In order to avoid the effect of light, this apparatus was operated in a dark room.

The PEG 8M-10-modified capillary was produced in our laboratory according to the temperature protocols recommended by Innophase (Portland, CT, USA).

Procedures

Capillaries were initially washed with 1 *M* NaOH for 10 min, except the PEG-modified column, then washed with water. In most of cases, the capillaries were equilibrated with buffer overnight. The detector noise (peak-to-peak) was measured with capillaries filled with buffer (*i.e.*, the visualization agent solution) and without voltage. The total noise was measured from a 2–3 min segment of a stable baseline while a certain voltage was applied.

Stock solutions of 50 m*M* 4-nitrophenol (NPH), 10 m*M* 1,3,5-benzenetricarboxylic acid (BTA) and 2 m*M* 1-naphthylacetic acid (NAA) were prepared by dissolving the chemicals in boiling pure water (17 MΩ). After cooling, the final volume was adjusted and the solution was filtered through a 0.45-μm membrane. Lower concentration solutions were obtained by dilution. pH 4 buffers were made by adding NaOH solution or Tris solution, pH 8 buffers by adding Tris solution–Tris solid.

Propionic acid and hexanoic acid solutions ($1.1 \cdot 10^{-2}$ *M* each) were prepared and adjusted to pH 4.1 or 8.0 by Tris solution in order to keep the sample pH close to the buffer pH, then diluted to the desired concentration with distilled water. Just before injection, the sample solutions were further diluted with buffer at a 1:1 ratio, and the indicated concentration was that after dilution with buffer.

Chemicals

BTA, NPH, NAA and hexanoic acid were obtained from Aldrich (Milwaukeek, WI, USA), PEG 8M-10 from Innophase, Tris from Bio-Rad Labs. (Richmond, CA, USA) and all other chemicals from Fisher (Fair Lawn, NJ, USA).

RESULTS AND DISCUSSION

Noise from visualization agent

For indirect fluorescence and indirect absorption detection, the major factors determining the detection limits have been reported to be the concentration of the visualization agent, C_v, the dynamic reserve, D_r (*i.e.*, the ratio of the background absorbance to the noise), and the displacement ratio, R (*i.e.*, the number of visualization agent molecules transferred by one analyte molecule) [17–20]. The detectable concentration, C_{det}, can be estimated from eqn. 1 [17]:

$$C_{det} = C_v/(RD_r) \quad (1)$$

According to eqn. 1, lowering C_v and increasing D_r will reduce the detection limit. However, there are two questionable points in eqn. 1. First, it has been found that the D_r value somehow depends on C_v [17,19]. Therefore, one may not reduce detection limits according to eqn. 1 by lowering C_v, because D_r is reduced simultaneously. Secondly, in eqn. 1, the function of molar absorptivity of the visualization agent is not clear, although some authors

TABLE I

RELATIONSHIP OF NOISE TO VISUALIZATION AGENT CONCENTRATION IN A ROUND CAPILLARY

Conditions: 75 μm I.D. fused-silica capillary; BTA–NaOH buffer, pH 4.22; 355 V/cm.

C_v (mM)	Background (a.u.)	Slope (a.u./mM)[a]	σ_v ($\times 10^{-5}$)	K_n ($\times 10^{-15}$)
0.40	0.072	0.162	0.47	7.2
1.00	0.162	0.135	1.2	8.9
2.00	0.275	0.095	1.6	8.4
4.00	0.403	0.038	1.5	9.8

[a] Tangent of the regression curve at each concentration.

[19,20] recommend the use of visualization agent with high molar absorptivity.

In this research, it is found that the noise in indirect absorption detection includes at least two sources: the visualization agent and the detector (electronic, source, etc.). From the viewpoint of absorption measurements [21], noise is the unwanted fluctuations in the desired signal, and the noise magnitudes are typically expressed as either root-mean-square (rms) or peak-to-peak (p–p) values. Since the square values of independent rms noises are additive, for indirect absorption detection in CZE, we have

$$\sigma_{tot}^2 = \sigma_v^2 + \sigma_d^2 \quad (2)$$

where σ_{tot} is the total rms noise, σ_v the rms noise from the visualization agent and σ_d the rms noise from the detector. In experiments, the peak-to-peak noise is more easily to be measured, with the rms noise being approximately one fifth of the p–p noise [21]. Therefore,

$$(5\sigma_{tot})^2 = (5\sigma_v)^2 + (5\sigma_d)^2 \quad (3)$$

or

$$N_{tot}^2 = N_v^2 + N_d^2 \quad (4)$$

where N_{tot} is the total p–p noise, N_v the p–p noise from the visualization agent and N_d the p–p noise from the detector.

The noise measurements indicate that, when keeping the voltage constant, the σ_v value varies with the visualization agent, as it is seen from Tables I and II. However, between concentration and noise, there is a factor, K_n, which remains approximately constant, and a new relationship can be established as follows:

$$\sigma_v = K_n C_v S_p \quad (5)$$

where K_n is named the noise coefficient, and S_p is the slope of concentration *versus* absorbance. Within the linear range, S_p is equal to εb, where ε is molar absorptivity and b is the equivalent optical path length of capillary. In Table I (round capillary), the K_n values of BTA fall between $7.2 \cdot 10^{-5}$ and $9.8 \cdot 10^{-5}$, which are approximately a constant within the measurement error. It is also noticed that the calibration curve using the round capillary is not linear (non-constant slopes in Table I), which may interfere the measurement. In order to eliminate any possible effect due to the deviations from Beer's law, the noise measurement was performed using a rectangular capillary, which gave an excellent straight line in the concentration *versus* absorbance plot, and the K_n values of NPH fall between $3.2 \cdot$

TABLE II

RELATIONSHIP OF NOISE TO VISUALIZATION AGENT CONCENTRATION IN A RECTANGULAR CAPILLARY

Conditions: 0.05 × 0.5 mm Pyrex rectangular capillary; NPH–Tris buffer, pH 8.29; 200 V/cm.

C_v (mM)	Background (a.u.)[a]	N_{tot} (10^{-4} a.u.)	N_d (10^{-4} a.u.)	σ_v (10^{-4} a.u.)	K_n ($\times 10^{-4}$)
1.0	0.074	3.6	3.6	–	–
3.0	0.224	7.2	5.2	1.0	4.4
6.0	0.448	12	9.2	1.5	3.3
15.0	1.136	43	39	3.6	3.2

[a] Constant slope (0.0075 a.u./mM) from the regression equation.

10^{-4} and $4.4 \cdot 10^{-4}$ (Table II). These data indicate that in each case K_n is approximately a constant.

A very important phenomenon observed in the noise measurement is that the N_{tot} values are obviously affected by the applied voltage, both in rectangular and round capillaries. Assuming the N_d remains constant during voltage changes, the σ_v, then the K_n values, according to eqns. 4 and 5, respectively, will be affected by the applied voltage. One of the changes of K_n values is presented in Fig. 1. The changes of N_{tot} values with the electric field strength indicate that the noise contribution from the visualization agent is not caused by the absorbance measurement such as the source fluctuation, but presumably caused by the concentration fluctuation.

In order to determine what factors are responsible for the additional noise, the noise was measured under different pH values and different columns, and the results are tabulated in Table III. It is found that using BTA–Tris buffer, the noise contribution from the visualization agent is almost undetectable in the PEG-bonded capillary. The dramatic reduction in noise when using a PEG capillary was unexpected, and the results suggest that interactions such as adsorption between the visualization agent and the capillary wall could be responsible for the noise. If adsorption is one of the reasons leading to extra noise in a bare silica capillary, a higher pH value would lead to lower noise, due to enhanced repulsion between the BTA and the silica surface in basic buffers. This inference has been verified experimentally. The data in Table III demonstrated that when the pH is increased from 4.25 to 8.25, the σ_v value is decreased from $1.3 \cdot 10^{-5}$ to $0.57 \cdot 10^{-5}$ a.u., and the K_n value is simultaneously reduced from $4.6 \cdot 10^{-5}$ to $2.0 \cdot 10^{-5}$.

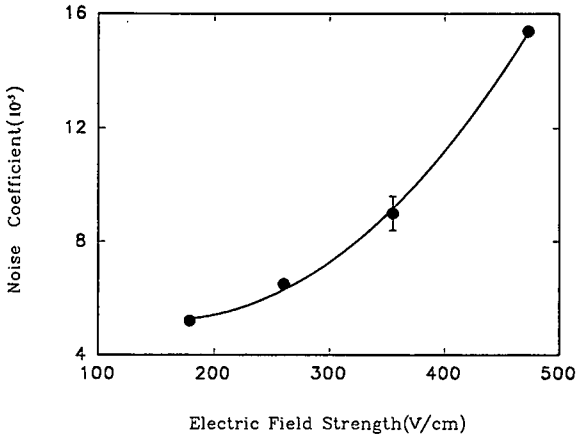

Fig. 1. Relationship of the noise coefficient to the electric field strength. Conditions: 75 μm I.D. × 360 μm O.D. fused-silica capillary; 2.0 m*M* BTA–NaOH buffer, pH 4.22; detector wavelength 210 nm; rise time 0.5 s. The bar represents the range of three measurements in different days.

Based on the results mentioned above, it is reasonable to assume that σ_v is created by the concentration fluctuation of the visualization agent, ΔC_v, although it is hard to tell how such a fluctuation is generated. Thus,

$$\sigma_v = \Delta C_v S_p \quad (6)$$

Combining eqns. 5 and 6, we have

$$K_n = \Delta C_v / C_v \quad (7)$$

Eqn. 7 suggests the physical meaning of the noise coefficient: the ratio of concentration fluctuation to concentration of the visualization agent. Different visualization agents may have different K_n values. K_n is independent of the concentration of the visualization agent, but is dependent on the applied voltage and surface chemistry of capillaries.

TABLE III

EFFECT OF pH AND SURFACE MODIFICATION ON THE NOISE COEFFICIENT

Column[a]	Conditions	σ_v (10^{-5} a.u.)	K_n ($\times 10^{-5}$)
Bare	2 m*M* BTA–Tris, pH 4.25; 306 V/cm	1.3	4.6
PEG-bonded	2 m*M* BTA–Tris, pH 4.21; 306 V/cm	<0.2	<0.7
Bare	2 m*M* BTA–Tris, pH 8.25; 306 V/cm	0.57	2.0

[a] All are 75 μm I.D. fused-silica capillaries.

Detection limit

The detection limit depends on the signal-to-noise (S/N) ratio. Ideally, the signal in indirect absorption detection is

$$\Delta A = (R\varepsilon_v - \varepsilon_s)bC_s \quad (8)$$

where ΔA is the reduction of background absorbance, R is the displacement ratio (the number of visualization agent molecules transferred by one analyte molecule), ε_s and ε_v are the molar absorptivity of the sample and the visualization agent, respectively, b is the equivalent optical path length of the capillary and C_s is the sample concentration. When the molar absorptivity of the analyte is much smaller than that of the visualization agent, $R\varepsilon_v - \varepsilon_s \approx R\varepsilon_v$, thus

$$\Delta A = R\varepsilon_v bC_s \quad (9)$$

Combining eqns. 4, 5 and 9 (within the linear range, $S_p = \varepsilon_v b$), we have

$$S/N = \left[\frac{\Delta A^2}{N_{tot}^2}\right]^{0.5} = \left[\frac{(R\varepsilon_v bC_s)^2}{(5\,K_nC_v\varepsilon_v b)^2 + N_d^2}\right]^{0.5} \quad (10)$$

The detection limit, C_{lim}, is usually measured at an S/N of 3, thus

$$C_{lim} = C_s = 3\left[\frac{(5\,K_nC_v\varepsilon_v b)^2 + N_d^2}{(R\varepsilon_v b)^2}\right]^{0.5} \quad (11)$$

In practice, $\varepsilon_v b$ may be replaced by the real slope, thus

$$C_{lim} = 3\left[\frac{(5\,K_nC_v\varepsilon_v b)^2 + N_d^2}{(RS_p)^2}\right]^{0.5} \quad (12)$$

Eqn. 11 indicates that ε_v contributes both signal and noise; simply selecting visualization agents with higher ε_v may not necessarily lead to lower detection limits. There are two extreme conditions in eqn. 11.

(a) $(5K_nC_v\varepsilon_v b)^2 \gg N_d^2$: eqn. 11 becomes

$$C_{lim} \approx 15\,K_nC_v/R \quad (13)$$

The detection limit cannot be improved by increasing ε_v, but lowering C_v will reduce the detection limit. It is noticed that eqn. 13 is very similar to eqn. 1. In other words, eqn. 1 could be treated as a specific expression of eqn. 12.

(b) $(5K_nC_v\varepsilon_v b)^2 \ll N_d^2$: eqn. 11 becomes

$$C_{lim} \approx 3\,N_d/R\varepsilon_v b \quad (14)$$

Lowering V_v does not reduce detection limits any more, instead, increasing ε_v will improve detection limits.

From these extreme conditions, a reasonable inference is that combinations of high ε_v and low C_v will give a lower detection limit, and such an experimental result has been observed by Foret *et al.* [15]. However, the requirements of buffer capacity, buffer conductivity and adequate background absorbance which is corresponding to a lower detection error and falls in the linear range of the detector must be considered when one selects the values of ε_v and C_v.

The function of K_n is obvious in eqn. 11, that is, the lower the better. Since the mechanism of the concentration fluctuation is not clear at present, experimental selection of visualization agents and surface modification have to be done in order to obtain lower detection limits.

Fig. 2 illustrates the effect of ε_v on detection. The electropherograms were obtained from one injection but monitored at two wavelengths. The background absorbance ratio, which is equal to the ε_v ratio, is 5.21, and higher peaks are generated by the higher ε_v value. The peak-height ratios are 4.92–

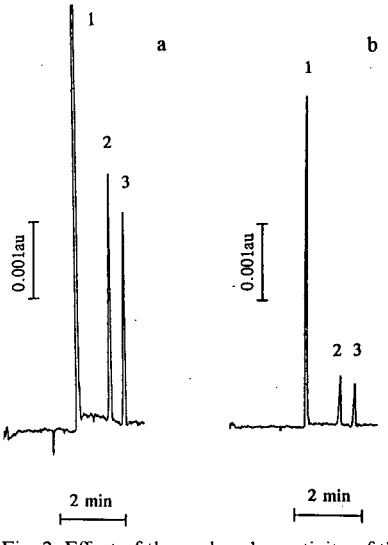

Fig. 2. Effect of the molar absorptivity of the visualization agent on detection. (a) Detector wavelength 210 nm; (b) detector wavelength 240 nm. Conditions: 75 μm I.D. × 360 μm O.D. fused-silica capillary; 0.5 mM BTA–Tris buffer, pH 8.20. Peaks: 1 = water; 2 = $5.5 \cdot 10^{-5}$ M hexanoic acid; 3 = $5.5 \cdot 10^{-5}$ M propionic acid.

4.93, quite close to the background absorbance ratio. Since the noise at 210 nm is a little higher than that at 240 nm, the calculated detection limit (S/N = 3) for propionic acid at 210 nm is only a 3.3-fold improvement compared to that at 240 nm.

Linearity of detection

The indirect absorption detection in CZE was estimated to have a narrow dynamic linear range [15], because the concentration of the analyte must be much lower than that of the buffer in order to reduce the disturbance of the local electric field. However, it has been found that the dynamic linear range depends on what parameter is measured. From Fig. 3 it is seen that the linearity in terms of peak height is poor, but the linearity in terms of peak area is very good (except the outlier at $1.1 \cdot 10^{-6}$ M) and the dynamic linear range extends at least two orders of magnitude from $3.3 \cdot 10^{-6}$ to $3.3 \cdot 10^{-4}$ M (buffer concentration is only 1 mM) with a linear regression coefficient (r^2) of 0.99996, even though the asymmetric factor of the peaks changes from 1.2 to 12.8. It should be mentioned that, although the quantitation is available at high sample concentration, the peak becomes broad and the resolving power is sacrificed. At $1.1 \cdot 10^{-6}$ M, noise obviously interferes with area integration, thus deteriorating linearity.

CONCLUSIONS

In this paper, the factors which contribute to the noise and signal in indirect absorption detection in CZE are studied. Two independent noise sources are distinguished, *i.e.*, the visualization agent and the detector. Although the mechanism of the noise from the visualization agent is not clear at present, the experimental results indicate that the noise has both chemical and physical natures, because the noise can be affected by the surface modification of a capillary and the applied voltage, as well as the concentration of the visualization agent. A new factor, named the noise coefficient, is found which represents the contribution to the noise from the visualization agent, and the coefficient is interpreted as the ratio of the concentration fluctuation to the concentration of the visualization agent. The factors that contribute to the noise and the signal are summarized in eqn. 11, and the functions of the molar absorptivity and the concentration of the visualization agent, the noise coefficient and the detector noise are discussed.

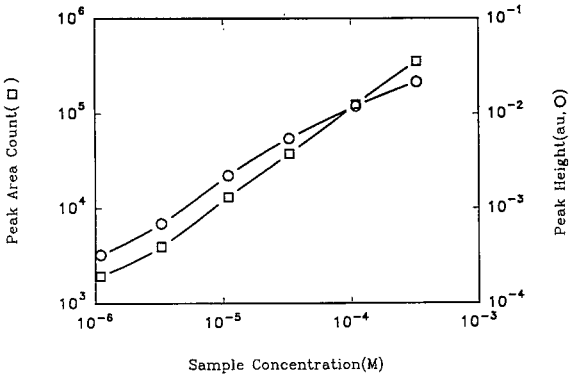

Fig. 3. Linearity of detection. Conditions: 1.0 mM NAA–Tris buffer, pH 8.09. Sample: propionic acid; 1.0-s hydrodynamic injection.

ACKNOWLEDGEMENTS

This research was supported by the Center for Biotechnology of the State University of New York at Stony Brook and by the Spectra-Physics Analytical Instrument Division.

REFERENCES

1 F. E. P. Mikkers, F. M. Everaerts and Th. P. E. M. Verheggen, *J. Chromatogr.*, 169 (1979) 11.
2 P. Gebauer, M. Deml, P. Boček and J. Janák, *J. Chromatogr.*, 267 (1983) 455.
3 J. L. Beckers, Th. P. E. M. Verheggen and F. M. Everaerts, *J. Chromatogr.*, 452 (1988) 591.
4 X. Huang, T. J. Pang, M. J. Gordon and R. N. Zare, *Anal. Chem.*, 59 (1987) 2747.
5 X. Huang, J. A. Luckey, M. J. Gordon and R. N. Zare, *Anal. Chem.*, 61 (1989) 766.
6 X. Huang, M. J. Gordon and R. N. Zare, *J. Chromatogr.*, 480 (1989) 285.
7 X. Huang, R. N. Zare, S. Sloss and A. G. Ewing, *Anal. Chem.*, 63 (1991) 189.
8 R. A. Wallingford and A. G. Ewing, *Anal. Chem.*, 60 (1988) 1972.
9 T. M. Olefirowicz and A. G. Ewing, *J. Chromatogr.*, 499 (1990) 713.
10 W. G. Kuhr and E. S. Yeung, *Anal. Chem.*, 60 (1988) 1832.
11 W. G. Kuhr and E. S. Yeung, *Anal. Chem.*, 60 (1988) 2642.
12 L. Gross and E. S. Yeung, *J. Chromatogr.*, 480 (1989) 169.
13 T. M. Garner and E. S. Yeung, *J. Chromatogr.*, 515 (1990) 639.
14 S. Hjertén, K. Elenbring, F. Kilar, J. L. Liao, A. J. C. Chen, C. J. Siebert and M. D. Zhu, *J. Chromatogr.*, 403 (1987) 47.

15 F. Foret, S. Fanali, L. Ossicini and P. Boček, *J. Chromatogr.*, 470 (1989) 299.
16 W. R. Jones and P. Jandik, *J. Chromatogr.*, 546 (1991) 445.
17 T. Takeuchi and E. S. Yeung, *J. Chromatogr.*, 370 (1986) 83.
18 W. D. Pfeffer, T. Takeuchi and E. S. Yeung, *Chromatographia*, 24 (1987) 123.
19 T. Takeuchi and D. Ishii, *J. Chromatogr.*, 393 (1987) 419.
20 D. Ishii and T. Takeuchi, *J. Liq. Chromatogr.*, 11 (1988) 1865.
21 J. D. Ingle, Jr. and S. R. Crouch, *Spectrochemical Analysis*, Printice-Hall, Englewood Cliffs, NJ, 1988, Ch. 5.

Journal of Chromatography, 607 (1992) 126–130
Elsevier Science Publishers B.V., Amsterdam

CHROM. 24 440

Short Communication

Concerning the role of face-to-edge π–π interactions in chiral recognition

William H. Pirkle and Christopher J. Welch*

School of Chemical Sciences, University of Illinois, Urbana, IL 61801 (USA)

Myung H. Hyun

Department of Chemistry, Pusan National University, Pusan 609-735 (South Korea)

(First received January 8th, 1992; revised manuscript received June 16th, 1992)

ABSTRACT

A simplified chiral recognition mechanism involving face-to-edge π–π interaction is advanced to account for chromatographic data previously rationalized by invoking two competing, opposite sense chiral recognition mechanisms.

INTRODUCTION

Accumulation of evidence from a variety of sources often leads to general acceptance of a reaction mechanism. Mechanistic hypotheses have played an invaluable role in advancing the understanding of chemical processes, including processes involving chiral recognition. It is widely understood that mechanistic hypotheses can be disproven, but never proven.

To be generally accepted, a mechanism must be in accord with all relevant experimental data and should comply with the Occam's razor maxim. This maxim, attributed to William of Occam, a fourteenth-century English philosopher, cautions against excessive and unjustifiably elaborate assumptions. In the present paper, we simplify a rationalization presented earlier to explain chromatographic data obtained from a homologous series of racemates on several related chiral stationary phases (CSPs).

DISCUSSION

In several papers published in the mid 1980s [1–3], we described a curious relationship between enantioselectivity, the length of the alkyl substituent in a type 1 analyte, the length of the tether connecting the chiral selector to the support, and the orientation of the selector with respect to the tether. This relationship is illustrated in Fig. 1.

To rationalize the unusual α *versus* n curves obtained from normal-phase chromatography (α is the separation factor for enantiomers and n is the number of methylene units in the alkyl substituent), two

Correspondence to: Dr. W. H. Pirkle, School of Chemical Sciences, University of Illinois, Urbana, IL 61801, USA.

* Present address: Regis Chemical Company, Morton Grove, IL, USA.

0021-9673/92/$05.00

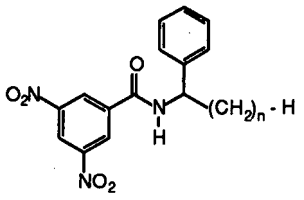

Type 1 analyte

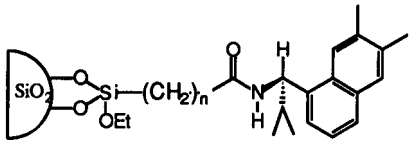

(*R*) CSP 1 n = 4
(*R*) CSP 2 n = 10

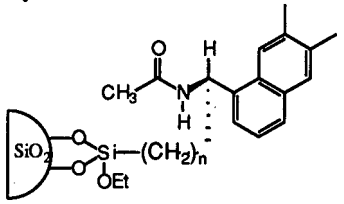

(*R*) CSP 3 n = 5
(*R*) CSP 4 n = 11

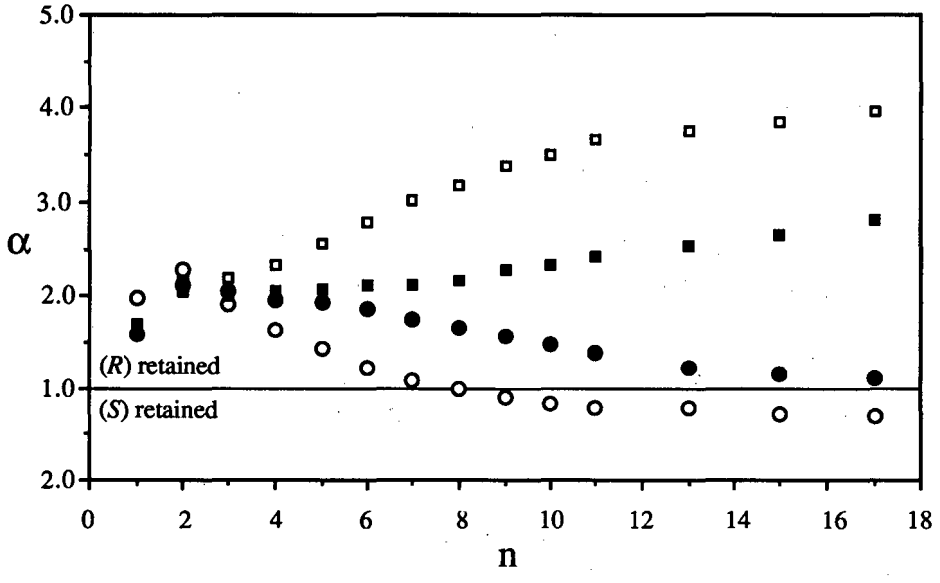

Fig. 1. Enantioselectivities observed for type 1 analytes on CSPs 1 (○), 2 (●), 3 (□) and 4 (■).

chiral recognition processes were proposed. A "dipole stacking" process was suggested to selectively retain one enantiomer while a "hydrogen bonding" process selectively retains the other. Both processes involve "face-to-face" approaches of the analytes and the CSP owing to π–π interactions between the π-basic naphthyl groups in the CSPs and the π-acidic 3,5-dinitrobenzoyl groups in the analytes. Both processes invoked steric interaction between the alkyl substituents of the analytes and the tethers and/or silica as the alkyl substituents were intercalated between adjacent strands of bonded phase. These steric interactions were suggested to become more severe as the alkyl substituents became longer or the tethers became shorter. These steric interactions were suggested to be nonidentical for the enantiomers and to depend upon the orientation of the selector with respect to the tethers. Both processes were predicated upon the presumption that the aromatic substituent (phenyl, *p*-anisyl,

α-naphthyl, β-naphthyl) in the analytes behaved as if it were effectively larger than the alkyl group and that this size difference (and the consequent differential steric interactions with the CSP) was the source of the chiral recognition.

A confluence of events and observations leads us to reconsider the earlier data in terms of face-to-edge bonding interactions between aromatic systems. By invoking such an interaction, the earlier observations can be rationalized more simply and, in our view, more plausibly.

There is ample precedent for attractive face to edge interaction between aromatic rings. Such arrangements are found in the crystal structures of proteins [4], peptides [5] and small molecules [6], and have been the subject of theoretical calculations [7]. Moreover, in other chiral recognition studies, we are encountering chromatographic and nuclear magnetic resonance spectroscopic data which can be rationalized in terms of such interactions. Contemplation of an attractive interaction between the face of the aryl substituent of the analyte and the edge of the naphthyl group of CSPs 1–4 leads to the conclusion that a single chiral recognition process will suffice to rationalize the data.

Fig. 2 shows the simplified postulate in which the previously invoked face-to-face π–π interaction and the hydrogen bond between the analyte's dinitrobenzamide N–H and the carbonyl oxygen of the CSP are retained. As before, both selector and analyte are shown in presumed low energy conformations in which the methine hydrogens on the stereogenic centers are approximately eclipsed with the carbonyl oxygens and approximately in the plane of the naphthyl and dinitrobenzoyl rings, respectively. These are held to be relatively low energy conformations which are significantly populated prior to complexation. In the case of the homochiral (*i.e.* the *R*:*R* or *S*:*S*) complex, π–π and hydrogen bonding interactions lead to a structure where the face of the analyte's aryl substituent is presented to the edge of the CSPs naphthyl ring, a bonding interaction ensuing. This arrangement also positions the methine hydrogen of the CSP such that it may simultaneously undergo weak hydrogen bonding to the π cloud of the aryl ring of the analyte. In addition, the analyte's alkyl substituent is directed more or less parallel to the CSP's acyl substituent. In acyl-tethered CSPs 1 and 2, this orientation of the alkyl group is viewed as an intercalative orientation where the resultant steric difficulties reduce retention (relative to the non-intercalating antipode) as the alkyl substituent is lengthened or the tether is shortened. Since the analyte enantiomer involved in the homochiral complex is normally the more retained, the reduction in enantioselectivity noted as the alkyl substituent is lengthened or the tether is shortened is explained, as is the eventual inversion of elution order on CSP 1.

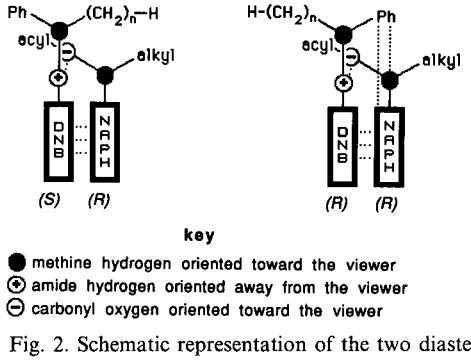

Fig. 2. Schematic representation of the two diastereomeric adsorbates proposed to account for chiral recognition of type 1 analytes on CSPs 1–4. The homochiral (*R*:*R*) adsorbate allows for simultaneous hydrogen bonding, face-to-face π–π interaction, and face-to-edge π–π interaction.

In the corresponding heterochiral complex, the aryl substituent of the analyte is directed toward the acyl group of the CSP. The alkyl substituent of the analyte is oriented more or less alongside the alkyl group of the CSP where, in CSPs 3 and 4, this constitutes an intercalative arrangement. Since the heterochiral analyte enantiomer is the least retained, increasing the length of the alkyl group or shortening the length of the alkyl tether in CSPs 3 and 4 increases enantioselectivity by decreasing the retention of the least retained enantiomer relative to its non-intercalating antipode. The effect is most profound on the short-tethered CSP 3.

A computer-generated space-filling molecular model representation of an exploded view of the two diastereomeric adsorbates which more clearly illustrates the face–edge π–π interaction is illustrated in Fig. 3 (the interested reader is also encouraged to constuct space-filling models). For clarity in this depiction, the 3,5-dinitrobenzamide derivative of α-phenylethylamine is used to represent a generic type 1 analyte (bottom structure) and the acetamide

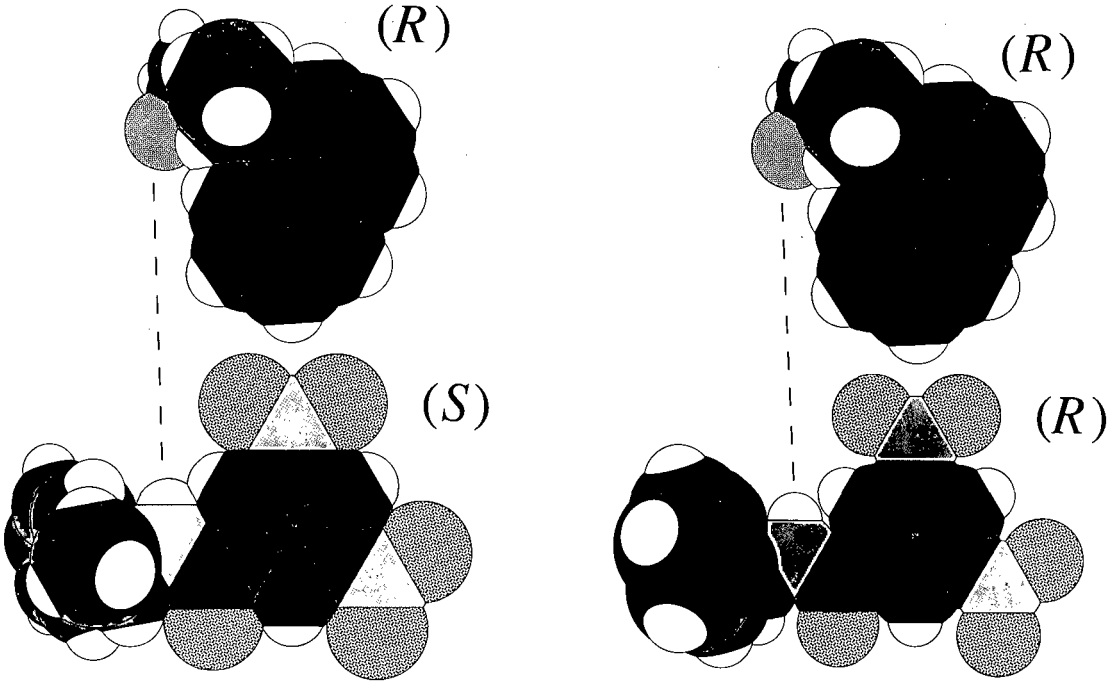

Fig. 3. Exploded view of computer-generated space-filling molecular model representations of the two diastereomeric adsorbates pictured in Fig. 2. The dashed line indicates a hydrogen bond between the upwardly oriented amide hydrogen of the analyte and the downwardly oriented carbonyl oxygen of the CSP. As the distance along this line is decreased by sliding the two structures together within the x–y plane, the proposed face-to-edge π–π interaction of the homochiral (R:R) adsorbate can be visualized.

derivative of (R)-α-naphthylethylamine is used to represent the stationary phase (top structure). A hydrogen bonding interaction between the upwardly oriented DNB amide hydrogen and the downwardly oriented amide carbonyl oxygen of the CSP is indicated by a dashed line. In the postulated adsorbates, the analyte and CSP are closer together than depicted so as to allow the face-to-face geometry necessary if the homochiral (R:R) adsorbate is to simultaneously undergo hydrogen bonding, face-to-face π–π interaction, and face-to-edge π–π interaction.

Some aspects of the original rationalization remain unchanged, the principal refinement stemming from a growing appreciation that aromatic substituents can serve as sites for a variety of bonding as well as steric interactions. By recognizing the occurance of face-to-edge π–π interaction, competing "opposite sense" dipole stacking and hydrogen bonding chiral recognition processes need not be invoked to rationalize the α vs n plots shown in Fig. 1. While multiple adsorption processes are thought to be common (if not universal), the simplest adequate rationalization is, according to Occam, to be preferred. Obviously, those mechanistic model which conform most closely to reality are of the greatest value in the design of improved chiral stationary phases.

ACKNOWLEDGEMENTS

This work has been supported by a grant from the National Science Foundation and by a Department of Education Advanced Opportunites in Chemistry Graduate Fellowship. We thank Drs. Scott Kahn and Edward Voss Jr. for valuable discussions concerning face-to-edge π–π interactions.

REFERENCES

1 W. H. Pirkle, M. H. Hyun and B. Bank, *J. Chromatogr.*, 316 (1984) 585.

2 W. H. Pirkle, M. H. Hyun, A. Tsipouras and B. Bank, *J. Pharm. Biomed. Anal.*, 2 (1985) 173.
3 W. H. Pirkle and M. H. Hyun, *J. Chromatogr.*, 328 (1985) 1.
4 S. K. Burley and G. A. Petsko, *Science (Washington, D.C.)*, 229 (1985) 23.
5 I. Z. Siemion, *Z. Naturforsch., B: Chem. Sci.*, 45 (1990) 1324.
6 A. V. Muehldorf, D. Van Engen, J. C. Warner and A. D. Hamilton, *J. Am. Chem. Soc.*, 110 (1988) 6561.
7 P. Linse, *J. Am. Chem. Soc.*, 114 (1992) 4367.

Journal of Chromatography, 607 (1992) 131–134
Elsevier Science Publishers B.V., Amsterdam

CHROM. 24 426

Short Communication

Quantitative reproducibility study with automated microcolumn liquid chromatography

Hernan J. Cortes, Jeffrey R. Larson and Gerald M. McGowan

The Dow Chemical Company, 1897B Building, Midland, MI 48667 (USA)

(First received April 21st, 1992; revised manuscript received June 10th, 1992)

ABSTRACT

Studies were conducted to evaluate the quantitative reproducibility and long-term system stability for a reversed-phase microcolumn liquid chromatographic system. The relative standard deviation found was 0.38% for a major component and 0.7–1.6% for minor impurities using external standard calibration and automated sample injection. System longevity was studied over an eight-month operating period using repetitive injections of synthetic samples in an automated fashion. Excellent column stability was observed with minimal increase in operating pressure or observable loss in resolution. The results obtained suggest that microcolumn liquid chromatography is well-suited for routine applications.

INTRODUCTION

Miniaturization of a packed column liquid chromatography (LC) system using fused-silica columns was initially investigated almost a decade ago [1–5] with the recognized benefits of reduced consumption of mobile and stationary phases, increased mass sensitivity with concentration sensitive detectors, high separation efficiencies and posibility of new detection techniques [6,7]. More recently, the low volumetric dispersion given by such microcolumns has been exploited by interfacing in a multidimensional approach with capillary gas chromatography [8–11], conventional liquid chromatography [12,13], and capillary supercritical fluid chromatography [14]. Although studies in column preparation and system use have continued, the use of microcolumn LC has not yet found widespread routine utilization, mainly due to perceived difficulties of operation, instrument availability, and to the relative lack of published information concerning quantitative reproducibility and long-term system stability, which are of great importance to analysts involved in the solution of day-to-day problems. Recent reviews have summarized the practical details, theory and applications of microcolumn LC [15,16]. In order for the benefits of the technique to be fully exploited and for the technique to be more widely practiced, a microcolumn LC system should yield quantitative results which are equivalent to those obtained using conventional systems. Unfortunately, few quantitative studies using microcolumn LC have been reported [17].

In this paper, studies conducted in the evaluation of an automated microcolumn LC (Micro LC) system in terms of quantitative reproducibility and long-term system stability are described.

Correspondence to: Dr. H. J. Cortes, The Dow Chemical Company, 1897B Building, Midland, MI 48667, USA.

EXPERIMENTAL

The system used consisted of an Isco LC 500 (Isco, Lincoln, NE, USA) syringe pump operated at constant flow-rate, which was connected to a Model A2N14W injection valve (Valco Instruments, Houston, TX, USA) equipped with a 100-nl internal rotor. The injection valve was either operated manually, or was automated using an air-driven Digital Valve Interface (Valco). In either case, the valve was allowed to remain in the inject position for two seconds prior to returning the load position.

An ABI 757 variable-wavelength detector (Applied Biosystems, Santa Clara, CA, USA) with a longitudinal flow cell [18] of 8-mm path length and 70-μm diameter (LC Packings, San Francisco, CA, USA) was operated at 214 and 254 nm.

Columns were made from fused silica (Polymicro Technologies, Phoenix, AZ, USA), 15 cm × 250 μm I.D. equipped with a porous ceramic bed support [19] and were packed at 400 atm with Spherisorb ODS, 5-μm particle diameter (Phase Separations, Haupagge, NJ, USA) as a slurry (5:1; in acetonitrile. The eluent used was acetonitrile–0.05 *M* KH_2PO_4 (30:70) at a flow-rate of 4.5 μl/min. An NEC portable 30386SX computer (NEC Information Systems, Boxborough, MA, USA) was used to control pump filling, sample introduction, collect raw data, integrate the chromatogram and store and plot the results, utilizing user-written software.

An Eldex Model A high-pressure metering pump (Anspec, Ann Arbor, MI, USA) equipped with a 0.5-μm in-line filter (Alltech, Milwaukee, WI, USA) was used to continuously circulate sample through the injection valve. A diagram of the Micro LC system set-up is included in Fig. 1. A program was written for the computer to allow automated refilling of the pump, which has a 50-ml capacity. The slide switch at the back of the pump was set to external, and the interfacing to the Isco pump was accomplished through 5-V TTL level signals to the 37 pin D-sub connector. The manual 3-way valve of the pump was replaced with an air actuated 6-port valve (Valco). During pump filling, the outlet port of the pump and the line to the 4-port injection valve were blocked. After the pump piston reached the bottom of its stroke, the 6-port valve was rotated and the pump was switched to the constant pressure mode in order to rapidly repressurize the system. After allowing one minute to reach the desired column pressure, the pump was switched to the constant flow mode.

The sample used for the quantitative study consisted of 2,4-dichlorophenoxyacetic acid (2,4-D) as a major component and various related compounds, *o*-chlorophenoxyacetic acid (OCPAA), *p*-chlorophenoxyacetic acid (PCPAA), 2,6-dichlorophenoxyacetic acid (2,6-D), *p*-chlorophenol (PCP), 2,4,6-trichlorophenoxyacetic acid (2,4,6-T) and 2,4-dichlorophenol (2,4-DCP) (Pfaltz & Bauer, Waterbury, CT, USA and Aldrich Chemicals, Milwaukee, WI, USA). Compounds were dissolved in acetonitrile–water (50:50). Long-term system stability was studied using a solution containing acetophenone, phenol and methyl benzoate (Aldrich).

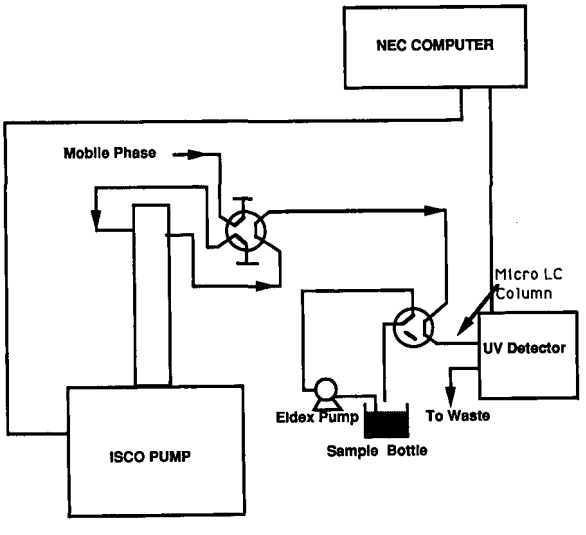

Fig. 1. Diagram of the automated microcolumn LC system.

RESULTS AND DISCUSSION

Reproducibility studies were conducted using synthetic samples containing a major component and a series of minor impurities, as this represents a typical analysis conducted in the assay of chemical products.

Due to the geometry of the valco injection valve sample loops typically used for microcolumn LC [20] and because the components of interest were not soluble in a weaker solvent than the mobile phase in order to allow peak focussing [21] tailing

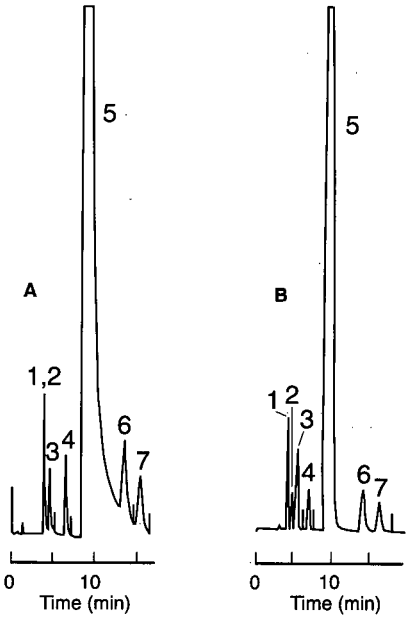

Fig. 2. Chromatograms of 2,4-D and related impurities. (A) Injection valve left in the inject position for the duration of the analysis. (B) Injection valve returned to the load position after 2 s. Column: 15 cm × 250 μm I.D. fused silica packed with Spherisorb ODS, particle diameter (d_p = 5 μm; eluent: acetonitrile–0.05 *M* KH_2PO_4 (30:70); flow: 4.5 μl/min; Injection loop size: 100 nl; detector: ABI 757, longitudinal flow cell of 8 mm path length; wavelength: 214 nm. Peaks: 1 = *o*-Chlorophenoxyacetic acid, 2 = *p*-chlorophenoxyacetic acid, 3 = 2,6-dichlorophenoxyacetic acid, 4 = *p*-chlorophenol, 5 = 2,4-dichlorophenoxyacetic acid, 6 = 2,4,6-trichlorophenoxyacetic acid and 7 = 2,4-dichlorophenol.

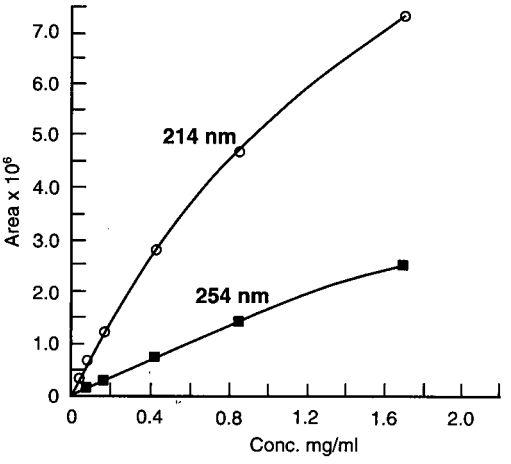

Fig. 3. Plot of response *versus* concentration obtained for 2,4-dichlorophenoxy acetic acid.

was observed in the resulting peak profiles when, during sample introduction, the valve was turned to the inject position and left there for the duration of the analysis, as illustrated in Fig. 2A. Returning the valve to the load position after a few seconds eliminated this problem as illustrated in Fig. 2B.

Detector linearity was evaluated by injection of varying concentrations of 2,4-D at 214 and 254 nm. In both cases deviations from linearity were observed at concentrations above 0.5–0.8 mg/ml (Fig. 3). Initial reproducibility experiments were conducted using a manual injection procedure (manual

TABLE I

REPRODUCIBILITY FOR THE ANALYSIS OF 2,4-DICHLOROPHENOXY ACETIC ACID USING MICROCOLUMN LIQUID CHROMATOGRAPHY (MICRO LC)

Compound	Manual injection (n = 11)			Automated injection (n = 11)		
	$\bar{x}^a$ (%)	T (%)	R.S.D. (%)	$\bar{x}^a$ (%)	T (%)	R.S.D. (%)
o-Chlorophenoxyacetic acid	1.43	0.03	2.0	2.45	0.02	0.73
p-Chlorophenoxyacetic acid	1.04	0.05	4.8	2.78	0.04	1.5
2,6-Dichlorophenoxy acetic acid	1.63	0.10	6.1	2.45	0.02	0.74
p-Chlorophenol	1.36	0.05	3.7	2.55	0.04	1.6
2,4-Dichlorophenoxyacetic acid	92.4	1.11	1.2	86.7	0.33	0.38
2,4,6-Trichlorophenoxyacetic acid	1.27	0.01	3.9	2.48	0.02	0.82
2,4-Dichlorophenol	1.52	0.05	3.3	2.28	0.03	0.40

[a] $\bar{x}$ = Mean value.

valve switching to the load position after injection), however the reproducibility obtained using this approach was considered unacceptable when compared to typical reproducibility values obtained using conventional LC systems (Table I). Automation of the injection process as described in the experimental section yielded much improved results, as illustrated in Table I. The reproducibility values [relative standard deviation (R.S.D.) of 0.38% for the major component] are comparable to results obtained using conventional LC systems.

The long-term system stability was evaluated using a solution containing acetophenone, phenol and methyl benzoate, and the system was automated to inject every 20 min. The Eldex pump was used to continuously circulate the sample solution through the 4-port injection valve. Filtering of the sample stream was considered important to insure that pressure buildup in the column due to particulate material did not occur. The system was operated continuously for eight months, using computer controlled refill of the pump cylinder. The same column was used throughout the study, and injections were performed at a rate of twenty per day during the first three weeks of the study. Thereafter, the injection rate was 3–5 per day for the remainder of the eight-month period. Retention time reproducibility over the eight-month period was 1% without any temperature control of the column or pump. Peak area response (R.S.D.) ranged from 0.7% to 1.2%. No significant pressure increase or column performance deterioration was observed.

Microcolumn LC has been shown to yield quantitative reproducibility which is considered as good as that obtained using conventional size liquid chromatographic systems. Automation of the injection process significantly improved reproducibility results. The stability and reliability observed over an eight-month operating period suggest that microcolumn LC is very suitable for routine applications.

REFERENCES

1 V. McGuffin and M. Novotny, *Anal. Chem.*, 53 (1981) 946.
2 T. Takeuchi and D. Ishii, *J. Chromatogr.*, 238 (1982) 409.
3 F. J. Yang, *J. Chromatogr.*, 236 (1982) 265.
4 J. Gluckman, A. Hirose, V. McGuffin and M. Novotny, *Chromatographia*, 17 (1983) 303.
5 Y. Hirata and K. Jinno, *J. High Resol. Chromatogr.*, 6 (1983) 196.
6 S. Folestad, L. Johnson and B. Josefsson, *Anal. Chem.*, 54 (1982) 925.
7 V. McGuffin and M. Novotny, *Anal. Chem.*, 55 (1983) 2296.
8 H. J. Cortes, in H. J. Cortes (Editor), *Multidimensional Chromatography*, Marcel Dekker, N.Y., 1990, Ch. 7, p. 251.
9 H. J. Cortes, L. S. Green and R. M. Campbell, *Anal. Chem.*, 63 (1991) 2719.
10 H. J. Cortes, E. L. Olberding and J. H. Wetters, *Anal. Chim. Acta*, 236 (1990) 173.
11 H. J. Cortes, C. D. Pfeiffer and B. E. Richter, *US Pat.*, 4 935 145 (1990).
12 T. Takeuchi and D. Ishii, *J. Chromatogr.*, 499 (1990) 549.
13 H. J. Cortes, G. E. Bormett and J. D. Graham, *J. Microcol. Sep.*, 4 (1992) 51.
14 H. J. Cortes, R. M. Campbell, R. P. Himes and C. D. Pfeiffer, *J. Microcol. Sep.*, 4 (1992) 239.
15 M. Novotny, *Anal. Chem.*, 60 (1988) 500A.
16 Y. Hirata, *J. Microcol. Sep.*, 2 (1990) 214.
17 P. Brunmark, M. Darlene, C. Sango, G. Skarping, P. Erlandsson and C. Dewaele, *J. Microcol. Sep.*, 371 (1991) 371.
18 J. P. Chervet, M. Ursem, J. P. Salzmann and R. W. Vannoort, *J. High Resolut. Chromatogr.*, 12 (1989) 278.
19 H. J. Cortes, C. D. Pfeiffer, B. E. Richter and T. S. Stevens, *J. High Resolut. Chromatogr. Chromatogr. Commun.*, 10 (1987) 446.
20 R. P. W. Scott and C. F. Simpson, *J. Chromatogr. Sci.*, 20 (1982) 62.
21 D. Duquet, C. Dewaele, M. Verzele and S. McKinley, *J. High. Resolut. Chromatogr. Chromatogr. Commun.*, 11 (1988) 824.
22 B. L. Ling, W. Baeyens and C. Dewaele, *J. Microcol. Sep.*, 4 (1992) 17.

Journal of Chromatography, 607 (1992) 135–138
Elsevier Science Publishers B.V., Amsterdam

CHROM. 24 343

Short Communication

Simultaneous cation and reversed-phase chromatography

Tetsuo Okada

Faculty of Liberial Arts, Shizuoka University, Shizuoka 422 (Japan)

(First received March 10th, 1992; revised manuscript received April 29th, 1992)

ABSTRACT

Micellar mobile phases facilitate the simultaneous separation of inorganic cations and organic neutral species. With an anionic micellar mobile phase transition metal ions and organic neutral species can be separated, whereas with a non-ionic micellar mobile phase containing a trace anionic surfactant separation of alkali and alkaline earth metal ions can be separated —the elution of alkali or alkaline earth metal ions can be monitored with a conductivity detector, if the trace anionic surfactant incorporated in a mobile phase is used in its acidic form.

INTRODUCTION

A number of advantages of micellar mobile phases over the usual aqueous–organic mobile phases have been pointed out, *e.g.*, non-flammability, non-toxicity, stable baselines and a short reconditioning time for repeated analyses in gradient elution and facilitation of the evaluation of partition coefficients to micellar and stationary phases [1-10]. In addition the easy modelling and prediction of the retention behaviours of ions is an advantage of inorganic micellar chromatography [11], and simultaneous separations of transition metal ions and phenols with anionic micelles have been presented [12].

Although micellar mobile phases facilitate the simultaneous separation of ions and neutral species, there are some problems with detection. With transition metal ions and aromatic organic compounds, selective detection is easy; the former are detectable by applying postcolumn reaction with, *e.g.*, pyridyl azoresorcinol, and the latter by UV absorption. However, it is difficult to detect alkali or alkaline earth metal ions in solutions containing an anionic micelle. To overcome this problem, the use of mixed micellar mobile phases composed of a non-ionic surfactant as a principal component and a trace anionic surfactant has been investigated; the former permits the separation of neutral species and the latter the separation of cations. In this work, simultaneous cation and reversed-phase chromatography using micellar mobile phases was studied and the usefulness of micellar chromatography for such a purpose was reconfirmed.

EXPERIMENTAL

A Tosoh chromatographic system was used, consisting of a CCPD computer-controlled pump, a Rheodyne injection valve, a CO-8000 column oven set at 25°C, a UV-8000 UV detector and a CM-8000 conductivity detector. The separation column was Inertsil ODS (Gaskro Kogyo) of 150 mm × 4 mm

Correspondence to: Dr. T. Okada, Faculty of Liberal Arts, Shizuoka University, Shizuoka 422, Japan.

0021-9673/92/$05.00

I.D., packed with octadecylsilylated silica gel of 5 μm particle size. All solutions were prepared with distilled, deionized water. Anionic surfactants were recrystalized from methanol. Other reagents were of analytical-reagent grade and were used as received.

The amounts of surfactants adsorbed in the column were determined with a breakthrough method.

RESULTS AND DISCUSSION

Simultaneous separation and detection of organic neutral species and transition metal ions

As reported previously [11,12], organic neutral species and transition metal ions can be separated with an anionic micellar mobile phase containing appropriate complexing agents such as tartaric acid. In this instance, transition metal ions are detectable by applying a postcolumn reaction using, *e.g.*, pyridylazo resorcinol; organic neutral species, most of which are detectable by UV spectrometry, do not interfere with the detection of transition metal ions, and *vice versa*. Optimization of the separation is therefore performed in a simple manner [12]. The elution of organic neutral species obeys the usual retention model developed by Armstrong [1,2], and that of transition metal ions can be described by an equation involving complex formation and mass action by a counter cation as shown previously [11]. Fig. 1 shows an example of the simultaneous separation of transition metal ions and some aromatic organic compounds with a sodium dodecyl sulphate (SDS) micellar mobile phase containing tartaric acid.

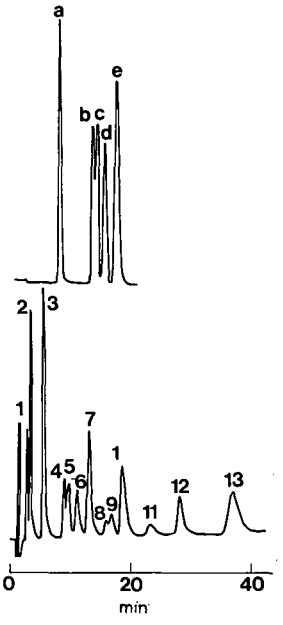

Fig. 1. Simultaneous separation of (top) transition metal ions and (bottom) aromatic neutral species. Mobile phase, 0.1 *M* sodium dodecyl sulphate–0.05 *M* tartaric acid (pH 3.6). Detection, UV at 254 nm for aromatic neutral species and visible at 540 nm for transition metal ions following postcolumn reaction with pyridylazoresorcinol. Peaks: a = Cu^{2+}; b = Zn^{2+}; c = Ni^{2+}; d = Co^{2+}; e = Mn^{2+}; 1 = *p*-hydroxybenzyl alcohol; 2 = resorcinol; 3 = *p*-hydroxybenzaldehyde; 4 = benzyl alcohol; 5 = phenol; 6 = *p*-nitrophenol; 7 = 2-phenylethanol; 8 = *p*-cresol; 9 = acetophenone; 10 = 3-phenyl-1-propanol; 11 = *p*-ethylphenol; 12 = 1-naphthol; 13 = *p*-*tert*-butylphenol.

Simultaneous separation and detection of organic neutral species and alkali and alkaline earth metal ions

The elution of alkali and alkaline earth metal ions cannot be monitored with a postcolumn reaction and another detection method should therefore be considered. Although these ions are usually detected by conductivity in ion chromatography [13,14], conductivity detection has the limitation that the ionic strength of the mobile phase should be low. To separate organic neutral species such as phenols within an acceptable time, 0.05–0.1 *M* surfactant solutions should be used as mobile phases. If the mobile phase contains an ionic surfactant alone, the ionic strength of the solution is too high for conductivity detection to be used for monitoring ions. This problem can be solved as follows.

Non-ionic micellar mobile phases have been successfully used in reversed-phase chromatography, although the poor separation efficiency has been pointed out and its use is not as common as that of ionic micelles [3,4]. Borgerding and Hinze [3] outlined some premises concerning poor separation efficiency when using a non-ionic micellar mobile phase. Non-ionic surfactant molecules adsorbed on the stationary phase cause an increase in the effective film thickness of the stationary phase, produce a more polar stationary phase and disturb the effective mass diffusion of analytes in the stationary phase. In this study, though no enhancement of the separation efficiency was observed, the use of Brij

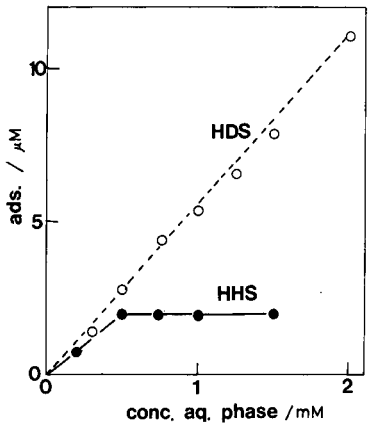

Fig. 2. Adsorption isotherms of HDS and HHS from 0.05 *M* Brij 35 solution to the stationary phase.

35 brought about a significant advantage for the present purpose.

It is obvious that non-ionic micelles do not influence the conductivity detection of ions. Although there remain some questions about the separation performance as stated above, the use of non-ionic micelles containing a trace anionic surfactant permits the conductivity detection of Group 1A and 2A metal ions and the UV detection of neutral species after their simultaneous separation. Fig. 2 shows the adsorption of dodecylsulphuric acid (HDS) and hexadecylsulphuric acid (HHS) in the presence of Brij 35 as a major mobile phase component. The amounts of adsorbed HDS increase linearly with increase in concentration, whereas the adsorption of HHS becomes constant when the concentration reaches *ca.* 0.5 m*M*. An adsorption equilibrium of an ionic surfactant is usually established between the monomeric surfactant and the adsorbed surfactant, and micelles do not participate in the equilibrium. The break point of the adsorption isotherm curve of HHS is therefore due to the formation of the micelle, whereas HDS does not give any break point, suggesting that HDS forms no micelles over this concentration range. Although these anionic surfactants may form mixed micelles with Brij 35, conductivity measurements did not give a clear break point owing to the mixed micelle formation. It is predictable from Fig. 2 that HDS is a better additive than HHS because the low adsorption of HHS causes weak retention and poor resolution.

TABLE I

PARTITION COEFFICIENTS OF ANALYTES BETWEEN WATER AND BRIJ 35 MICELLAR PHASE (K_{MW}) AND BETWEEN WATER AND THE STATIONARY PHASE (K_{SW})

Partition coefficients were determined on the basis of the following equation.

$$1/(V_r - V_0) = [(K_{MW} - 1)\bar{v}_m + 1] / K_{SW} V_s$$

where V_r, V_0 (= 1.56 ml) and V_s (= 1.25 ml) are retention volume, void volume and volume of the stationary phase, $\bar{v}$ is the partial molal volume of the micelle (= 1120 ml/mol for Brij 35 micelles) and C_m is the concentration of micelles.

Analyte	K_{MW}	K_{SW}
Phenol	56.6	46
p-Cresol	145	160
p-Ethylphenol	323	380
p-*tert*-Butylphenol	1100	1850
p-Hydroxybenzaldehyde	52.6	32
Resorcinol	59.2	31
Benzyl alcohol	9.48	6.3
2-Phenylethanol	13.3	10

The non-ionic compounds tested and the partition coefficients are listed in Table I. Partition coefficients between water and Brij 35 micelles were determined on the basis of Armstrong's model. As trace ionic surfactants do not affect the retention of non-ionic compounds, the separation of these neutral species is first optimized using the partition coefficients listed in Table I. The results are shown in Fig. 3, which indicates that 0.043 *M* Brij 35 gives the best resolution. Also, the analysis time, which is determined by the elution of *tert*-butylphenol in this instance, is acceptably short. Therefore, the concentration of Brij 35 was fixed at 0.04 *M* for the following investigation.

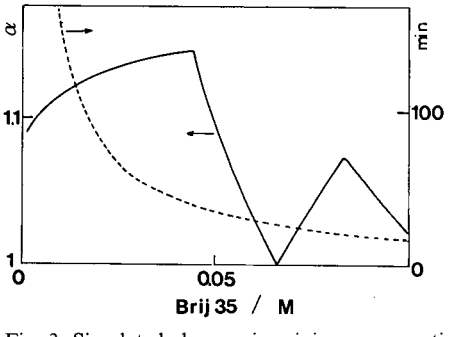

Fig. 3. Simulated changes in minimum separation ratios (solid line) and retention times of *p*-*tert*-butylphenol (broken line) with the concentration of Brij 35.

TABLE II

CHANGES IN RETENTION TIMES OF SELECTED CATIONS WITH THE CONCENTRATION OF HDS IN 0.04 *M* BRIJ 35 MOBILE PHASE

Concentration of HDS (m*M*)	Retention time (min)			
	Na^+	K^+	Mg^{2+}	Ba^{2+}
0.5	2.95	3.15	7.35	10.5
0.75	2.80	3.20	8.25	12.2
1.0	3.0	3.45	8.0	12.0

Table II shows changes in the retention of Na^+, K^+, $Mg2^+$, and Ba^{2+} with the concentration of HDS in 0.04 *M* Brij 35. The retention times are almost constant, and do not vary with the concentration of HDS. This phenomenon can be explained as follows. The capacity factor of a metal ion can be described by

$$k' = \phi\,[M^{n+}]_s/[M^{n+}]$$
$$= \phi\,K_{IE}[H^+]_s^n/[H^{n+}]^n$$

where ϕ is a phase ratio, K_{IE} is the ion-exchange equilibrium constant of $M^{n+} + nH^+(s) \rightleftharpoons M^{n+}(s) + nH^+$ at the stationary phase surface and s denotes the stationary phase. As shown in Fig. 1, the amounts of adsorbed HDS linearly increase with increasing concentration of HDS in the mobile phase, indicating that $[H^+]_s$ is also proportional to the concentration of HDS. $[H^+]$ is also proportional to the concentration of HDS. Therefore, the capacity factor is independent of the concentration of HDS.

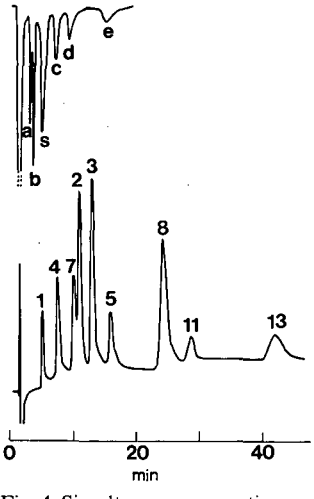

Fig. 4. Simultaneous separation and detection of (top) metal ions and (bottom) aromatic neutral species. Mobile phase, 0.04 *M* Brij 35–0.75 m*M* HDS. Detection, conductivity (10 μS/cm full-scale) for metal ions and UV at 254 nm for organic neutral species. Peaks: a = Na^+; b = K^+; c = Mg^{2+}; d = Ba^{2+}; e = Pb^{2+}; s = system peak; and aromatic compounds as in Fig. 1.

Fig. 4 shows examples of the simultaneous separation of cations and organic neutral species. When HHS was used in Brij 35 mobile phase, the resolution between cations was poorer, as predicted, although the results are not shown. On the other hand, as can be seen in Fig.4, the separation between cations obtained with a Brij 35 mobile phase containing HDS is much better, but still poor in comparison with the usual cation chromatography. Although the poor separation is obviously due to weak adsorption of anionic surfactants in the presence of Brij 35, monovalent cations and divalent cations are simultaneously separated. This is known to be difficult in the usual ion-exchange chromatography.

The present scheme may be applied to the separation and detection of various amines, which are separated with simultaneous partition and ion-exchange modes, and measured by UV and/or conductimetric detection. To accomplish such separations, the low separation efficiency should be overcome by optimizing the mobile phase conditions. This task remains to be studied.

REFERENCES

1 D. W. Armstrong and F. Nome, *Anal. Chem.*, 53 (1981) 1662.
2 D. W. Armstrong, *Sep. Purif. Methods*, 14 (1985) 213.
3 M. F. Borgerding and W. L. Hinze, *Anal. Chem.*, 57 (1985) 2183.
4 M. F. Borgerding, F. H. Quina, W. L. Hinze, J. Bowemaster and H. M. McNair, *Anal. Chem.*, 60 (1988) 2520.
5 M. G. Khaledi, J. K. Strasters, A. H. Rodgers and E. D. Breyer, *Anal. Chem.*, 62 (1990) 130.
6 E. Pramauro, C. Minero, G. Saini, R. Graglia and E. Pelizzetti, *Anal. Chim. Acta*, 212 (1988) 171.
7 F. G. P. Mullins and G. F. Kirkbright, *Analyst (London)*, 109 (1984) 1217.
8 F. G. P. Mullins, *ACS Symp. Ser.*, 342 (1987) 115.
9 L. J. C. Love, J. G. Habata and J. G. Dorsey, *Anal. Chem.*, 56 (1984) 1132A.
10 T. Okada, *J. Chromatogr.*, 538 (1991) 341.
11 T. Okada, *Anal. Chem.*, 64 (1992) 589.
12 T. Okada, *Anal. Sci.*, submitted for publication.
13 J. S. Fritz, D. T. Gjerde and R. M. Becker, *Anal. Chem.*, 52 (1980) 1519.
14 H. Sato, *J. Chromatogr.*, 469 (1989) 339.

Journal of Chromatography, 607 (1992) 139–144
Elsevier Science Publishers B.V., Amsterdam

CHROM. 24 418

Short Communication

Separation of vanadyl and nickel petroporphyrins on an aminopropyl column by high-performance liquid chromatography

Hao Xu and Suzanne Lesage

National Water Research Institute, 867 Lakeshore Boulevard, Burlington L7R 4A6 (Canada)

(First received March 31st, 1992; revised manuscript received June 9th, 1992)

ABSTRACT

The nickel(II) and vanadyl(II) petroporphyrins in fuel oil and crude oil samples are separated by normal-phase high-performance liquid chromatography on an aminopropyl column. Separation mechanisms presented include hydrogen bonding as well as Van der Waals interactions between the petroporphyrin and the amino group on the column surface. The method is simple and efficient for the fingerprinting of petroporphyrins in crude oils and oil products.

INTRODUCTION

Vanadyl [VO(II)] and nickel(II) petroporphyrins (PPs) were identified in fossil fuels as products derived from chlorophyll [1,2]. Since then, they have been used as biomarkers in the study of the origin and the formation of petroleum and as an important parameter for oil exploration [3]. However, the PPs have not been used as extensively as other biomarkers, probably because of the complexity of their chemical structure, the large number of closely similar isomers, and the lack of simple and accurate analytical techniques [3–5].

The interest for the PPs has increased in the last 10 years because the oil refinery industry is dealing with increasingly heavier crude oils. Vanadium and nickel are the most abundant metals found in crude oils [1–4], often in the form of petroporphyrins or other organic chelates. These metals can block the activity of the catalyst in the hydrogenation process by precipitation as metal sulphides [6,7]. Therefore, metal speciation in crude oils is important for the selection of refining methods and for the assessment of the quality of crude oils. In environmental studies, PPs are potentially useful as biomarkers for determining the origin of spills.

The PPs are a group of macrocyclic aromatic compounds consisting of a porphin ring, to which a metal ion is bound. There are eight alkyl substituents on the porphin ring (Fig. 1). The most abundant series found in crude oils are etioporphyrins (ETIOs) and deoxophylloerythroetioporphyrins (DPEPs) with the total carbon number from 29 to 39 [8]. Differences of the alkyl substituents and their steric structure lead to a large number of homologues and isomers which are characteristic of each

Correspondence to: Dr. H. Xu, National Research Institute, 867 Lakeshore Boulevard, Burlington L7R 4A6, Canada.

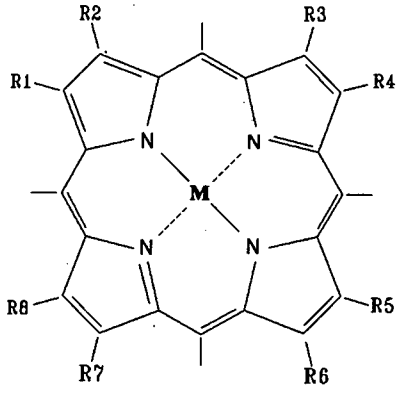

Fig. 1. Generalized chemical structure of petroporphyrins (R stands for an alkyl group with 1 to 8 carbon numbers). ETIO-I: $R_{1,3,5,7}$ = CH_3, $R_{2,4,6,8}$ = C_2H_5; ETIO-III: $R_{1,3,5,8}$ = CH_3, $R_{2,4,6,7}$ = C_2H_5; octaethylporphyrin: R_{1-8} = C_2H_5; DPEPs: the porphyrins bearing an isocyclic ring [8].

petroleum deposit. Thus, PPs are ideal as fingerprint chemicals.

Techniques for the analysis of PPs can be divided into two categories: indirect (after removal of the chelated metal) and direct. Amongst the indirect analytical techniques, the most efficient separation reported is by normal-phase high-performance liquid chromatography (HPLC). The analytical procedures involve isolation of the PPs by liquid chromatography, demetallation by acid, and finally separation of the demetallated porphyrins by HPLC [9–13]. This analytical procedure is time consuming and, moreover, the demetallation reaction may degrade the alkyl substituents on the porphin ring. However, the most significant drawback, is that the indirect analytical techniques cannot provide information on the original forms of metal chelates. Therefore, recent studies have focused on the development of direct analytical techniques. Several researchers have used size-exclusion chromatography (SEC) to separate the PPs [6,7], but the separation is limited by the poor resolution of the SEC. By using reversed-phase octadecylsilane columns or normal-phase silica columns, separation of the standard mixtures [Ni(II) and VO(II) octaethylporphyrins] has been achieved [14–16]. In oil samples, however, only VO(II)petroporphyrins could be sep-

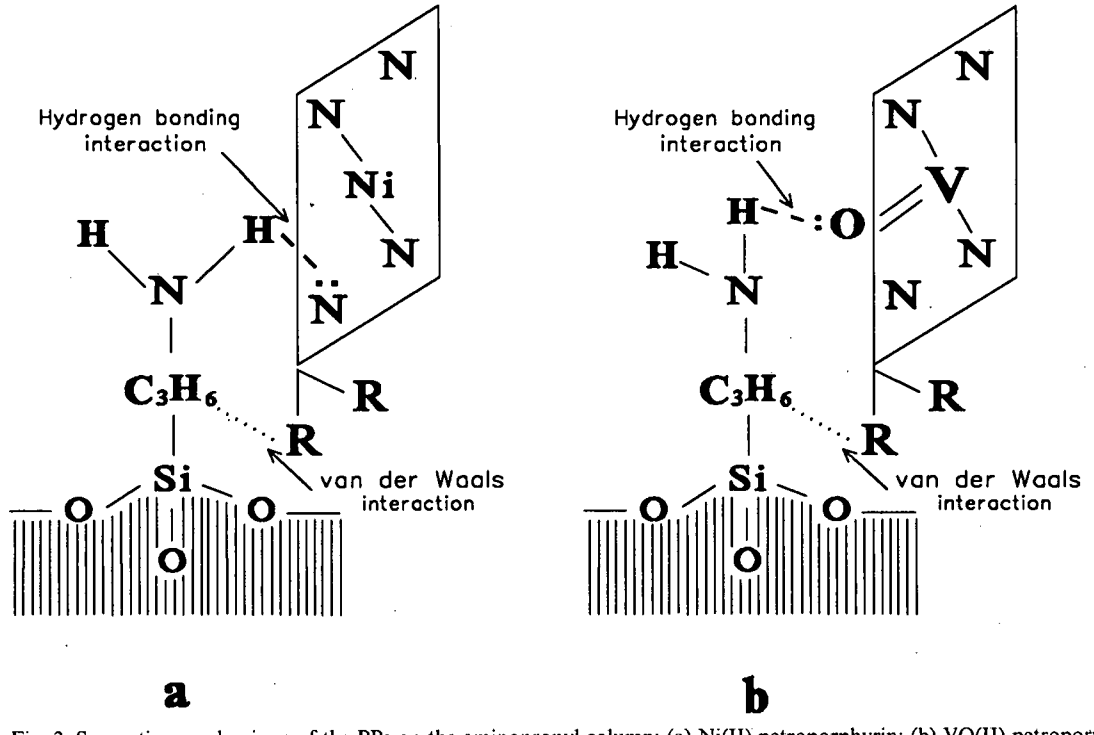

Fig. 2. Separation mechanisms of the PPs on the aminopropyl column: (a) Ni(II) petroporphyrin; (b) VO(II) petroporphyrin.

arated [15,16]. The resolution for Ni(II) petroporphyrins was very poor [16].

In the present study, separation of PPs was conducted by normal-phase HPLC because PPs are poorly soluble in methanol and acetonitrile. In contrast to the previous methods using silica columns, an aminopropyl column was chosen in this study in order to improve the selectivity for the PPs. Separation of the petroporphyrin homologues and isomers on the amino column is based on the differences in the adsorption energy of each. As shown in Fig. 2, two types of interactions between the porphyrin and the stationary phase may occur. The first is hydrogen bonding between the free electron pair from the nitrogen [in the case of Ni(II) petroporphyrins, Fig. 2a] or from the oxygen [VO(II) petroporphyrins, Fig. 2b] and the hydrogen of the amino group. The other is Van der Waals interaction between the alkyl substituents of the porphyrin and the propyl group on the stationary phase. Unger *et al.* [17] found a slight reversed-phase effect of diol bonded phase due to the influence of hydrophobic interactions between the long alkyl group of the diol bonded phase and solutes. The selectivity of the diol bonded phase as well as amino bonded phase was also improved for both acidic and basic compounds. Thus, chemical or steric differences in the alkyl substituents will lead to differences in adsorption energy by both hydrogen bonding and Van der Waals forces. Therefore, the homologues and isomers can be separated better on an aminopropyl column than on a silica column where only hydrogen bonding prevails.

This paper presents an improved method for the separation of the PPs directly on the aminopropyl column by HPLC. The method is applied to fuel oil and crude oil samples and fingerprints of these samples are compared.

EXPERIMENTAL

HPLC system and conditions

The HPLC system consists of a quaternary solvent delivery pump (600E; Waters, Milford, MA, USA), a Waters autoinjector (WISP 700), an UV–VIS detector (SP8440; Spectra-Physics), a fluorescence detector (470; Waters) and a computer work station. The UV–VIS detector was set at 400 nm for the analysis of metal porphyrin standards and at

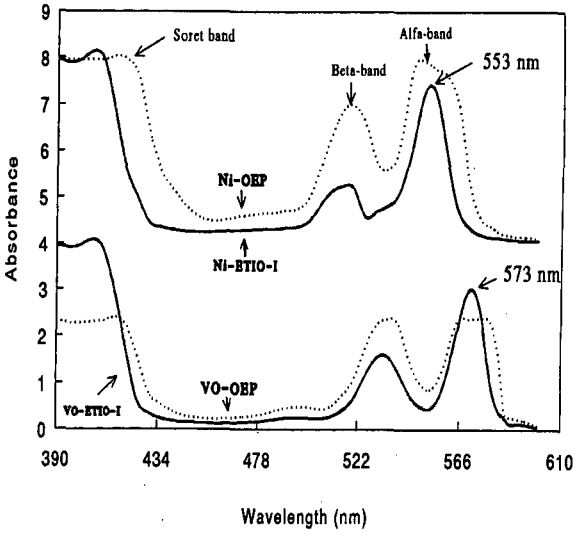

Fig. 3. Adsorption spectra of Ni-OEP, Ni-ETIO-I, VO-OEP and VO-ETIO-I in toluene.

400, 553 and 573 nm for the analysis of the oil samples. The wavelength of 553 nm and 573 nm was considered as an α-band for Ni(II) and VO(II) petroporphyrins, respectively (Fig. 3). The fluorescence detector was set at 400 nm for the excitation and at 620 nm for the emission to detect free base porphyrins in the oil samples.

A μBondapak-NH_2 column (300 × 3.9 mm) obtained from Waters was employed. The μBondapak-NH_2 column contained aminopropyl groups chemically bonded to irregular-shaped 10 μm porous silica.

Hexane, toluene and dichloromethane (DCM) were employed as mobile solvents. A mixture of hexane and toluene in the ratio of 55:45 was established in a linear gradient across the column and maintained for 10 min. This mixture was then modified to 30:20:50 of hexane, toluene and DCM respectively over a period of 15 min, maintained at this ratio for 20 min, and returned to the initial condition over a period of 5 min.

Preparation of standards

The standards employed included VO(II)-etioporphyrin-I (VO-ETIO-I) and Ni(II)-etioporphyrin-I (Ni-ETIO-I) (Midcentury Chemicals, Posen, USA), VO(II)-octaethylporphyrin (VO-OEP) and Ni(II)-octaethylporphyrin (Ni-OEP) (Porphyrin

Products, Logan, UT, USA). All standards were dissolved in toluene except for VO-ETIO-I, which was dissolved in DCM and then diluted with toluene. Absorption spectra of the standards were measured by a spectrophotometer (UV-260, Shimadzu) and shown on Fig. 3.

Preparation of sample

One fuel oil sample and four crude oil samples were analyzed. They included Bunker C oil from Venezuela, Alberta sweet mixed blend crude oil from western Canada, Atkinson crude oil from the Canadian North West Territories, Terra Nova crude oil and Avalon crude oil from off-shore exploration in the northern Atlantic. The samples (about 4 g) were extracted with 5 ml of pyridine–water–toluene (4:1:1) for four consecutive repetitions. The extract was then dried by evaporation, the residue dissolved in toluene (2 ml) and stored in the dark.

RESULTS AND DISCUSSION

The separation of Ni-OEP, Ni-ETIO-I, VO-OEP and VO-ETIO-I standards on the aminopropyl column by HPLC is shown on Fig. 4. The four standards were well separated with the retention time at 5.70, 7.17, 21.78 and 22.93 min for Ni-OEP, Ni-ETIO-I, VO-OEP and VO-ETIO-I, respectively.

The PPs in the Bunker C fuel oil sample from Venezuela were also well separated. The chromatograms of the fuel oil sample on the UV–VIS detector at the wavelength of 400, 553 and 573 nm, respectively, are shown on Fig. 5. Three Ni(II) petroporphyrin and four VO(II) petroporphyrin peaks were detected at the retention time from 8 to 11 and 23 to 27 min. There are no commercially available standards for many of these compounds.

The separations of VO(II) petroporphyrins in the four crude oil samples are shown on Fig. 6. Peaks at the retention time between 9 to 12 min are not attributable to Ni(II) petroporphyrins because of their lack of absorbance at 553 nm, a specific adsorption wavelength for Ni(II) porphyrins (Fig. 3). This indicates that the content of Ni(II) porphyrins is much less than VO(II) porphyrins in these Canadian crude oils.

In the first 7 min, there were also large unresolved peaks detected by both UV–VIS and fluorescence detectors in all samples. These peaks are probably due to the presence of carotenoids or flavonoids [18]. After 7 min there were porphyrin peaks detected by the UV–VIS detector but not by the fluorescence detector. Because free base porphyrins are fluorescent while metallated porphyrins are not, this result implies that the mature oils contain mainly the metallated porphyrins.

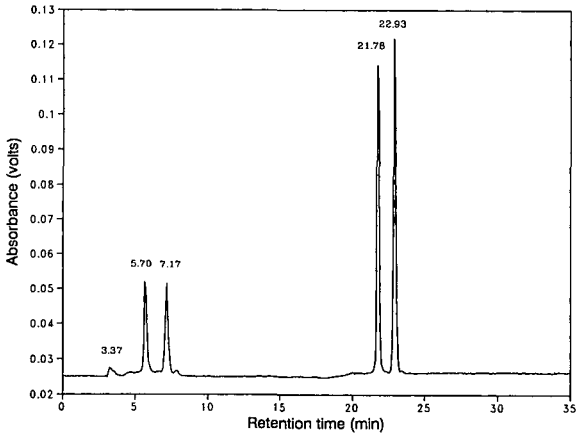

Fig. 4. HPLC chromatogram of Ni-OEP, Ni-ETIO-I, VO-OEP and VO-ETIO-I standards (134 ng each) on the aminopropyl column under normal-phase conditions (injection volume: 10 μl; flow-rate: 1.0 ml/min; UV–VIS detector: 400 nm).

It is interesting to note that the four crude oils show three types of PPs fingerprints based on their geographic locations. The Alberta crude oil from

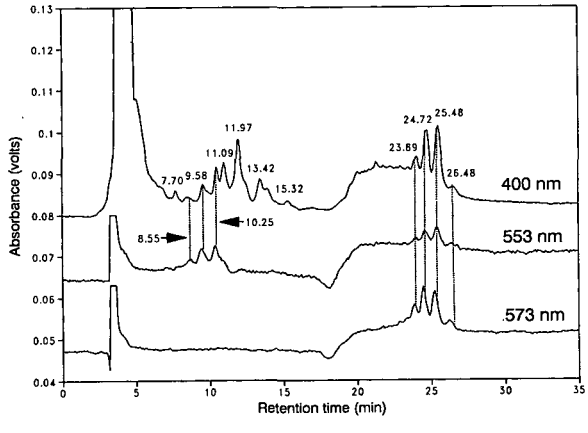

Fig. 5. HPLC chromatograms of Ni and VO petroporphyrins in Bunker C oil (Venezuela) on the UV–VIS detector [injection volume: 10 μl (2.8 mg fuel oil) at 400 nm and 50 μl (14 mg fuel oil) at 553 and 573 nm; other conditions as in Fig. 4].

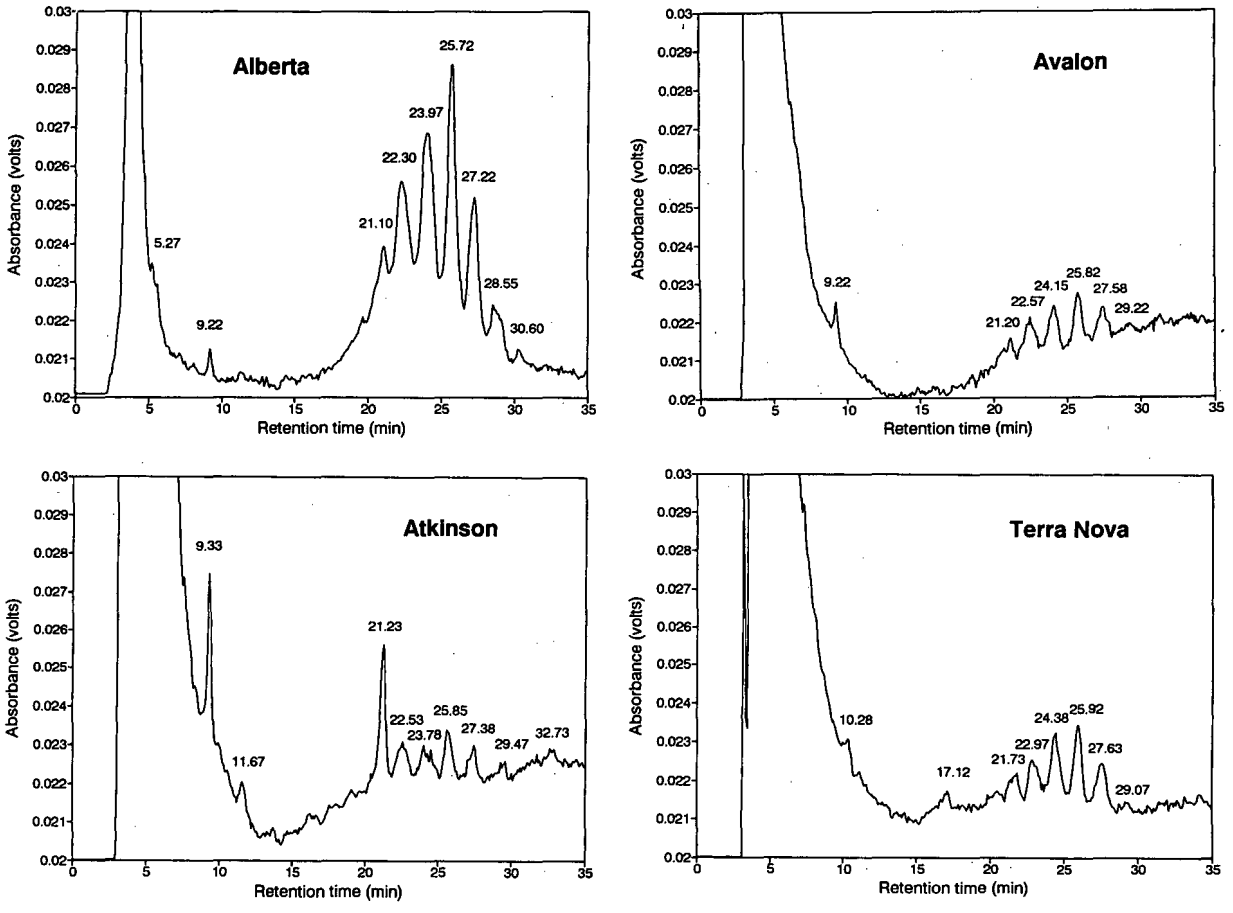

Fig. 6. HPLC chromatograms of VO petroporphyrins in the crude oil samples on the UV–VIS detector (400 nm) (injection volume: 20 μl, which is equal to 81, 153, 237 and 230 mg Alberta, Atkinson, Avalon and Terra Nova crude oils, respectively; other conditions as in Fig. 4).

western Canada contains seven peaks of PPs with a dominant peak at 25.72 min and the Atkinson crude oil from the Northwest Territories contains seven peaks with a dominant peak at 21.23 min. The Avalon and Terra Nova crude oils, offshore oils from the Canadian east coast, have a similar type of PPs fingerprints. The content of PPs decreases in the order of Alberta > Atkinson > Avalon ≈ Terra Nova.

The resolution of both VO(II) and Ni(II) petroporrphyrins in the present study is much better than that observed in previous studies using either silica columns or octadecylsilane columns [15,16]. This is expected because as discussed in the introduction, the aminopropyl column provides better selectivity for the PP isomers which often only differ in a few alkyl substituents.

CONCLUSION

The PPs can be directly separated on an aminopropyl column by HPLC. The possible mechanisms involved are interactions due to hydrogen bonding and the Van der Waals forces between the PPs and the aminopropyl group.

This method is valuable for fingerprinting PPs in crude oils and fuel oils, which is useful in oil exploration, assessment of oil quality for refining, and in environmental impact studies. The method is more straightforward and efficient than the previously published methods.

ACKNOWLEDGEMENTS

This study was financially supported by Environment Canada. We are also indebted to Ms. Karen Sims of the Waste Technology Centre and to Dr. Rick Bourbonniere at the National Water Research Institute of Canada for the gift of the crude oil and fuel oil samples.

REFERENCES

1 A. Treibs, *Ann. Chem.*, 510 (1934) 42.
2 A. Treibs, *Angew. Chem.*, 49 (1936) 682.
3 E. W. Baker, in A. A. Prashnowsky (Editor), *The Impact of the Treibs' Porphyrin Concept on the Modern Organic Geochemistry, International Alfred-Treibs-Symposium, Munich, 1979*, Halbig Druck, Würzburg, 1980, p. 1.
4 R. H. Filby and G. J. Van Berkel, in R. H. Filby and J. F. Branthaver (Editors), *Metal Complexes in Fossil Fuels*, American Chemical Society, Washington, DC, 1987, p. 2.
5 M. I. Chicarelli and J. R. Maxwell, *Trends Anal. Chem.*, 6 (1987) 158.
6 A. Gratzfeld-Hüsgen, *LC · GC*, 7 (1990) 836.
7 W. A. L. De Waal, C. C. H. M. Kuiper, F. J. M. J. Maessen, J. C. Kraak, R. Wijnands and F. J. Jonker, *J. Chromatogr.*, 462 (1989) 115.
8 J. M. E. Quirke, L. L. Cuesta, R. A. Yost, J. Johnson and E. D. Britton, *Org. Geochem.*, 14 (1989) 43.
9 S. K. Hajibrahim, P. J. C. Tibbetts, C. D. Watts, J. R. Maxwell and G. Eglingon, *Anal. Chem.*, 50 (1978) 549.
10 S. K. Hajibrahim, *J. Liq. Chromatogr.*, 4 (1981) 749.
11 A. J. G. Barwise, R. P. Evershed, G. A. Wolff, G. Eglinton and J. R. Maxwell, *J. Chromatogr.*, 368 (1986) 1.
12 M. I. Chicarelli, G. A. Wolff and J. R. Maxwell, *J. Chromatogr.*, 368 (1986) 11.
13 S. Kaur, J. P. Gill, R. P. Evershed, G. Eglinton and J. R. Maxwell, *J. Chromatogr.*, 473 (p1989) 135.
14 J. S. Flynn and D. H. Freeman, *J. Chromatogr.*, 386 (1987) 111.
15 Z. Aizenshtat and P. Sundararaman, *Geochim. Cosmochim. Acta*, 53 (1989) 3185.
16 W. A. J. De Waal, S. Heemstra, J. C. Kraak and R. J. Jonker, *Chromatographia*, 30 (1990) 38.
17 K. K. Unger, N. Becker and P. Roumeliotis, *J. Chromatogr.*, 125 (1976) 115.
18 J. W. Louda and E. W. Baker, in M. L. Sohn (Editor), *Organic Marine Geochemistry*, American Chemical Society, Washington DC, 1986, p.107.

Journal of Chromatography, 607 (1992) 145–149
Elsevier Science Publishers B.V., Amsterdam

CHROM. 24 369

Short Communication

Measurement of infinite dilution diffusion coefficients of ε-caprolactam in nylon 6 at elevated temperatures by inverse gas chromatography

Luisa Bonifaci and Gian Paolo Ravanetti

Enichem Polimeri, Mantua Research Centre, Via G. Taliercio 14, 46100 Mantua (Italy)

(First received March 16th, 1992; revised manuscript received May 25th, 1992)

ABSTRACT

The diffusion coefficients of ε-caprolactam in nylon 6 were measured by inverse gas chromatography on a capillary column at temperatures between 250 and 280°C. The values obtained ranged between $2 \cdot 10^{-8}$ and $4 \cdot 10^{-8}$, in good agreement with the reported values obtained by a static technique. The activity coefficients at infinite dilution of ε-caprolactam in nylon 6 were also determined and compared with values obtained previously using packed columns. The two data sets differed by less than 7%.

INTRODUCTION

The knowledge of diffusion and activity coefficients of small molecules in melt polymers is useful in order to analyse fundamental processing steps, such as devolatilization, bulk polymerization and plasticization of polymers.

Inverse gas chromatography (GC) has been recognized [1,2] as a useful tool for the determination of the infinite dilution activity coefficient (Ω^{∞}) of a solvent in a polymer. This technique is simpler, more economical and less time consuming than the static method, and requires only small amounts of polymer and solvent.

Inverse GC has also been proposed [3–6] for studying the diffusion of a solute within a polymer. Owing to the slow diffusion of the sample in the stationary phase, the chromatographic peak turns out broadened and distorted. Under suitable experimental conditions, the shape of the elution curve can be related to the diffusion coefficient of the probe at infinite dilution in the polymer (D_p).

Most of these studies have been performed using packed columns. However, there is considerable uncertainty about the accuracy of diffusion data obtained by inverse GC, owing to the difficulty in describing correctly the stationary phase geometry in the column [7]. According to Pawlisch *et al.* [8], this difficulty can be overcome by using capillary columns with a uniform distribution of polymeric stationary phase on the wall of the tube. This technique allows the simultaneous determination of the diffusion and activity coefficients.

In a previous work [9] we studied the thermodynamic properties of nylon 6–solvent systems by inverse GC on packed column and we determined

Correspondence to: Dr. L. Bonifaci, Enichem Polimeri, Mantua Research Centre, Via G. Taliercio 14, 46100 Mantua, Italy.

0021-9673/92/$05.00

the infinite dilution activity coefficient of ε-caprolactam (CPL) and the specific retention volume of its cyclic dimer in nylon 6 at temperatures ranging from 250 to 290°C.

The main purpose of this work was to determine the diffusion coefficients of ε-caprolactam at infinite dilution in nylon 6 at elevated temperatures using inverse GC on a capillary column, according to Pawlisch *et al.*'s method [8]. Moreover, we aimed to compare the chromatographic data and the activity coefficients obtained using capillary columns with those obtained with packed columns.

Very few experimental data of the activity and diffusion coefficients for nylon 6 systems are available. Newman and Prausnitz [10] measured Ω^{∞} for some solvents but at temperatures well below those considered here and using a stationary phase with very different characteristics. Nagasubramanian and Reimschuessel [11] measured the diffusion of CPL in melted nylon 6 using a non-chromatographic method.

EXPERIMENTAL

Equipment

The analyses were performed using a Carlo Erba HRGC Mega series gas chromatograph, equipped with a flame ionization detector and a split-splitless injector. The splitting ratio was 100:3.

Helium was used as the carrier gas and the flow-rates were measured by a soap-bubble flow meter at the column outlet. They ranged from 0.3 to 1 ml/min for CPL and from 1.1 to 2 ml/min for the cyclic dimer. The influence of the flow-rate was examined, performing tests at three different flow-rates at each temperature.

The samples were dissolved in ethanol and injected using a 1-μl Hamilton syringe. Three consecutive injections were made for each set of measurements.

For data acquisition, the Baseline program (Millipore) was used for monitoring the detector output. The raw data were corrected for the baseline offset and then the mean retention time (μ_1), the second central moment (μ_2^*) and the area of the elution peak were calculated by numerical integration.

The whole system was tested by performing experiments on several capillary columns coated with polystyrene in order to obtain data corresponding to those obtained by Pawlisch *et al.* [8].

Materials

Nylon 6 (Nivionplast) and CPL were supplied by Enichem (Porto Marghera, Italy). The number-average molecular weight and the melting point of the polymer were 18 000 and 220°C, respectively.

An oligomers mixture was obtained by extraction of nylon 6 with water. In order to obtain a standard sample of dimer, fractional sublimation according to Heikens [12] was carried out. The chosen dimer fraction had a purity of 96.7%, as measured by high-performance liquid chromatography [13].

Glass capillary tubing was supplied by Carlo Erba (Milan Italy) with I.D. = 0.32 and O.D. = 1 mm.

Column preparation

The column was prepared using an 8-m long glass capillary tube. The nylon 6 film was applied on the wall by a static coating technique that allows deposition of films with uniform and known thickness [14].

The polymer solution in 2,2,2-trifluoethanol (Janssen) was forced into the tube using a nitrogen back-pressure and the filled column was then sealed at one end with a silicone-rubber–glass plug. This was a critical step of the experimental procedure as it is crucial that no air bubbles are trapped in the column, especially at the sealed end.

The tube was then placed in a water-bath and connected to vacuum via the open end until the complete evaporation of the solvent was obtained (about 48 h). The column was conditioned in the chromatographic oven, raising the temperature at 0.5°C/min until a satisfactory baseline was obtained.

The final coating film on the wall was uniform and even. Its thickness (2.037 μm at 250°C) was evaluated from the concentration of the coating solution [14]:

$$\tau = \frac{Rc}{2\rho_p} \quad (1)$$

where τ = film thickness (μm), R = column inner radius (mm), c = coating solution concentration (g/l) and ρ_p = polymer density (g/ml)

Data analysis

Inverse gas chromatography on capillary columns was proposed by Pawlisch *et al.* [8] in order to obtain simultaneously infinite dilution activity and diffusion coefficients of a sample in a polymer. A solvent injected into a capillary column arrives at the

detector after a time (or with a retention volume) that depends on the interaction between the solvent and the polymer, and therefore on the activity coefficient Ω^{∞}. If experimental parameters are properly selected, the shape and the broadening of the elution peak depend on the diffusion coefficient of the probe in the stationary phase.

The model used by Pawlisch *et al.*, in order to relate chromatographic data with thermodynamic and transport properties, was described in detail elsewhere in the original paper [8]; here we examine only its fundamental equations for the determination of Ω^{∞} from the first statistical moment, μ_1 (mean retention time), and D_p from the second statistical moment, μ_2^*, of the elution curve.

The mean retention time, μ_1, is related to the partition coefficient, K, by the equation

$$\mu_1 = \frac{\sum t_i A_i}{\sum A_i} = \frac{1 + 2\tau K}{R} \cdot t_c \qquad (2)$$

[where A_i = slice area of the peak at the time t_i, t_c = residence time of the gas carrier = L/V, where L is the column length and V the mean carrier gas velocity, and K = partition coefficient. The knowledge of the partition coefficient allows the evaluation of thermodynamic parameters, such as Henry constant, Flory–Huggins interaction parameter and activity coefficient at infinite dilution in a polymer.

It is common practice to express the chromatographic results as a function of specific retention volume (V_g^0) rather than partition coefficient:

$$V_g^0 = \frac{273.2K}{T\rho_p} \qquad (3)$$

where T is the column temperature.

The relationship which correlates the specific retention volume with the activity coefficient is

$$\ln \Omega^{\infty} = \ln\left(\frac{273.2R_g}{p_1^0 V_g^0 M_1}\right) - \frac{p_1^0(B_{11} - V_1)}{R_g T} \qquad (4)$$

where R_g is the universal gas constant, M_1 the molecular weight, p_1^0 the vapour pressure, B_{11} the second virial coefficient and V_1 the molar volume, all referring to the sample.

The shape and broadening, and therefore the second central moment of the elution curve (variance of the concentration distribution), can be related to the diffusion coefficient of the probe in the polymeric phase:

$$\mu_2^* = \frac{\sum(t_i - \mu_1)^2 A_i}{\sum A_i} =$$

$$\left[\frac{4\tau^3 K}{3Rt_c D_p} + \frac{2D_g t_c}{L^2} \cdot \left(1 + 2\tau \cdot \frac{K}{R}\right)^2\right] t_c^2 \qquad (5)$$

where L = column length and D_g = diffusion coefficient of the sample in the gas phase.

For polymeric stationary phases, the diffusion coefficient in the stationary phase (D_p) can be 8–10 orders of magnitude smaller than D_g. In this case the term containing D_g in eqn. 5 is negligible and it is possible to calculate D_p by a single elution curve [15]. Otherwise, D_p can be obtained from the slope of the straight line obtained plotting μ_2^*/t_c^3 *versus* $1/t_c^2$, carrying out several tests at different flow-rates.

RESULTS AND DISCUSSION

The peculiarities of the nylon 6–CPL system have been underlined in our previous study, carried out using packed columns. Nylon 6 degrades [16] at elevated temperatures, and the resulting weight loss produces unreliable values of the retention volume. Therefore, tests at elevated temperatures should be performed as quickly as possible, and at the end of experiments the weight of the stationary phase in the column should be checked.

In the particular case of a capillary column it should be taken into account that the coated film can deteriorate at high temperatures. On the other hand, the chromatographic tests have to be performed at least 30°C above the melting temperature, in order to avoid the presence of a crystalline fraction in the stationary phase.

In this study, optimum experimental conditions (in particular the flow-rate for dimer elution) were rapidly found with the aid of partition coefficient values previously measured by means of packed columns. In fact, if partition coefficient is known the elution time can be predicted at a particular flow-rate.

Table I shows the values of the diffusion coefficient obtained at temperatures from 250 to 280°C (average values calculated from measurements at three different flow-rates).

According to the theory [17], the diffusion coefficient increases with increase in temperature, but the

TABLE I

DIFFUSION COEFFICIENT OF ε-CAPROLACTAM IN NYLON 6 AT VARIOUS TEMPERATURES

Temperature (°C)	D_p (cm^2/s)	Standard deviation (cm^2/s)
250	$2.5 \cdot 10^{-8}$	$6.9 \cdot 10^{-9}$
260	$1.7 \cdot 10^{-8}$	$4.2 \cdot 10^{-9}$
270	$3.3 \cdot 10^{-8}$	$1.5 \cdot 10^{-8}$
280	$3.8 \cdot 10^{-8}$	$9.1 \cdot 10^{-9}$

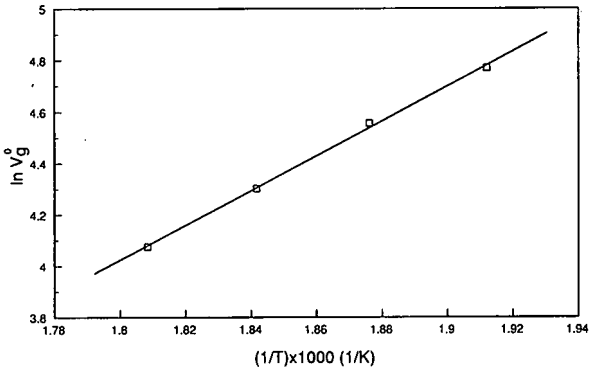

Fig. 1. Retention plot for ε-caprolactam in nylon 6.

rate of increase is smooth, because the temperatures of measurement are well above the T_g of the polymer (40°C [18]). The data obtained appear to be reliable within the experimental errors (30%).

To our knowledge, only one study concerning the diffusion of CPL in nylon 6 has been published [11]. There, D_p was measured at 265°C without using a chromatographic method, and the reported average value was $8 \cdot 10^{-8}$ cm^2/sec, with limiting values of $1 \cdot 10^{-8}$ and $15 \cdot 10^{-8}$ cm^2/sec, therefore in good agreement with out data.

Table II shows the specific retention data; as expected, V_g^0 varies with temperature. The data were plotted on a retention diagram (*i.e.*, ln V_g^0 *versus* 1 T). It is known that such plots are linear, except in the proximity of a phase transition of the polymer, where a discontinuity can exist owing to a change in the retention mechanism. In this study, a linear plot was obtained (Fig. 1), indicating that the retention volume was determined by bulk retention over the whole range of experimental temperatures.

A comparison between the values of V_g^0 and Ω^∞ obtained on packed and capillary columns is also shown in Table II. Except for those obtained at 250°C, the values differ by less than 5%. By common opinion an acceptable error in the IGC technique is between 2 and 5% [19], so the two sets of data can be considered to be consistent. The agreement suggest also that the stationary phase of the capillary column has not undergone a significant weight loss.

Finally, by using the data obtained at temperatures ranging from 260 to 280°C (Table II), the thermodynamic parameters of the system were calculated [20], as summarized in Table III, which also gives the thermodynamic data for CPL.

TABLE II

SPECIFIC RETENTION VOLUMES AND WEIGHT FRACTION ACTIVITY COEFFICIENTS AT INFINITE DILUTION OF ε-CAPROLACTAM AND DIMER IN NYLON 6 AT VARIOUS TEMPERATURES MEASURED ON PACKED AND CAPILLARY COLUMNS

Temperature (°C)	ε-Caprolactam					
	V_g^0 (ml/g)		Ω^∞		Dimer: V_g^0 (ml/g)	
	Packed column	Capillary column	Packed column	Capillary column	Packed column	Capillary column
250	127.1	117.84	2.68	2.89		
260	98.6	95.21	2.76	2.86		
270	77.5	73.86	2.84	2.98		
280	61.3	58.91	2.94	3.06	4571	4555

TABLE III

PARTIAL MOLAR HEATS OF MIXING AND HEATS OF SOLUTION OF CPL IN NYLON 6 AND HEATS OF VAPORIZATION AND SOLUBILITY PARAMETER AT 270°C OF CPL

Parameter	Packed column	Capillary column
$\Delta\bar{H}_1^{\infty} = R \cdot \frac{\partial \ln \Omega^{\infty}}{\partial(1/T)}$ (kcal/mol)	−2.00 ± 0.2	−1.76 ± 0.07
$\Delta H_s = -R \cdot \frac{\partial \ln V_g^0}{\partial(1/T)}$ (kcal/mol)	−13.36 ± 0.35	−13.96 ± 0.03
$\Delta H_v = \Delta\bar{H}_1^{\infty} - \Delta H_s$ (kcal/mol)	11.36 ± 0.55	12.2 ± 0.1
$\delta_{270} = \left(\frac{\Delta H_v - RT}{V_1}\right)^{\frac{1}{2}}$ $(cal/cm^2)^{\frac{1}{2}}$	8.7 ± 0.2	9.02 ± 0.04

REFERENCES

1 J. R. Laub and L. R. Pecsok, *Physicochemical Applications of Gas Chromatography*, Wiley, New York, 1978.
2 J. M. Braun and J. E. Guillet, *Adv. Polym. Sci.*, 21 (1976) 107.
3 D. G. Gray and J. E. Guillet, *Macromolecules*, 6 (1973) 223.
4 J. M. Braun, S. Poos and J. E. Guillet, *Polym. Lett.*, 14 (1976) 257.
5 M. Oner and S. Dincer, *Polymer*, 28 (1987) 279.
6 J. Miltz, *Polymer*, 27 (1986) 105.
7 S. T. Hu, C. D. Han and L. I. Stiel, *J. Appl. Polym. Sci.*, 33 (1987) 551.
8 A. C. Pawlisch, A. Macris and L. R. Lawrence, *Macromolecules*, 20 (1987) 1564.
9 L. Bonifaci, G. Cavalca, D. Frezzotti, E. Malaguti and G. P. Ravanetti, *Polymer*, in press.
10 J. D. Newman and J. M. Prausnitz, *J. Paint Technol.*, 45 (1973) 33.
11 K. Nagasubramanian and H. K. Reimschuessel, *J. Appl. Polym. Sci.*, 17 (1973) 1663.
12 D. Heikens, *Recl. Trav. Chim. Pays-Bas*, 75 (1956) 1199.
13 L. Bonifaci, G. Cavalca, D. Frezzotti, E. Malaguti and G. P. Ravanetti, *J. Chromatogr.*, 585 (1991) 333.
14 W. Jennings, *Gas Chromatography with Glass Capillary Columns*, Academic Press, New York, 2nd ed., 1980.
15 C. A. Pawlisch, *Ph.D. Dissertation*, University of Massachusetts, Amherst, MA, 1985.
16 A. A. Hanna, *Thermochim. Acta*, 76 (1984) 97.
17 J. L. Duda, J. S. Vrentas and H. T. Liu, *AIChE J.*, 28 (1982) 279.
18 P. Engler and S. H. Carr, *Polym. Eng. Sci.*, 18 (1978) 450.
19 I. Kikic, P. Alessi and M. Fermeglia, *Fluid Phase Equilib.*, 14 (1983) 363.
20 G. Di Paola-Baranyi and J. E. Guillet, *Macromolecules*, 11 (1978) 228.

Journal of Chromatography, 607 (1992) 150–153
Elsevier Science Publishers B.V., Amsterdam

CHROM. 24 368

Short Communication

Determination of phenolics from propolis by capillary gas chromatography

V. Bankova, R. Christov, G. Stoev and S. Popov

Institute of Organic Chemistry with Centre of Phytochemistry, Bulgarian Academy of Sciences, 1113 Sofia (Bulgaria)

(First received December 10th, 1991; revised manuscript received April 28th, 1992)

ABSTRACT

A procedure using capillary gas chromatography with an internal standard has been developed for the determination of the main biologically active phenolics of propolis (bee glue): the flavonoid aglycones pinocembrin and galangin, and caffeic acid and its β-phenylethyl ester.

INTRODUCTION

Phenolics are widespread components of all parts of higher plants and are used in medicine, the food industry, chemosystematics, etc. [1,2]. In plants they are found as complex mixtures, containing numerous representatives of different structural groups. Paper, column and thin-layer chromatography (TLC) and spectrophotometric methods have been used for separation and identification of phenolic compounds, but these methods are time consuming or limited in separation power [3]. High performance liquid chromatography (HPLC) gives better results [4,5], but the best separation has been achieved by capillary gas chromatography (cGC). Recent investigations showed the potential of cGC for the qualitative analysis of phenolic mixtures [3,6]. Some problems are created by flavonoids, which are liable to break down under the conditions used [5] and they produce smaller signals per unit mass then other phenolics [6]. This is the reason why so far cGC has not been applied to the determination of flavonoids.

In order to develop a method for the standardization of propolis (bee glue) we had to solve this problem. Propolis is a resinous hive product, collected by bees, and known to possess valuable biological activity [7]. It is widely used in folk medicine and has recently found application in clinics [7]. It is very promising for application in drugs and cosmetics but there is a problem with its standardization [8]. Propolis is a very complex mixture, containing more than 160 components [9], mainly phenolics, their relative concentrations depending on the origin of the sample. Most of these phenolics belong to three structural groups: flavonoid aglycones, phenolic acids and their esters. The determination of propolis flavonoids had been performed by HPLC [4,5] but there is no method for the simultaneous determination of all three groups of propolis phe-

Correspondence to: Professor Simeon Popov, Institute of Organic Chemistry with Centre of Phytochemistry, Bulgarian Academy of Sciences, Acad. G. Bonchev str., bl. 9, 1113 Sofia, Bulgaria.

0021-9673/92/$05.00

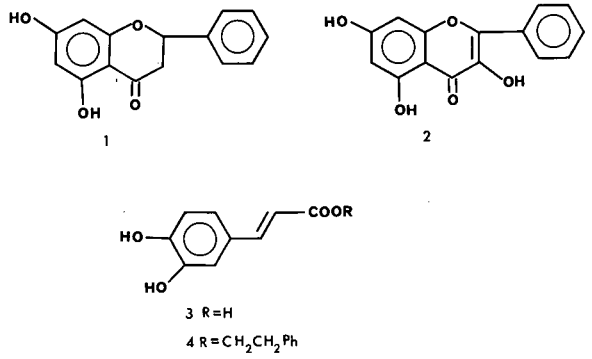

Fig. 1. Main phenolic components of propolis. Ph = Phenyl.

nolics, which is needed for development of new drugs and cosmetics.

Owing to the complex composition of propolis, its quantitative analysis of all components is virtually impossible. For this reason, we decided to determine only the few main representatives from each group of propolis phenolics which possess biological activity characteristic for propolis. Our recent investigations showed [10] that the main flavonoid aglycones appeared to be pinocembrin (**1**) and galangin (**2**), while the main aromatic acid in propolis is caffeic acid (**3**) and its β-phenylethyl ester (**4**) is one of the main representatives of the group of aromatic acid esters (Fig. 1). These compounds have shown antibacterial activity [7,11], which is characteristic for propolis preparations. The structure and biological activity of these compounds allowed us to use them as typical representatives of the main groups of propolis phenolics. Mild chromatographic conditions, preventing thermal destruction as far as possible, must be used.

EXPERIMENTAL

The flavonoids pinocembrin (**1**) and galangin (**2**) were obtained from propolis and purified by several passages through polyamide and silica gel columns, followed by recrystallization, and their purity was confirmed by TLC, melting point determination and mass, UV and ^{1}H NMR spectrometry [10]; the substances were compared with authentic samples. β-Phenylethyl caffeate (**4**) was synthesized as described elsewhere [12]. Caffeic acid (**3**) was purchased from Merck. The propolis used was a commercial Bulgarian sample.

Extraction of propolis

Propolis (1 g) was cut into small pieces and extracted with 20 ml of solvent (see Table II) overnight at room temperature. The extracts were evaporated to dryness.

Thin-layer chromatography

The propolis extracts were chromatographed on DC-Alufolien Kieselgel 60 F_{254} plates with chloroform–ethyl acetate (7:3) or *n*-hexane–ethyl acetate (7:3) as mobile phase and detection by UV irradiation and treatment with sulphuric acid and heating, in order to control the extraction process.

Silylation

The silylation of the standard mixtures and the model mixture was performed with bis(trimethylsilyl)trifluoroacetamide (BSTFA) at 65°C for 30 min in a screw-capped vial. About 1.5 mg of propolis extract was silylated with 95 μl of BSTFA. The large excess of BSTFA ensured reproducible results. The resulting derivatives were stable for at least 24 h.

Gas chromatography

A 9 m × 0.25 mm I.D. fused-silica capillary column with SE-54 as stationary phase was used. The linear velocity of the carrier gas (nitrogen) was 9 cm s^{-1} and the splitting ratio was 1:100. The injector temperature was 300°C. The column temperature was programmed from 80 to 280°C at 20°C min^{-1}, then from 280 to 300°C at 2°C min^{-1}, with a 10-min hold at 300°C. A flame ionization detector was used at 320°C. The sample volume injected was 1 μl.

TABLE I

CONCENTRATIONS OF STANDARD SOLUTIONS USED FOR MEASURING THE CALIBRATION GRAPHS

Compound	Concentration (mg ml^{-1})			
	Solution 1	Solution 2	Solution 3	Solution 4
1	8.33	3.81	2.61	1.01
2	5.50	1.36	1.03	0.32
3	1.66	0.43	0.26	0.10
4	3.16	0.76	0.63	0.21

TABLE II

EXTRACTION OF PROPOLIS WITH DIFFERENT SOLVENTS

No.	Solvent	Extract (% of native propolis)	Note
1	70% ethanol	58	Minimum waxes
2	90% ethanol	64	
3	Hexane, followed by acetone	64 (acetone extract)	
4	Acetone	81	

Quantitative analysis

Quantitative analysis was performed by the internal standard method, using *n*-pentacosane (*n*-$C_{25}H_{52}$). For each of the components analysed a calibration graph was constructed. Four standard mixtures were prepared, containing pinocembrin (**1**), galangin (**2**) caffeic acid (**3**) and β-phenylethyl caffeate (**4**) in proportions of about 10:4:1:2. These proportions were chosen to be similar to those in propolis. The concentrations of the standard mixtures are given in Table I. The concentration of the internal standard in each standard mixture was 1.2 mg ml^{-1}.

TABLE III

PARAMETERS OF CALIBRATION GRAPHS

b = Slope of the calibration graph (response factor of the detector to the sample component relative to the internal standard); S.D. = standard deviation of b; ε = mean error of b; $(\varepsilon/b) \cdot 100$ = relative error (%) of b; r = correlation coefficient.

Compound	b	S.D.	ε	$(\varepsilon/b) \cdot 100$ (%)	r
Pinocembrin (**1**)	0.58	0.02	0.04	6.8	0.99
Galangin (**2**)	0.59	0.02	0.04	6.7	0.99
Caffeic acid (**3**)	0.91	0.02	0.04	4.3	0.99
Caffeate (**4**)	0.67	0.02	0.04	6.0	0.99

Analysis of extract from propolis

A 1.50-mg amount of dry propolis extract (obtained with 70% ethanol) was dissolved in 95 μl of BSTFA and heated at 65°C for 30 min in a screw-capped vial. After cooling, 4 μl of internal standard solution were added and the sample was injected three times into the gas chromatograph.

RESULTS AND DISCUSSION

The main components of propolis are phenolics and waxes [9] and GC analysis of the former cannot be performed in the presence of waxes. For this reason, we tried some solvents for the extraction of

TABLE IV

PRECISION AND ACCURACY OF THE DETERMINATION OF COMPOUNDS **1–4**

A (%) = $([\text{compound}]_{\text{actual}} - [\text{compound}]_{\text{calculated}}) \cdot 100/[\text{compound}]_{\text{actual}}$. V (%) = $(S/x) \cdot 100$; S = calculated value, x = standard deviation (n = 8).

Compound	Concentration (mg/ml^{-1})		Precision, V (%)	Accuracy, A (%)
	Model mixture	Calculated value + S.D.		
1	5.5	5.7 ± 0.2	3.5	3.7
2	2.20	2.17 ± 0.2	9.2	1.4
3	0.64	0.66 ± 0.02	3.0	3.0
4	1.20	1.18 ± 0.05	4.2	1.7

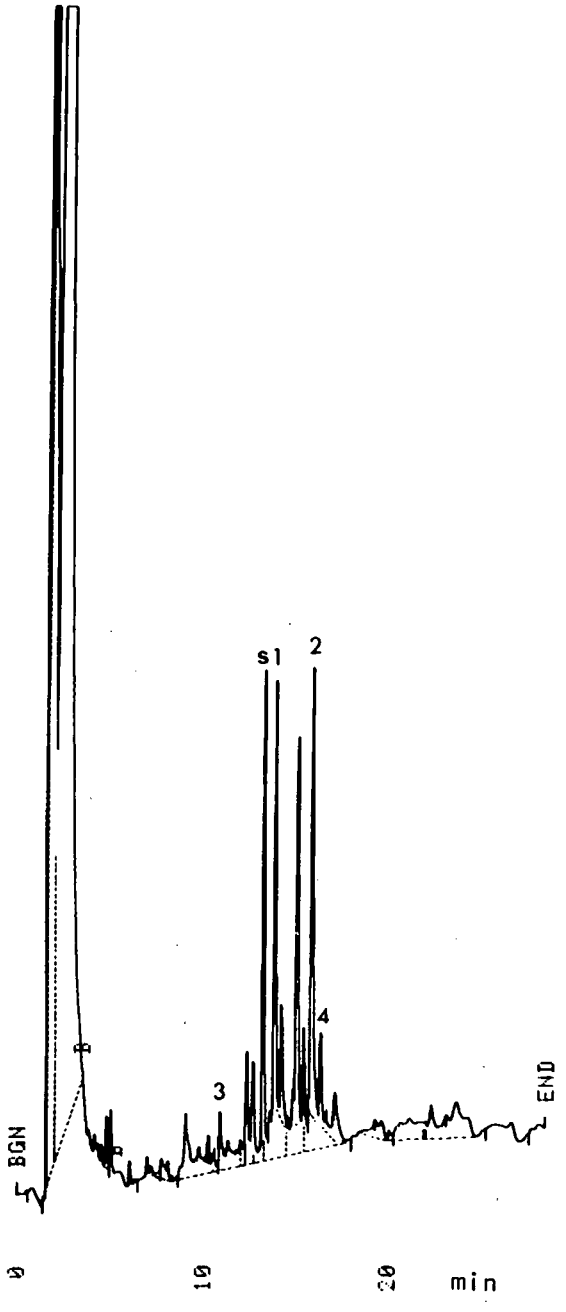

Fig. 2. Capillary GC of a wax-free propolis sample. For conditions, see Experimental. Peaks numbers correspond to compounds 1–4; s = internal standard (n-$C_{25}H_{52}$).

propolis in order to prepare an extract with less waxes. The results obtained are summarized in Table II. TLC and GC showed that extraction with 70% ethanol gave the best results, which is in agreement with the results obtained by Greenaway *et al.* [6].

Thermal destruction could be reduced if the separation was performed in a shorter time. This can be achieved by using shorter but highly effective non-polar capillary columns. The high efficiency is necessary because of the complex composition of propolis. The model mixture of **1–4** was chromatographed for 18 min, and the components were determined by the internal standard method with n-$C_{25}H_{52}$, a calibration graph being constructed for each of the components. The parameters of the calibration graphs are given in Table III.

The precision and accuracy of the proposed method are indicated in Table IV. It is evident that in all instances the relative error is less than 4%, which is a very good result for the analysis of natural products. This is due to the prior enrichment of the phenolic mixtures and to the high efficiency of the short quartz capillary column. This is an indication that the procedure developed is suitable for the analysis of phenolic mixtures, including propolis.

The GC analysis of the propolis extract was repeated three times (Fig. 2), and the concentrations of the components in the BSTFA solution were **1** = 2.33 ± 0.02, **2** = 1.39 ± 0.03, **3** = 0.21 ± 0.02 and **4** = 0.19 ± 0.01 mg ml^{-1}. With the proposed method the limits of detection are of **1** = 0.5, **2** = 0.2, **3** = 0.05 and **4** = 0.1 μg at S/N ⩾ 3.

REFERENCES

1 E. E. Conn, *The Biochemistry of Plants*, Vol. 7, Academic Press, New York, 1981, p. 425.
2 J. W. McClure, in J. B. Harborne, T. J. Mabry and H. Mabry (Editors), *The Flavonoids*, Chapman and Hall, London, 1975, Ch. 18, p. 970.
3 C. S. Creaser, M. R. Koupai-Abyazani and G. R. Stephenson, *J. Chromatogr.*, 478 (1989) 415.
4 V. Bankova, S. Popov and N. Marekov, *J. Chromatogr.*, 242 (1982) 135.
5 M. Vanhaelen and R. Vanhaelen-Fastre, *J. Chromatogr.*, 187 (1980) 255.
6 W. Greenaway, T. Scaysbrook and F. Whatley, *Proc. R. Soc. London, Ser. B*, 232 (1987) 249.
7 E. Ghisalberti, *Bee World*, 60, No. 2 (1979) 59.
8 V. Bankova and N. Marekov, *Farmatsiya (Sofia)*, 32, No. 2 (1984) 8.
9 P. Walker and E. Crane, *Apidologie*, 18 (1987) 327.
10 V. Bankova, S. Popov and N. Marekov, *J. Nat. Prod.*, 46 (1983) 471.
11 V. Bankova, A. Kujumgiev, A. Ignatova, Al. Dyulgerov, O. Pureb, J. Zamyansan and S. Popov, in R. Vlakov (Editor), *Proceedings of Vth International Conference on the Chemistry and Biotechnology of Biologically Active Natural Products, September 18–23, 1989, Varna, Bulgaria*, Bulgarian Academy of Sciences, Sofia, 1989, Vol. 2, p. 239.
12 V. Bankova, *J. Nat. Prod.*, 53 (1990) 821.

Journal of Chromatography, 607 (1992) 154–158
Elsevier Science Publishers B.V., Amsterdam

CHROM. 24 360

Short Communication

Glass capillary gas chromatographic identification of volatile components recovered from orange essence by continuous liquid extraction

Hideaki Ohta, Yoichi Nogata, Koh-Ichi Yoza and Mari Maeda

Chugoku National Agricultural Experiment Station, Ministry of Agriculture, Forestry and Fisheries, Fukuyama City, Hiroshima 721 (Japan)

(First received July 26th, 1991; revised manuscript received May 7th, 1992)

ABSTRACT

Volatile components extracted from two different commercial orange essences by continuous liquid–liquid extraction were analyzed by glass capillary gas chromatography. From the evaluation of identified volatile components, one of the essences seemed to be a true orange essence, whereas the other seemed to be a refined citrus peel oil. We also showed that the continuous liquid–liquid extraction provided an easy, useful and very convenient procedure for the preparation of samples.

INTRODUCTION

The recovery of flavour compounds from fruits and their products prior to gas chromatographic (GC) separation is one of most important aspects of flavour chemistry, even though the development of glass capillary GC and GC–mass spectrometry (MS) has also contributed significantly to recent advances in flavour analytical chemistry. The concentration and nature of the flavour compounds detected often depend on the sample preparation methods, and three general procedures have been used: analysis of the headspace above the sample, steam distillation of the sample, and extraction (either cold or at room temperature) of the sample with a low-boiling organic solvent followed by evaporation of the solvent. Of these three methods, solvent extraction procedures have been widely used in citrus flavour analysis [1–5]. Solvent extraction procedures, however, are often tedious and time consuming using a separating funnel.

Orange essence recovered during industrial concentration processes is often added to a number of citrus fruit products to impart fresh flavour. Recently, flavour loss of citrus juices and drinks packed in flexible pouches has become a serious problem [6–8], and in this study we applied a continuous liquid–liquid solvent extractor for analysing flavour compounds in the orange essence.

This paper deals with the identification of volatile components extracted from two different commercial orange essences by a continuous liquid–liquid extraction, using wall-coated open-tubular (WCOT) glass capillary GC and GC–MS.

Correspondence to: Dr. H. Ohta, Chugoku National Agricultural Experimental Station, Ministry of Agriculture, Forestry and Fisheries, Fukuyama City, Hiroshima 721, Japan.

0021-9673/92/$05.00

EXPERIMENTAL

Materials

Two commercial orange essences, (A) W-9735 and (B) P-0522, were purchased from Takasago Perfume (Tokyo, Japan). W-9735 was produced from volatiles recovered during the concentration of orange juice and P-0522 was prepared from peel oil recovered from the extraction of orange fruits [9].

Flavour recovery from orange essence solution

Distilled water (250 g) was added to 250 g of orange essence. The essence solution obtained was continuously extracted for 8 h with 360 ml of *n*-pentane–diethyl ether (2:1) at room temperature using a liquid–liquid extractor as shown in Fig. 1. The flask which contained the solvent was heated to and maintained at 45°C. The combined solvent extract was dehydrated with sodium sulphate and then the extract was concentrated *in vacuo* (28°C, 10 mmHg). The yields of extract concentrates were 1.535 and 8.483 g for essences A and B, respectively.

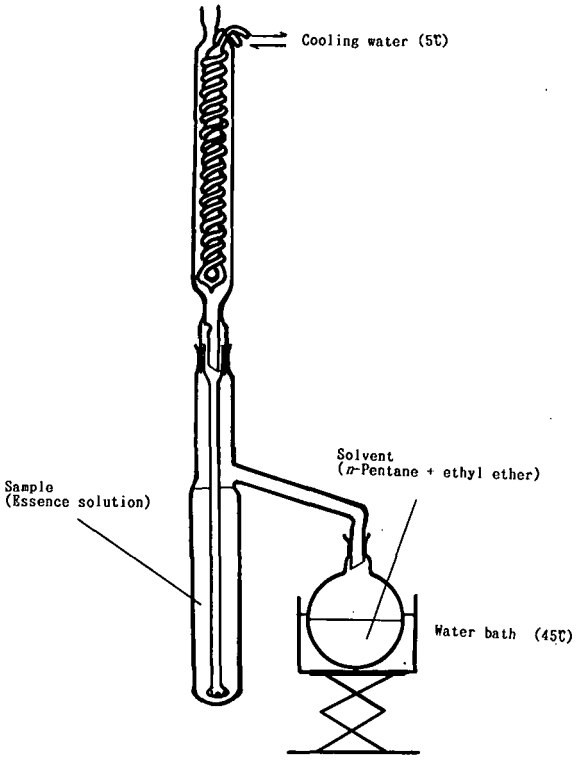

Fig. 1. Schematic diagram of the continuous liquid–liquid extractor.

Apparatus

Analytical GC was carried out on a Shimadzu Model 8A gas chromatograph with flame ionization detection (FID). A WCOT glass capillary column (50 m × 0.25 mm I.D.) coated with Carbowax 20M was used. The temperature of both the injection port and detector were maintained at 250°C. The column oven temperature was maintained at 65°C for 4 min and then programmed from 65 to 195°C at 2°C/min. Helium was used as the carrier gas at a flow-rate of 0.93 ml/min with a splitting ratio of 108:1. The sample size was 0.2 μl. Peak areas were integrated by means of a Shimadzu Chromato-pack C-R3A integrator.

GC–MS was performed on a Hitachi Model M-80A mass spectrometer combined with a Hitachi Model 063 gas chromatograph, under similar conditions to the GC analysis. Other operating parameters were as follows: carrier gas, helium; ionizing voltage, 20 eV; ion source temperature, 200°C.

RESULTS AND DISCUSSION

The yields (w/w) of extract concentrates were 0.61% for essence A and 3.39% essence B.

Gas chromatograms of the extract concentrates A and B from two orange essences using FID are given in Figs. 2 and 3, respectively. The presence of peaks of *m/z* 127 for A and *m/z* 121 for B was demonstrated; 50 components for A and 44 for B were identified as known compounds by comparing and matching the mass spectra and GC retention times or from the mass spectra only (Table I).

The peak-area percentages, excluding peaks for the solvents and ethanol, were calculated; ethanol is used in preparing commercial fruit essence [9].

Concerning the identified terpene content, there was a great difference between essences A and B. As expected, the largest fraction of the extract concentrate B consisted of terpene carbohydrates; principally *d*-limonene and 1,8-cineole (89.71%), myrcene (1.81%) and α-pinene (0.64%) were present in the greatest quantities. Methyl butyrate, ethyl 2-methylbutyrate, dihydrolinalool, isopulegol and nonanol were lacking with essence B compared with essence

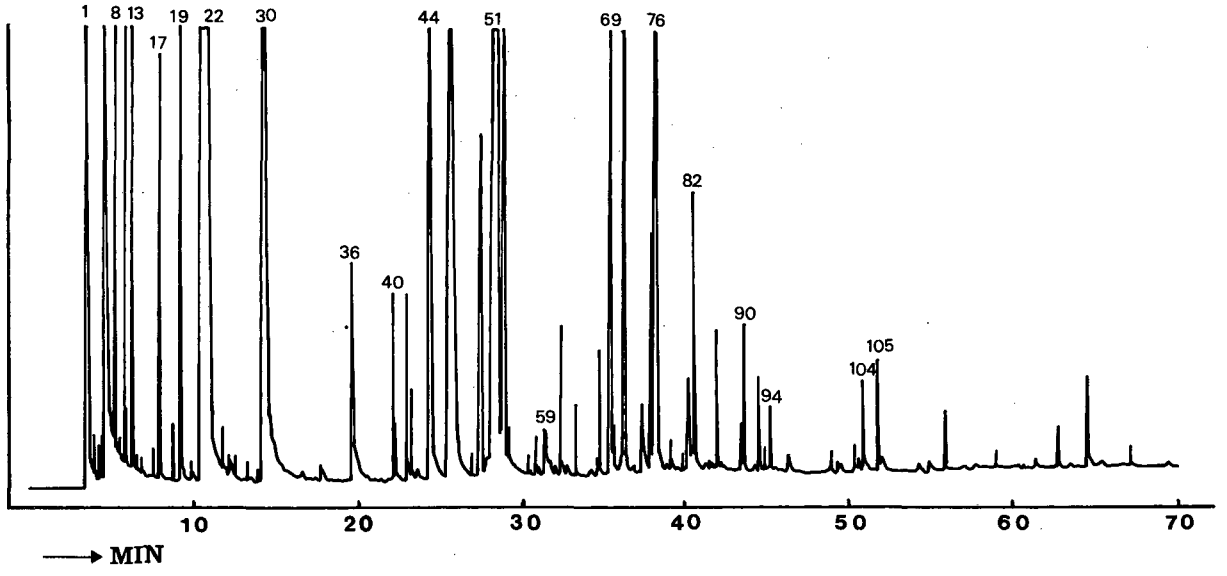

Fig. 2. Gas chromatogram recorded with FID of an extract concentrate of orange essence W-9735 (A). Sample size, 0.2 μl. A WCOT glass capillary column (50 m × 0.25 mm I.D.) coated with Carbowax 20M was used. The column oven temperature was kept at 65°C for 4 min and then programmed from 65 to 195°C at 2°C/min. Other operating conditions were as given under Experimental and peak identities are given in Table I.

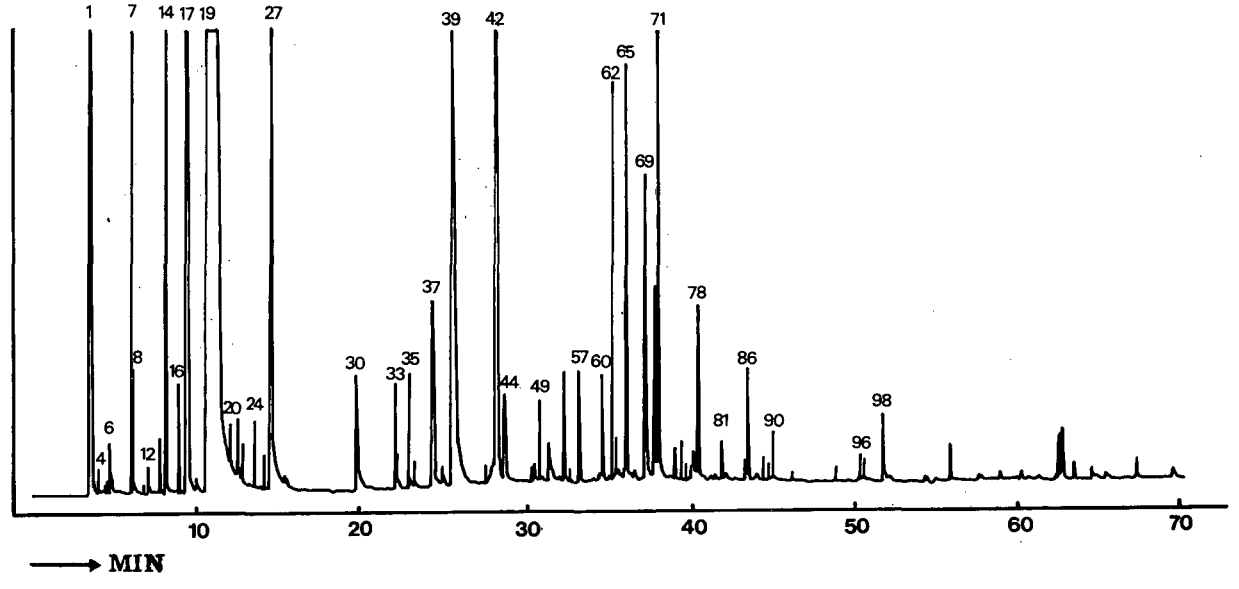

Fig. 3. Gas chromatogram recorded with FID of an extract concentrate of orange essence P-0522. (B) GC conditions and peaks as in Fig. 2.

TABLE I

VOLATILE COMPOUNDS IDENTIFIED IN THE ORANGE ESSENCES W-9735 (A) and P-0522 (B)

Peak No.[a] (Fig. 2)	Compound	Peak area (%)		Evidence	
		A	B	GC	GC–MS
1	*n*-Pentane (solvent)			+	+
2	Diethyl ether (solvent)			+	+
5	Ethyl acetate	0.02	Tr[b]	+	+
7	Ethanol			+	+
8	Methyl butyrate	0.26	–[b]	+	+
10	α-Pinene	0.32	0.64	+	+
11	Ethyl butyrate	0.03	0.04	+	+
13	Ethyl 2-methylbutyrate	0.57	–	+	+
16	β-Pinene	0.02	–	+	+
17	Sabinene	0.27	0.38	+	+
18	δ-3-Carene	0.05	0.09	+	+
19	Myrcene	1.23	1.81	+	+
20	Heptanal	0.02	0.01	+	+
21'[c]	*d*-Limonene + 1,8 cineole	58.05	89.71	+	+
22'	Ocimene + ethyl caproate	0.03	0.02	+	+
24	α-Terpinene	0.02	0.03	+	+
26	4-Cymene	0.01	0.02	+	+
27	Terpinolene	0.01	0.03	+	+
30	Octanal	3.56	0.67	+	+
36	Nonanal	0.37	0.13	+	+
41	Limonene-1,2-oxide	0.18	0.07		+
42	Linalool-3,6-oxide	0.09	0.02		+
44	Citronellal	0.75	0.18	+	+
47	Decanal	2.10	0.91	+	+
49	Dihydrolinalool	0.43	–	+	+
51	Linalool	21.80	2.08	+	+
52	Octanol	0.67	0.08	+	+
53	Isopulegol	0.07	–	+	+
57	Terpinen-4-ol	0.05	0.06	+	+
59	Undecanal	0.07	0.05	+	+
67	Nonanol	0.03	–	+	+
68	3-Pinen-2-ol	0.12	0.07	+	+
69	Neral	1.38	0.25	+	+
72	α-Terpineol	1.77	0.28	+	+
74	Dodecanal	0.16	0.29	+	+
75	α-Terpinyl acetate	0.22	0.13	+	+
76	Geranial	2.29	0.47	+	+
81	β-Citronellol	0.12	0.03	+	+
82	Perillaldehyde	0.30	0.12	+	+
86	Nerol	0.15	0.03	+	+
90	*cis*-Carveol	0.15	0.08		+
92	Geraniol	0.10	0.02	+	+
94	*trans*-Carveol	0.07	0.04		+
102	Laurinal	0.04	0.03	+	+
104	Dodecanol	0.11	0.02	+	+
105	*p*-Menta-1,8-dien-9-ol	0.13	0.06		+

[a] Peak numbers on the left-hand side give the elution order on the 50-m Carbowax 20M column in Fig. 2.

[b] Tr, <0.01%; –, not detectable.

[c] In the case of two overlapped peaks in Fig. 2, the peak numbers are marked with primes. The overlapped peaks were separated by GC (column temperature 60°C).

A. In contrast, some terpene alcohols (including linalool, nerol and citronellol) and aldehydes (including octanal, decanal, neral and geranial) were relatively abundant in essence A. Especially the linalool ratio relative to *d*-limonene and 1,8-cineole of essence A (37.6%) is sixteen times greater than that of essence B (2.3%).

Of the compounds in Table I, the oxygen-containing components, including carbonyls (octanal, decanal and neral, etc.) and alcohols (linalool, citronellol and nerol, etc.), are recognized as the major contributors to the fresh and pleasant flavour of orange essences, because of their low threshold and their olfactory characteristics [5,10,11].

The yield of extract concentrate B was approximately five times higher than that of extract A, owing to its higher content of terpene hydrocarbons (Table I). On the other hand, essence A was evaluated as a higher quality flavouring ingredient for orange product processors, as it contained a relatively larger proportion of the oxygen-containing compounds. These results suggested that essence A was a true orange essence whereas the GC profile of concentrate B was very similar to that of a refined citrus peel oil [9,12].

Although the convenient headspace analysis procedure for sample preparation has been widely applied recently by flavour chemists using Tenax resins, etc., solvent extraction is also necessary for the identification of high-boiling flavour compounds, although tedious and time consuming using a separating funnel. In this study to evaluate chemically the flavour compounds from commercial citrus essence, we have demonstrated that a continuous liquid–liquid extractor provides an easy, useful and very convenient procedure for preparing samples.

ACKNOWLEDGEMENTS

The authors acknowledge the cooperation and assistance of Mr. Y. Washizu of the Tokyo Research Institute, Takasago Perfume. This research was partly funded by a grant from the Ministry of Agriculture, Forestry and Fisheries of Japan.

REFERENCES

1 R. E. Wolford, G. E. Alberding and J. A. Attaway, *J. Agric. Food Chem.*, 10 (1962) 297.
2 Yajima, T. Yanai, M. Nakamura, H. Sakakibara and K. Hayashi, *Agric. Biol. Chem.*, 43 (1979) 259.
3 M. G. Moshonas and P. E. Shaw, *J. Agric. Food Chem.*, 31 (1983) 334.
4 H. Ohta and Y. Osajima, *J. Chromatogr.*, 268 (1983) 336.
5 H. E. Nordby and S. Nagy, in P. E. Nelson and D. Tressler (Editors), *Fruit and Vegetable Juice Processing Technology*, Avi, Westport, CT, 3rd ed., 1980, p. 35.
6 M. Shimoda, T. Nitanda, N. Kadota, H. Ohta, K. Suetsuna and Y. Osajima, *Nippon Shokuhin Kogyo Gakkaishi (J. Jpn. Soc. Food Sci. Technol.)*, 31 (1984) 697.
7 C. H. Mannheim, J. Miltz and A. Letzter, *J. Food Sci.*, 52 (1987) 737.
8 O. Y. Kwapong and J. H. Hotochkiss, *J. Food Sci.*, 52 (1987) 761.
9 F. Fujimaki, T. Hattori, K. Hayashi and S. Arai (Editors), *Koryo no Jiten (Perfume Dictionary)*, Asakura, Tokyo, 1980, p. 228.
10 J. F. Kefford and B. V. Chandler, in C. O. Chichester, E. M. Mark and G. F. Stewart (Editors), *The Chemical Constituents of Citrus Fruit (Advances in Food Research)*, Suppl. 2, Academic Press, New York, 1970, Ch. 11, p. 85.
11 P. E. Shaw, in S. Nagy, P. E. Shaw and M. K. Veldhuis (Editors), *Citrus Science and Technology*, Vol. 1, Avi, Westport, CT, 1977, Ch. 12, p. 463.
12 P. E. Shaw and C. W. Wilson, *Importance of Selected Components to Natural Orange, Grapefruit, Tangerine, and Mandarin Flavors (ACS Symposium Series*, No. 143), American Chemical Society, Washington, DC, 1980 p. 167.

Journal of Chromatography, 607 (1992) 159–162
Elsevier Science Publishers B.V., Amsterdam

CHROM. 24 367

Short Communication

Development of a specific device for densitometry of thin-layer chromatographic sheets in planar chromatography

C. Regnault, P. Delvordre and H. Bonnier

Department of Clinical Pharmacy and Biotechnique, School of Pharmacy, 5 Rue J. B. Clément, 92290 Chatenay Malabry (France)

E. Postaire

Department of Clinical Pharmacy and Biotechnique, School of Pharmacy, 5 Rue J. B. Clément, 92290 Chatenay Malabry, and Central Pharmacy of Paris Hospitals, 7 Rue du Fer à Moulin, 75005 Paris (France)

(First received March 2nd, 1992; revised manuscript received May 21st, 1992)

ABSTRACT

A specific device for densitometry of Empore TLC sheets is described and it is compared with two other devices using one or two glass plates as support. This comparison lie on a reading by densitometry at 225, 275 and 520 nm in reflectance and transmittance on silica gel and C_{18} sheets. The results of an application to the determination of aspartame are presented.

INTRODUCTION

The flexibility and easy cutting of Empore thin-layer chromatographic (TLC) sheets (Analytichem International, Harbor City, CA, USA) offer attractive features [1,2]. However, the distortion of the sheet during scanning densitometry is a drawback and leads to a risk of a decrease in the performance obtained in previous steps. This is the reason why scanning optimization has been carefully studied on new sheets: experiments have already been reported by Poole and co-workers using a support on glass plates [3] or a sheet of aluminium foil [4]. Hence, densitometry using a glass plate support on which a sheet is placed, or a "sandwich" configuration confining the sheet between two plates, has been carried out in comparison with the use of a new fixation system of the sheet. It is a rigid fixation, which is placed around the plate and allows it to be held firmly on its four sides. This system is composed of two elements: a pedestal fixed on a plane support and a double frame which can be opened and the superposed parts of which are fixed with a hinge and clips as a slide. Experiments were carried out in reflexion and transmittance, by scanning spectra and densitometry at 225–275 and 520 nm, with silica gel and C_{18} sheets with a fluorescence indicator. Application to the study of background noise on aspartame (tripeptided) was investigated.

The first results make the impossibility of using a "glass sandwich" obvious on account of the significant absorbance of the support due to the use of

Correspondence to: Dr. E. Postaire, Central Pharmacy of Paris Hospitals, Laboratory of Analytical Development, 7 Rue du Fer à Moulin, 75005 Paris, France.

0021-9673/92/$05.00

two glass plates. The results obtained with the new rigid device seem to be interesting because scanning densitometry in reflectance is made on a stretched, flat plate, and scanning densitometry in transmittance is not interfered with by the obstruction of a possible element as in scanning with a glass support. Moreover, this device is helpful in the manipulation and storage of plates.

EXPERIMENTAL

Chemical and reagents

Empore silica gel and reversed-phase TLC sheets with fluorescence indicator were obtained from Analytichem International. Ethanol, acetic acid, ninhydrin, 2,4,6-collidine and copper nitrate of analytical-reagent grade were supplied by E. Merck (Darmstadt, Germany). The aspartame used was the commercialy available product.

Instrumentation

The densitometric evaluations of plates after derivatization (for measurement of aspartame) and of plates without spots (for measurement of indirect interference of the support) were carried out with CD 60 TLC scanner from Desaga (Heidelberg, Germany), each with three steps. Spots of a 25 mg per 100 ml solution of aspartame dissolved in water–ethanol (10:90, v/v) were applied using 1-μl Microcaps.

Densitometry

The plates were scanned at 225, 275 and 520 nm in transmittance and reflectance for plates without spots and 225, 490 and 520 nm for plates after derivatization with ninhydrin. The monochromator band width was 10 nm and slit dimension of 0.1 x 1 mm was used. Aspartame was streaked on a reversed-phase (C_{18}) sheet and ninhydrin reagent for derivatization was applied [5] using overpressured derivatization [6] to avoid errors arising from spraying or dipping the sheets [7]. After OPD the sheets were heated at 100°C in a drying oven for 30 min. Aspartame appeared as a red spot. After cooling to room temperature the chromatograms were evaluated by densitometry (λ = 275, 490 and 520 nm; slit dimensions 0.2 × 3 mm; eight points per measurement; in the reflectance with deuterium and tungsten lamps).

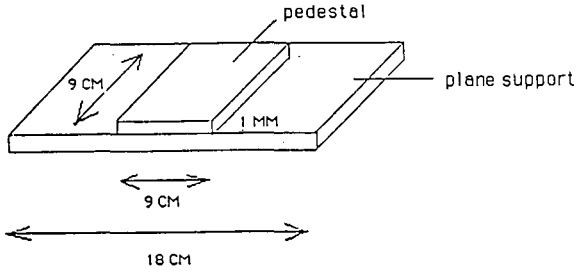

Fig. 1. Support for Empore TLC sheet (10 × 10 cm).

Description of the specific device for densitometry of sheets

The device is a rigid fixation made of plastic material, which is placed around the plate and allows it to be held firmly on its four sides. This system is composed of two elements: a pedestral fixed on a plane support (Fig. 1) and a double frame (Fig. 2) which can be opened and the superposed parts of which are fixed with a hinge and clips as a slide. In this case, no support is needed for scanning.

RESULTS AND DISCUSSION

The densitometric measurements of the EMPORE TLC sheets were carried out under conditions identical with those used for the commercially available glass-supported sorbent layers, in three steps: (A) the sheet was placed on a glass plate support; (B) the sheet was placed between two glass-plates ("Sandwich" configuration); and (C) the sheet was fixed with the new specific device.

Spectra of the same sheet (without spots) in steps A, B and C were recorded and adsorbances were measured at 225, 275 and 520 nm. All the spectra

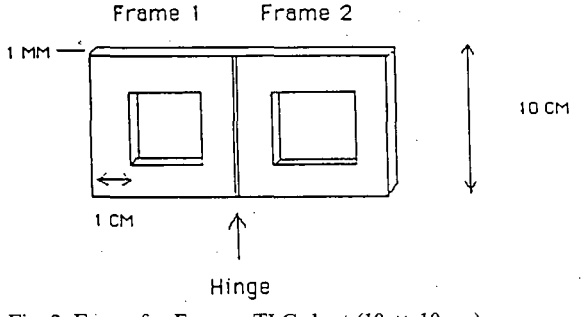

Fig. 2. Frame for Empore TLC sheet (10 × 10 cm).

TABLE I

ABSORBANCES AT 225, 275 AND 520 nm OF EMPORE SHEETS (REVERSED PHASE AND SILICA GEL) IN REFLECTANCE AND TRANSMITTANCE USING STEPS A, B and C

Absorbances expressed in milliabsorbance units, mean results of five measurements.

Mode	Step	Reflectance			Transmittance		
		225 nm	275 nm	520 nm	225 nm	275 nm	520 nm
Reversed phase	C	–[a]	160	550	5250	6300	5000
	A	–	225	580	5100	6250	5100
	B	2700	4400	650	4800	6300	5000
Silica gel	C	–	20	645	5750	6200	4700
	A	–	10	645	5800	6150	4750
	B	3100	4500	700	6300	8000	4750

[a] No absorbance.

TABLE II

STUDY OF NOISE OF 225, 275 AND 520 nm OF EMPORE SHEETS (REVERSED PHASE AND SILICA GEL) IN REFLECTANCE AND TRANSMITTANCE, B AND C *VERSUS* A

Values represent the % increase or decrease in absorbance in of steps B and C *versus* step A, mean results of five measurements.

Mode	Step	Reflectance			Transmittance		
		225 nm	275 nm	520 nm	225 nm	275 nm	520 nm
Reversed phase	C/A	−0.9	−0.5	+0.1	−3.1	−10.6	−1.1
	B/A	+11	+15.4	+11,2	+11.2	+14.0	+0.3
Silica gel	C/A	+0.7	+0.7	+0.7	−12.6	−2.2	−3.8
	B/A	+10	+14.8	+10.8	+3.3	−0.3	+0.2

TABLE III

SIGNAL-TO-NOISE RATIO OF NINHYDRIN-DERIVATIZED ASPARTAME AT 275, 490 AND 520 nm IN STEPS A, B AND C

Mean results of eight measurements.

Step	Signal-to-noise ratio		
	275 nm	490 nm	520 nm
C	2.9	5.1	3.7
A	2.5	3.05	3.46
B	2.42	1.0	2.0

are identical with respect to qualitative data (aspect, shape, ...); only quantitative values of the absorbance differ with the steps used (Table I). The results show a high noise level in reflectance with the sandwich configuration (B). In transmittance, A, B and C seem to be identical. Chromatograms were recorded at 225, 275 and 520 nm to compare the noise using steps A, B and C. Results are expressed as the percentage of increasing (+) or decreasing (−) noise *versus* step A as a reference (Table II). Results show the lowest noise using the new specific device (C) and the greatest noise with the sandwich configuration (B). It is likely that these differences

are essentially characteristic of the glass plate support. To confirm these data, a signal-to-noise ratio study was performed in the reflectance on aspartame after ninhydrin derivatization [5]. The results are given in Table III. The signal-to-noise ratios were found to be essentially identical except at 490 nm, the classical wavelength for evaluating ninhydrin-derivatized aspartame by densitometry [5]. In this case results clearly favour step C.

REFERENCES

1 L. Boltz, Sz. Nyiredy, E. Wehrlt and O. Sticher, *J. Liq. Chromatogr.*, 13 (1990) 2809.
2 C. Regnault, P. Delvordre and E. Postaire, *J. Chromatogr.*, 547 (1991) 403.
3 S. K. Poole and C. F. Poole, *J. Planar Chromatogr.*, 2 (1989) 478.
4 S. K.Poole, W. P. N. Fernando and C. F. Poole, *J. Planar Chromatogr.*, 3 (1990) 331.
5 D. Waldi in E. Stahl (Editor), *Dünnschicht Chromatographie*, Springer, Berlin, 1962, p. 510.
6 E. Postaire, C. Sarbach, P. Delvordre and C. Regnault, *J. Planar Chromatogr.*, 3 (1990) 247.
7 J. Grösz and O. Jonas, *J. Planar Chromatogr.*, 3 (1990) 261.

Journal of Chromatography, 607 (1992) 163–167
Elsevier Science Publishers B.V., Amsterdam

CHROM. 24 365

Short Communication

Thin-layer chromatographic behaviour of substituted phenolic compounds on silica gel layers impregnated with Al(III) and Cu(II)

M. Petrović, M. Kaštelan-Macan and A. J. M. Horvat

Faculty of Chemical Engineering and Technology, Institute of Analytical Chemistry, Marulićev trg 20, 41000 Zagreb (Croatia)

(First received February 19th, 1992; revised manuscript received May 20th, 1992)

ABSTRACT

The chromatographic behaviour of some substituted phenolic compounds on silica gel layers impregnated with Al(III) and Cu(II) was studied. Addition of metal ions gives very good separations of some structural isomers. In order to establish whether any improvment in the separation could be achieved by varying the concentration of impregnant, three different concentrations of $CuSO_4 \cdot 5H_2O$ and $AlCl_3 \cdot 6H_2O$ (1, 2 and 4%, w/w) were used. A very good separation of hydroquinone and resorcinol on silica gel layers impregnated with $CuSO_4$ was achieved. Aminophenols can be successfully separated using silica gel layers modified by $CuSO_4$ addition. The optimum resolution of *meta* and *para* isomers was achieved on silica gel containing 0.51% Cu(II) ions (2% $CuSO_4 \cdot 5H_2O$).

INTRODUCTION

Thin-layer chromatography (TLC) is commonly used for the identification of phenolic compounds. The separation of substituted phenols using various chromatographic systems has been reported. Silica gel [1-4] is the material preferred by most workers, but examinations showed that structural isomers cannot be succesfully separated, although a certain separation by variation of the solvent system can be achieved. Therefore, difficulties in obtaining adequate resolution of closely related structural isomers have led to the application of modified sorbents.

Correspondence to: Dr. M. Kaštelan-Macan, Faculty of Chemical Engineering and Technology, Institute of Analytical Chemistry, Marulićev trg 20, 41000 Zagreb, Croatia.

Improved resolution has been achieved by impregnating silica gel with some inorganic or organic substances. Thielmann [5] obtained good results in the resolution of a mixture of naphthols and some polyphenols using silica gel layers impregnated with amonium molybdate. Hadžija and co-workers [6,7] studied the chromatographic behaviour of phenolic acids and aldehydes on precoated silica gel plates impregnated with iron(III) nitrate and while some other researchers [8-11] suggested the use of different impregnants such as silver nitrate, sodium nitrite, aniline chloride and oxalic, tartaric and citric acid. The improved resolution and changed mobility on the modified silica gel plates is a result of complex interactions between phenolic compounds and impregnants.

In this work we studied the chromatographic behaviour of some structural isomers of phenolic

0021-9673/92/$05.00

TABLE I

SOLVENT SYSTEMS USED

Solvent system	Components	Ratio of components (v/v)
S_1	Chloroform	
S_2	Chloroform–acetone	65:35
S_3	Chloroform–ethyl acetate	95: 5
S_4	Chloroform–ethyl acetate	95:10
S_5	Toluene–chloroform–acetone	40:25:15
S_6	Toluene–chloroform–acetone	40:25:25
S_7	Hexane–acetone	80:20
S_8	Hexane–acetone	80:40
S_9	Benzene	
S_{10}	Benzene–acetone	70:30

compounds on silica gel thin layers modified with copper and aluminium.

EXPERIMENTAL

Chromatographic plates were prepared by spreading a slurry of silica gel GF_{254} (Merck) and an aqueous solution of $CuSO_4 \cdot 5H_2O$ or $AlCl_3 \cdot 6H_2O$, by means of a Camag applicator on to 20 × 20 cm glass plates. The layer thickness was 300 μm. The plates were dried in air and activated for 1 h at 105°C.

Stock standard solutions containing 1 mg/ml of phenol, *o* -, *m*- and *p*-cresol, *o*-, *m*- and *p*-nitrophenol, *o*- and *p*-chlorophenol, *o*-, *m*- and *p*-aminophenol, salicylic acid, hydroquinone, resorcinol and pyrogallol in acetone were prepared. Samples of 5 μl were applied to the activated plates with a Camag micropipette.

The chromatograms were developed with the solvent systems listed in Table I in saturated chambers to a distance of 12 cm.

Phenolic compounds were detected by spraying with a 5% (w/v) aqueous solution of $FeCl_3 + K_3Fe(CN)_6$ to obtain blue spots on a white background or by UV irradiation at 254 nm.

RESULTS AND DISCUSSION

The chromatographic separation of sixteen substituted phenols was carried out on silica gel layers modified with various concentrations of $CuSO_4$ and $AlCl_3$. R_F-values of the compounds examined on impregnated plates were compared with those ob-

TABLE II

R_F VALUES ON SILICA GEL LAYERS

Compounds examined	R_F values					
	S_1	S_2	S_3	S_4	S_5	S_6
Phenol	0.24	0.63	0.73	0.38	0.22	0.91
o-Cresol	0.42	0.74	0.80	0.49	0.33	0.91
m-Cresol	0.27	0.63	0.73	0.39	0.23	0.90
p-Cresol	0.27	0.65	0.72	0.37	0.24	0.90
o-Nitrophenol	0.94	0.94	0.92	0.70	0.82	1
m-Nitrophenol	0.16	0.57	0.65	0.25	0.11	0.85
p-Nitrophenol	0.14	0.52	0.61	0.22	0.09	0.82
o-Chlorophenol	0.68	0.83	0.75	0.41	0.51	0.93
p-Chlorophenol	0.25	0.61	0.70	0.37	0.22	0.90
o-Aminophenol	0.22	0.27	0.45	0.21	0.05	0.68
m-Aminophenol	0	0.15	0.26	0.10	0	0.57
p-Aminophenol	0	0.13	0.23	0.09	0	0.52
Salicylic acid	0	0	0	0	0	0.05
Hydroquinone	0	0.12	0.34	0.08	0	0.58
Resorcinol	0	0.12	0.34	0.09	0	0.62
Pyrogallol	0	0.10	0.17	0.06	0	0.40

tained on plain silica gel plates. The influence of different solvent systems, chosen on the basis of published data, was studied.

The introduction of functional groups into a phenol molecule generally raises its adsorption affinity on the silica gel layers, but the position of functional groups, and especially steric effects, have to be taken into acount. The R_F values obtained for phenolic compounds using different solvent systems are listed in Table II. The R_F values of *m*- and *p*-cresol show little difference from those of phenol, whereas a methyl group in the *ortho* position increases the R_F value. This decreased adsorption of *ortho* isomers is attributed to steric effects, which are particularly marked in the case of *o*-nitrophenol. Adsorption of phenols on silica gel layers is a result of hydrogen bonding with silica surface, but in the *ortho*-substituted compounds the formation of intramolecular hydrogen bonds between the hydroxyl group and the *ortho* substituent is possible. The consequence of this chelation is a reduced adsorption affinity of *ortho* isomers.

Aminophenols are more weakly acidic than phenol, owing to the inhibited resonance of the hydroxyl group with the benzene ring caused by the amino group. An amino group in the *ortho* or *para* position has a much greater inductive effect than one in the *meta* position. The R_F values of aminophenols obtained on silica gel layers show that *m*- and *p*-aminophenol cannot be succesfully separated, although some resolution by variation of the solvent system can be achieved. Examining the chromatographic separation of aminophenols using modified layers, it can be concluded that addition of metal ions to the silica gel during the layer preparation gives an opportunity for very good separations of *meta*- and *para*-isomers.

In order to establish whether any improvment in the separation of aminophenols could be made by varying the concentration of impregnants, three different concentrations of $CuSO_4 \cdot 5H_2O$ and $AlCl_3 \cdot 6H_2O$ (1, 2 and 4%, w/w) were used. The addition of $CuSO_4$ leads to a significant increase in adsorption of *p*-aminophenol, which is shown by a rapid decrease in R_F values (Fig. 1), whereas adsorption of *m*-aminophenol is gradually increased.

On Cu(II)-impregnated plates pyrogallol has smaller R_F values than on plain plates. On the other hand, the mobility of resorcinol is almost the same

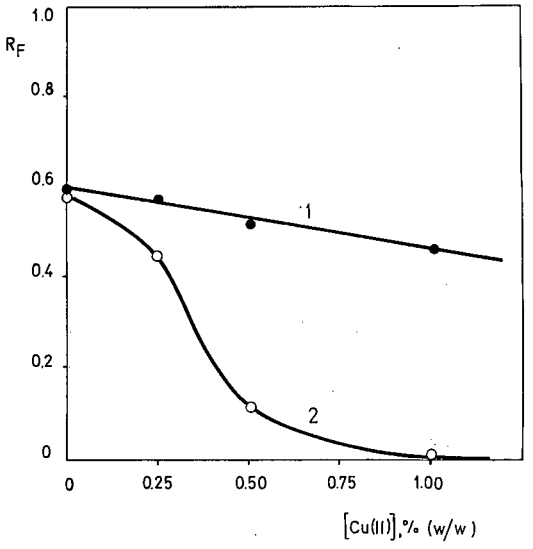

Fig. 1. R_F values of aminophenols as a function of Cu(II) mass fraction in the layer; solvent system S_2. 1 = *m*-aminophenol; 2 = *p*-aminophenol.

on the impregnated and plain silica gel plates (Fig. 2).

This increased adsorption of pyrogallol can be considered to be a result of a copper(II) complex, which is expected to be formed during the chro-

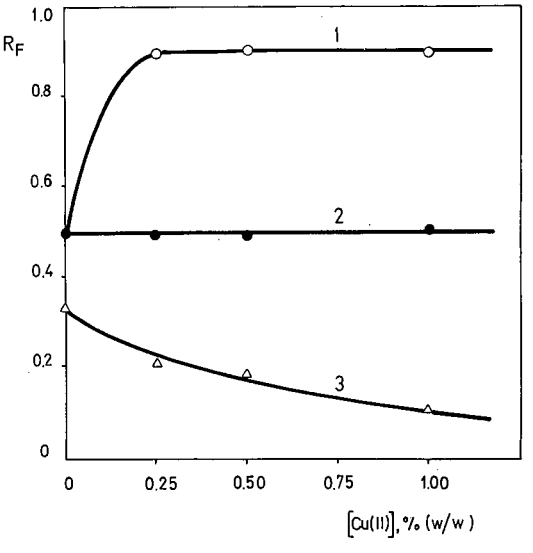

Fig. 2. R_F values of polyphenols as a function of Cu(II) mass fraction in the layer; solvent system S_6. 1 = Hydroquinone; 2 = resorcinol; 3 = pyrogallol.

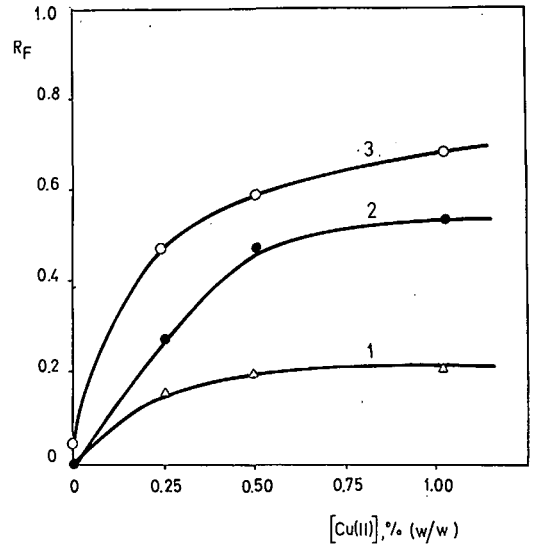

Fig. 3. R_F values of salicylic acid as a function of Cu(II) mass fraction in the layer. Solvent system: 1 = S_3; 2 = S_5; 3 = S_{10}.

matographic process on the copper-impregnated plates.

An interesting phenomenon is observed on examining hydroquinone. The addition of copper to the silica gel layer leads to a rapid decrease in the adsorption of hydroquinone. As copper(II) is an oxidizing agent, the significant increase in R_F values using different solvent systems can be explained as a consequence of oxidation of hydroquinone to the *p*-benzoquinone. The high R_F values of hydroquinone obtained on copper-impregnated plates correspond to those obtained by testing a genuine reference sample of *p* -benzoquinone on silica gel layers. On the other hand, hydroquinone cannot be oxidized by Al(III) ions. Therefore, the chromatographic behaviour of hydroquinone on the Al(III) impregnated plates is identical with that on plain silica gel layers.

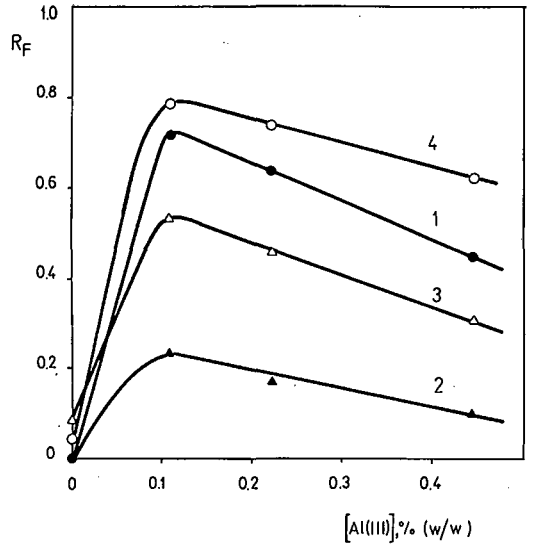

Fig. 4. R_F values of salicylic acid as a function of Al(III) mass fraction in the layer. Solvent system: 1 = S_2; 2 = S_4; 3 = S_5; 4 = S_{10}.

We also examined the chromatographic behaviour of salicylic acid on copper- and aluminium-impregnated plates. On the impregnated plates salicylic acid has higher R_F values than on plain plates (Figs. 3 and 4).

Adsorption of phenolic compounds is a result of hydrogen bonding between the oxygen atom of the phenolic group and hydrogen atoms of the hydroxyl groups on the silica gel surface. As salicylic acid forms stable complexes with Cu(II) and Al(III) ions [12], in which the metal ions are coordinated between the oxygen atom of the phenolic group and the oxygen atom of the carboxyl group, which is present in an *ortho* position, adsorption of salicylic acid on metal impregnated plates is reduced.

On examining the behaviour of other phenolic compounds (cresols, nitrophenols and chlorophenols) on Cu(II)- and Al(III)-impregnated plates, no improvement in resolution was observed.; the $R_F$values obtained on impregnated plates were similar to those obtained on plain silica gel plates.

It can be concluded that the formation of phenol–metal interaction products, different solubilities of the phenol and the interaction product in the solvent system used and the changed adsorption properties of impregnated silica gel play prominent roles in the TLC separation of phenols.

REFERENCES

1 J. I. Koreman and A. I. Krikov, *Zh. Anal. Khim.*, 45 (1990) 1140.
2 K. J. Bajaj and Y. K. Arora, *J. Chromatogr.*, 196 (1980) 309.
3 K. C. Khulbe and R. S. Mann, *Fresenius' Z. Anal. Chem.*, 330 (1988) 642.
4 H. Thielmann, *Fresenius' Z. Anal.Chem.*, 327 (1987) 722.
5 H. Thielmann, *Fresenius' Z. Anal. Chem.*, 330 (1988) 531.

6 O. Hadžija, S. Iskrić and M. Tonković, *J. Chromatogr.*, 464 (1989) 220.
7 O. Hadžija, M. Tonković and S. Iskrić, *J. Liq. Chromatogr.*, 9 (1986) 3473.
8 R. S. Dhillon, J. Sing, V. K. Gautan and B. R. Chhabra, *J. Chromatogr.*, 435 (1988) 256.
9 B. R. Chhabra, R. S. Gulati, R. S. Dhillon and P. S. Kalsi, *J. Chromatogr.*, 135 (1977) 521.
10 S. P. Srivastava and L. S. Chauhan, *Chromatographia*, 13 (1980) 353.
11 M. Petrović and M. Kaštelan-Macan, *Prehrambeno-Tehnol. Biotehnol. Rev.*, 29 (1991) 91.
12 S. Kotrly and L. Sucha, *Handbook of Chemical Equilibria in Analytical Chemistry*, Ellis Horwood, Chichester, 1985.

Announcement from the Publisher

ELSEVIER SCIENCE PUBLISHERS

prefers the submission of electronic manuscripts

Electronic manuscripts have the advantage that there is no need for the rekeying of text, thereby avoiding the possibility of introducing errors and resulting in reliable and fast delivery of proofs.

The preferred storage medium is a $5\frac{1}{4}$ or $3\frac{1}{2}$ inch disk in MS-DOS format, although other systems are welcome, e.g. Macintosh.

Your disk and (**exactly matching**) printed version (printout, hardcopy) should be submitted together to the accepting editor. In case of revision, the same procedure should be followed such that, on acceptance of the article, the file on disk and the printout are **identical**. Both will then be forwarded by the editor to Elsevier.

Please follow the general instructions on style/arrangement and, in particular, the reference style of this journal as given in 'Instructions to Authors'.

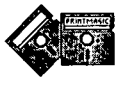

Please label the disk with your name, the software & hardware used and the name of the file to be processed.

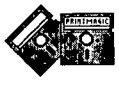

Further information can be found under 'Instructions to Authors - Electronic manuscripts'.

Contact the Publisher for further information.

ELSEVIER SCIENCE PUBLISHERS B.V.
P.O. Box 330, 1000 AH Amsterdam
Netherlands
Fax: (+31-20) 5862-304

4/92

PUBLICATION SCHEDULE FOR 1992

Journal of Chromatography and *Journal of Chromatography, Biomedical Applications*

MONTH	O 1991–M 1992	J	J	A	S	O	N	D
Journal of Chromatography	Vols. 585–600	602/1 + 2 603/1 + 2 604/1	604/2 605/1 605/2 606/1	606/2 607/1 607/2	608/1 + 2 609/1 + 2			
Cumulative Indexes, Vols. 551–600		[a]						
Bibliography Section	610/1	610/2			611/1			611/2
Biomedical Applications	Vols. 573–577/1	577/2	578/1 578/2	579/1	579/2 580/1 + 2	[b]		

[a] Cumulative Indexes will be Vol. 601, to appear early 1993.
[b] The publication schedule for further issues will be published later.

INFORMATION FOR AUTHORS

(Detailed *Instructions to Authors* were published in Vol. 558, pp. 469–472. A free reprint can be obtained by application to the publisher, Elsevier Science Publishers B.V., P.O. Box 330, 1000 AH Amsterdam, The Netherlands.)

Types of Contributions. The following types of papers are published in the *Journal of Chromatography* and the section on *Biomedical Applications:* Regular research papers (Full-length papers), Review articles and Short Communications. Short Communications are usually descriptions of short investigations, or they can report minor technical improvements of previously published procedures; they reflect the same quality of research as Full-length papers, but should preferably not exceed five printed pages. For Review articles, see inside front cover under Submission of Papers.

Submission. Every paper must be accompanied by a letter from the senior author, stating that he/she is submitting the paper for publication in the *Journal of Chromatography*.

Manuscripts. Manuscripts should be typed in double spacing on consecutively numbered pages of uniform size. The manuscript should be preceded by a sheet of manuscript paper carrying the title of the paper and the name and full postal address of the person to whom the proofs are to be sent. As a rule, papers should be divided into sections, headed by a caption (*e.g.*, Abstract, Introduction, Experimental, Results, Discussion, etc.). All illustrations, photographs, tables, etc., should be on separate sheets.

Introduction. Every paper must have a concise introduction mentioning what has been done before on the topic described, and stating clearly what is new in the paper now submitted.

Abstract. All articles should have an abstract of 50–100 words which clearly and briefly indicates what is new, different and significant.

Illustrations. The figures should be submitted in a form suitable for reproduction, drawn in Indian ink on drawing or tracing paper. Each illustration should have a legend, all the *legends* being typed (with double spacing) together on a *separate sheet*. If structures are given in the text, the original drawings should be supplied. Coloured illustrations are reproduced at the author's expense, the cost being determined by the number of pages and by the number of colours needed. The written permission of the author and publisher must be obtained for the use of any figure already published. Its source must be indicated in the legend.

References. References should be numbered in the order in which they are cited in the text, and listed in numerical sequence on a separate sheet at the end of the article. Please check a recent issue for the layout of the reference list. Abbreviations for the titles of journals should follow the system used by *Chemical Abstracts*. Articles not yet published should be given as "in press" (journal should be specified), "submitted for publication" (journal should be specified), "in preparation" or "personal communication".

Dispatch. Before sending the manuscript to the Editor please check that the envelope contains four copies of the paper complete with references, legends and figures. One of the sets of figures must be the originals suitable for direct reproduction. Please also ensure that permission to publish has been obtained from your institute.

Proofs. One set of proofs will be sent to the author to be carefully checked for printer's errors. Corrections must be restricted to instances in which the proof is at variance with the manuscript. "Extra corrections" will be inserted at the author's expense.

Reprints. Fifty reprints of Full-length papers and Short Communications will be supplied free of charge. Additional reprints can be ordered by the authors. An order form containing price quotations will be sent to the authors together with the proofs of their article.

The most useful chiral separation column,
ULTRON ES-OVM, for enantiomeric drugs.

Substance	Rs	Substance	Rs	Substance	Rs
Acetylpheneturide	2.74	Disopyramid	2.04	Nisoldipine	2.36
Alimemazine	6.06	Eperisone	1.15	Nitrendipine	1.80
Alprenolol	1.09[1]	Ethiazide	1.42	Oxazepan	2.65[2]
Arotinolol	1.95	Fenoprofen	0.80	Oxprenolol	1.38
Bay K 8644	5.92	Flurbiprofen	1.27	Pindolol	2.04
Benproperine	3.27	Glutethimide	1.36	2-Phenylpropionic acid	0.80
Benzoin	8.41	Glycopyrronium	1.73	Pranoprofen	0.63
Biperiden	3.17	Hexobarbital	1.70	Prenylamine	0.86
Bunitrolol	3.08	Homochlorcyclizine	3.04	Profenamine	3.31
Bupivacaine	1.26	Hydroxyzine	2.15	Promethazine	1.42
Chlormezanone	6.48	Ibuprofen	1.72	Propranolol	1.24
Chlorphenesin	2.23	Ketoprofen	1.37	Terfenadine	2.22
Chlorpheniramine	2.36	Lorazepam	2.55[2]	Thioridazine	0.72
Chlorprenaline	2.34	Meclizine	3.71	Tolperisone	1.50
Cloperastin	2.85	Mepenzolate	1.40	Trihexyphenidyl	5.16
Dimethindene	4.33	Mephobarbital	1.70	Trimipramine	3.69
1,2-Diphenylethylamine	1.74	Methylphenidate	1.13[1]	Verapamil	1.49

NOTE: 4.6×150mm column at room temp. except[1] 6.0×150mm at room temp. and[2] 6.0×150mm at 10°C

From trace analysis for metabolites ***to preparative scale***

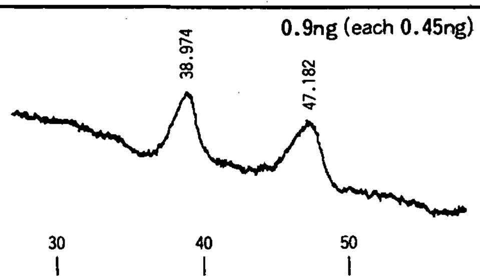

Column : ULTRON ES-OVM 2.0ϕ×150mm
Mobile Phase : 20mM-KH_2PO_4 (pH 6.8)/ CH_3CN=100/35
Flow Rate : 0.1ml/min
Temperature : 25°C
Pressure : 40kg/cm²
Detection : UV-220nm/0.5×10⁻³AUFS
Sample : Propranolol

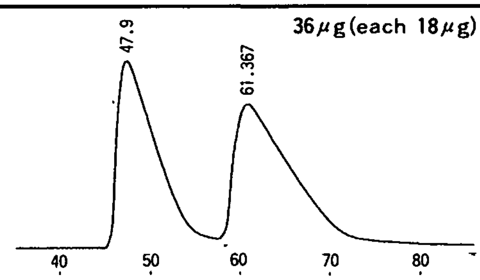

Column : ULTRON ES-OVM 20.0ϕ×250mm
Mobile Phase : 20mM-KH_2PO_4 (pH 6.8)/ CH_3CN=100/30
Flow Rate : 10ml/min
Temperature : 25°C
Pressure : 47kg/cm²
Detection : UV-220nm/6×10⁻³AUFS
Sample : Propranolol

SHINWA CHEMICAL INDUSTRIES, LTD

50 Kagekatsu-cho, Fushimi-ku, Kyoto 612, JAPAN

Phone: 80-75-621-2360 Fax : 80-75-602-2660

Please contact in United States of America and Europe to :

Rockland Technologies, Inc. 538 First State Boulevard, Newport, DE 19804, U.S.A.

Phone : 302-633-5880, Fax : 302-633-5893

This product is licenced by Eisai Co., Ltd.